Carbenes and Nitrenes in Reactive Matrices

Dissertation

To obtain the degree of

Doctor of natural science (Dr. rer. nat.)

by

Enrique Méndez Vega

from La Habana, Cuba

RUHR UNIVERSITÄT BOCHUM

RUB

Bochum 2018

This work was carried out from February 2013 to October 2017 at the Department of Organic Chemistry II of the Ruhr-Universität Bochum under the supervision of Prof. Dr. Wolfram Sander. Part of the work reported in this thesis was performed in collaboration with Prof. Dr. Yuan-Pern Lee at the Department of Applied Chemistry and Institute of Molecular Science, National Chiao Tung University, Taiwan.

First Referee: Prof. Dr. Wolfram Sander

Second Referee: Prof. Dr. Patrick Nürnberger

Day of submission: 28/02/2018

Day of disputation: 05/04/2018

Publications

Mieres-Perez, J.; Mendez-Vega, E.; Velappan, K.; Sander, W., Reaction of Triplet Phenylnitrene with Molecular Oxygen. J. Org. Chem. 2015, 80 (24), 11926-11931.

Richter, G.; Mendez-Vega, E.; Sander, W., Singlet Halophenylcarbenes as Strong Hydrogen-Bond Acceptors. J. Phys. Chem. A 2016, 120 (20), 3524-32.

Mieres-Perez, J.; Henkel, S.; Mendez-Vega, E.; Schleif, T.; Lohmiller, T.; Savitsky, A.; Sander, W., Dinitreno pentaradicals: organic sextet molecules. J. Phys. Org. Chem. 2017, 30 (4).

Mendez-Vega, E.; Maehara, M.; Mieres-Perez, J.; Raut, A. H.; Tsuge, M.; Lee, Y.-P.; Sander, W., Hydrogen Activation by Triplet Carbenes, in preparation.

Mendez-Vega, E.; Trosien, I.; Maehara, M.; Mieres-Perez, J.; Sander, W., Spin-Selective Hydrogenation of Carbenes, in preparation.

Mendez-Vega, E.; Mieres-Perez, J.; Chapyshev, S. V.; Sander, W., Trinitrenes, in preparation.

Scientific Meetings

Graduate School Solvation Science Autumn Workshop, RUB, 10/2016 (Oral Contribution, Award).

Chemistry and Physics at Low Temperature (CPLT 16), France, 07/2016 (Poster).

Graduate School Solvation Science Workshop Area A, RUB, 10/2015 (Poster).

European Symposium of Organic Reactivity (ESOR 15), Kiel, 07/2015 (Poster, Award).

Graduate School Solvation Science Workshop, RUB, 10/2014 (Poster, Award).

Graduate School Solvation Science Summer School, RUB, 06/2014 (Poster).

International Symposium on Reactive Intermediates and Unusual Molecules (ISRIUM 14), Japan, 04/2014 (Poster).

Graduate School Solvation Science Autumn Workshop, RUB, 11/2013 (Poster).

International Internship

From 05/2015 to 07/2015 in the research group of Prof. Dr. Yuan-Pern Lee at the Department of Applied Chemistry and Institute of Molecular Science, National Chiao Tung University, Taiwan.

Contents

Summary

Reactive intermediates are typically short-lived, high-energy species that quickly convert into more stable molecules. Herein, the low-temperature reactivity of carbenes and nitrenes toward small molecules like H_2, O_2, and H_2O is investigated, by covering a range of molecules from highly reactive triplet carbenes to relatively stable septet trinitrenes. The systems studied have been grouped according to the observed reactivity as: triplet reactivity, spin-selective reactivity, and stable trinitrenes.

Low-temperature reactivity against H_2, O_2, and H_2O

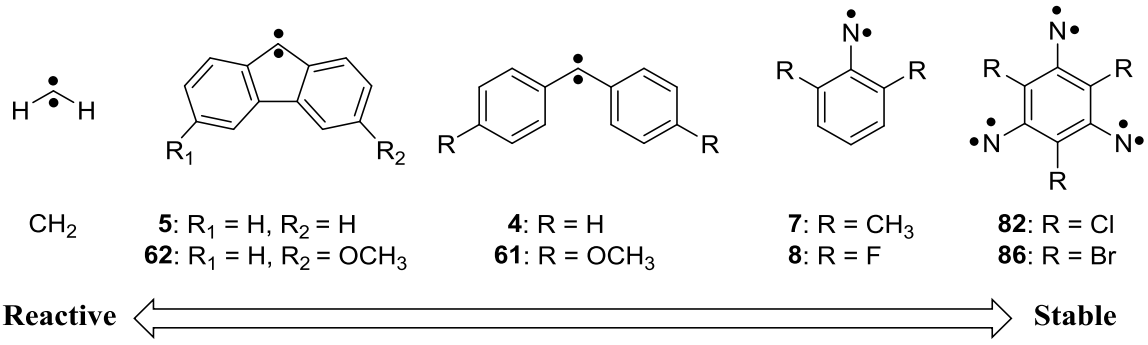

The reactions of triplet ground state carbenes (CH_2, **4**, and **5**) and nitrenes (**7** and **8**) with H_2 were studied by means of the matrix isolation technique. Irradiation of precursor CH_2I_2 with UV light in *p*-H_2 matrices mainly produces CH_2I radical and CH_4. Triplet CH_2 is not detected, although high-level theoretical methods predict high barriers for the H-abstraction by triplet CH_2. Likewise, fluorenylidene **5** readily inserts into H_2 to form fluorene **41**, at temperatures as low as 3 K. In D_2 matrices, carbene **5** is formed, and decays in the dark to produce d_2-**41** by quantum mechanical tunneling, as indicated by the large kinetic isotope effect, temperature-independent rates between 3–6 K, and a high activation barrier estimated by calculations. Triplet diphenylcarbene **4** selectively reacts with H_2 in Ar matrices containing both H_2 and D_2 at 30 K to produce diphenylmethane **47**. However, carbene **4** is stable in solid H_2 and D_2 matrices at 3 K, showing a remarkable temperature-dependence that is unusual under these conditions. It is hence suggested that H-abstraction occurs through vibrationally-assisted tunneling. In contrast to the singlet-chemistry observed in polar solvents, H_2 activation by carbenes **4** and **5** is governed by triplet reactivity, with the carbenic angle as the key factor. Triplet 2,6-dimethylphenylnitrene **7** and 2,6-difluorophenylnitrene **8** are found to be unreactive toward H_2 even at 50 K, which can be rationalized by the high barriers and endothermicity

predicted for the H-abstraction step. Accordingly, triplet nitrenes are found to be less reactive than triplet carbenes toward H_2 activation (Scheme I).

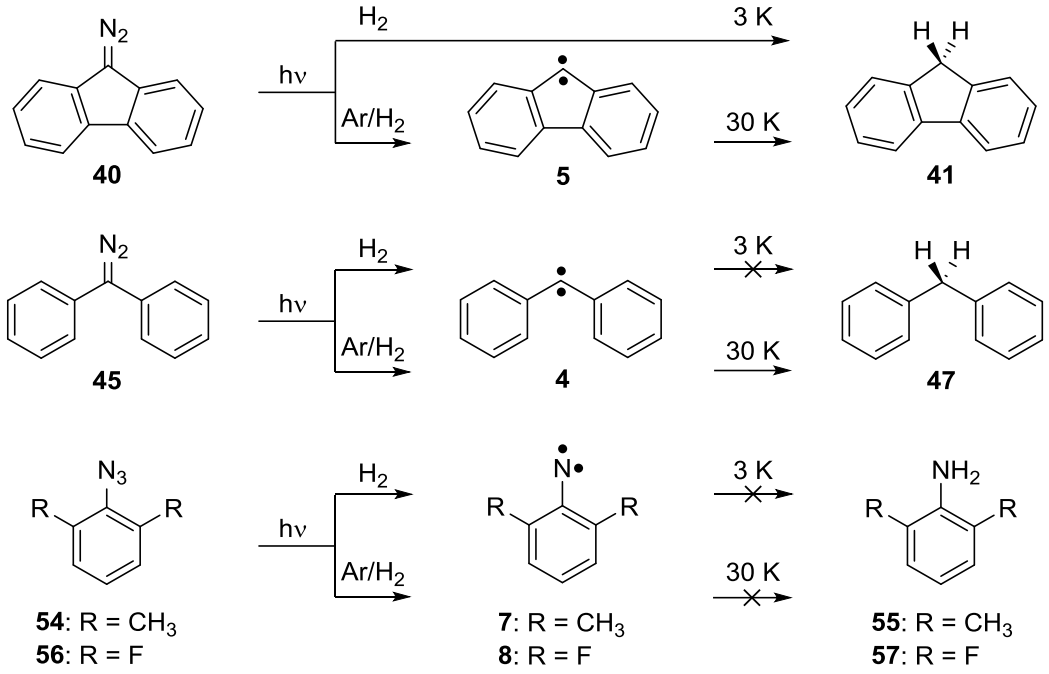

Scheme I. Reactivity of triplet intermediates toward H_2 in low-temperature matrices: diphenylcarbene **4**, fluorenylidene **5**, 2,6-dimethylphenylnitrene **7**, and 2,6-difluorophenylnitrene **8**.

Trapping experiments with H_2 provide chemical evidence for the formation of triplet carbenes in low-temperature matrices. Bis(*p*-methoxyphenyl)carbene **61** is a magnetically bistable carbene, whose lowest singlet S-**61** and triplet T-**61** states indefinitely coexist in inert gas matrices at 3 K. Spectroscopic measurements (IR, UV–vis, and EPR) show that T-**61** is only present as traces in solid H_2 and D_2, whereas S-**61** is stable, which corresponds to a spin-selective hydrogenation. Kinetic measurements in H_2-doped Ar matrices suggest that a rapid thermal equilibration at 30 K results in the conversion of S-**61** into T-**61**, and the latter reacts with H_2 to form bis(*p*-methoxyphenyl)methane **64**. Another bistable carbene, 3-methoxy-9-fluorenylidene **62**, reacts quantitatively in solid H_2 from both S-**62** and T-**62** states to produce 3-methoxy-9-fluorene **69** at 3 K. In pure D_2 matrices, S-**62** and d_2-**69** are generated in a similar ratio to that of the carbene spin states (S-**62**/T-**62**) in Ar matrices (45:55), hence displaying a quantitative and spin-selective D_2 activation by T-**62**. Hydrogenation of bistable carbenes allows to probe the reactivity of singlet and triplet states in a single experiment (Scheme II).

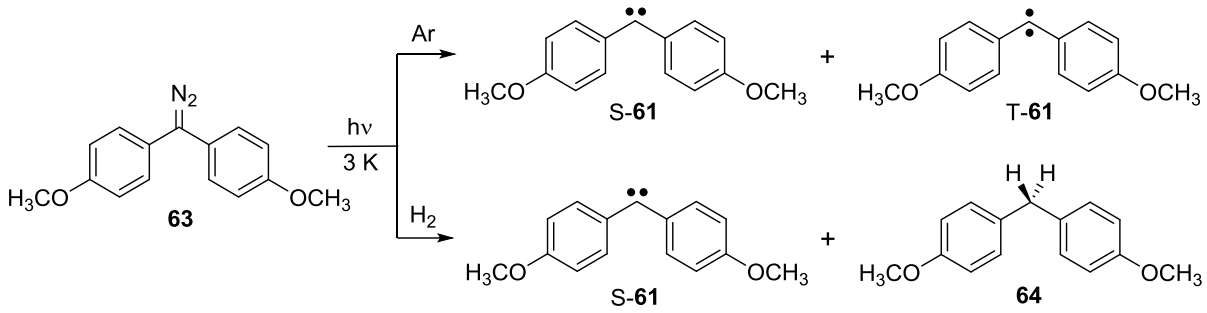

Scheme II. Spin-selective reactivity of bis(*p*-methoxyphenyl)carbene **61** toward H_2 in low-temperature matrices.

Two highly symmetrical trinitrenes, 1,3,5-trichloro-2,4,6-trinitrenobenzene **82** and 1,3,5-tribromo-2,4,6-trinitrenobenzene **86** were isolated in both inert gas (Ne, Ar, and Xe) and reactive host (H_2, O_2, and H_2O) matrices. Trinitrenes **82** and **86** have robust septet ground states and unprecedent stability under cryogenic conditions. Irradiation of triazide precursors **79** and **83** with UV light results in the quantitative formation of trinitrenes **82** and **86**, respectively. A complete photoconversion of **79**→**82** and **83**→**86** was obtained, whereas the corresponding low-spin intermediates such as triplet mononitrenes **80**, **84**, and quintet dinitrenes **81**, **85** were not present at the end of the photolysis. For the first time, IR and UV–vis spectra were recorded for septet organic molecules free from side products. In water matrices, trinitrene **82** was surprisingly stable up to 160 K, where water ice starts subliming. The stability, robust septet ground states, and strong magnetic properties of trinitrenes **82** and **86** suggest that they can potentially be used as building blocks for the design of molecular magnets (Scheme III).

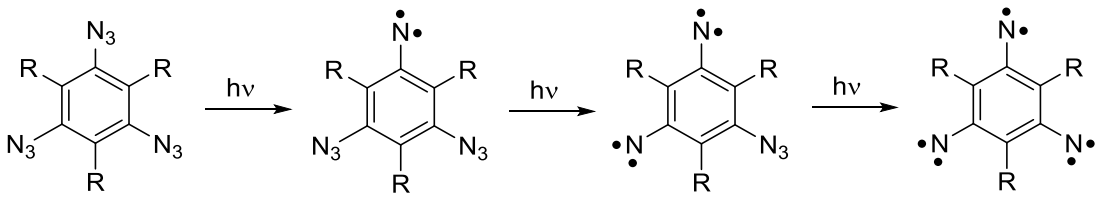

Scheme III. Photochemical synthesis of trinitrene 1,3,5-trichloro-2,4,6-trinitrenobenzene **82** and 1,3,5-bromo-2,4,6-trinitrenobenzene **86** in low-temperature matrices.

Background

Carbenes

Carbenes are neutral, divalent derivatives of carbon. Together with carbanions, carbocations, and carbon-centered radicals, carbenes are among the fundamental intermediates in the reactions of carbon compounds. Because of their electron-deficient nature, carbenes are usually highly reactive and have a short lifetime at room temperature.[1] The divalent carbon atom of a carbene has only six electrons in its valence shell. Four are shared forming covalent bonds with the two substituents, and hence two nonbonding electrons remain. These two electrons are distributed in two nonbonding molecular orbitals (NBMOs) of the carbene and can have antiparallel spins (singlet state) or parallel spins (triplet state). If the carbene is linear, the two NBMOs are degenerate (p_x, p_y), and the carbon center adopts sp hybridization. In this case, according to Hund's rule, the lowest energy is achieved when a triplet configuration is present. Bending the molecule breaks such degeneracy and stabilizes the p_x orbital that acquires some s character, causing the carbon center to adopt sp^2 hybridization, whereas the p_y orbital remains almost unchanged. Accordingly, for bent carbenes, the p_x orbital is renamed as σ, and the p_y orbital therefore as π orbital (Figure 1).[2]

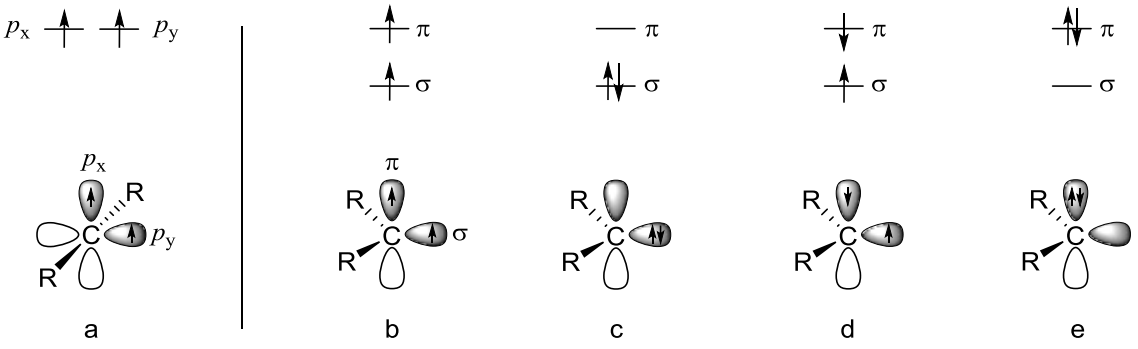

Figure 1. Schematic depiction of the electronic configurations of carbenes. a) Triplet $p_x^1p_y^1$ configuration with a linear geometry. b) Triplet $\sigma^1\pi^1$ configuration with a bent geometry. c) Closed-shell singlet $\sigma^2\pi^0$ configuration with a bent geometry. d) Open-shell singlet $\sigma^1\pi^1$ configuration with a bent geometry. d) Closed-shell singlet $\sigma^0\pi^2$ configuration with a bent geometry.

The electronic occupation of the σ and π orbitals depends on the energy separation between them and determines the carbene ground state multiplicity. If the electron-electron Coulombic repulsion is higher in energy than the pairing energy, the two electrons will occupy two different orbitals, and thus either triplet or open-shell singlet configurations will be formed. Otherwise, the electrons will remain in the same orbital leading to a closed-shell configuration.

Hoffmann estimated that an energy separation of at least 2 eV is necessary to impose a singlet ground state, whereas a value smaller than 1.5 eV leads to a triplet ground state.[3] In practice, most of carbenes are bent and the two lowest electronic states are triplet $\sigma^1\pi^1$, in which the two electrons occupy separate orbitals with parallel spins, and a singlet $\sigma^2\pi^0$, where the two electrons are spin-paired in the in-plane orbital. The other possible electronic configurations, with singlet $\sigma^1\pi^1$ and $\sigma^0\pi^2$ electron occupations, are usually much higher in energy. The difference in energy between triplet and singlet state is called "singlet-triplet splitting" (ΔE_{ST}), and usually refers to the energetic gap between the triplet and closed-shell singlet state. Conventionally, ΔE_{ST} is defined as $\Delta E_{ST} = E_S - E_T$, and hence triplet ground state carbenes have positive singlet-triplet energy gaps. Ground state multiplicity and ΔE_{ST} of carbenes are defined by geometry and electronic structure and have a profound impact on chemical reactivity.

The structure and energetics of methylene CH_2, the simplest carbene, was subjected to a long debate, starting in 1932 with Mulliken`s qualitative predictions,[4] until 1961 when Herzberg suggested a linear triplet ground state based on the analysis of the experimental electronic spectra.[5] Later on, electron paramagnetic resonance (EPR) experiments at low temperatures demonstrated that CH_2 has a triplet ground state.[6] However, analysis of the zero-field splitting parameter E estimated the bond angle H–C–H to be around 136°, challenging the hypothesis of Herzberg. These finding were also confirmed by using different precursors for CH_2, as well as preparing several of its isotopomers (CHD, CD_2, and $^{13}CD_2$),[7,8] concluding that triplet CH_2 adopts a bent structure with an sp^2 hybridized carbon atom (Figure 1b). The ΔE_{ST} was found to be 9.05 ± 0.06 kcal/mol according to far-infrared laser magnetic resonance spectroscopic measurements.[9]

Regarding carbenes more complex than CH_2, the ΔE_{ST} may easily be overturned by the effects of substituents attached to the carbene center. The factors which influence the spacing can be analyzed in terms of electronic, hyperconjugation, and steric effects. Attachment of π-donor and σ-acceptor groups (e.g. halogen atoms) stabilize the singlet state by raising the energy of the π orbital of the carbene, while the σ orbital remains basically unperturbed. In contrast, π-acceptor or conjugating groups (e.g. aryl groups) have the opposite effect, by lowering the energy of the π orbital of the carbene. In either case, the ground state for these carbenes is expected to be triplet, although the magnitude of ΔE_{ST} may change. On the other hand, alkyl groups stabilize the singlet through hyperconjugative interactions with the empty 2p orbital,

which is the case for dimethylcarbene **1**. For bulky alkyl groups, this effect is less effective. For example, the steric repulsion between the two *tert*-butyl groups in di(*tert*-butyl)carbene **2** widens the central bond angle favoring the triplet state.[10]

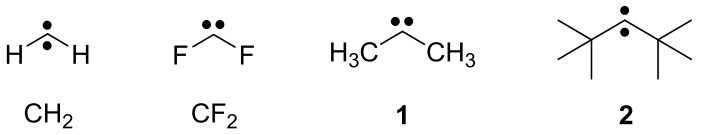

CH_2 CF_2 **1** **2**

The effect of aryl substitution on carbenes spin states is more complex since both electronic and steric effects might contribute. It has been demonstrated by EPR studies that most aryl and diarylcarbenes have triplet ground states, although with smaller singlet-triplet gaps than the parent CH_2.[11] Among the carbenes of this class, the most studied ones are phenylcarbene **3**, diphenylcarbene **4**, and fluorenylidene **5**.

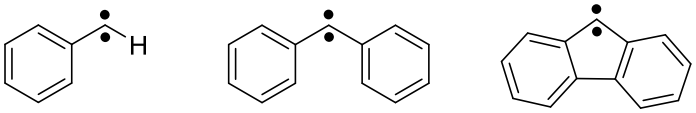

3 **4** **5**

Chemical reactivity of carbenes depends on their multiplicity because of fundamental differences in the reaction mechanism.[12] Triplet carbenes display a reactivity in solution similar to that of radicals. They add to olefins to generate intermediate triplet diradicals that subsequently form cyclopropanes with loss of the alkene stereochemistry. Likewise, triplet carbenes also abstract H atoms from C–H bonds to produce triplet radical pairs. Those radicals can spin-flip to singlet pairs, which recombine to give C–H insertion products. In contrast, singlet carbenes react with olefins in a concerted fashion, affording cyclopropanes with retained stereochemistry, as well as inserting directly into C–H bonds. The observation of stereospecific or nonstereospecific addition remains as one of the most used experimental test of singlet or triplet reactivity.[13]

Although carbenes have two electronic states of different stability, it is not always the ground state which is involved in the reaction. For example, in trapping solution experiments, carbenes are frequently generated by photolysis of diazo or diazirine precursors. Irradiation of the precursor should initially produce singlet carbenes (via the singlet excited state of the precursor), regardless of the ground state multiplicity. On the other hand, triplet-sensitized photolysis can directly produce triplet carbenes. However, when the energy difference between such electronic states (ΔE_{ST}) is small, the reaction from the upper state can compete with the

ground state reaction. Then, regardless of the mode of generation, singlet and triplet products can be formed depending on their relative rates of formation (k_S and k_T) and the energy separation ΔG_{ST} between the singlet and triplet state of the carbene. This sequence of processes was rationalized by Eisenthal et al. and is depicted in Scheme 1.[14]

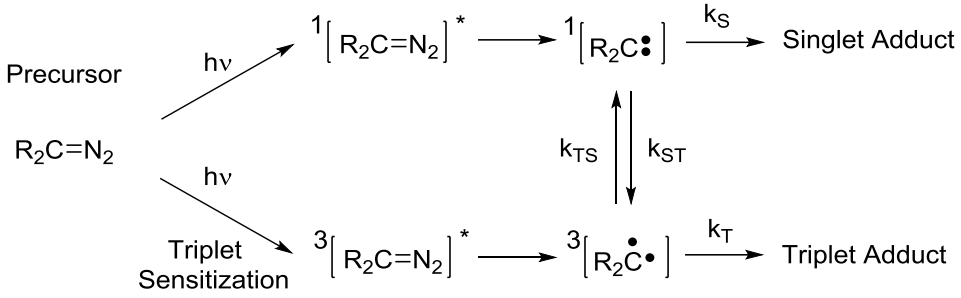

Scheme 1. Spin-specific generation and reactions of singlet and triplet carbenes.

In addition, Tomioka suggested several guidelines, which are summarized as follows:[15]

- Carbenes with singlet states lying well below triplets will react in the singlet state even if they were produced by triplet-photosensitization.
- Carbenes with triplet states lying well below singlets (ΔE_{ST} > 5 kcal/mol) react through a multiplicity that depends on the mode of generation.
- Triplet ground state carbenes with a small singlet-triplet gap (ΔE_{ST} < 3 kcal/mol) react via singlet, irrespective of the mode of generation.

These criteria can be overridden if choosing a molecule that effectively quenches a particular electronic state such as molecular oxygen. Triplet carbenes add readily to triplet O_2 in a spin-allowed reaction; in contrast, singlets tend to react slowly, or are even unreactive.[16] Another variable to take into account, which was only discovered recently, is the role of solvent as a spin controller. For instance, triplet ground state diphenylcarbene **4** switches its spin to singlet upon interaction with methanol and water, by forming strong hydrogen-bond complexes.[17,18] Stabilization of the singlet state of **4** is also achieved by interaction with halogen-bond donors (CF_3I and CF_3Br)[19] as well as with strong Lewis acids like BF_3.[20]

Nitrenes

Nitrenes are carbene analogs, where a monovalent nitrogen replaces the carbon atom. In most of the stable compounds, nitrogen is trivalent, and therefore it is no surprise that nitrenes are typically very reactive and short-lived intermediates.[21,22] Arylazides (with nitrenes as

photoproducts) have important applications as photoresists in lithography,[23] and in biochemistry as photoaffinity labeling reagents.[24] Similar to carbenes, nitrenes have nonbonding electrons that occupy the valence molecular orbitals on different ways, resulting in several possible electronic configurations. Common electronic configurations of nitrenes are shown in Figure 2, with the nitrogen atom depicted as adopting sp hybridization.

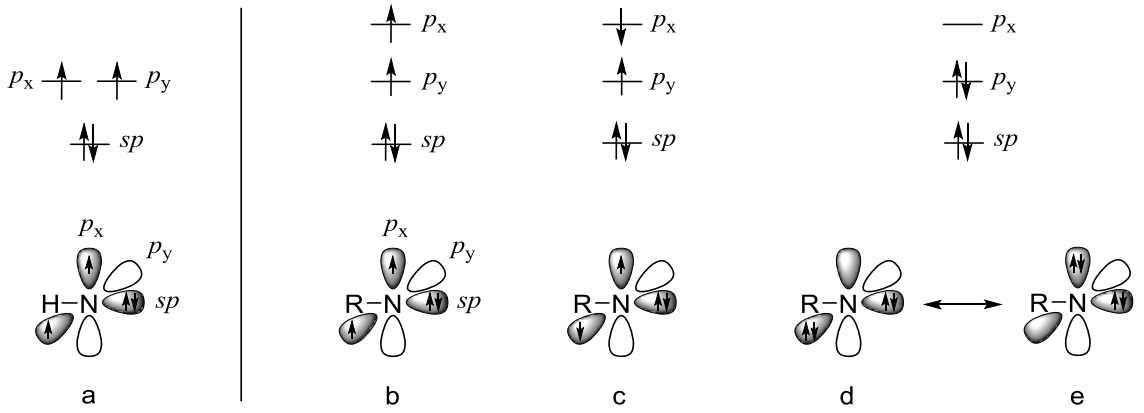

Figure 2. Schematic depiction of the electronic configurations of nitrenes. a) Triplet configuration of NH. b) Triplet configuration of a substituted nitrene. c) Open-shell singlet configuration of a substituted nitrene. d-e) Closed-shell singlet configurations of a substituted nitrene.

Imidogen NH, the simplest nitrene, is a highly symmetric molecule with an sp hybridized nitrogen atom. It possesses four nonbonding electrons that are distributed in a sp orbital and two degenerate p_x and p_y orbitals, hence generating several possible electronic configurations. The two lowest electronic states of NH are triplet $^3\Sigma^-$ and singlet $^1\Delta$, the latter being a doubly degenerate state formed by a linear combination of closed-shell and open-shell singlet configurations.[25] The ground state of NH is triplet since the Coulombic electron-electron repulsion is less severe than in the singlet state. A value of 36 kcal/mol for the singlet-triplet splitting of NH was determined by spectroscopy of neutral NH[26] as well as by negative ion photoelectron spectroscopy (NIPES) of the NH anion.[27] Triplet NH and its deutero-substitute analogue ND were also trapped in inert gas matrices at low temperatures, and fully characterized by infrared (IR) and ultraviolet–visible (UV–vis) spectroscopy.[28,29] To this date, the EPR spectrum of triplet NH in cryogenic matrices has not been reported.[30]

When the H atom of NH is substituted by a molecular group (e.g. a π-donor group), the degeneracy of the p_x and p_y orbitals is removed, and the p_x orbital increases its energy. This destabilizing effect can be explained by the interaction between lone pairs of the substituent and the out-of-plane p_x orbital on the nitrene center. The lowest-energy states are usually

triplet, open-shell singlet, and closed-shell singlet. The relative stability of the electronic states of nitrenes can be rationalized in terms of two contributions, the magnitude of the exchange integral between both unpaired electrons in the triplet state, and the energy separation between the frontier orbitals. In analogy to carbenes, if the frontier orbital energy gap (as result of introducing a substituent) is larger than the exchange integral between the two unpaired electrons in the triplet state, then a singlet ground state is obtained. Since ΔE_{ST} of the parent NH is very large, only few substituents can switch the spin from triplet to singlet ground state (e.g. an amino group).[31] Indeed, most of the reported nitrenes have a triplet ground state, although ΔE_{ST} is not as large as in NH.[32]

Similar to carbenes, singlet and triplet nitrenes show different chemical reactivity. Triplet nitrenes insert into alkyl C–H bonds by abstraction-recombination mechanism and react thermally with O_2. Singlet nitrenes insert into aryl C–H bonds, undergo ring expansion reactions to benzazirines, and form nitrenium ions in acidic media.[22,33,34]

Arylnitrenes, which exhibit robust triplet grounds states, have received the most attention in the literature.[32,35] Among the nitrenes of this class, some of most studied ones are phenylnitrene **6**, 2,6-dimethylphenylnitrene **7**, and 2,6-difluorophenylnitrene **8**.

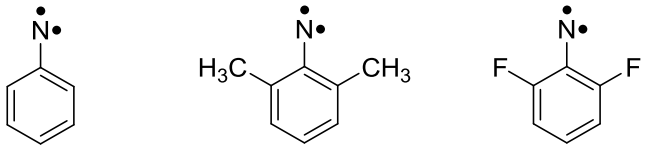

6 **7** **8**

Unraveling the chemistry of arylnitrenes took a long and difficult way because trapping experiments in solution were not very informative. For instance, photolysis or pyrolysis of most arylazides in hydrocarbons leads to polymeric tars, instead of diagnostic insertion products.[36] A fortunate exception is the formation of azepines in the presence of primary and secondary amines.[37] Therefore, much of the current understanding of arylnitrenes has come from direct observational methods such as spectroscopy in the gas phase, solution, low-temperature glasses, and inert gas matrices.[35,38-40] Scheme 2 represents a simplified view of the mechanism of photolysis and thermolysis of phenylazide **9** in different media.

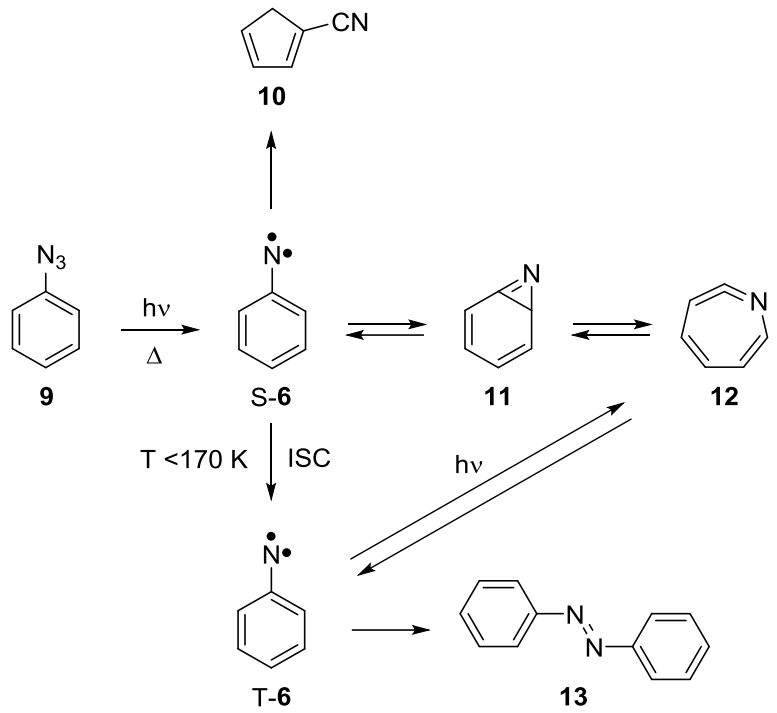

Scheme 2. Photolysis and thermolysis of phenylazide **9**.

Photolysis of **9** initially produces open-shell singlet phenylnitrene S-**6** and the following step depends on temperature and phase.[41] In the gas phase, hot S-**6** is formed with excess of vibrational energy and isomerizes to cyanocyclopentadiene **10**.[40] In solution at ambient temperature, S-**6** rearranges to benzazirine **11** that subsequently forms ketenimine **12**.[42] At temperatures below 170 K, S-**6** decays to T-**6** by intersystem crossing (ISC).[43] Triplet T-**6** is stable in inert gas matrices and forms azobenzene **13** upon annealing of the matrix.[44] Furthermore, T-**6** undergoes ring expansion to form ketenimine **12** upon irradiation.[45]

Phenylnitrene **9** has a triplet ground state ($^3A_2$), in which the NBMOs are singly occupied. The next higher-lying states are open-shell singlet ($^1A_2$) and closed-shell singlet ($^1A_1$). The energy separation between the ground state and those two excited states was estimated to be 15 and 31 kcal/mol, respectively.[46,47]

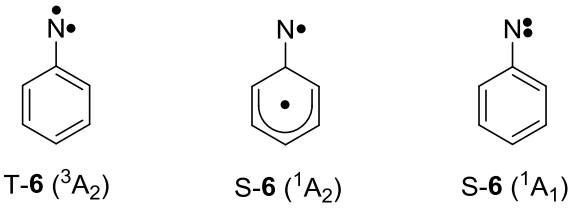

The stabilization of the open-shell singlet state is the result of the delocalization of the unpaired electron (located in the p_x orbital) into the phenyl ring; this tends to minimize the

electron-electron Coulombic repulsion. Such delocalization is not as extensive as for the triplet state, due to the high exchange integral resulting from having both electrons with the same spin at the nitrogen center. Indeed, calculations estimate a longer Ph–N bond (1.34 Å) in the triplet state with respect to the open-shell singlet (1.28 Å), the latter value indicates a substantial double bond character. Consequently, the triplet state can be thought as a more nitrogen-centered diradical, while the open-shell singlet state has more 1,3-diradical character.[47,48]

Carbenes vs. Nitrenes

Phenylcarbene **3** and phenylnitrene **6** are isoelectronic triplet ground state intermediates, however, they show a very different chemical reactivity in solution at ambient temperatures. A comparison of the dynamics of these reactive species is illustrated in Figure 3.

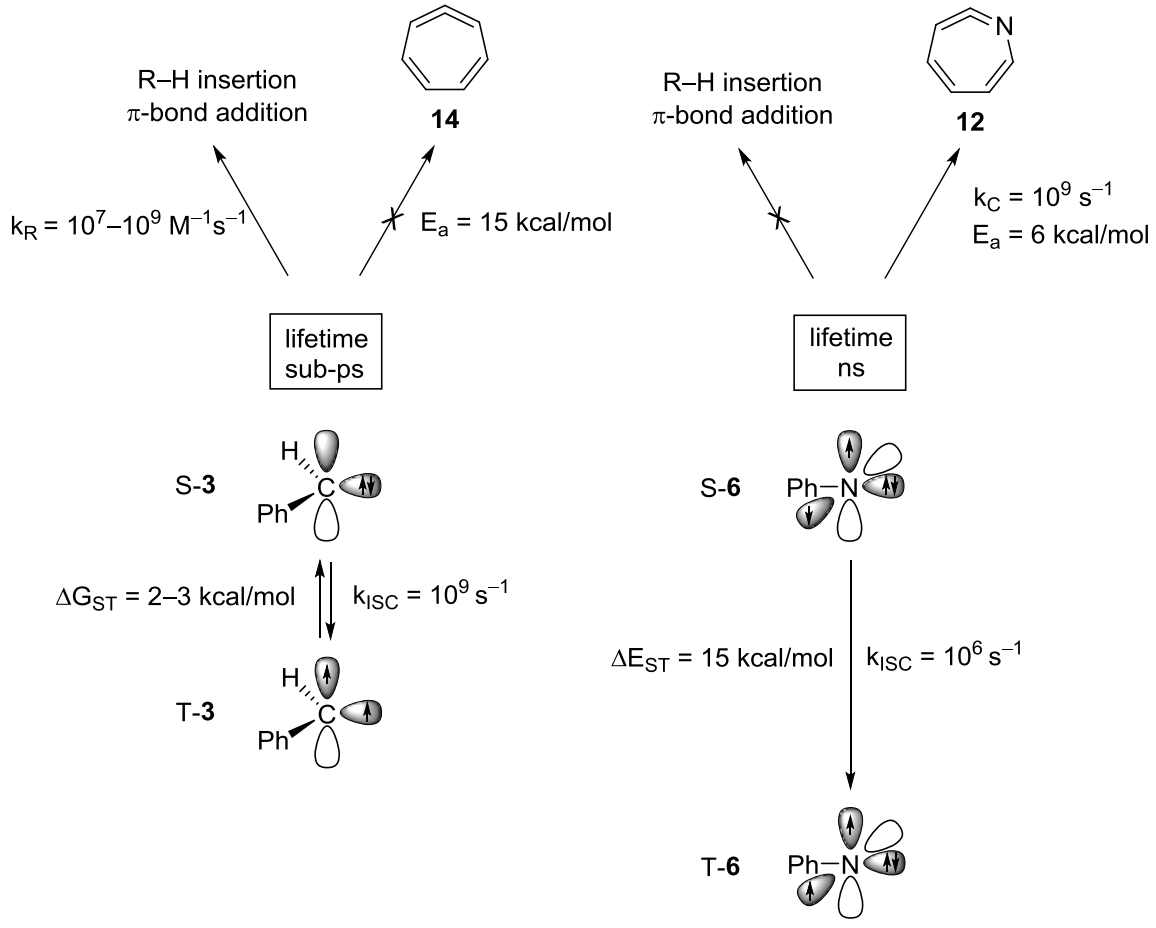

Figure 3. Representation of some of the possible reactions of phenylcarbene **3** (left) and phenylnitrene **9** (right) such as intersystem crossing (ISC) process, cyclization, and bimolecular reactions with organic substrates.

In the solution phase, singlet phenylcarbene S-**3** readily reacts with many functional groups such as alcohols, alkenes, and alkanes to form stable products.[49,50] In contrast, photolysis of

phenylazide **9** just leads to the formation of polymeric tars without application in synthetic chemistry.[36] In contrast to the fast rearrangement of **6**, the ring expansion of singlet phenylcarbene S-**3** to form cumulene **14** proceeds much slower than that of singlet phenylnitrene S-**6**.[51,52] This contrasting reactivity was explained by combining experimental data from kinetics and spectroscopy measurements with theoretical calculations.[53-56] Several questions arise like why nitrene **6** has a higher ΔE_{ST}, decays at a slower ISC rate, undergoes faster cyclization, and is less reactive toward organic solvents. These topics are discussed in the next paragraphs.

Phenylcarbene **3** has a triplet ground state with a small ΔG_{ST} of 2–3 kcal/mol, depending on the solvent used.[50,57] The small energy gap is a consequence of the stabilization gained by keeping the nonbonding electrons farther apart (triplet state), or placing them on a lower-energy sp^2 orbital (singlet state). In contrast, the open-shell singlet state of phenylnitrene S-**6**, although stabilized by delocalization into the phenyl ring, does not have the energetic advantage of placing both electrons into a σ orbital rich in 2s character.[55] Hence, the ΔE_{ST} of nitrene **6** is with 15 kcal/mol much larger than that of carbene **3** (2–3 kcal/mol).[46]

For many arylcarbenes such as **3**, singlet-triplet splittings are so small that the two states reversibly interconvert with rates that are faster than bimolecular reactions[1] (although such assumption has been recently challenged by the role of solvent-carbene interactions).[58] Relaxation of singlet nitrene **6** to the corresponding triplet state is always irreversible (both in solution and cryogenic matrices) because of the large ΔE_{ST}. Indeed, the rate of ISC for **3** is three orders of magnitude faster than for **6** ($k_{ISC} = 10^9$ vs. 10^6 s^{-1}).[14,52] This can be explained by the smaller ΔE_{ST} of the carbene, although spin-orbit coupling must be taken into account. For instance, the ISC is facilitated by the change in orbital angular momentum of carbene **3** ($\sigma^2\pi^0 \rightarrow \sigma^1\pi^1$), but not in **6** because both S-**6** and T-**6** have the same orbital occupancy ($\sigma^1\pi^1 \rightarrow \sigma^1\pi^1$).[56]

Cyclization of S-**6** requires that the nitrogen slightly bends out of the molecular plane, in order to facilitate the overlapping of the N-centered p_x orbital with a singly occupied π orbital of the benzene ring. In contrast, cyclization of S-**3** requires changes in the electronic structure. A double bond to the exocyclic ring carbon must be created and the corresponding charge separation in the transition state (TS) is energetically costly. Consequently, the activation energy (E_a) is about 9 kcal/mol higher in S-**3** with respect to that in S-**6**; that is consistent with the higher rate for the cyclization of S-**6** ($k_C = 10^9$ s^{-1}).[52,54,59]

In terms of intermolecular reactivity, S-**3** reacts much faster with electron donors than does S-**6**.[50] The empty π orbital of S-**3** interacts (as electrophile) with electron pairs, e.g. inserting into C–H bonds and adding to alkenes.[49] However, similar reactions with S-**6** are not that favored because its π orbital is partially occupied, and hence proceed much slower than the cyclization. Since both low-lying states of **6** are open-shell, they are expected to undergo radical-like reactions. However, H-abstraction by triplet phenylnitrene T-**6** is even slower than the dimerization under the conditions of flash photolysis experiments.[36] In contrast, S-**6** readily abstracts H atoms from suitable donors. In order to find an explanation for this trend, it is worth to move back to the simplest systems, CH_2 and NH.

Scheme 3 shows the thermochemistry of the C–H and N–H bond dissociation of CH_4 and NH_3, respectively. Moreover, isodesmic reactions involving $^3CH_2$ and ^3NH, as well as triplet phenylcarbene T-**3** and triplet phenylnitrene T-**6** are also represented.

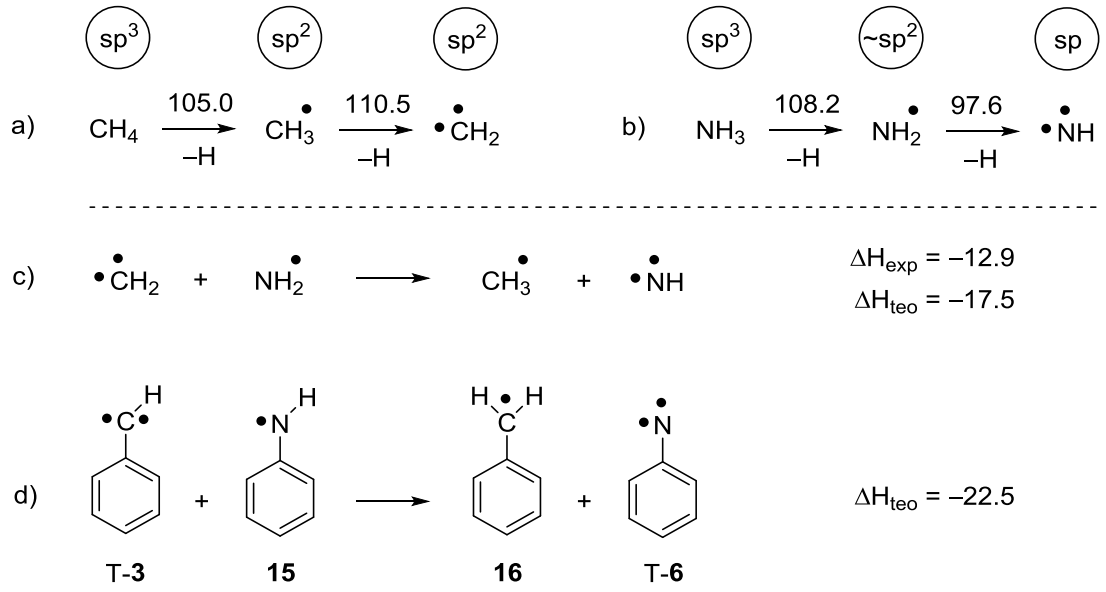

Scheme 3. Thermochemistry of some H-abstraction processes. a-b) Experimental bond dissociation energies (BDE) of CH_4, CH_3, NH_3, and NH_2.[60] Approximated hybridization of the involved species are shown on top. c) Isodesmic reaction showing the relative stability of $^3CH_2$ and ^3NH. Enthalpy (ΔH_{exp}) is derived from the energy values in (a, b). Enthalpy (ΔH_{teo}) was reported at the CASPT2/6-31G* level of theory.[55] d) Isodesmic reaction showing the relative stability of triplet phenylcarbene T-**3** and triplet phenylnitrene T-**6**. Enthalpy (ΔH_{teo}) was reported at the CASPT2/6-31G* level of theory.[55] Energies are given in kcal/mol.

The first BDE of NH_3 is slightly larger (3.2 kcal/mol) than that of CH_4, as expected for a more polar bond. However, the second BDE of methane is substantially larger (12.9 kcal/mol) than that of NH_3. Those differences in energies can be explained by using the concept of rehybridization.[55,56] In the first bond dissociation of CH_4 and NH_3, the approximated

hybridization of the central atom is changing from sp^3 to sp^2 in both cases. In contrast, in the second bond dissociation, only the nitrogen center changes its hybridization ($sp^2 \rightarrow sp$). Hence, the lone pair of the nitrogen lowers its energy by occupying an orbital with more 2s character. Such rehybridization should make ^3NH more stable than $^3CH_2$ since, in the latter, the nonbonding electrons occupy the more energetic 2p orbitals. The isodesmic reactions involving ^3NH and $^3CH_2$, as well as the more complex T-**3** and T-**6**, show a remarkable release of energy (12–22 kcal/mol) on transferring a H atom from the aminyl radical to the carbene center. Moreover, based on the BDEs, $^3CH_2$ would react exothermic with CH_4 (ΔH = –5.6 kcal/mol); whereas a similar reaction of ^3NH would be endothermic (ΔH = 7.4 kcal/mol).[25,53] Overall, it seems that the large amount of 2s character in the lone pair orbital on the nitrogen atom makes triplet nitrenes thermodynamically more stable and less reactive to H-donors than triplet carbenes.

Quantum Tunneling

Tunneling of a particle through a barrier arises from the wave-particle duality. It is a quantum mechanical phenomenon, whereby particles can penetrate through areas with a potential energy higher than their total energy. If the de Broglie wavelength of a particle approaching a barrier is approximately equal or longer than the thickness of the barrier, tunneling can take place. As an illustration, one can consider particles having kinetic energies of 5 kcal/mol (0.22 eV), which is comparable to barriers found in chemical reactions. Under such conditions, the de Broglie wavelength for an electron is 26 Å and it should be able to tunnel through distances equal to many molecular diameters. This enables scanning tunneling microscopy, tunnel junctions, and tunnel diodes. However, when considering atoms, smaller wavelengths (although still chemically relevant) are obtained for H (0.6 Å), D (0.4 Å) and C (0.2 Å), the latter being almost at the limit for considering quantum mechanical tunneling (QMT).[61]

QMT increases the rate of a chemical reaction because it occurs in addition to crossing over the barrier. Since it proceeds through less energetic pathways, it can happen even when the available thermal energy is lower than the activation energy. Thermally- or vibrationally-assisted tunneling means that most of the tunneling contribution to the rate comes from excited vibrational levels of the reactant (ν = 1, 2, 3 …), instead of from the zero-point energy level (ZPE or ν = 0).[62] The occurrence of tunneling depends on the shape of the barrier, the atomic masses, and the temperature, those parameters will be discussed below. The tunnel effect can

be described by using a simple qualitative model, a particle approaching a rectangular barrier (Figure 4).

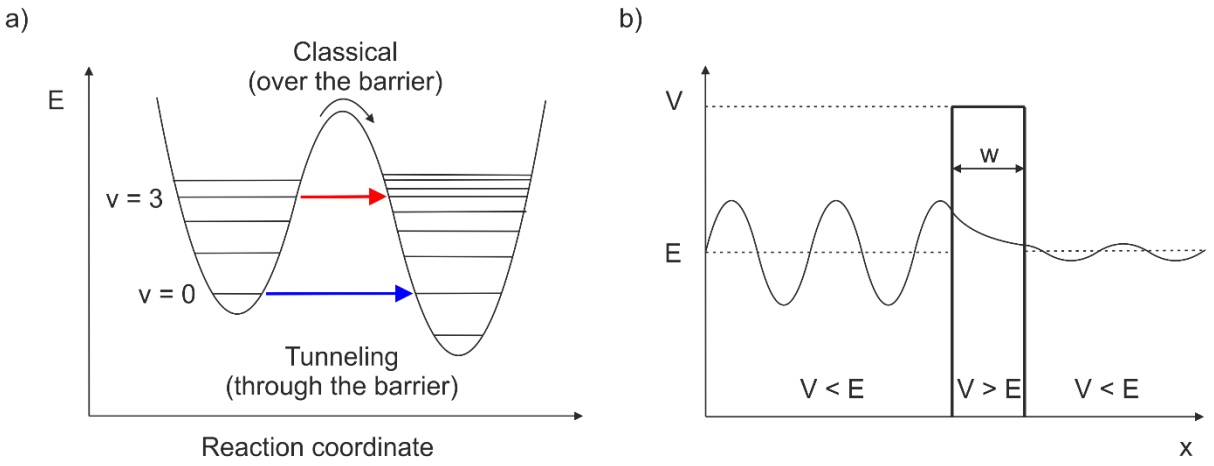

Figure 4. Tunneling scenarios. a) One-dimensional potential energy surface of an exothermic reaction. Several competing pathways are shown: over the barrier and through the barrier from the lowest (blue) or an excited vibrational level (red). b) A particle with a kinetic energy E penetrates a rectangular barrier with width w and potential energy V.

For a barrier with a finite potential V, there is a certain probability to find the particle on the other side of the potential wall, even if the kinetic energy of the particle E is lower than the height of the potential barrier (E < V). In this case, the wave function of the particle does not decay abruptly to zero, but rather decays exponentially with the distance inside the barrier and oscillates on the other side with a lower amplitude. If the particle has mass m and energy E, and the barrier has height V and width w, the tunneling probability is:[63]

$$P = e^{-4\pi w\sqrt{2m(V-E)}/\hbar} \quad (1)$$

Equation (1) shows that the probability of tunneling decreases exponentially with the width of the barrier and with the square root of both the particle mass and the energy deficiency (V – E). This simple example illustrates the strong dependence of the tunneling rate on the barrier shape and weaker dependence on the mass and the barrier height, in contrast to the thermal rate described by the Arrhenius equation, which mainly depends on the barrier height.

Bell investigated the effect of tunneling on the reaction rates in detail, and developed a theoretical model for describing tunneling through a parabolic barrier.[61] He introduced the quantum tunneling correction factor Q into the Arrhenius rate expression as shown in Eq. (2) and Eq. (3).

$$k = Q\ A\ e^{-\frac{E_a}{R\,T}} \tag{2}$$

$$Q = \frac{e^{\alpha}}{\beta-\alpha}\left(\beta e^{-\alpha} - \alpha e^{-\beta}\right) \tag{3}$$

$$Q \approx \frac{\beta}{\beta-\alpha} \tag{4}$$

$$\text{with } \alpha = \frac{E}{R\,T} \text{ and } \beta = \frac{2w\pi^2(2mE)^{\frac{1}{2}}}{h}$$

Moreover, Eq. (3) can be simplified to Eq. (4) since parameter β is usually larger than α for chemical reactions.[64] Hence, the effect of the tunneling correction Q is to increase the rate of reaction at a given temperature, relative to the classical rate based on A and E_a. According to Eq. (4), the smaller the ratio β/α, the greater will be the tunneling "acceleration". Moreover, the equations show that Q increases as the temperature is lowered, thus predicting that tunneling should be more relevant at low temperatures.

Unfortunately, quantification of tunneling contributions to reaction rates cannot be experimentally determined. Experimental evidence for tunneling is based on deviations from the classical kinetic behavior. Some of those anomalies are nonlinear Arrhenius plots, temperature-independent reaction rates, reactions that are faster than expected, strong kinetic isotope effects, and anomalous values of A and E_a.[65] Those key experimental observations are described in the next paragraphs.

For most organic reactions, the reaction rates follow the Arrhenius law, which results in linear plots of ln k versus 1/T. However, when QMT is involved, rate constants decay less steeply as the temperature is lowered, resulting in curved Arrhenius plots. At low temperatures, available thermal energy is insufficient to overcome the activation barrier, so tunneling would completely control the reaction. The reaction rate is therefore temperature-independent as tunneling occurs exclusively from the lowest vibrational level (deep tunneling).[66] Therefore, nonlinear Arrhenius plots and temperature independence on reaction rates can be taken as indication of a tunneling reaction (Figure 5a).[67]

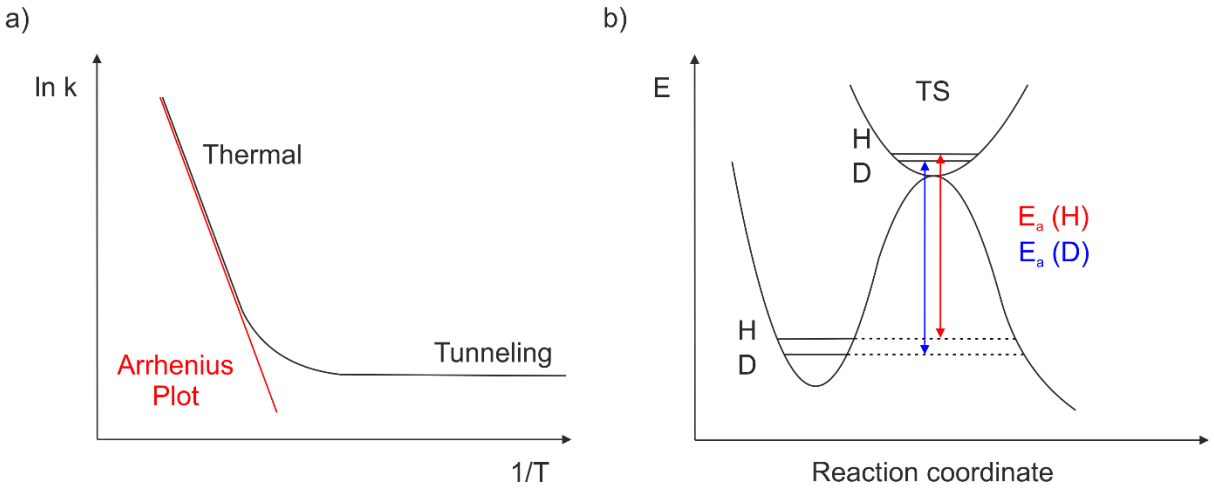

Figure 5. Effect of temperature and mass on reaction rates. a) Schematic Arrhenius plot with (black) and without (red) tunneling. At higher temperatures, the reaction is dominated by thermal transitions; at low temperatures, the reaction is controlled by tunneling. b) One-dimensional potential energy surface illustrating the kinetic isotope effect (KIE). The exchange of isotopes (hydrogen and deuterium) influences the classical reaction (height of the barrier) as well as the probability of tunneling (mass of the isotope and width of the barrier).

On the other hand, QMT allows reactions to proceed much faster than expected based on calculations or extrapolation from rates measured at higher temperatures (classical temperature regime). For instance, in a hypothetical unimolecular reaction with a barrier of only 1 kcal/mol and a pre-exponential factor A of 10^{12} s^{-1} (estimation from k_bT/h), the Arrhenius expression would predict a rate constant in the order of 10^{-10} s^{-1} and a half-life time of approximately 100 years at 10 K.[68] This classical estimation is several orders of magnitude slower than the experimental rates found for many tunneling reactions in inert matrices at 10 K. For example, isomerization of carboxylic acids[69] and hydroxycarbene derivatives[70,71] take place within a time range of minutes/hours at 10 K, although their activation barriers are predicted to be larger than 5 kcal/mol.

Another way to experimentally assess the importance of tunneling is to measure the kinetic isotope effect (KIE = k(light isotope)/k(heavy isotope)). As reactants follow the reaction coordinate toward the TS, bonds can become weaker which results in slightly different ZPEs for reactants and TS. Because of the mass dependence of the vibrational energy, isotopes would have distinct activation barriers and reaction rates, resulting in a semi-classical KIE (Figure 5b). However, because of the mass-dependence on the probability of tunneling, isotope effects on rates of reaction can be more dramatic than the semi-classical estimations. This effect is most pronounced for the isotopes of hydrogen, since the atomic mass of deuterium is twice that of hydrogen. For tunneling processes at room temperature involving a H atom, some criteria are applied: (i) $k_H/k_D > 7$; (ii) $A_H/A_D < 0.7$; and (iii) E_a (D) – E_a (H) > 1.2 kcal/mol.[72]

The greater probability of tunneling in H- vs. D-transfer reactions comes from several effects. First, the smaller de Broglie wavelength of the D isotope results in a smaller tendency to penetrate the barrier. Moreover, as the frequency of the active mode decreases (e.g. ν(C–D) < ν(C–H)), the tunneling particle makes fewer attempts to penetrate the barrier. Finally, C–D bonds have lower ZPEs, therefore, facing broader barriers to penetrate. Nevertheless, large KIEs at low temperatures are not a direct indication of tunneling, since ln (KIE) vary linearly with the inverse of the temperature at the Arrhenius expression.

Kinetics at the high- and low-temperature regime have been described, but the crossover region has not been covered yet. At those intermediate temperatures, reactions sometimes proceed faster than combining the (extrapolated) thermal rate and the low-temperature limit of the tunneling rate. This is due to vibrationally-assisted tunneling (VAT) and can be explained by narrower barriers at excited vibrational levels below the top of the barrier.[73] Moreover, at excited vibrational levels, the density of states is higher at both the reactant and product sides, increasing the probability of overlapping. Likewise, vibrational excitation also explains why endothermic reactions might proceed by tunneling, although the ZPE level of the reactants cannot match any energy level of the products. Therefore, deep tunneling at very low temperatures is mostly restricted to thermoneutral or exothermic reactions.[61]

It should be noticed that low-temperature tunneling reactions in solid media can often be interpreted better based on the assumption of a continuous Boltzmann energy distribution (that is fully justified in bimolecular gas reactions), rather than using a quantum model with discrete vibrational levels.[61] This can be attributed to the effect of lattice vibrations of the solid (phonons), resulting in "broadening" the molecular energy levels or by providing a range of barriers of different dimensions. For example, in H-transfer reactions, C–H stretching vibrational levels can be broadened by the superposition of lower-frequency levels from C–H bending or ring deformation modes.[74]

Far from just being a correction to classic transition-state theory (TST), tunneling plays a role in many important areas such as enzymology,[75] interstellar chemistry,[76] catalysis,[77] and organic chemistry.[78] Tunneling in chemical transformations is usually classified into light- and heavy-atom tunneling depending on the atomic mass of the atoms involved. Some of the first chemical processes that were rationalized to proceed via tunneling are the inversion of ammonia (light),[61] and the automerization of cyclobutadiene (heavy).[79] Since then, many other chemical reactions of this nature have been observed at cryogenic temperatures, where thermal contributions can

be ruled out. Scheme 4 shows some examples of intra- and intermolecular H-atom tunneling, involving neutral molecules, radicals, carbenes, and nitrenes.

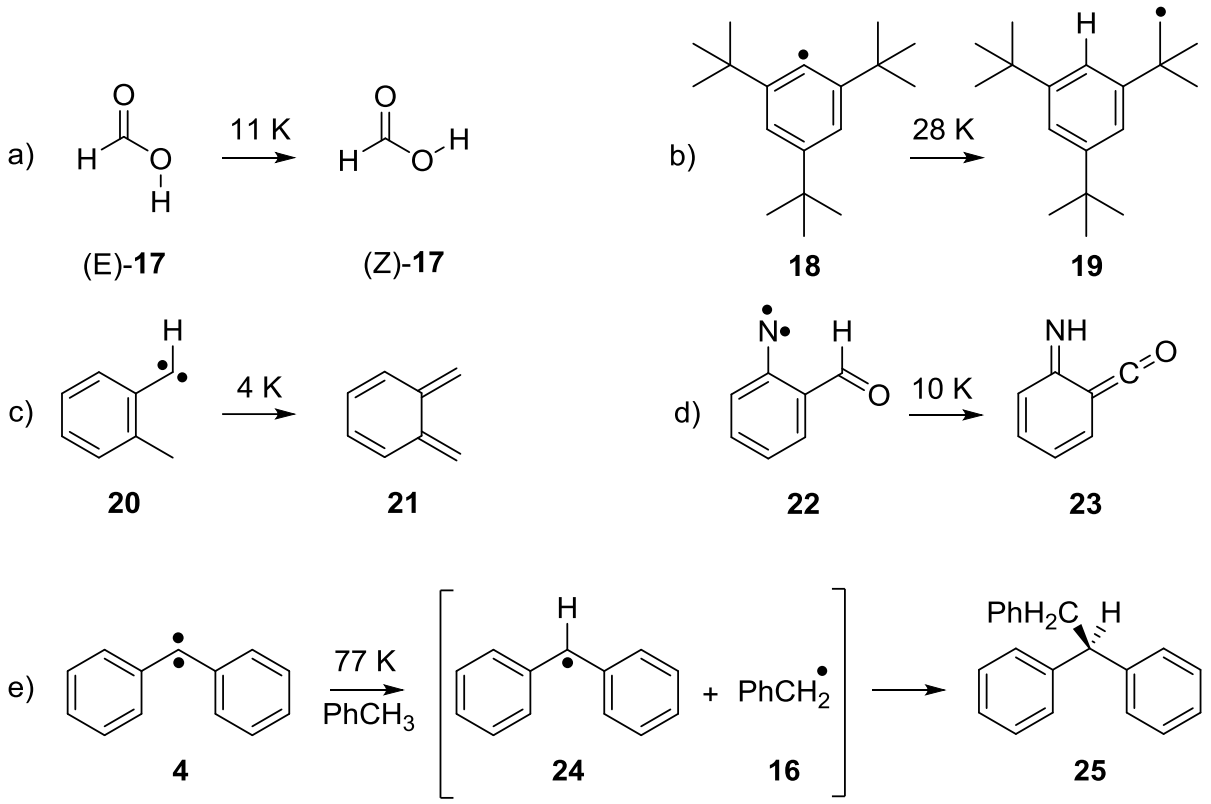

Scheme 4. Selected examples of hydrogen tunneling at low temperatures. a) Rotamerization of formic acid **17**.[80,81] b) Intramolecular H-abstraction by 2,4,6-tri-*tert*-butylphenyl radical **18**.[74] c) 1,4-Hydrogen shift of *o*-tolyl methylene **20**.[82] d) 1,4-Hydrogen shift of 2-formylphenylnitrene **22**.[83] e) Intermolecular H-abstraction from toluene by diphenylcarbene **4**.[84]

As a result of the high sensitivity of QMT to the tunneling atom's mass, H-atom tunneling has received the most attention in organic chemistry. For instance, in 2002, Pettersson et al. generated the higher-energy conformer of formic acid (E)-**17** and observed the isomerization to the more stable isomer (Z)-**17** in inert gas matrices at 11 K.[80,81] Later on, Schreiner et al. contributed to the understanding of tunneling rotamerization by measuring a series of substituted benzoic acid derivatives.[69] Regarding H-abstractions by radicals, one of the earliest tunneling examples was the isomerization of 2,4,6-tri-*tert*-butylphenyl radical **18** to 3,5-di-*tert*-butylneophyl radical **19**.[74] For this reaction, a KIE (H/D) of 13000 was measured, which is much larger than the classical estimation of 260 at –150 °C, thus suggesting the presence of tunneling. Many examples of intramolecular H-transfer via tunneling have been reported for carbenes.[65,85] For example, the isomerization of *o*-tolylmethylene **20** to *o*-xylylene **21** proceeds in darkness at temperatures as low as 4 K ($\tau_{1/2}$ = 64 h).[82] In contrast, arylnitrenes are stable in Xe matrices up to 80 K giving no H-shifted products.[86] The first direct evidence of a tunneling

reaction involving a nitrene was reported recently, which is the 1,4-hydrogen shift of 2-formylphenylnitrene **22** to form 6-imino-2,4-cyclohexadien-1-ketene **23**.[83]

In addition to unimolecular reactions, the role of tunneling on the H-abstraction from hydrocarbons by triplet carbenes came from investigations by Platz[87] and Gaspar[88] in 1980. They monitored the decay of triplet diphenylcarbene **4** in low-temperature organic glasses by EPR spectroscopy. For example, when carbene **4** is photochemically generated in toluene matrices at 77 K, it decays by abstracting a H atom from the matrix and forms a triplet radical pair (diphenylmethyl radical **24** and benzyl radical **16**).[84] Moreover, thawing the matrix yields the C–H insertion product **25** in quantitative yields. Kinetic measurements at various temperatures gave Arrhenius parameters of E_a = 2.1 kcal/mol and log A = 2.4 s^{-1}, which are much smaller than expected. Based on analogous free radical processes, one expects E_a and log A values to be in the range of 6–12 kcal/mol and 8–11 s^{-1}, respectively. The experimentally observed rate constant of 6.3 × 10^{-4} s^{-1} at 77 K, was higher than the classical estimation of <10^{-6}, again indicating the involvement of a tunneling process.

In addition, such kinetic studies were extended for several triplet arylcarbenes (such as phenylcarbene **3** and fluorenylidene **5**) in different glassy matrices, resulting in several general observations.[89] The decay of triplet carbenes is slowed down in perdeuterated matrices, suppressed in perfluoroalkane matrices, and correlates with the relative H-donating ability of the glassy materials. Overall, it was proposed that the mechanism of carbene decay was H-abstraction through QMT.

Finally, it has been suggested that abstraction and insertion reactions of triplet and singlet carbenes with H_2 may be representative of the analogous reactions with saturated hydrocarbons.[90] Hence, this brief review about the well-documented chemistry of such reactive intermediates in organic solvents and glasses might serve as guide for understanding hydrogenation reactions in cryogenic matrices. Low-temperature hydrogen activation by carbenes is thoroughly discussed in the next two chapters.

Hydrogenation of Triplet Intermediates

Introduction

The activation and subsequent utilization of molecular hydrogen is one of the most fundamental processes in synthetic chemistry. However, the majority of the processes involve transition metals.[91] Metal-free activation of H_2 has therefore attracted great interest in the scientific community.[92] Splitting of the H–H bond at room temperature using stable carbenes,[93] frustrated Lewis pairs,[94] and heavier analogues of carbenes such as germylenes and stannylenes[95] has been reported. Under cryogenic conditions, super-electrophilic carbenes,[96,97] triplet,[98,99] and singlet carbenes[100] have been reported to react with H_2.

The mechanisms for the reactions of singlet and triplet carbenes with H_2 (and saturated hydrocarbons) are distinctively different (Scheme 5). Singlet carbenes are predicted to react with H_2 via a concerted path including electrophilic and nucleophilic phases.[101] Molecular hydrogen approaches the singlet carbene to form a three-centered bond with the "empty" π orbital of the carbene (electrophilic phase), while the lone pair of the carbene populates the σ^* orbital of H_2 (nucleophilic phase). On the other hand, triplet carbenes are expected to react through an abstraction-recombination mechanism, hence behaving like diradicals. The first and rate-determining step of the hydrogenation of a triplet carbene is H-abstraction that leads to the formation of a triplet radical pair. In the second step, intersystem crossing followed by radical recombination takes place to form the H_2-insertion product, this step is typically barrierless and highly exothermic.

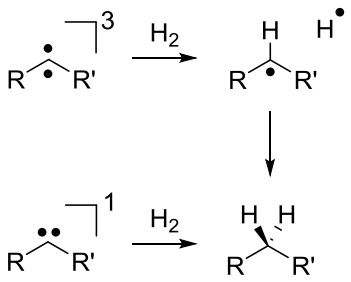

Scheme 5. General mechanism of the hydrogenation reaction of triplet and singlet carbenes.

A compilation of all singlet and triplet carbenes for which the reaction with H_2 has been studied at cryogenic temperatures is shown in Figure 6.

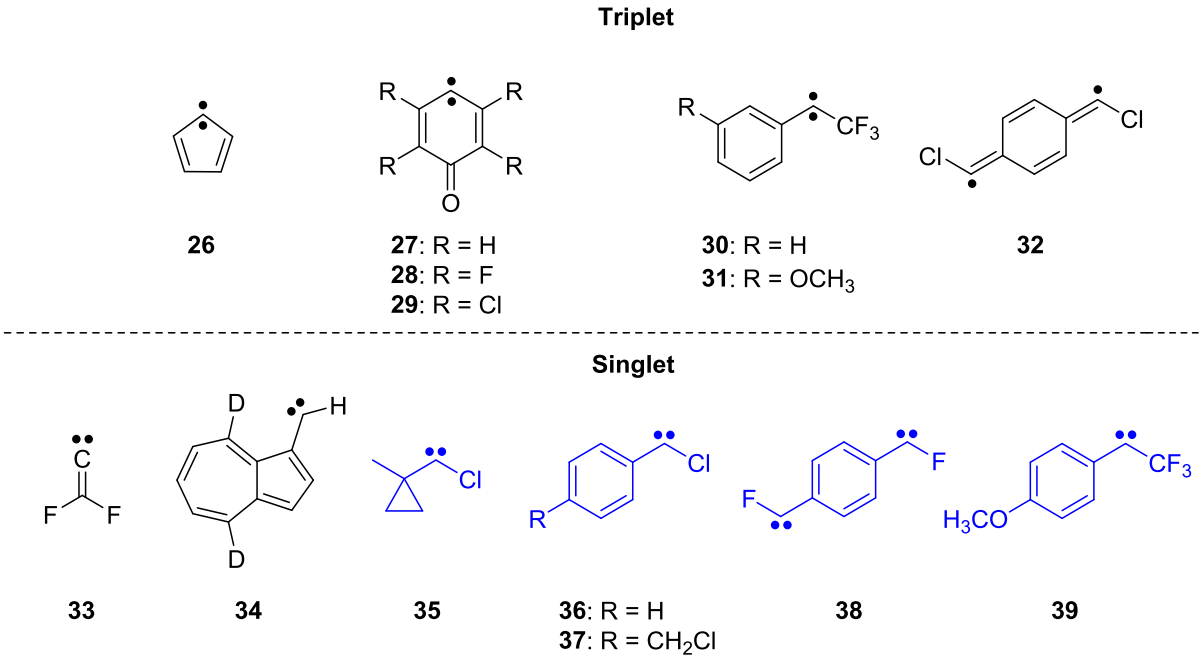

Figure 6. Triplet and singlet carbenes for which the reaction with H_2 has been investigated at low temperatures. Triplet carbenes **26**–**31**, open-shell singlet diradical **32**, and singlet carbenes **33**, **34** react with H_2, but singlet carbenes (in blue) **35**–**39** do not react.

Zuev and Sheridan investigated the reaction of H_2 with a series of singlet and triplet carbenes using the matrix isolation technique.[98] They generated the carbenes in 2% H_2-doped Ar matrices at 10 K and subsequently warmed the matrix to 30 K to allow diffusion of H_2. Under these conditions, it was found that triplet carbenes **26**, **27**, **30**, as well as singlet diradical **32** react thermally with H_2 to give the corresponding H_2-insertion products. Moreover, such triplet carbenes were completely unreactive with D_2 under comparable conditions, indicating a large kinetic isotope effect. In contrast, singlet carbenes **35**–**39**, could not be induced to react with H_2 at temperatures up to the degradation point of the Ar matrix (ca. 35 K). Interestingly, isomeric aryl(trifluoromethyl)carbenes showed different reactivity toward H_2 under the same conditions, triplet *m*-methoxyphenyl(trifluoromethyl) carbene **31** reacted with H_2 but the *para* isomer (singlet ground state) **39** did not.[102]

In general, the concerted addition of singlet carbenes to H_2 is calculated to have higher barriers (5−13 kcal/mol) than the H-abstraction by triplet carbenes (2−5 kcal/mol).[65,98] Hence, it is suggested that direct insertion of singlet carbenes into the H–H bond via QMT is less facile than the stepwise reaction of triplet carbenes with H_2, either because of higher classical barriers or because of the lower probability of QMT involving two H atoms simultaneously. Nevertheless, a few singlet carbenes are reported to react with H_2 at low temperatures. One example is difluorovinylidine **33**, which inserts into H−H and C−H bonds with almost no

activation barrier.[96] This family of highly electrophilic carbenes, including singlet **33** and triplet **28**, **29**, is shown to be extremely reactive.[97,103] So far, carbene **33** and 4,8-d_2-1-azulenylcarbene **34** are the only singlet carbenes that undergo insertion reactions with H_2 at low temperature.[100]

The effects of spin multiplicity and electrophilicity of carbenes, as well as the overall exothermicity and barrier of the hydrogenation reaction, have been under extensive discussion.[98,103,104] However, less attention has been paid on the structural rigidity of the carbenes, as well as the enthalpy and the shape of the barrier associated with the H-abstraction step. So far, all triplet carbenes investigated have been shown to react with H_2 either in pure H_2 or in H_2-doped Ar matrices. It is interesting to extend such study to the bulky triplet diarylcarbenes, where the access of H_2 to the unpaired electrons is limited. In this work, the low-temperature reactivity of two triplet carbenes, diphenylcarbene **4** and fluorenylidene **5**, toward H_2 and D_2 is investigated by means of the matrix isolation technique. As for comparison, studies are also extended to the simplest carbene, CH_2, as well as to two arylnitrenes, 2,6-dimethylphenylnitrene **7** and 2,6-difluorophenylnitrene **8**.

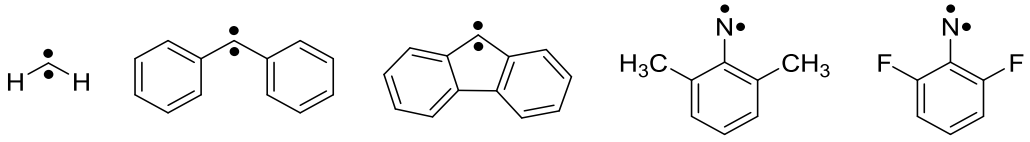

CH_2 **4** **5** **7** **8**

Methylene

Addition of H_2 to methylene CH_2 is one of the simplest organic reactions one can think of. This reaction was experimentally studied by Braun, Bass, and Pilling by irradiating both diazomethane and ketene (as well as the corresponding isotope-labeled compounds CD_2N_2 and CD_2CO) with vacuum ultraviolet flash radiation in the gas phase at 298 K.[105] Quenching of triplet and singlet CH_2 was monitored by kinetic spectroscopy in N_2 and H_2 atmosphere. With rate constants at 298 K given in $cm^3\,molec^{-1}\,s^{-1}$, they have summarized their results as follows:

Singlet reaction: $CH_2\,(^1A_1) + H_2 \rightarrow CH_4^* \rightarrow CH_3 + H$ $\quad k_5 = 7.0 \pm 1.5 \times 10^{-12}$ (5)

Singlet deactivation: $CH_2\,(^1A_1) + H_2 \rightarrow CH_2\,(^3B_1) + H_2$ $\quad k_6 < 1.5 \times 10^{-12}$ (6)

Triplet reaction: $CH_2\,(^3B_1) + H_2 \rightarrow CH_3 + H$ $\quad k_7 < 1.5 \times 10^{-14}$ (7)

No reaction between triplet CH_2 with H_2 was experimentally observed at 298 K, and the value given is an upper limit to the true rate constant. Moreover, the absolute reaction rates for singlet CH_2 are apparently independent of the source (ketene or diazomethane), suggesting that the reactions occur via vibrationally cold singlet CH_2. The reported values (according to the Chemical Kinetic Database for Combustion Chemistry) for k_5 and k_7 are 1.2×10^{-10} and $< 5 \times 10^{-15}$ $cm^3\,molec^{-1}\,s^{-1}$, respectively.[106,107] Shock-wave kinetics experiments at high temperatures (1850−2040 K) show that reaction (5) proceeds without noticeable barrier and does not depend on temperature. In case of reaction (7), numerical simulations (TST with Eckert correction) suggest slower rates, especially at lower temperatures.[108,109]

Singlet reaction rate: $k_5 = 1.27 \pm 0.36 \times 10^{-10}$ $E_a = 0$, experiment

Triplet reaction rate: $k_7 = 7.32 \times 10^{-19} T^{2.3}\, e^{-3699/T}$ simulation

with k in $cm^3\,molec^{-1}\,s^{-1}$ and E_a in kcal/mol

Overall, hydrogenation reaction of CH_2 at higher temperatures is quite complex since the collisional energy transfer ($^3CH_2 \rightarrow {}^1CH_2$) is very fast, and hence singlet CH_2 can compete for H_2 as well as decay to the triplet.[110] However, under cryogenic conditions, only the triplet ground state is expected to be trapped in the matrix.

p-Hydrogen Matrices

These experiments were performed in the laboratory of Prof. Yuan-Pern Lee at NCTU, Taiwan. Spectra were kindly provided in order to get any insight into the reactivity of CH_2 in *para*-hydrogen (*p*-H_2) matrices. The use of *p*-H_2 as matrix host offers several advantages because of its quantum nature.[111] Due of the large amplitude of the zero-point lattice vibrations, the matrix is considered to be "soft", hence reducing inhomogeneous broadening of signals of the guest molecules. Associated with this softness is the diminished matrix cage effect that allows generating free radicals by in situ photodissociation of molecular precursors (e.g. organic halides).[112] In this work, the matrix isolation set up and experimental procedures were similar to those reported previously by Lee et al. for generating ICH_2OO.[113] Likewise, the spectroscopic assigments are based on this reference unless otherwise indicated. The IR spectrum of a gaseous mixture of CH_2I_2/*p*-H_2 (1/1000) after deposition at 3.2 K for 3 h is shown in Figure 7.

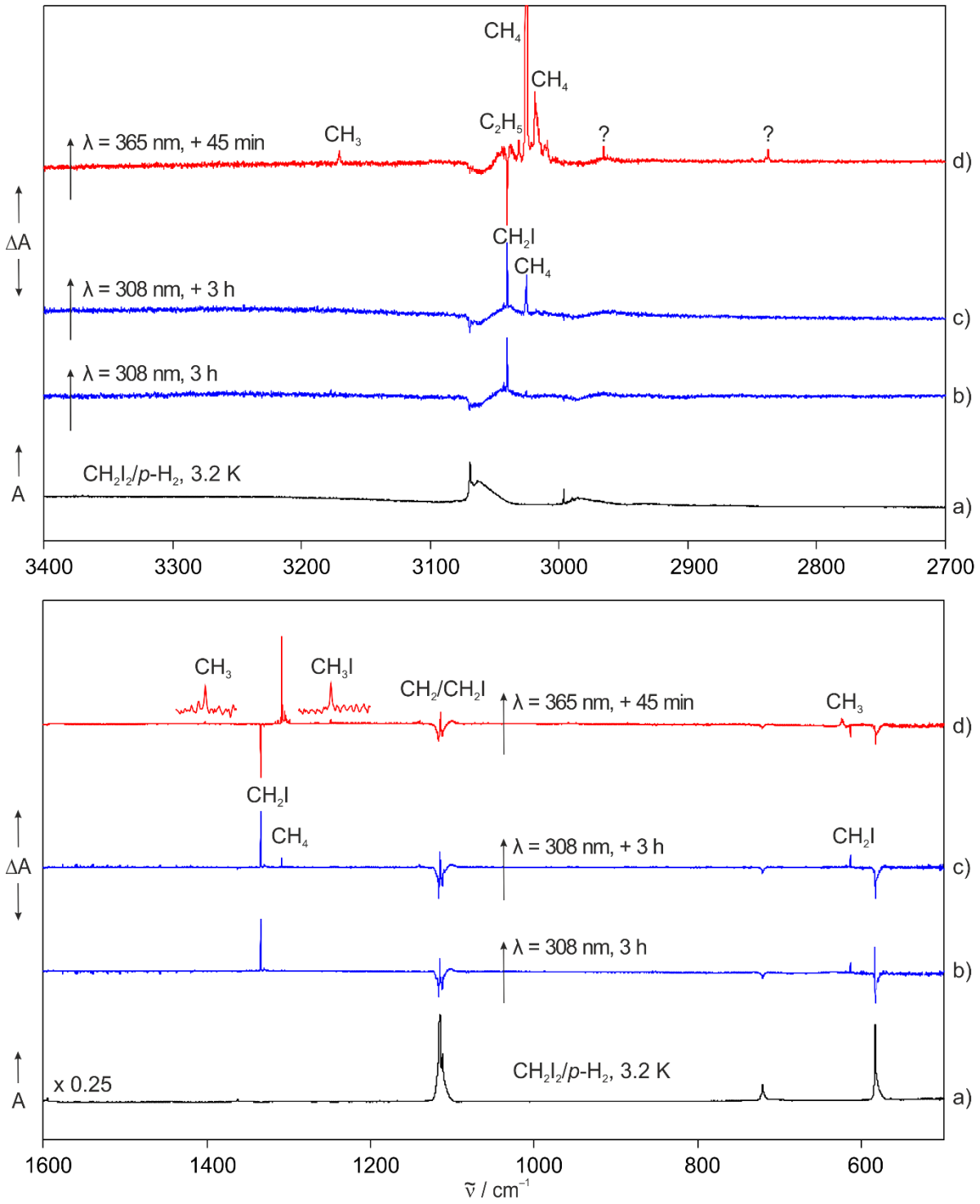

Figure 7. IR spectra (region 3400–2700 and 1600–500 cm^{-1}) showing the photochemistry of CH_2I_2 in *p*-H_2 matrices. a) IR spectrum of a CH_2I_2/*p*-H_2 (1/1000) matrix at 3.2 K. b) Difference IR spectrum obtained after irradiating the matrix with λ = 308 nm for 3 h at 3.2 K. c) Difference IR spectrum obtained after irradiating the matrix with λ = 308 nm for 3 h more at 3.2 K. d) Difference IR spectrum obtained after irradiating the matrix with λ = 365 nm for additional 45 min at 3.2 K.

Intense signals observed at 1116.3, 1112.0, 721.0, and 583.4 cm^{-1}, and weaker ones at 3068.9, 2996.1, and 1362.7 cm^{-1} are assigned to fundamental modes of CH_2I_2. When the matrix is irradiated with 308 nm light (excimer laser) for 3 h, all signals belonging to the precursor

decrease in intensity and a new set of signals is formed. These new signals at 3040.1, 1334.3, and 613.7 cm^{-1} are assigned to CH_2I radical, and grow proportionally over the time of irradiation (45 min, 90 min, and 3 h). Upon further irradiation with 308 nm light over 3 h more, CH_4 shows up with signals at 3026.0, 3025.2, and 1308.3 cm^{-1}. The amount of CH_4 formed upon photolysis (308 nm, 6 h) is very less compared to that of the experiments performed in O_2-doped *p*-H_2 matrices (280 nm, 20 h).[113] When comparing the intensities of CH_2I (1334.3 cm^{-1}) and CH_4 (1308.3 cm^{-1}) for the experiments with and without O_2, a CH_2I/CH_4 ratio of approximately 1:1 is obtained in O_2-doped *p*-H_2 matrices; in contrast, it is 5:1 in pure *p*-H_2 matrices. That can be explained since CH_2I has a strong absorption centered at 280 nm.[114]

The CH_2I/CH_4 ratio is drastically changed after secondary photolysis with a 365 nm light-emitting diode (LED) for 45 min. All signals corresponding to CH_2I disappear and those belonging to CH_4 increase. It is noteworthy that the 365 nm irradiation was much more efficient in converting CH_2I into CH_4 than using the excimer laser for 3 h, albeit the amount of precursor photolyzed was quite low in both cases. New weak signals are also observed, which are assigned to CH_3 (3170.5, 1401.7, and 624.1 cm^{-1}), CH_3I (1248.5 cm^{-1}), as well as a couple of unidentified spectral features (2965.2 and 2837.4 cm^{-1}). In *p*-H_2 matrices, CH_2I radical is expected to be stable since its C–H bond dissociation energy (103 kcal/mol) is slightly smaller than that of H–H (104 kcal/mol).[60] This was also confirmed by the experiments in O_2-doped *p*-H_2 matrices; annealing of the matrix at 4.0 K yielded syn-ICH_2OO radical, whereas CH_4 was only obtained upon photolysis.[113] As for CH_3 radical, Momose et al. reported that its reaction with H_2 does not proceed at 5 K within a week's time. The upper limit of such tunneling rate is estimated to be 8×10^{-8} s^{-1}.[115]

Concerning the photochemical conversion of CH_2I into CH_4, several mechanisms can be considered. Excited CH_2I could be formed, which reacts via radical chain reactions involving CH_3I or CH_3. However, the most probable pathway might involve the formation of the reactive CH_2. Spin conservation requires that CH_2 be initially produced in the singlet state, when generated from singlet precursors like CH_2N_2 or CH_2CO. In case of cleaving the C–I bond in CH_2I radical (doublet state), either singlet or triplet CH_2 could be formed as excited states and could react with H_2 before relaxing to the triplet ground state. For instance, Fushitani et al. reported that irradiation of a CH_3I/*p*-H_2 matrix with 253.7 nm produces only CH_3 radical, whereas 184.9 nm light yields both CH_3 and CH_4.[112] The authors concluded that excited CH_3 decomposes to singlet CH_2, which reacts with *p*-H_2 to form CH_4.

However, the photochemical generation of CH_2 is very difficult even at cryogenic temperatures. Moore and Pimentel showed that the photolysis of ^{15}N-labeled diazomethane or diazirine in solid N_2 produces CH_2, which subsequently reacts with neighboring N_2 molecules to form diazomethane.[116] Later on, Maier and Reisenauer reported that irradiation of CH_2I_2 with 254 nm light in N_2 matrices forms CH_2N_2 as main product, along with CH_3I radical, ethylene, and acetylene. Upon switching to 313 nm light, a halogen-bonded isomer of CH_2I_2 is formed in both N_2 and Ar matrices (Scheme 6).[117]

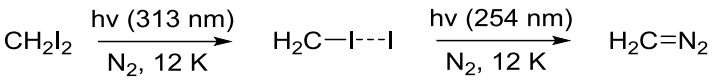

Scheme 6. Photolysis of CH_2I_2 in N_2 matrices at 12 K.

The identification of triplet CH_2 by matrix IR spectroscopy is difficult because it has only three active modes in the IR region, but only one signal is intense enough to allow detection (Table 1). The bending mode of matrix-isolated triplet CH_2 was first reported at 1114 cm^{-1} by Milligan and Pimentel,[118] and later, reassigned by Lee and Pimentel at 1115 cm^{-1} (in Ar) and 1109 cm^{-1} (in Xe).[119] Such bending mode appears at higher frequencies in matrix compared to gas phase because CH_2 rotates freely in the matrix, resulting in a rotation-vibration line.

Table 1. Experimental and calculated vibrational frequencies of methylene.

Spin State	Matrix[119]	Gas phase[120]	CCSD/aug-cc-PVQZ	Assignment
Triplet ($^3B_1$)	–	3190	3384 (0.326)	C–H str. as
	–	–	3158 (0.289)	C–H str. s
	1109–1115	963	1103 (7.726)	bend
Singlet ($^1A_1$)	–	2865	3012 (67.549)	C–H str. as
	–	2806	2942 (69.443)	C–H str. s
	–	1353	1416 (1.835)	bend

Frequencies in cm^{-1} and absolute intensities in km/mol.

A closer look at the region (1130–1100 cm^{-1}) where the bending mode of triplet CH_2 should appear is shown in Figure 8. Irradiation of the precursor CH_2I_2 with 308 nm light produces a weak signal at 1115.5 cm^{-1}, and when switching to 365 nm light, an additional signal at 1114.5 cm^{-1} is formed. Both signals match with the reported experimental IR frequency of matrix-isolated triplet CH_2. However, they overlap with the bending mode of the precursor CH_2I_2 (1116.3 cm^{-1}). As there is a large amount of precursor remaining and the photolysis is quite inefficient, these weak signals coming up and down in the difference IR spectra could

just be an artefact due to relaxation of the precursor in the matrix. Hence, there are no clear spectroscopic evidences on the formation of triplet CH_2 in the matrix.

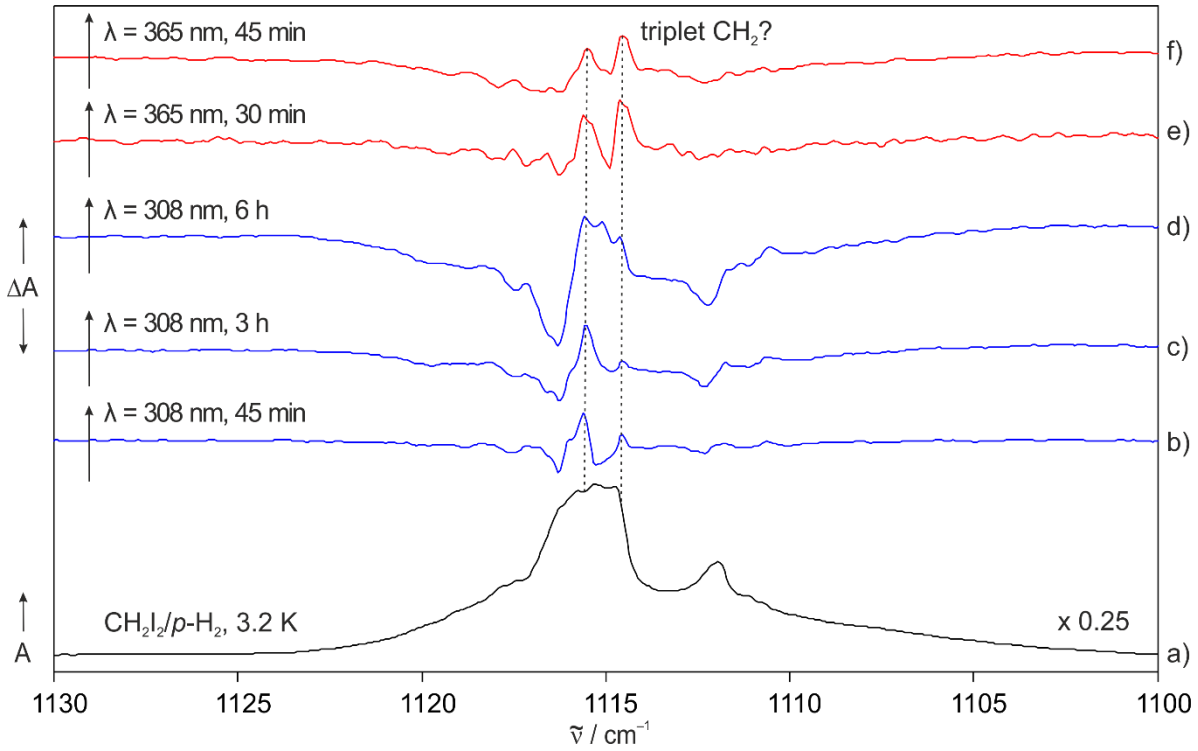

Figure 8. IR spectra showing the photochemistry of CH_2I_2 in *p*-H_2 matrices. a) IR spectrum of a CH_2I_2/*p*-H_2 (1/1000) matrix at 3.2 K. b-d) Difference IR spectra obtained after irradiating the matrix with λ = 308 nm for 45 min, 3 h, and 6 h, respectively at 3.2 K. e-f) Difference IR spectra obtained after irradiating further the matrix with λ = 365 nm for 30 and 45 min, respectively at 3.2 K.

Calculations

The mechanisms of the addition of H_2 to singlet and triplet CH_2 were early studied by Schaefer et al. and are described in the following:[121-123]

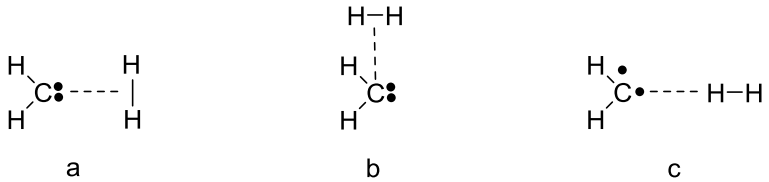

The least-motion insertion (a) of singlet CH_2 into H_2 to yield CH_4 is forbidden under thermal conditions, as explained by the Woodward–Hoffmann selection rules.[124] As a result, a large barrier of 27 kcal was predicted corresponding to the constrained TS.[122] However, if the occupied σ orbital of H_2 interacts with the unoccupied π orbital of singlet CH_2 (b), then the reaction involves two electrons and becomes allowed. This non-least-motion pathway

maintaining Cs symmetry has no orbital symmetry restrictions, and it was reported to have no barrier at all.[123] The absence of barrier for the insertion of singlet CH_2 into H_2 and F_2 is confirmed by more accurate ab-initio calculations.[125]

Triplet CH_2 is expected to react with H_2 through a two-step abstraction-recombination mechanism, with H-abstraction as the rate-determining step. Such reaction step is predicted to have a TS structure as depicted in (c), and with a considerable barrier height. Reaction model (c) has been used as prototype for the reaction of triplet CH_2 with CH_4, which was predicted to have an analogous TS and a barrier height of 20 kcal/mol.[90]

After the report that claimed no reaction of triplet CH_2 with H_2 to occur at 298 K in the gas phase,[105] several groups tried to explain the lack of reaction. Early studies by Carr et al. were able to rationalize the nonreactivity of CH_2 by predicting a quite high barrier, 19.7 kcal/mol, using the bond energy bond order (BEBO) method.[126] Later on, Schaefer et al. reported a slightly smaller value of 15.5 kcal/mol as well as the enthalpy of reaction (–5.4 kcal/mol), the latter in good agreement with an experimental value of –5.7 kcal/mol.[121] Recently, Matsui et al. estimated a barrier of 10.1 kcal/mol and an enthalpy of –5.6 kcal/mol at the G2M(RCC2) level of theory.[109] Overall, the rather large differences found for the computed energy barrier of this reaction, do not allow to draw a conclusion.

Therefore, the performance of different methods in predicting the energy difference between singlet and triplet CH_2 is initially assessed. In addition, the reaction barrier for the hydrogenation reaction of triplet CH_2 is explored at the same levels of theory and the results are shown in Table 2. It is reasonable to expect that being able to match the experimental singlet-triplet energy gap, would be a good indication before turning attention to activation energies. Several high accurate ab-initio approaches have been selected such as couple-cluster (CC), quadratic configuration interaction (QCI), and multi-reference configuration interaction (MRCI) methods in combination with a quadruple-zeta basis set as well as the complete basis set (CBS) method. Moreover, density functional theory (DFT) calculations that are commonly used when computing bigger molecules like arylcarbenes are therefore also included as for comparison.

Table 2. Calculated singlet-triplet energy gap of methylene and activation energy for the reaction between triplet CH_2 and H_2.

Method	ΔE_{ST}	ΔE_{ST} + ZPE[a]	E_a	E_a + ZPE[a]
B3LYP-D3/def2-TZVP	11.75	11.37	3.67	4.63
CCSD(T)/aug-cc-PVQZ	9.28	8.85	8.37	9.00
QCISD(T)/aug-cc-PVQZ	9.32	8.91	8.21	8.83
MRCI/aug-cc-PVQZ	8.91	8.48	9.16	7.91
CBS-APNO (0 K)	–	8.97	–	7.83
Experimental[9]	9.05 ± 0.06		–	

[a]Including zero-point energy (ZPE) correction. Energies are given in kcal/mol.

All the ab-initio approaches used for this benchmarking predict the ΔE_{ST} to be close to the experimental value (9.05 kcal/mol).[9] In contrast, the B3LYP calculation gives a rather high value, and this trend has also been observed for arylcarbenes.[127,128] Such underestimation (~2 kcal/mol) of the stability of the singlet species relative to the triplet can be explained since density functionals do not include a Coulomb correlation term, nor do they treat nondynamic electron correlation accurately. The activation energy of the reaction is predicted by the ab-initio calculations to be around 8–9 kcal/mol. This value is almost half of what was reported in the pioneering work by Schaefer et al. (15.5 kcal/mol).[121] Similar to the discrepancies found in estimating the S–T gap, the B3LYP calculation gives an activation energy of 4.6 kcal/mol that is much lower than the values estimated by correlated methods. Likewise, the concerted insertion of singlet CH_2 into H_2 or F_2 is not properly described by DFT methods.[125] For instance, they predict small reaction barriers involving transition states with low imaginary frequencies, however, these TS disappear employing higher levels of theory. This underlines the importance of using correlated methods for a proper modelling of carbenes and their chemical reactions.[129]

Overall, singlet CH_2 is several orders of magnitude more reactive toward H_2 than triplet CH_2 at room temperature. In the singlet case, hydrogenation reaction tends to occur via direct insertion with zero or negative activation energies, in contrast to reactions of the triplet ground state, which generally have significant and positive activation energies. Matrix experiments did not provide sufficient elements for detecting the "less reactive" triplet CH_2 in the matrix. Most likely, any CH_2 formed reacted as hot singlet state before relaxing to the triplet ground state. In addition, triplet CH_2 could abstract H atoms by tunneling at low temperatures. Given that CH_2 is surrounded by many molecules of H_2, the H atoms would not need to travel long distances

to form the new C–H bond. Consequently, a thin barrier is expected for the H-atom transfer, which would result in fast rates of tunneling even from the lowest vibrational level.[130] This carbene may be subjected to further investigations in D_2 matrices and potentially by using EPR spectroscopy. Deuterium matrices should slow down the tunneling process and even if a very small amount of triplet CH_2 is trapped in the matrix, it can be easily detected and monitored over time in case of decaying.

Fluorenylidene

Hydrogen Matrices

The spectrum of 9-diazofluorene **40** in solid H_2 at 3 K is shown in Figure 9. Irradiation of **40** with UV light (λ = 365 nm) at 3 K results in a complete depletion of the IR signals assigned to **40** and formation of a new set of signals. Observed new signals at 1483, 1456, 744, 695, and 622 cm^{-1} are in agreement with the IR spectrum of matrix-isolated fluorene **41** in Ar at 3 K. The most intense feature (744 cm^{-1}) is slightly red-shifted in Ar matrices (741 cm^{-1}).

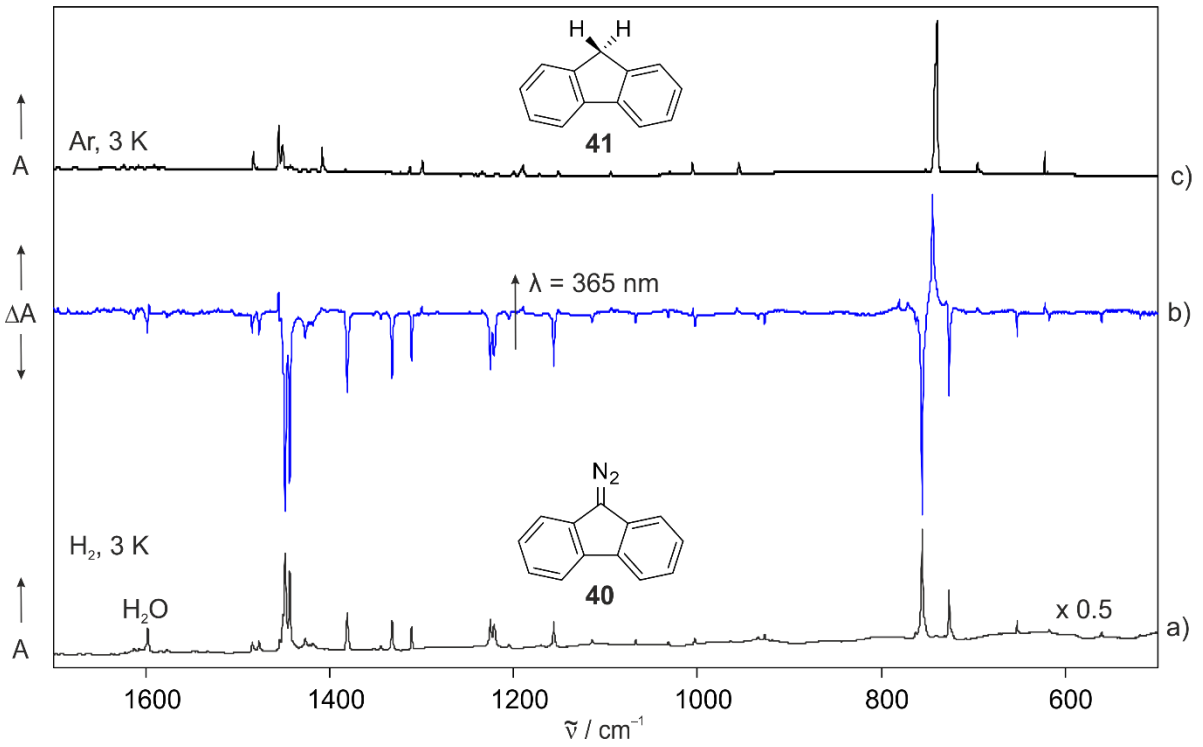

Figure 9. IR spectra showing the photochemistry of 9-diazofluorene **40** in H_2 matrices. a) IR spectrum of **40** in H_2 at 3 K. b) Difference IR spectrum obtained after irradiating **40** with λ = 365 nm in H_2 at 3 K. c) IR spectrum of fluorene **41** in Ar at 3 K.

A spectrum of triplet fluorenylidene **5** in solid Ar is shown in Figure 10; signals at 1408, 1208, 753, 713, and 564 cm^{-1} are assigned to **5**. Such reference spectrum is obtained after photolysis of **40** with $\lambda = 365$ nm in Ar matrices and agrees with the one reported in N_2 matrices by Dunkin et al.[131] On comparison of the spectrum of **5** with the spectrum corresponding to the photolysis of the precursor in H_2 matrices, there are no signals ascribable to **5**. Carbene **5** is not formed throughout the photolysis, indicating that its reaction with H_2 is very fast even at temperatures as low as 3 K. Instead, H_2-insertion product **41** is detected even after irradiating precursor **40** for a few minutes and continues to form until **40** is completely consumed.

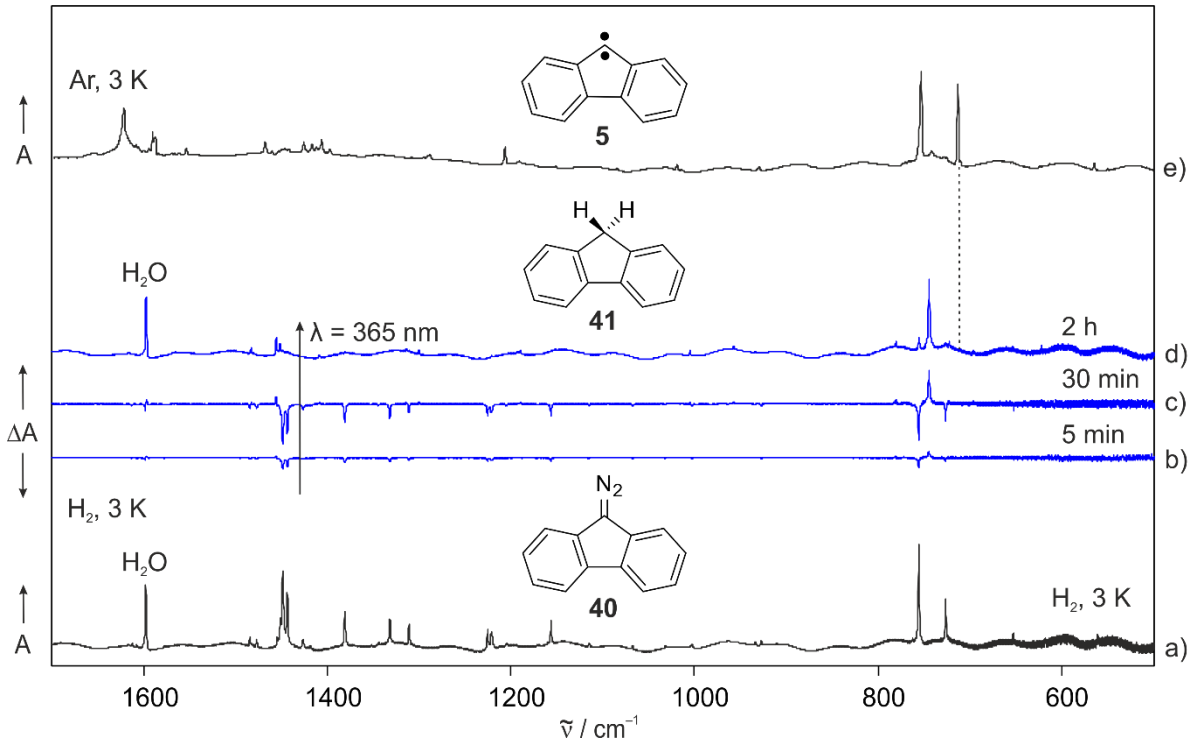

Figure 10. IR spectra showing the photochemistry of 9-diazofluorene **40** in H_2 matrices. a) IR spectrum of **40** in H_2 at 3 K. b-c) Difference IR spectra obtained after irradiating **40** with $\lambda = 365$ nm for 5 and 30 min, respectively in H_2 at 3 K. d) IR spectrum obtained after irradiating **40** with $\lambda = 365$ nm for 2 h in H_2 at 3 K. e) IR spectrum of fluorenylidene **5** in Ar at 3 K, obtained after irradiating **40** with $\lambda = 365$ nm. The dashed line indicates the signal position of carbene **5**; no corresponding signal was observed in (b-d).

An additional experiment was performed by depositing precursor **40** together with an excess of 5% H_2-doped Ar at 3 K. Photolysis with $\lambda = 365$ nm results in a clean transformation of precursor **40** into carbene **5**. Subsequent annealing at 30 K allows H_2 to diffuse in the matrix, and insertion product **41** is quickly formed. The thermal reaction of **5** and H_2 reaches an 80% yield after just 5 min of annealing. Experiments in pure H_2 and H_2-doped Ar matrices show that the reaction proceeds quantitatively even at such low temperatures and suggest that it is probably diffusion-controlled (see appendix, Figure A1).

Deuterium Matrices

Photolysis of **40** was also carried out in D_2 matrices as shown in Figure 11. In analogy to the experiments performed in pure H_2 matrices, the IR signals assigned to **40** in solid D_2 diminish completely upon irradiation at 3 K and a set of new signals at 1454, 1409, 1208, 755, 742, 713, 669, and 622 cm^{-1} is formed. After maintaining the matrix in darkness for 24 h, the intensity of the signals at 1454, 742, 669, and 622 cm^{-1} increases, whereas that of the signals at 1409, 1208, 755, and 713 cm^{-1} decreases. The positive signals (indicating formation) are assigned to 9,9-dideuterofluorene d_2-**41** and the downward signals (indicating decay) are assigned to carbene **5**. The hydrogen- and deuterium-substituted products of **41** generated in H_2 and D_2 matrices show the most intense signals at 744 and 742 cm^{-1}, respectively, which are assigned to out-of-plane (oop) ring deformation modes. The small isotopic shift of 2 cm^{-1} was also found in solid Ar matrices (741 and 739 cm^{-1}).

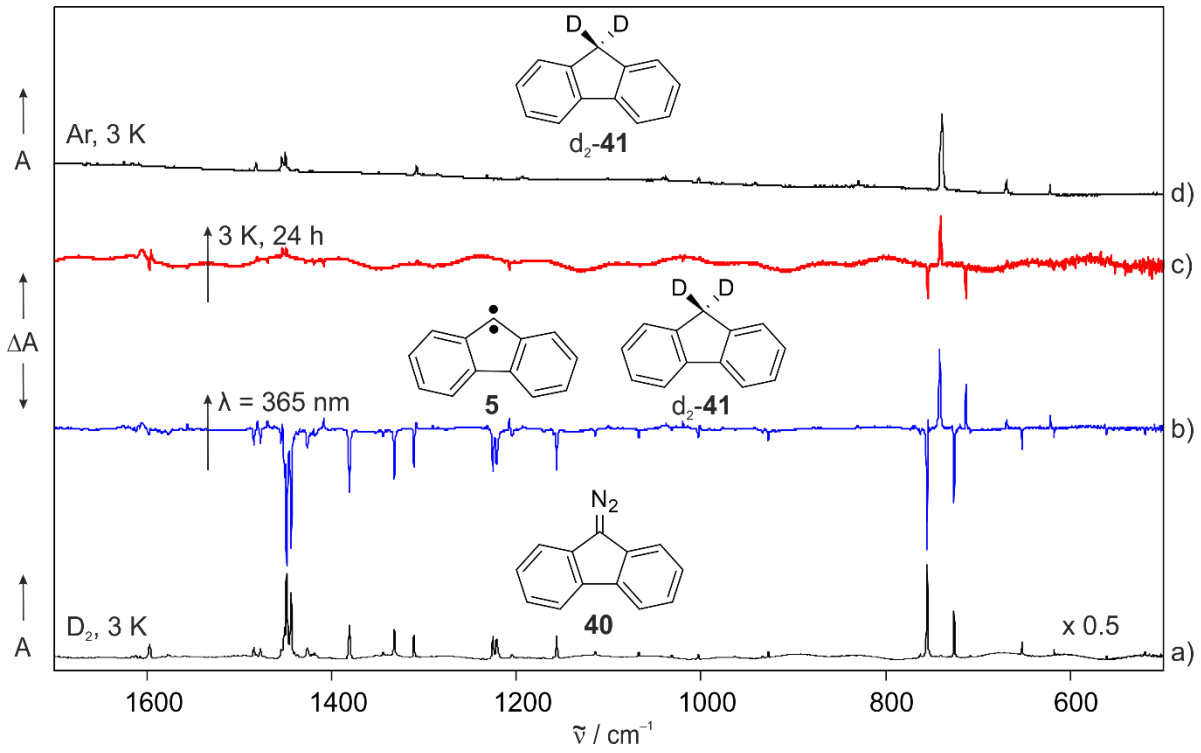

Figure 11. IR spectra showing the photochemistry of 9-diazofluorene **40** in D_2 matrices. a) IR spectrum of **40** in D_2 at 3 K. b) Difference IR spectrum obtained after irradiating **40** with λ = 365 nm for 1 h in D_2 at 3 K. c) Difference IR spectrum obtained after keeping the matrix at 3 K in darkness for 24 h. c) IR spectrum of 9,9-dideuterofluorene d_2-**41** in Ar at 3 K.

After keeping the matrix in darkness for 24 h at 3 K, the remaining carbene **5** is transformed to the corresponding product d_2-**41**. The conversion reaches a 70–80% in 24 h with a half-life time of approximately 5–6 hours. Irradiation with 365 nm for 2 h of precursor **40** in H_2 and D_2

matrices is necessary to photolyze the precursor completely, however, after irradiation of **40** in D_2 matrices for 1 h, 75% of the precursor is converted. If photolyzing for longer times, formation of carbene slows down and more product d_2-**41** is formed, as shown in Figure 12. Therefore, irradiation time was set to 1 h in order to have the maximal concentration of carbene when starting the kinetic measurements.

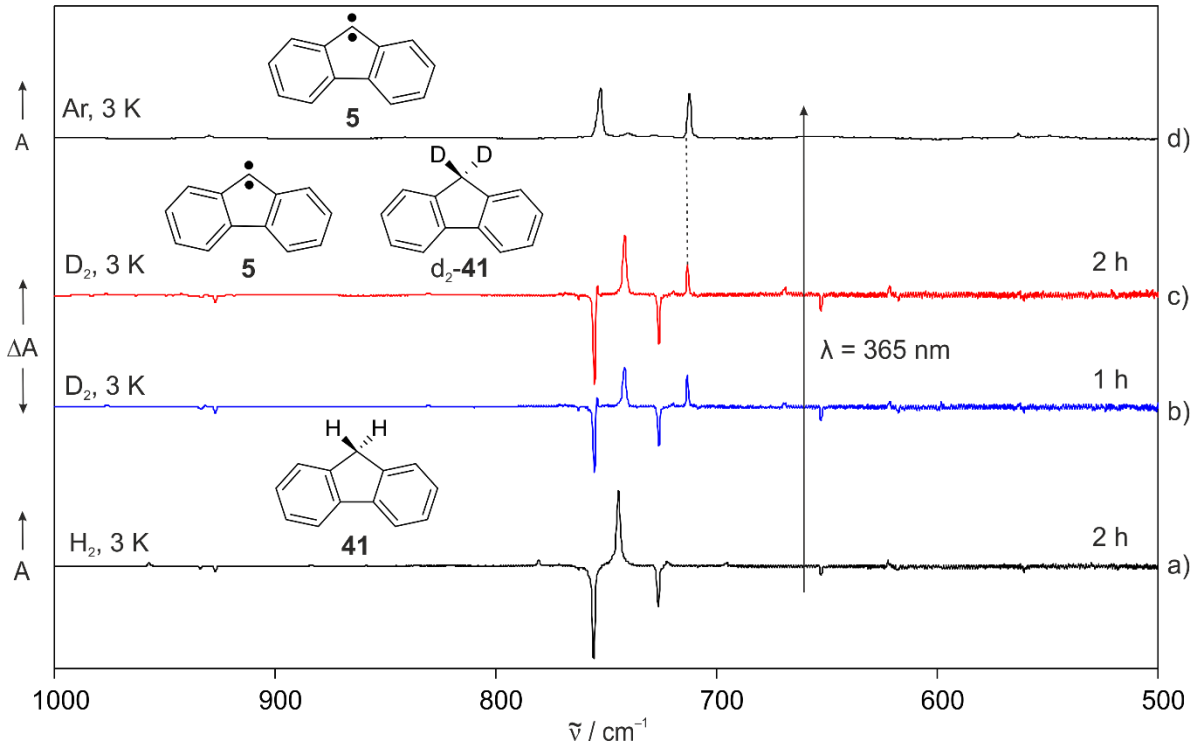

Figure 12. IR spectra showing the photochemistry of 9-diazofluorene **40** in H_2 and D_2 matrices. a) Difference IR spectrum obtained after irradiating **40** with λ = 365 nm for 2 h in H_2 at 3 K. b-c) Difference IR spectra obtained after irradiating **40** with λ = 365 nm for 1 and 2 h, respectively in D_2 at 3 K. d) IR spectrum of fluorenylidene **5** in Ar at 3 K, obtained after irradiating **40** with λ = 365 nm. The dash line shows the selective formation of carbene **5** in D_2.

The kinetics of the reaction of carbene **5** in D_2 matrices was followed by observing the decay of the intensity of its characteristic IR signal at 713 cm^{-1}, and the rise of that of product d_2-**41** at 742 cm^{-1}. The other intense signal of carbene **5** at 755 cm^{-1} was not used due to its severe overlap with precursor **40**. Integrated intensities of these two signals were measured in intervals of 15 min after irradiation and for a total time of 24 h (Figure 13). A careful inspection of the spectral signals of **5** and d_2-**41** revealed that both signals are red-shifted by 0.5 cm^{-1} at later reaction periods, likely indicating a change of matrix environments. Indeed, the low-temperature decay of triplet carbenes in solid media is frequently described by nonexponential funtions.[132] Instead of having a single rate constant, as expected for unimolecular reactions (with a large excess of host), interactions between substrate and the matrix environment result

in a distribution of rate constants. The kinetic data have therefore been fitted to a pseudo-first order by using the equation of Wildman and Siebrand.[133] This model assumes a distribution of reaction rates by introducing a dispersion coefficient β as shown in Eq. (8).

$$I = I_0\, e^{-(kt)^{\beta}} + C \quad with\ 0 < \beta < 1 \tag{8}$$

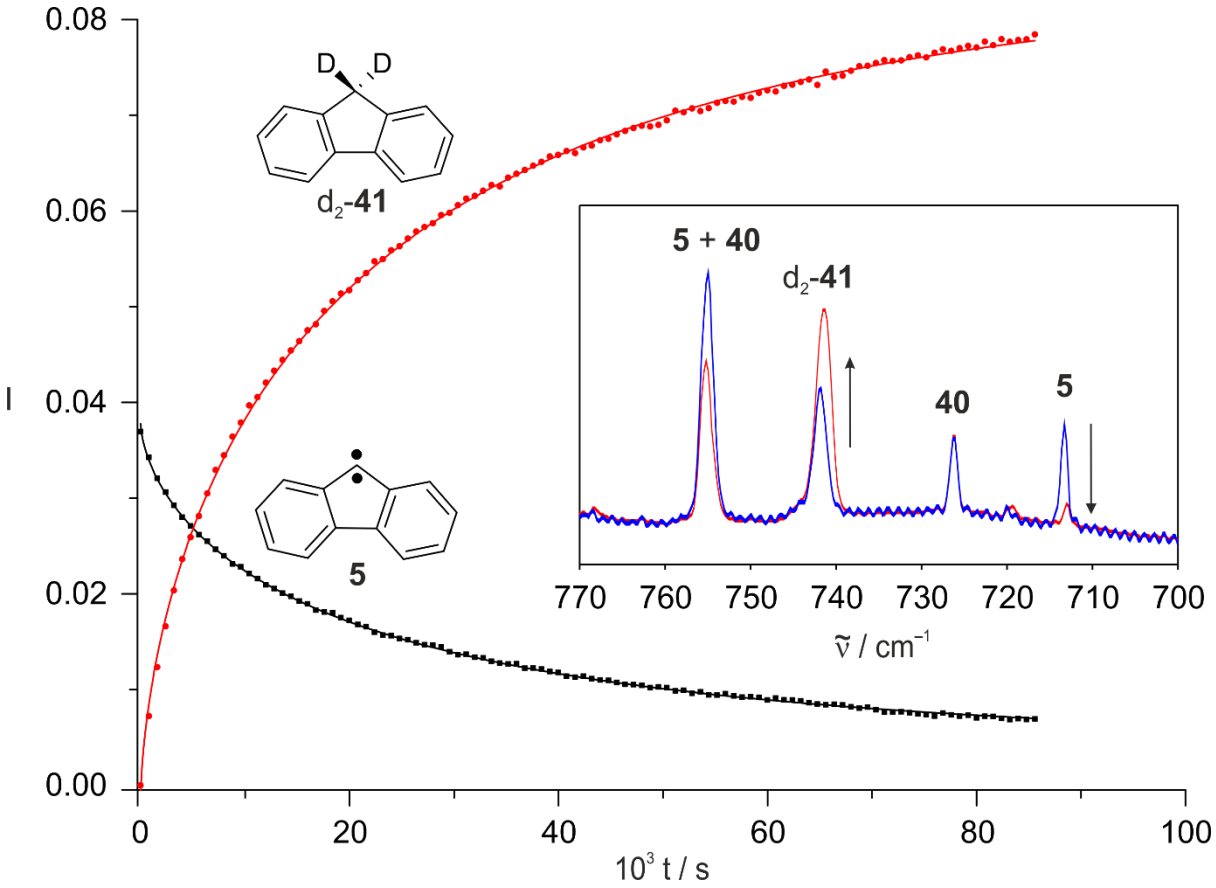

Figure 13. Plot of the increasing intensity of the IR signal at 742 cm^{-1} and the decreasing intensity of the IR signal at 713 cm^{-1} as fitted to Eq. (8) and recorded in D_2 matrices at 3 K. Integrated intensities of the signal at 742 cm^{-1} were subtracted by the initial value. Inset shows the spectroscopic features used for the kinetics.

Reaction rates are determined to be 2–5 × 10^{-5} s^{-1} in solid D_2 under different experimental conditions. It is found that the irradiation time, which has an influence on the initial reactant/product ratio, does not affect the reaction rate. Likewise, using IR cut-off filters that block light above 4000 cm^{-1} (LP2400) or 1000 cm^{-1} (LP9800) does not result in any discernible effect on the rate constants. Furthermore, rate constants in the same order of magnitude are obtained at different temperatures from 3 to 6 K, the latter value being an upper limit for annealing due to evaporation of the D_2 matrix (Table 3).

Table 3. Rate constants (as fitted to Eq. (8) with β = 0.75) for the insertion of fluorenylidene **5** into H_2 and D_2 under different experimental conditions.

Host	Temp	Cut-off filter	k ($\times 10^{-5}$ s^{-1})
H_2	3 K	–	–
H_2	3 K	> 4000 cm^{-1}	–
D_2	3 K	–	1.6 ± 0.1
D_2	3 K	> 4000 cm^{-1}	1.8 ± 0.1
D_2	5 K	> 4000 cm^{-1}	2.1 ± 0.1
D_2	6 K	> 4000 cm^{-1}	4.0 ± 0.2
D_2	6 K	> 1000 cm^{-1}	4.5 ± 0.1

The reaction rate increases by a factor of less than three on increasing the absolute temperature from 3 to 6 K. If proceeding as a classical thermal reaction, the Arrhenius model would predict a huge increase in the rates of about e^{100} for 3→6 K, even assuming a likely underestimated E_a of just 1 kcal/mol. Experimental data therefore supports a tunneling mechanism. The small increase in the rates might be caused by slight temperature-dependent changes in the matrix. For H_2, the reaction was too fast to be measured in the experimental setup, and hence it was not possible to determine the KIE for this reaction. Nevertheless, considering that the reaction of the carbene with H_2 occurs at a sub-minute scale, while in D_2 it takes several hours, a rough estimate suggests a lower limit for the KIE of 10^3. Overall, carbene **5** shows a reactivity similar to that of oxocyclohexadienylidene **27** in H_2/D_2 matrices. Indeed, carbene **27** readily inserts into H_2 upon formation, and reacts to D_2 with rates of 3–7 × 10^{-5} s^{-1} at 3–6 K to form the corresponding D_2-insertion product.[99]

Since carbene **5** has a triplet ground state, it can also be characterized by EPR spectroscopy, offering valuable information about the reaction mechanism (Figure 14). Precursor **40** was co-deposited along with an excess of D_2 on the tip of a copper rod at 5 K (lowest temperature achievable), allowing to trap D_2, but not the more volatile H_2. Photolysis of the matrix with 365 nm produces high yields of the triplet signals of **5**, which are consistent with literature data.[134,135] Similar to the IR experiments, the decay of **5** in D_2 matrices at 5 K was monitored for 24 h. A 71% of loss was determined for the signals at the z_1 and x_1 canonical transitions, agreeing with the 73% observed at 5 K by IR spectroscopy. At the same time, an increase of the signals corresponding to D atoms (3340, 3418, 3496 G; hyperfine coupling 78 G) was observed as well as a small amount of H atoms (3147, 3654 G; hyperfine coupling 507 G).[136]

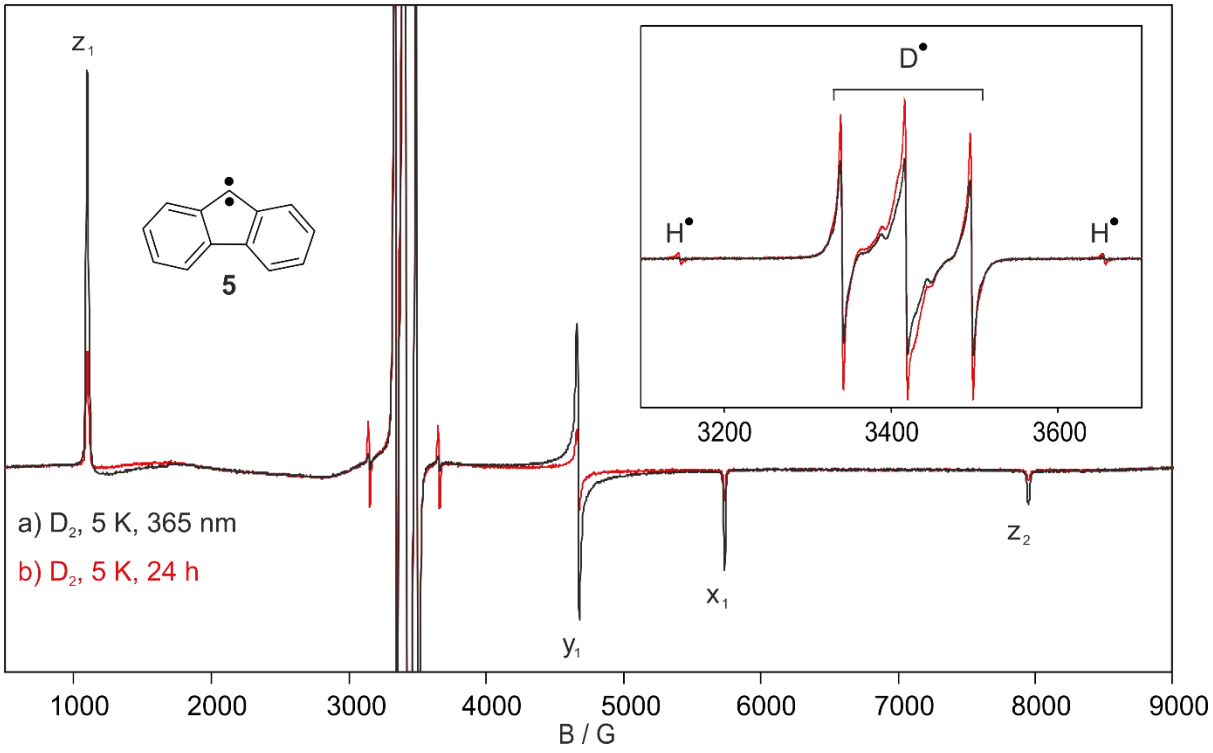

Figure 14. EPR spectra showing the decay of triplet fluorenylidene **5** in D_2 matrices. a) EPR spectrum obtained after irradiating 9-diazofluorene **40** with λ = 365 nm for 30 min in D_2 at 5 K. b) EPR spectrum obtained after keeping the matrix at 5 K in darkness for 24 h. Inset shows the radical region of the spectra where H and D atoms appear.

The formation of D atoms concomitant with the disappearance of **5** indicates that the D atoms are formed in the reaction of carbene **5** with D_2. The formation of D atoms is therefore consistent with an abstraction-recombination mechanism, as expected for triplet carbenes (Scheme 7).[98]

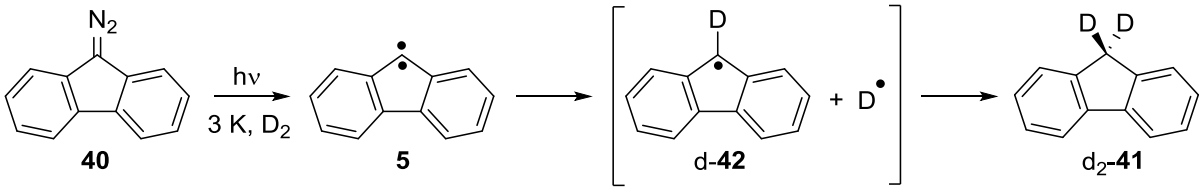

Scheme 7. Generation of fluorenylidene **5** and reaction with D_2 to form insertion product d_2-**41** through an abstraction-recombination mechanism.

The formation of the weak signals assigned to H atoms might be a consequence of impurities of H_2 in the D_2 matrix. Unfortunately, 9-deuterofluorenyl radical d-**42** cannot be identified, perhaps due to overlapping with the signals of D atoms. Barrierless recombination of the radical pair to give EPR-silent d_2-**41** is expected to be the major reaction pathway, so only the radicals that can escape the matrix cage of the initially formed radical pair would be detectable. In

agreement with this, IR spectroscopic experiments do not provide any evidence of the presence of radicals **42** and d-**42** in H_2 and D_2 matrices, respectively.

Calculations

The hydrogenation reaction of fluorenylidene **5** has also been studied computationally in order to support and interpret the experimental data. Carbene **5** has a triplet ground state, which lies below the closed-shell singlet state by only 1.1 kcal/mol, as determined in acetonitrile.[137] The high-level CBS-QB3 method also predicts an small S–T gap (1.91 kcal/mol) in the gas phase.[138] Therefore, both singlet and triplet potential energy surfaces (PES) have been explored and all relevant stationary points are subsequently reported (Figure 15).

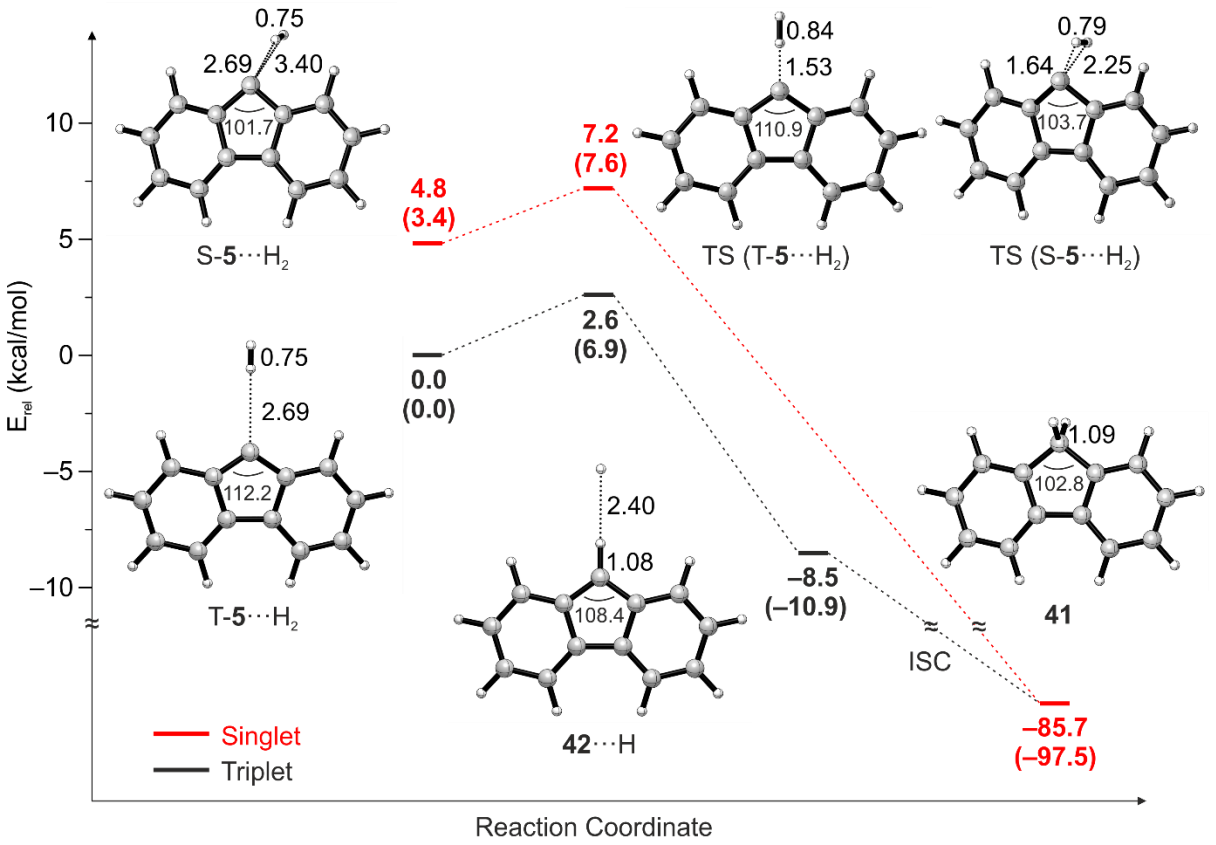

Figure 15. Hydrogenation of fluorenylidene **5** on the singlet (red) and triplet (black) PES calculated at the ZPE-corrected B3LYP-D3/def2-TZVP level of theory. Values in parentheses correspond to CCSD(T)/cc-PVDZ //B3LYP-D3/def2-TZVP energies. Energies are given in kcal/mol and selected bond lengths and angles are given in Å and °, respectively.

The hydrogen complex T-**5**···H_2 is energetically slightly below the non-interacting molecules with a quite large C···H distance of 2.69 Å. Such binding energy depends on the chosen method; a positive value of 0.2 kcal/mol was calculated at the B3LYP-D3/def2-TZVP level of theory, which turns into –0.2 kcal/mol if the energies are refined with CCSD(T)/cc-PVDZ. This shows

the formation of a weakly bounded van-der-Waals complex, although it could well be an artefact of the calculation. Similar cases were found for the singlet complex S-**5**···H_2 as well as for the radical pair **42**···H.

At the UB3LYP-D3/def2-TZVP level of theory, the triplet barrier for the H-abstraction by **5** is predicted to be 2.6 kcal/mol, although a higher value of 6.9 kcal/mol was found with CCSD(T)/cc-PVDZ. The first step of the triplet reaction is the exothermic formation of a radical pair **42**···H. The triplet radical pair undergoes ISC to the singlet surface and recombines to form **41** in a highly exothermic reaction. The barrier is much higher than the energy available at 3 K (kT = 0.006 kcal/mol), so a thermal reaction is prohibited at these low temperatures. This finding strongly supports the assumption that tunneling is involved in the D_2-insertion reaction of carbene **5** at low temperatures. In case of the insertion into H_2 where **41** is exclusively formed after irradiation, the role of photochemistry for driving the reaction cannot be ruled out. In principle, the very large KIE observed for the insertion of carbene **5** into D_2 can be explained for a conventional thermal reaction. The zero-point vibrational energy changes the activation barrier only very slightly for the isotopomers (E_a (H_2) = 2.61 kcal/mol, E_a (D_2) = 2.68 kcal/mol). A KIE of about e^{10} can be estimated at 3 K by applying the Arrhenius model (although such 0.07 kcal/mol energy difference is much lower than the accuracy of DFT methods). Such simple theoretical prediction, could explain the lower limit for the KIE in the order of 10^3 that was suggested based on the kinetic data.

Alternatively, the reaction proceeding through a singlet PES can also be formulated because of the small S–T gap of **5**. According to DFT calculations, the activation barriers corresponding to the reactions in the singlet and triplet state surfaces are quite similar (E_a (S-**5**···H_2) = 2.4 kcal/mol, E_a (T-**5**···H_2) = 2.6 kcal/mol), which means that the thermal reaction at low temperatures should follow an adiabatic pathway, without crossing between the surfaces (although CCSD(T) calculations predict a smaller S–T gap). Overall, these calculations suggest that the thermal hydrogenation of **5** at low temperatures should proceed along the triplet surface and through an abstraction-recombination mechanism. This agrees with the EPR experiments showing the formation of D atoms concomitant with the disappearance of **5** in darkness at 5 K. Concerning the experiments in H_2 matrices, it can be argued that photolysis could excite carbene **5** to the close-lying singlet state, from where the reaction proceeds faster than decaying to the triplet ground state. However, this would be an extremely rare example of an isotope-selective photochemistry.

The role of tunneling in the H-abstraction by triplet fluorenylidene **5** was previously investigated in low-temperature organic glasses.[87,89] In methylcyclohexane/toluene glasses, an Arrhenius plot of ln k versus 1/T was found to be linear over the range of 100–122 K, with E_a = 5.5 kcal/mol and log A = 15.8 s^{-1}. However, below 100 K, the decay of carbene **5** was less dependent on temperature, giving for example, E_a = 1.2 kcal/mol and log A = 6.2 s^{-1} at 90–100 K. It was therefore proposed that the H-transfer proceeds via classically at higher temperatures, and through QMT at lower temperatures.

In conclusion, fluorenylidene **5** is a reactive triplet carbene that is hydrogenated in solid H_2 and D_2 at temperatures as low as 3 K. The reaction proceeds via H-abstraction by the triplet carbene like other carbenes studied at low temperatures.[65,98] The reaction of **5** in D_2 matrices shows a very large kinetic isotope effect, temperature-independence between 3–6 K, and proceeds despite having an activation barrier that is prohibitively high for a reaction to occur thermally at those low temperatures. The experiments therefore provide clear evidence for both hydrogen tunneling and the rare deuterium tunneling (Scheme 8).

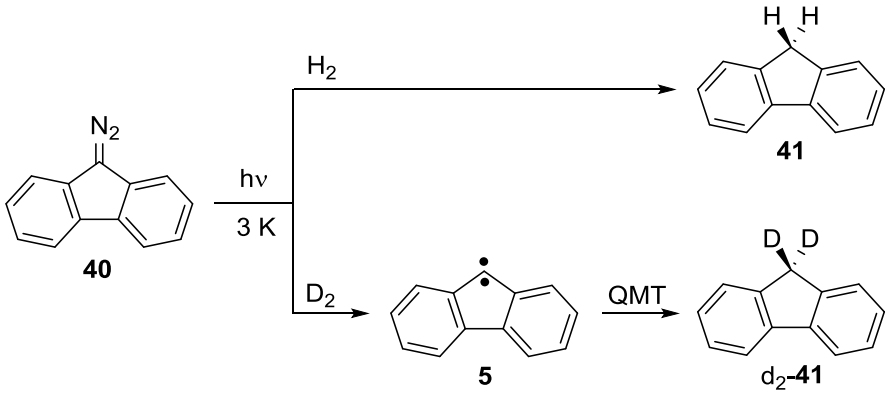

Scheme 8. Reactivity of fluorenylidene **5** in H_2 and D_2 matrices.

Diphenylcarbene

The hydrogenation of diphenylcarbene **4** was investigated in two different types of matrices: i) solid hydrogen matrices and ii) inert gas matrices doped with hydrogen. In both types of matrices, H_2 and D_2 were used to investigate isotope effects on the hydrogenation of **4**. In case of the mixtures of inert gases with H_2 or D_2, Ar or Ne were used as hosts. Due to the high volatility of H_2, temperatures below 4 K are necessary to keep solid H_2 from subliming, whereas the heavier isotope D_2 is stable up to 6 K under the experimental conditions of the matrix isolation technique. In solid Ar, H_2 can be trapped at much higher temperatures and

hydrogenation reactions can be studied up to 35 K. This sequence of experiments has already been used in studying the hydrogenation of triplet 4-oxocyclohexa-2,5-dienylidene **27** (Scheme 9).[98,99]

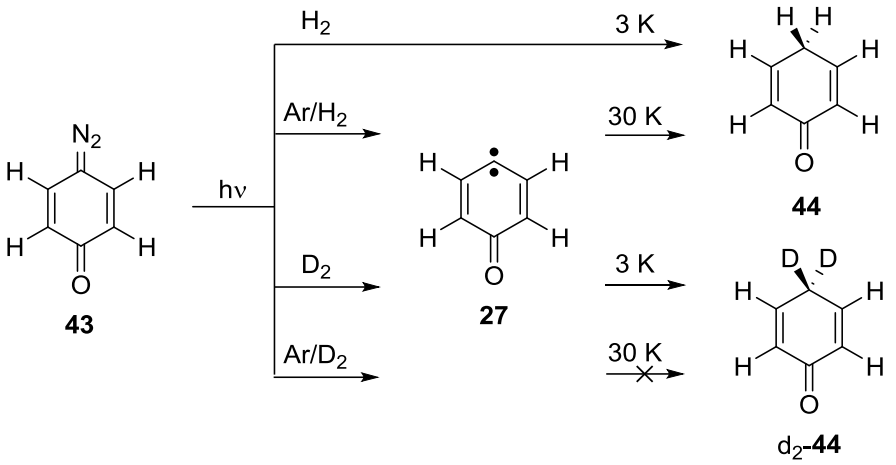

Scheme 9. Reactivity of 4-oxocyclohexa-2,5-dienylidene **27** with hydrogen and deuterium in solid H_2 and D_2 as well as in doped Ar matrices.

It is also desirable to study such reactions at intermediates temperatures. However, diffusion of H_2 in solid Ar is slow below 20 K, and thus bimolecular reactions are efficiently suppressed. In contrast, H_2-doped Ne matrices can be effectively annealed up to 8 K and offer an additional set of conditions for studying the influence of temperature and matrix host on hydrogenation reactions.

Hydrogen and Deuterium Matrices

The spectrum of diphenyldiazomethane **45** in solid H_2 at 3 K in the region of 500−1000 cm^{-1} is shown in Figure 16. Irradiation of **45** in H_2 matrices at 3 K with visible light (λ = 560 nm) results in a complete decrease of the IR signals assigned to **45** (758, 694, 651 cm^{-1}), accompanied by formation of a new set of signals, fundamentally two very intense at 674 and 744 cm^{-1}. The spectroscopic features observed after the photolysis are assigned to matrix-isolated diphenylcarbene **4**, and are in excellent agreement with the literature.[139] Under the same experimental conditions, photolysis of **45** in either H_2 or Ar matrices at 3 K, produces basically the same spectrum. Since H_2 is a more compact host, signals have a smaller bandwidth and look sharper than in Ar matrices. Indeed, a broad signal that appears at 674 cm^{-1} in Ar is splitted into two signals at 676.3 and 673.7 cm^{-1} in H_2. Contrary to fluorenylidene **5**, no matrix-

shifts are found for the positions of the out-of-plane deformations modes (674 and 744 cm^{-1}). The experiment was also repeated using D_2 as host and the same photoproduct was obtained.

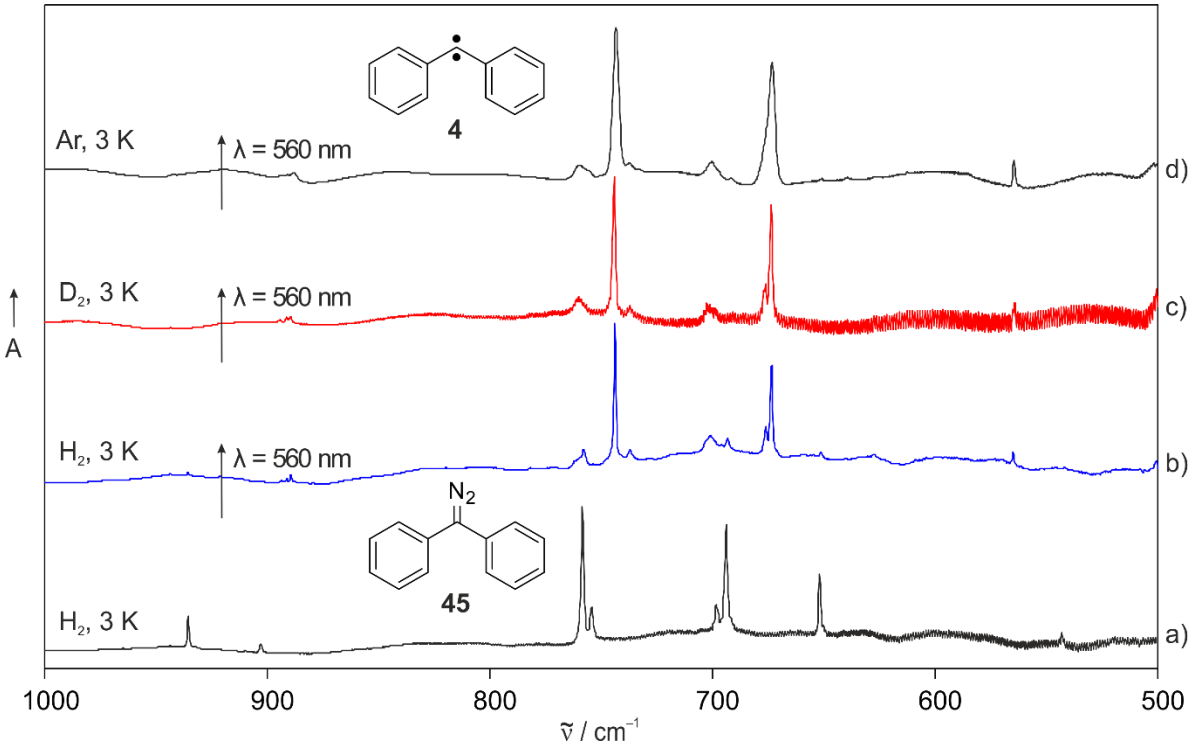

Figure 16. IR spectra showing the formation of diphenylcarbene **4** in H_2, D_2, and Ar matrices. a) IR spectrum of diphenyldiazomethane **45** in H_2 at 3 K. b) IR spectrum obtained after irradiating **45** with λ = 560 nm in H_2 at 3 K. c) IR spectrum obtained after irradiating **45** with λ = 560 nm in D_2 at 3 K. d) IR spectrum obtained after irradiating **45** with λ = 560 nm in Ar at 3 K.

Overall, photolysis of **45** in H_2, D_2 and Ar matrices at 3 K produces only carbene **4**, with hydrogen behaving like an inert gas under such conditions. However, perhaps the relatively mild visible irradiation used for generating the carbene and the low temperatures required to keep the H_2 matrix from evaporating do not provide enough energy to enhance a reaction with H_2. Two different strategies were therefore considered on trying to activate H–H. First, by carefully annealing the matrix at temperatures close to the evaporation point (4.8 K as measured on the cooper holder supporting the CsI window). The limit temperature is much lower than the standard boiling point of H_2 (20 K at 1 bar), as well as the triple point (14 K at 70 mbar), because of the high vacuum of around 10^{-6} mbar. The annealing procedure (3→4.5 K) should not increase the available thermal energy on the system too much, but will rather soften the host even more, allowing H_2 molecules to reorganize and perhaps find a better orientation toward the carbene center. Another idea would be trying to excite the carbene to a reactive high-energy state by irradiating the matrix at lower wavelengths.

Matrix isolated **4** was found to be stable in H_2 and D_2 matrices upon prolonged annealing at 4.5 K (H_2) and 6 K (D_2) and does not undergo any thermal reaction in any of those hosts. Upon 450 nm irradiation, it completely converts into tetraphenylethylene **46**. Observed new signals at 1483, 1033, 761, 701, 627, and 570 cm^{-1} are in agreement with the IR spectrum of matrix-isolated **46** in Ar at 3 K (Figure 17).

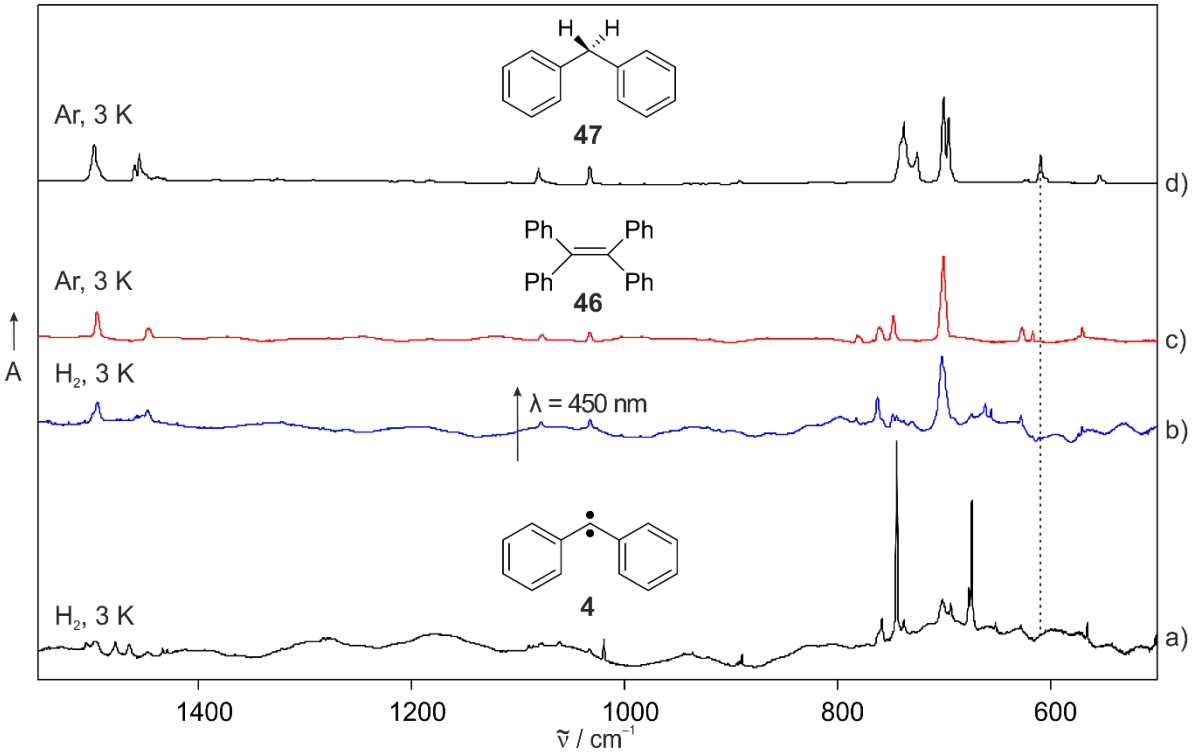

Figure 17. IR spectra showing the photochemistry of diphenylcarbene **4** in H_2 matrices. a) IR spectrum of **4** in H_2 at 3 K, obtained after irradiating **45** with λ = 560 nm. b) IR spectrum obtained after irradiating **4** with λ = 450 nm in H_2 at 3 K. c) IR spectrum of tetraphenylethylene **46** in Ar at 3 K. d) IR spectrum of diphenylmethane **47** in Ar at 3 K. The dashed line indicates the signal position of insertion product **47**; no corresponding signal was observed in (b).

Most of the signals of dimer **46** appear to be broad since torsion of the four rings can generate multiple conformers, which can be trapped in the matrix at low temperatures. Dimer **46** is formed when exposed to intense light or lower wavelengths are used (λ < 560 nm). However, carbene **4** remained unreactive toward H_2 upon both thermal and photochemical excitation. Even though most of the signals assigned to the H_2-insertion product **47** are expected to overlap with those of precursor **45** (due to a similar carbon skeleton), the characteristic signal at 609 cm^{-1} is clearly not present throughout the experiment.

The photochemistry of carbene **4** was also investigated in D_2 matrices in order to detect possible isotopic effects, as well as confirm its inertness toward H_2/D_2 at low temperatures. As

before, carbene **4** is stable in D_2 at 3 K and completely converts into tetraphenylethylene **46** upon photolysis (Figure 18).

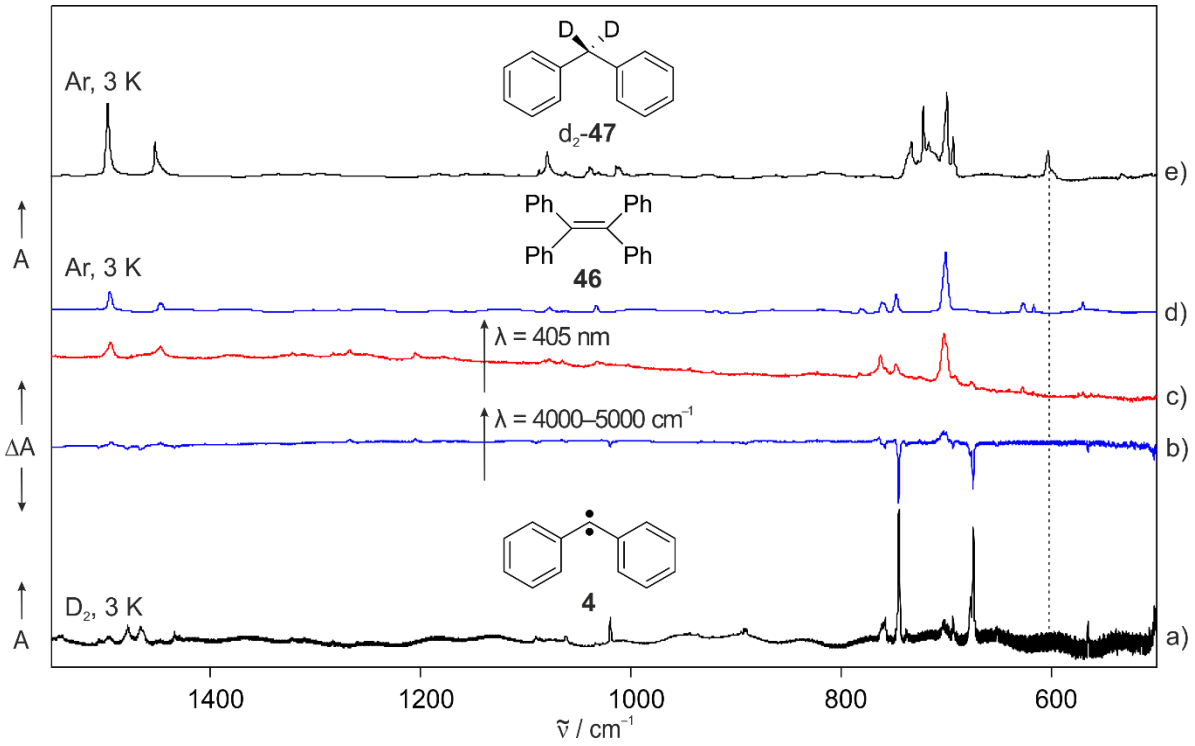

Figure 18. IR spectra showing the photochemistry of diphenylcarbene **4** in D_2 matrices. a) IR spectrum of **4** in D_2 at 3 K, obtained after irradiating **45** with λ = 560 nm. b) Difference IR spectrum obtained after irradiating **4** with λ = 4000–5000 cm^{-1} in D_2 at 3 K. c) IR spectrum obtained after irradiating **4** with λ = 405 nm in D_2 at 3 K. d) IR spectrum of tetraphenylethylene **46** in Ar at 3 K e) IR spectrum of 1,1-dideuterodiphenylmethane d_2-**47** in Ar at 3 K. The dashed line indicates the signal position of insertion product d_2-**47**; no corresponding signal was observed in (b-c).

Carbene **4** is generated in D_2 at 3 K by irradiation of precursor **45** with visible light (λ = 560 nm). Upon switching the light to lower wavelengths (e.g. 450, 405, and 365 nm), results in spectra that are very similar to the one obtained in H_2 matrices. IR irradiation at 4000–5000 cm^{-1} was also tried aiming at a vibrational excitation of either the carbene or solid D_2. However, the skeletal vibration of D_2-insertion product d_2-**47** at 603 cm^{-1} is not observed throughout the experiment, instead, tetraphenylethylene **46** is quantitatively formed. Carbene **4** just converts into the dimeric structure **47** irrespective of the photolytic conditions. Upon high intense UV light (405 nm), such process is favored even more.

Such light-induced aggregation does not happen in Ar matrices, but rather in the more volatile H_2 and D_2 hosts, which are quite soft even at 3 K. Neon matrices with a sublimation point between H_2 and Ar, were used in order to understand the aggregation process. Carbene **4** was generated in Ne matrices at 3 K by using 520 nm light (Figure 19).

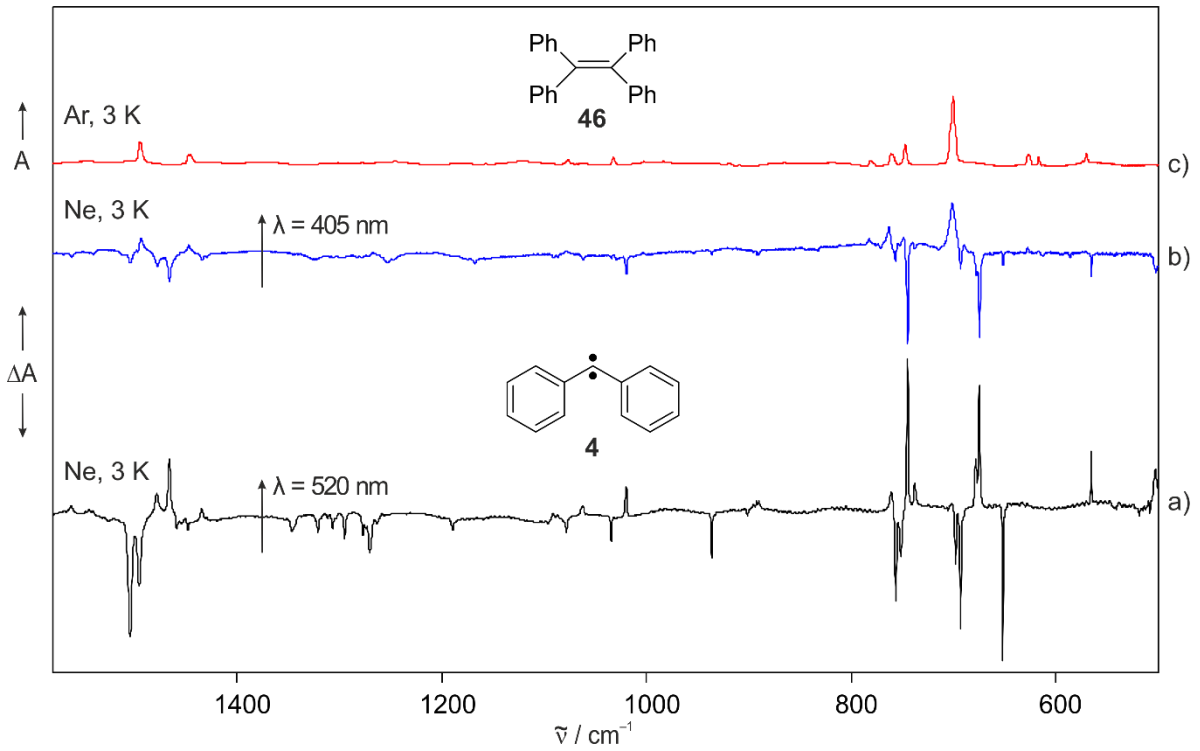

Figure 19. IR spectra showing the photochemistry of diphenylcarbene **4** in Ne matrices. a) Difference IR spectrum obtained after irradiating **45** with λ = 520 nm in Ne at 3 K. b) Difference IR spectrum obtained after irradiating **4** with λ = 405 nm in Ne at 3 K. c) IR spectrum of tetraphenylethylene **46** in Ar at 3 K.

Different photolytic conditions were applied, for instance visible light irradiation at 3 K, annealing the matrix at 8 K, as well as irradiating the matrix at 8 K. Under such conditions, carbene **4** is stable, however, when switching to wavelengths below 450 nm, dimeric compound **46** appears. Upon irradiation with 450 nm, dimerization is competing with the formation of 1-phenyl-1,2,4,6-cycloheptatetraene, as reported in literature.[140] However, highly intense 405 nm light efficiently induces the dimerization of **4** producing dimer **46** in high yields.

In practice, dimerization of carbenes is rare, primarily because carbenes are highly reactive species and are seldom generated in high enough concentrations that allow dimerization to occur. Instead, carbenes usually undergo reactions with other species present (e.g. solvent or precursor itself). The matrix isolation technique, however, provides a means of generating carbenes in high concentrations before the matrix is allowed to warm sufficiently to permit diffusion. One of the first reported examples of carbene dimerization in matrices is that of cyclopentadienylidene **26** (Scheme 10).[141]

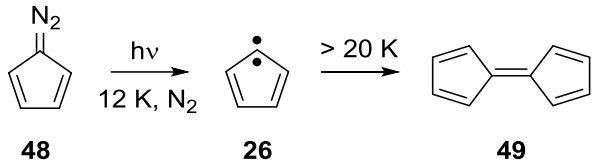

Scheme 10. Generation and dimerization of cyclopentadienylidene **26** in N_2 matrices.

Photolysis of diazocyclopentadiene **48** in N_2 matrices produces cyclopentadienylidene **26** at 12 K. When such matrix is warmed to 20–25 K, fulvalene **49** is formed. Several carbenes analogous to **26** (e.g. tetrachloro- and tetrabromocyclopentadienylidene and fluorenylidene **5**) failed to undergo similar dimerizations even at 30–35 K.[131,142] This was assumed to be a result of the increased size of these carbenes compared with **26**, which would hinder diffusion within the matrix, and would also destabilize the TS leading to the corresponding fulvalenes through unfavorable steric interactions.

Therefore, it is unexpected and surprising that the bulky diphenylcarbene **4** dimerizes so efficiently in volatile matrices upon UV photolysis. Such light-induced agglomeration could occur via excitation of **4** and with a subsequent transfer of energy to the lattice, which activates the mobility and/or produces a local lattice melting (photoannealing). Moreover, is also possible that the polar diazo precursor **45** forms dimeric aggregates in the gas phase while being sublimed to the cold window, resulting in a matrix containing precursor dimers or monomers that are not separated by many Ar atoms.

p-Hydrogen Matrices

Since diphenylcarbene **4** is found to be unreactive in H_2 matrices, such host could be a nice medium to study reactions with other small molecules at low temperatures. The reaction of triplet carbenes with O_2 is spin-allowed, and proceeds without apparent activation barrier in inert matrices at low temperatures.[143,144] The thermal and photochemical reactions of carbene **4** have been studied in O_2-doped Ar matrices (Scheme 11).[139,145] Upon annealing the matrix at temperatures higher than 10 K, benzophenone *0*-oxide **50** is formed with rates that approach diffusion control. Intermediate **50** is very photolabile toward long-wavelength irradiation (500–630 nm) and rearranges either to diphenyldiozirane **51** or benzophenone **52**. Further photolysis at lower wavelengths results in the formation of phenylbenzoate **53**.

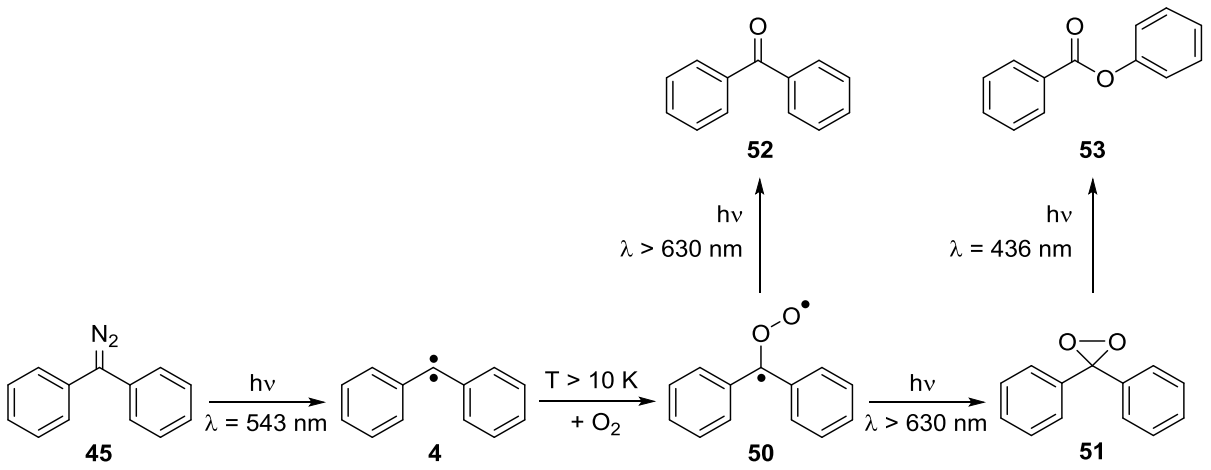

Scheme 11. Reaction of diphenylcarbene **4** with oxygen in Ar matrices at low temperatures.

Following that methodology, precursor **45** was deposited with an excess of *p*-H_2 doped with 1% of O_2 (Figure 20). Irradiation of **45** with visible light (λ = 520 nm) results in a complex spectrum containing several products. Assignment of the resulting signals is done by comparison to the experiments in pure *p*-H_2 and the studies on O_2-doped Ar matrices.[139] The resulting spectrum shows that along with carbene **4**, oxidation products **50** and **51** are also formed. In Ar matrices, the amount of oxidation products is found to correlate with increasing O_2 content. When the O_2 concentration is less than 0.5%, carbene **4** is mainly produced; but if increasing to 5%, such intermediate cannot be detected in the matrix. An O_2 concentration of 1% allows trapping carbene **4**, as well as the oxidation products; hence this concentration was used throughout the experiments in *p*-H_2 matrices.

Although enough O_2 is present in the matrix, the thermal reaction between carbene **4** and O_2 is not observed in *p*-H_2, as long as the matrix was kept at 3 K. On the other hand, the formation of oxidation products during irradiation can be explained by the direct photooxidation of **4** with molecules of O_2 in the same matrix cage. To investigate the thermal reaction of **4** with O_2, the matrix was warmed to 4.5 K and even for few seconds to 5.0 K, however, only a very small amount of **50** was formed, as indicated by its O–O stretching vibration at 896 cm^{-1}.[145] This vibration is very characteristic for carbonyl oxides; e.g. in cyclopentadienone *O*-oxide, it appears at 888 cm^{-1}.[146] Nevertheless, the yield of **50** in H_2 is much lower than in the experiments with O_2-doped Ar at 30 K. This lead to the assumption that there is a small activation barrier and temperatures of 3–5 K are too low to allow the reaction to proceed. Alternatively, the diffusion of O_2 in *p*-H_2 at 4.5 K might not be fast enough because of the extremely low temperatures. However, the concentration of O_2 is not the limiting step, since

upon additional photolysis with 405 nm, intense signals located 1200–1300 cm^{-1} appear and are assigned to ester **53**.[139]

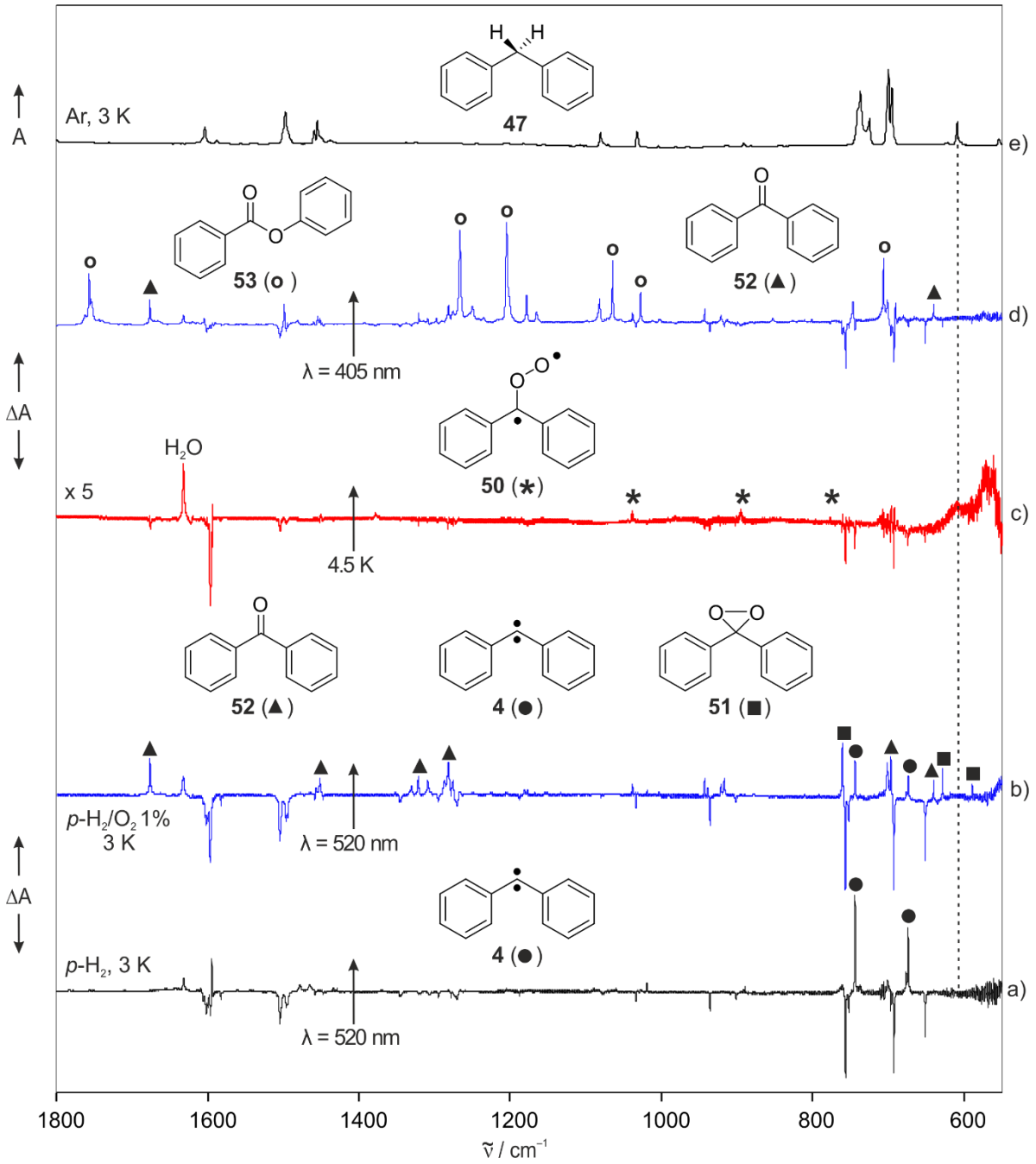

Figure 20. IR spectra showing the reaction of diphenylcarbene **4** with O_2 in *p*-H_2 matrices. a) Difference IR spectrum obtained after irradiating diphenyldiazomethane **45** with λ = 520 nm in *p*-H_2 at 3 K. b) Difference IR spectrum obtained after irradiating **45** with λ = 520 nm in 1% O_2-doped *p*-H_2 at 3 K. c) Difference IR spectrum obtained after annealing matrix (b) at 4.5 K. d) Difference IR spectrum obtained after irradiating matrix (c) with λ = 405 nm. e) IR spectrum of diphenylmethane **47** in Ar at 3 K. The dashed line indicates the signal position of insertion product **47**; no corresponding signal was observed in (a-d).

The H_2-insertion product **47** (signal at 609 cm^{-1}) is once again not formed throughout the experiment, which agrees with the results obtained from the experiments performed in normal H_2, *p*-H_2 and D_2 matrices. This experiment clearly shows the different reactivity of triplet carbene **4** toward O_2 and H_2 at low temperatures. Albeit H_2 is in excess in the matrix, carbene **4** selectively reacts both photochemically and thermally with such minor O_2. This can be depicted by simulating a H_2-box containing 1% of O_2 as well as carbene **4** (Figure 21). Typical host-to-guest ratios in matrix isolation experiments are 1000–2000 to 1, but in this case, were reduced to 500 to 1 in order to gain in clarity. An 8-nm^3-cubic cell was built around carbene **4** and was randomly filled with the gas molecules. Although this simple model is far from a proper description of a matrix cage, it gives a view of how selective the oxidation reaction is.

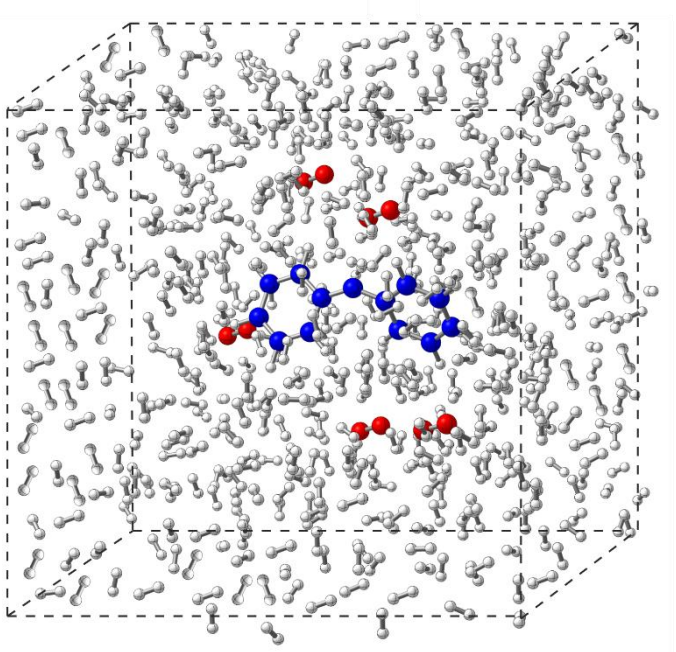

Figure 21. Representation of a cubic box containing H_2/O_2/**4** (500/5/1).

A summary of all the experimental procedures applied to induce a reaction of carbene **4** in H_2 matrices is shown in Table 4. Broadband irradiation with UV–vis and IR light sources were tried without success. Carbene **4** is found to be stable or to form the corresponding dimer **46**. The formation of **46** depends on how isolated the carbene is in the matrix, and how the matrix deposited onto the cold target is able to dissipate the excess of energy produced by the photolysis (photoannealing). It seems that gold-coated cooper plates provided better results than cesium iodide windows in isolating **4** in regular H_2 matrices. Moreover, annealing procedures were unsuccessful due to the narrow range of practically accessible temperatures in H_2 matrices (3–5 K).

Table 4. Summary of annealing and photolysis procedures applied to H_2 and *p*-H_2 matrices containing diphenylcarbene **4**.

Procedure	Bochum (H_2)[a]	Taiwan (H_2 and *p*-H_2)[b]
OPO Laser 560 nm	Stable	–
UV–vis light (530, 450, 405, 365 nm)	Dimer	Stable
OPO Laser (4000–5000 cm^{-1})	Dimer	–
NIR light (Globar internal and external) (Tungsten 6310–3080 cm^{-1})	–	Stable
Annealing at 4.5 K	–	Stable
Simultaneous NIR and 405 nm light	–	Stable

[a]Matrix is deposited on a cesium iodide window attached to a cooper holder by indium O-rings, cooled to 3 K with a Sumitomo closed-cycle refrigerator.
[b]Matrix is deposited on a gold-coated copper plate, cooled to 3 K with a Sumitomo closed-cycle refrigerator.

Further efforts were also dedicated to try to activate the H–H bond by means of infrared radiation. Selective and broadband IR irradiation was performed since solid H_2 (both normal and *para*) has a set of sharp signals (Q, S(0), and S(1)) in the region of 5000–4000 cm^{-1}, due to quadrupolar interaction.[147] For instance, Anderson et al. reported that broadband IR radiation from the globar source of an FTIR spectrometer (5000–4000 cm^{-1}) induces the reaction of atomic Cl with the *p*-H_2 matrix to form HCl at 2 K.[148] The infrared-induced process involves the formation of vibrationally excited H_2 ($v = 1$), which supplies the necessary energy to induce the reaction. In contrast, carbene **4** remains stable in *p*-H_2 matrices even with IR irradiation up to 6310 cm^{-1} (18 kcal/mol). Perhaps such excitation energy is not transferred to the reaction coordinate, but rather dissipated among all vibrational modes of **4** as well as to an efficient energy-quencher as solid *p*-H_2. Indeed, at liquid helium temperatures, the thermal conductivity of solid *p*-H_2 (ca. 200 W m^{-1} K^{-1}), is almost an order of magnitude greater than that of rare gas crystals.[149]

So far, no conditions were found under which carbene **4** reacts in solid H_2/D_2 at 3 K. However, most of the studies on hydrogenation of carbenes at low temperatures were conducted by using H_2-doped Ar matrices, with subsequent annealing at high temperatures (perhaps due to the more affordable 10 K closed-cycle cryostats).[98,102] Indeed, all triplet carbenes investigated so far, reacted with H_2 upon annealing the Ar matrices at 20–30 K (Figure 6). Therefore, the experiments on **4** were extended to those relatively high temperatures as for comparison.

Hydrogen-doped Inert Gas Matrices

Precursor **45** was deposited together with an excess of 5% H_2-doped Ar at 3 K. Visible light irradiation (520–560 nm) of the matrix at the lowest temperature results in the formation of carbene **4** with its characteristic IR absorptions at 674 and 744 cm^{-1} (Figure 22). Such spectrum is identical to the one obtained in pure Ar matrices. Subsequent annealing at 30 K allows the H_2 to diffuse in the Ar matrix, and results in a slow decrease of all bands assigned to **4**. Likewise, new signals at 609, 695, 700, 736, 1032, 1080, 1456, and 1498 cm^{-1} appear, which match those of diphenylmethane **47** isolated in Ar matrices at 3 K.

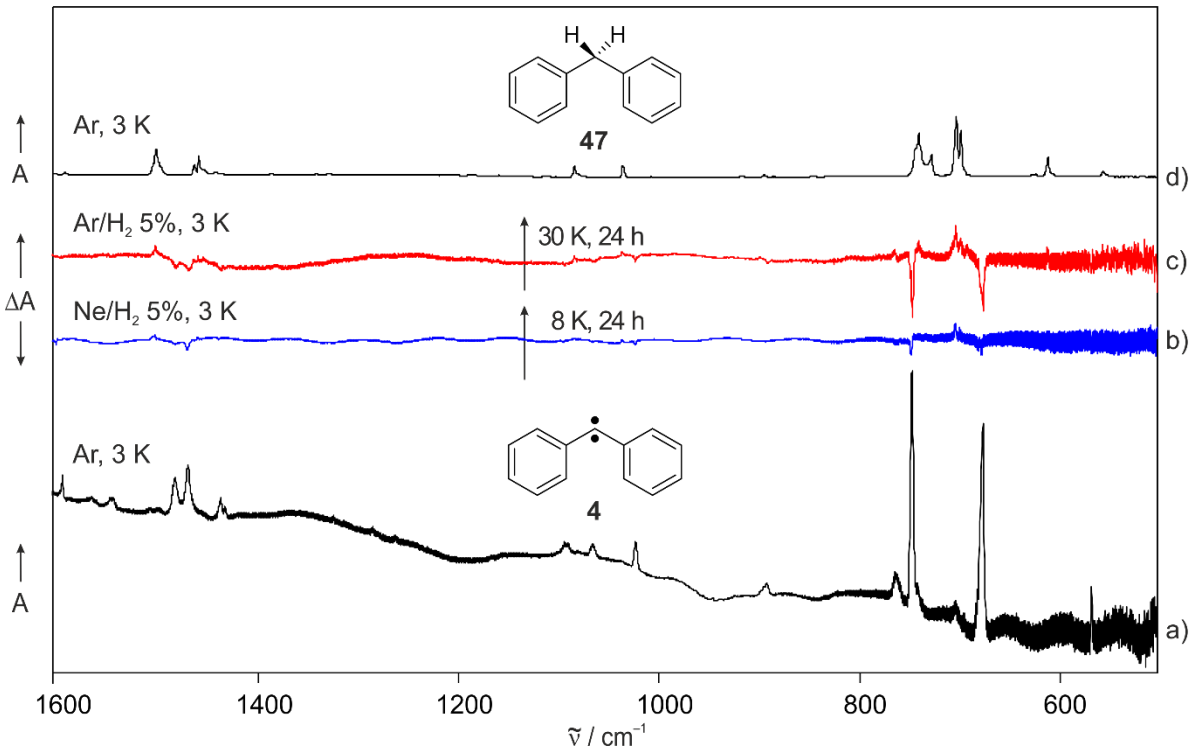

Figure 22. IR spectra showing the reaction of diphenylcarbene **4** with H_2 in Ar and Ne matrices. a) IR spectrum of **4** in Ar at 3 K, obtained after irradiating **45** with $\lambda = 560$ nm. b) Difference IR spectrum obtained after annealing **4** in 5% H_2-doped Ne at 8 K for 24 h. c) Difference IR spectrum obtained after annealing **4** in 5% H_2-doped Ar at 30 K for 24 h. d) IR spectrum of diphenylmethane **47** in Ar at 3 K.

Bimolecular reactions in matrix are intrinsically temperature-dependent since diffusion of molecules (in this case H_2) depends on the rigidity of the matrix host. For instance, carbene **4** is indefinitely stable in H_2-doped Ar matrices at 15 K, but starts to react with H_2 upon warming up the matrix to 20 K. The reaction becomes faster at 25–30 K; at this stage, Ar is soft enough to allow H_2 to freely diffuse in the matrix and find reactive carbene molecules. Hence, in these experiments, the methodology was to carefully increase the temperature of the matrix from 3 to 30 K (over 10 min), and then to keep the matrix at 30 K in darkness for 24 h. Upon warming

up the matrix to 30 K, the characteristic IR absorptions at 674 and 744 cm^{-1} of carbene **4** decay by a 20% and both dimer **46** and insertion product **47** are formed. At 30 K, carbene **4** exclusively transforms into product **47**, reaching a yield of 30% within 24 h. The faster decay of **4** while warming up is due to carbene molecules located in reactive sites, which immediately dimerize and/or react with nearby H_2 molecules upon softening of the matrix. This is a general phenomenon in disordered media as reactive intermediates are generated in a random distribution of different microenvironments, each with its own energy barrier.[84,133] Thus, disappearance plots are dominated at early times by reaction of these species in "fast sites", which have lower reaction barriers.

Comparing the reaction rates of the hydrogenation reaction of **4** at different temperatures in Ar matrices is not expected to yield information about the thermochemistry because of the temperature-dependent rigidity of solid Ar. Instead, it is possible to compare matrices of different material at temperatures where H_2 is freely diffusing, such as Ar at 30 K and Ne at 8 K. Irradiation of precursor **45** with λ = 560 nm in H_2-doped Ne matrices generates carbene **4** in good yields, although a small amount of dimer **46** is also formed. Upon warming up the matrix to 8 K (over 10 min), there is almost no decay of the signals of **4** since the matrix is already softened upon photolysis. The reaction at 8 K occurs with a slower rate than in Ar and only an 8% conversion of **4** into **47** is reached within 24 h. Unfortunately, a precise kinetic analysis is not possible due to noise in the low-frequency region, where the main peaks of **4** and **47** are located. However, rough estimations of the rates constants can be obtained by monitoring the decay of the signal at 1466 cm^{-1} (corresponding to **4**). Reaction rates were determined to be 1–3 × 10^{-5} s^{-1} at 30 K in Ar, and 0.7–2 × 10^{-6} s^{-1} at 8 K in Ne, as fitted to Eq. (8).[133]

These results should be analyzed with caution since Ar and Ne offer different matrix environments. For instance, host polarizability, cavity size, solvation, and phonon emission can influence reaction rates in low-temperature matrices (although their roles are not fully understood).[81] However, a simplified scenario can be assumed, where the reaction mainly depends on measurable variables like concentration of carbene/H_2 and temperature. In Ar and Ne matrices, the amount of precursor **46** deposited and irradiation conditions were similar, also a 5% content of H_2 was chosen, which is higher than the 0.5–2% that is typically used.[96,98,100] Likewise, the mobility of H_2 in the matrix should be comparable once the host is soft enough (e.g. Ar at 30 K and Ne at 8 K). Hence, the marked differences for the reaction of **4** with H_2 at

8–30 K might indicate a temperature dependence that resembles a classical behavior or, given such low temperatures, probably an interesting vibrationally-assisted tunneling.

Further investigations on this reaction were performed by repeating the experiment in 5% D_2-doped Ar matrices. Carbene **4** was generated as before and the matrix was kept in darkness at 30 K for 24 h, resulting in no spectroscopic changes. Since it is difficult to quantify the real amount of H_2 and D_2 deposited in the matrix, reactivity comparisons rely on the reproducibility of the experiments in H_2- and D_2-doped Ar matrices. As an alternative solution, an additional experiment was conceived by preparing an Ar matrix containing both H_2 and D_2 at 2.5% each (Figure 23). In this case, the IR cut-off filter was removed in order to increase the transmittance, and thus reduce the noise at the finger print region, making the separation between the two isotopomers **47** and d_2-**47** possible.

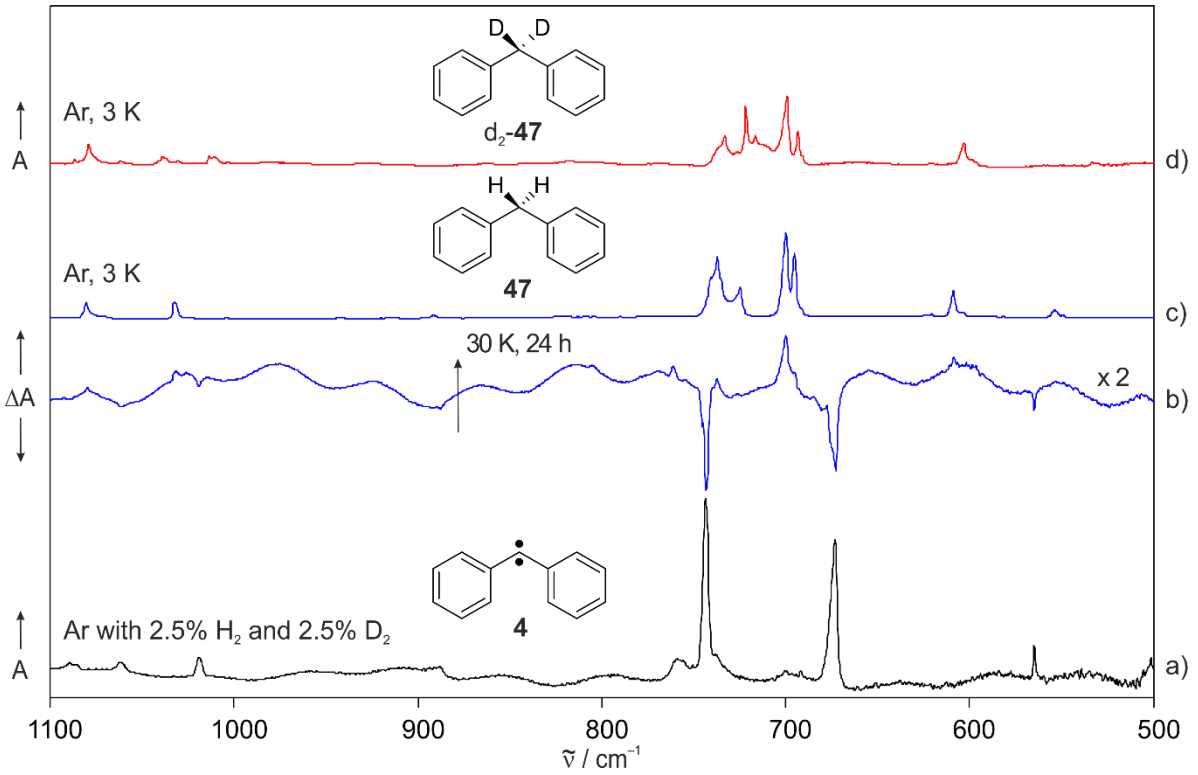

Figure 23. IR spectra showing the reaction of diphenylcarbene **4** with H_2 and D_2 in Ar matrices. a) IR spectrum of **4** in Ar doped with both 2.5% of H_2 and 2.5% of D_2 at 3 K, obtained after irradiating **45** with λ = 560 nm. b) Difference IR spectrum obtained after annealing the matrix at 30 K for 24 h. c) IR spectrum of diphenylmethane **47** in Ar at 3 K. d) IR spectrum of 1,1-dideuterodiphenylmethane d_2-**47** in Ar at 3 K.

Annealing of a matrix containing **4** in Ar doped with both 2.5% of H_2 and 2.5% of D_2 at 30 K results in a slowly decrease of all bands assigned to **4** and a simultaneous increase of the signals of **47**. Although the spectra corresponding to matrix-isolated **47** and d_2-**47** are very similar, increasing signals at 603 and 1032 cm^{-1} match with **47** in Ar, but not with d_2-**47**, which shows

signals at 609, 1012, and 1038 cm^{-1}. Also in this case, kinetics of the reaction of carbene **4** with H_2 was monitored at 30 K for 24 h by following the decay of the intensities of the IR signals at 565, 714, and 744 cm^{-1}, as well as the rise of that of product d_2-**47** at 695–700 cm^{-1}. The reaction rate was determined to be $1.5 \pm 0.5 \times 10^{-5}$ s^{-1} at 30 K in Ar, and the best correlation was obtained by using $\beta = 0.5$ in Eq. (8).[133] Such $t^{1/2}$ dependence was previously observed for the decay of carbene **4** in organic glasses at 77 K.[84] Moreover, conversion reached a 27% in 24 h, in agreement with the 30% observed in 5% H_2-doped Ar matrices at 30 K.

Overall, experiments in H_2/D_2-doped inert gas matrices showed that carbene **4** selectively inserts into H_2 but not into D_2. These results parallel the reactivity of triplet carbenes **26**, **27**, and **30**, which are also completely unreactive to D_2 under similar conditions (2% D_2-doped Ar matrices at 30 K).[98] This large kinetic isotope effect and the fact that the reaction takes place at temperatures as low as 8–30 K, indicates that the reaction rates are governed by QMT. However, tunneling reactions at such low temperatures usually shows no or very shallow temperature-dependence at such low temperatures (deep tunneling). Hence, it is quite puzzling that carbene **4** is stable in solid H_2 at 3–5 K, with H_2 molecules surrounding carbene **4**, but reacts in H_2-doped Ar matrices at 20–30 K (Scheme 12).

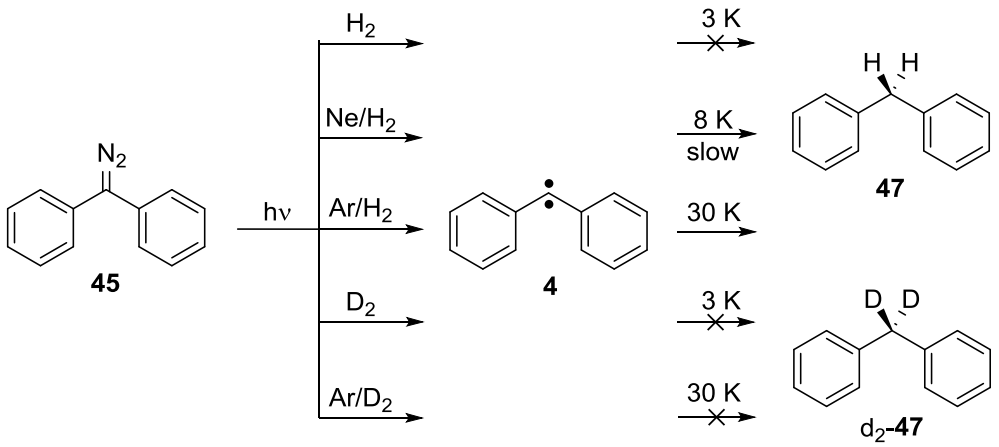

Scheme 12. Reactivity of diphenylcarbene **4** with hydrogen and deuterium in solid H_2 and D_2, as well as in doped inert gas matrices.

Calculations

The hydrogenation reaction of diphenylcarbene **4** was studied computationally to understand the reaction mechanism and the temperature-dependent reactivity observed in matrices. Carbene **4** has a triplet ground state with a relatively small ΔE_{ST}, as determinated experimentally in solution at RT. The value of ΔE_{ST} is sensitive to the solvent polarity and is

larger in isooctane (4.1 kcal/mol) than in acetonitrile (2.6 kcal/mol).[1,14] Hence, both the singlet and triplet PES have been explored and all relevant stationary points are reported (Figure 24).

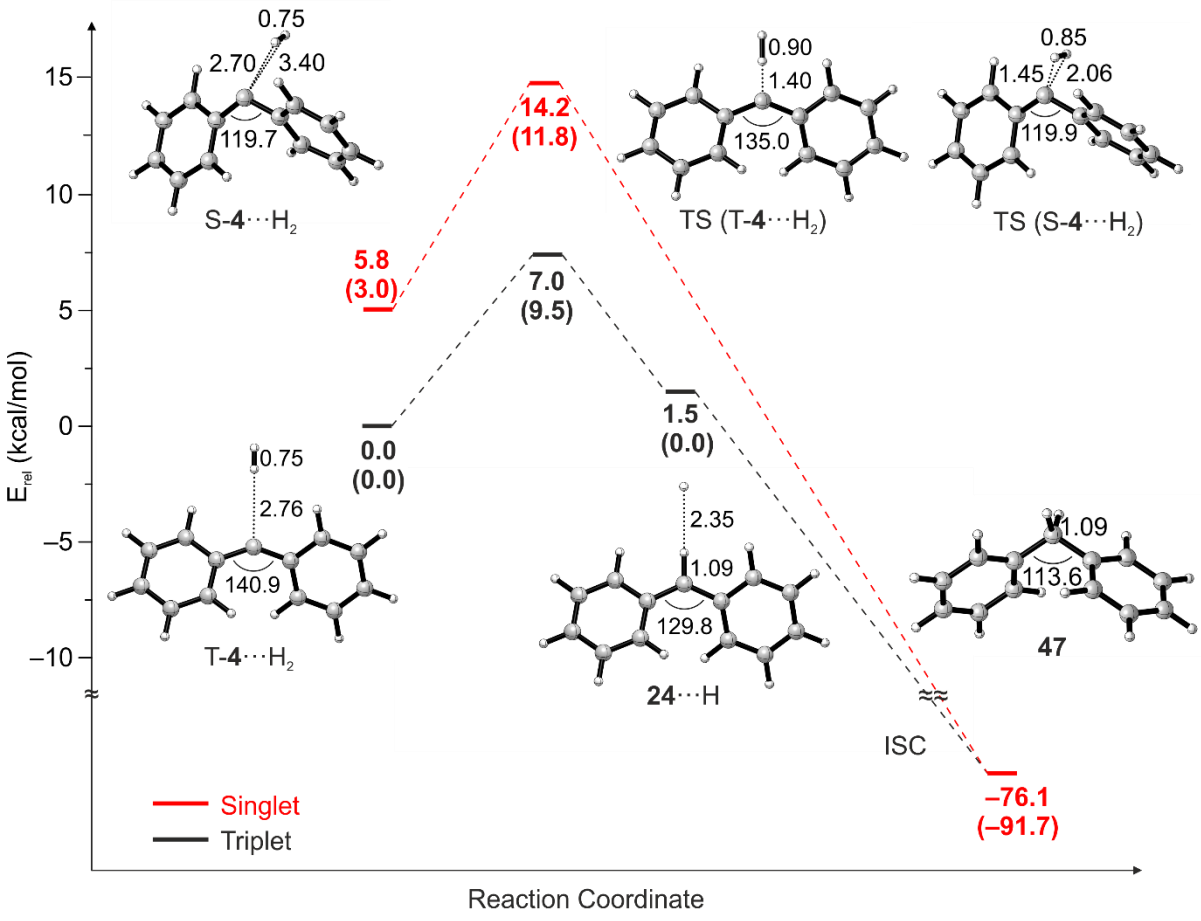

Figure 24. Hydrogenation of diphenylcarbene **4** on the singlet (red) and triplet (black) PES calculated at the ZPE-corrected B3LYP-D3/def2-TZVP level of theory. Values in parentheses correspond to CCSD(T)/cc-PVDZ //B3LYP-D3/def2-TZVP energies. Energies are given in kcal/mol and selected bond lengths and angles are given in Å and °, respectively.

Similar to carbene **5** (Figure 15), the hydrogen complexes T-**4**···H_2 and S-**4**···H_2, as well as the triplet radical pair **24**···H are predicted to be have near-zero binding energies. The triplet barrier for the H-abstraction is predicted to be 7.0 kcal/mol at the B3LYP-D3//def2-TZVP level of theory. Energy calculations with CCSD(T)/cc-PVDZ at the DFT-optimized geometry predict a value of 9.5 kcal/mol that is much higher than the thermal energy available at 30 K (kT = 0.06 kcal/mol). A thermal reaction of carbene **4** with H_2 is hence prohibited at low temperatures, which indicates that the reaction rates are governed by QMT. For tunneling reactions, large kinetic isotope effects are expected, as observed for the selective reaction with H_2 in Ar matrices containing both H_2 and D_2. A lower limit for the KIE of several hundred can be estimated based on the kinetic constants determined in H_2-doped Ar ($k \sim 10^{-5}$ s^{-1}) and

D_2-doped Ar ($k < 10^{-7}$ s^{-1}) at 30 K. An estimation of the classical KIE of 3.8 at 30 K is obtained by applying the Arrhenius expression (with $E_a(D) - E_a(H) = 0.08$ kcal/mol, according to DFT calculations). Hence, the large KIE observed experimentally can only be explained by tunneling.

Since carbene **4** has a small ΔE_{ST}, the reaction proceeding through the singlet PES was also taken into account. However, matrix-isolated **4** has a robust triplet ground state and does not switches its spin from triplet to singlet upon annealing Ar matrices at 30 K. In addition, experiments in H_2/D_2-doped Ar matrices do not show the formation of H-bonded complexes. Finally, DFT and CCSD(T) calculations predict similar activation barriers corresponding to the reactions in the singlet and triplet state PES (E_a (S-**4**$\cdots H_2$) = 8.4–8.8 kcal/mol, E_a (T-**4**$\cdots H_2$) = 7.0–9.5 kcal/mol). That means that at these temperatures the reaction of **4** and H_2 should proceed along the triplet surface (no crossing between surfaces before TS) and through abstraction-recombination mechanism.

The result that the low-temperature reaction of triplet **4** with H_2 proceeds via H-atom tunneling agrees with the conclusions obtained from low-temperature organic glasses experiments.[84,89] Carbene **4** decays within minutes in glassy matrices at 77 K forming a triplet radical pair as previously shown in Scheme 4. Moreover, KIE of up to 10^2 are found in perdeuterated solvents, and no Cl-abstraction is found in CCl_4 matrices. Experimental activation barriers in the range of 2.1–4.3 kcal/mol were determined for these reactions, which are lower than those predicted by calculations (6–12 kcal/mol), and correlate to the H-donor ability of the solvents (toluene > cyclohexene > methylcyclohexane > benzene). Additionally, the experimental rate constants are reproduced by tunneling calculations based on an Eckart barrier potential.

In conclusion, diphenylcarbene **4** is a triplet ground state carbene that can be isolated in solid H_2 and D_2 at 3 K and is stable upon IR and UV–vis irradiation. Nevertheless, it reacts with H_2 upon annealing of H_2-doped Ne and Ar matrices at 8 and 30 K, respectively, to form the H_2-insertion product **47**. The hydrogenation shows a large kinetic isotope effect and remarkable isotope selectivity, and proceeds despite having an activation barrier which is prohibitively high for a reaction to occur classically at such low temperatures (8–30 K). The experiments suggest that the H-abstraction proceeds through vibrationally-assisted tunneling. However, there are still two observations that remain unexplained which are the thermal activation of the reaction of carbene **4** with H_2, and the lower reactivity of **4** compared to fluorenylidene **5**. These topics will be discussed in the following section.

Diphenylcarbene vs. Fluorenylidene

Experimental evidences on the low-temperature hydrogenation of carbenes **4** and **5** suggest that these reactions proceed by QMT, instead of crossing over the barrier. Tunneling paths and rates can be predicted using elaborated methods such as canonical variational transition state (CVT) theory[150] combined with the small-curvature tunneling (SCT) approximation,[151] or by using instanton theory.[152] A simpler Wentzel–Kramers–Brillouin (WKB) tunneling model,[153] by using standard intrinsic reaction coordinate (IRC) calculations, is frequently used for H-transfer reactions.[69,70] Herein, a qualitative reaction model (based on IRC computations) for comparing the reactivity of carbenes **4** and **5** toward H_2 is presented.

Reaction profiles for the H-abstraction by carbenes **4** and **5** in their triplet ground states are shown in Figure 25. The reaction coordinate was chosen as both the distance between the carbene center and the H_2 molecule d(C–H), as well as the H–H distance in H_2 itself d(H–H). A three-dimension diagram is built up, where the potential energy (E) along the reaction path depends on both the geometrical parameters d(C–H) and d(H–H); these values are taken from the IRCs calculated at the B3LYP-D3/def2-TZVP level of theory. Likewise, energies and geometries corresponding to the stationary points (complex, TS, and triplet radical pair) are reported with and without ZPE corrections. Although much more vibrational modes (e.g. C–C–C bend, ring torsion) might also contribute to the multi-dimensional reaction coordinate, C–H and H–H distances are the main coordinates involved in the structural change from reactants to products. Since IRCs are not ZPE-corrected, vibrational levels are usually derived from the reaction mode, and by using the anharmonic oscillator model. Defining the reaction mode in intramolecular processes like isomerization of carboxylic acids is often straightforward, as torsional frequencies of reactant and product can easily be identified.[69,81] However, in bimolecular reactions of carbenes with H-donors, more complicated models arise, (e.g. assuming C–H vibrational states "broadened" by coupling with all other motions).[84] In this work, no explicit reaction mode is considered.

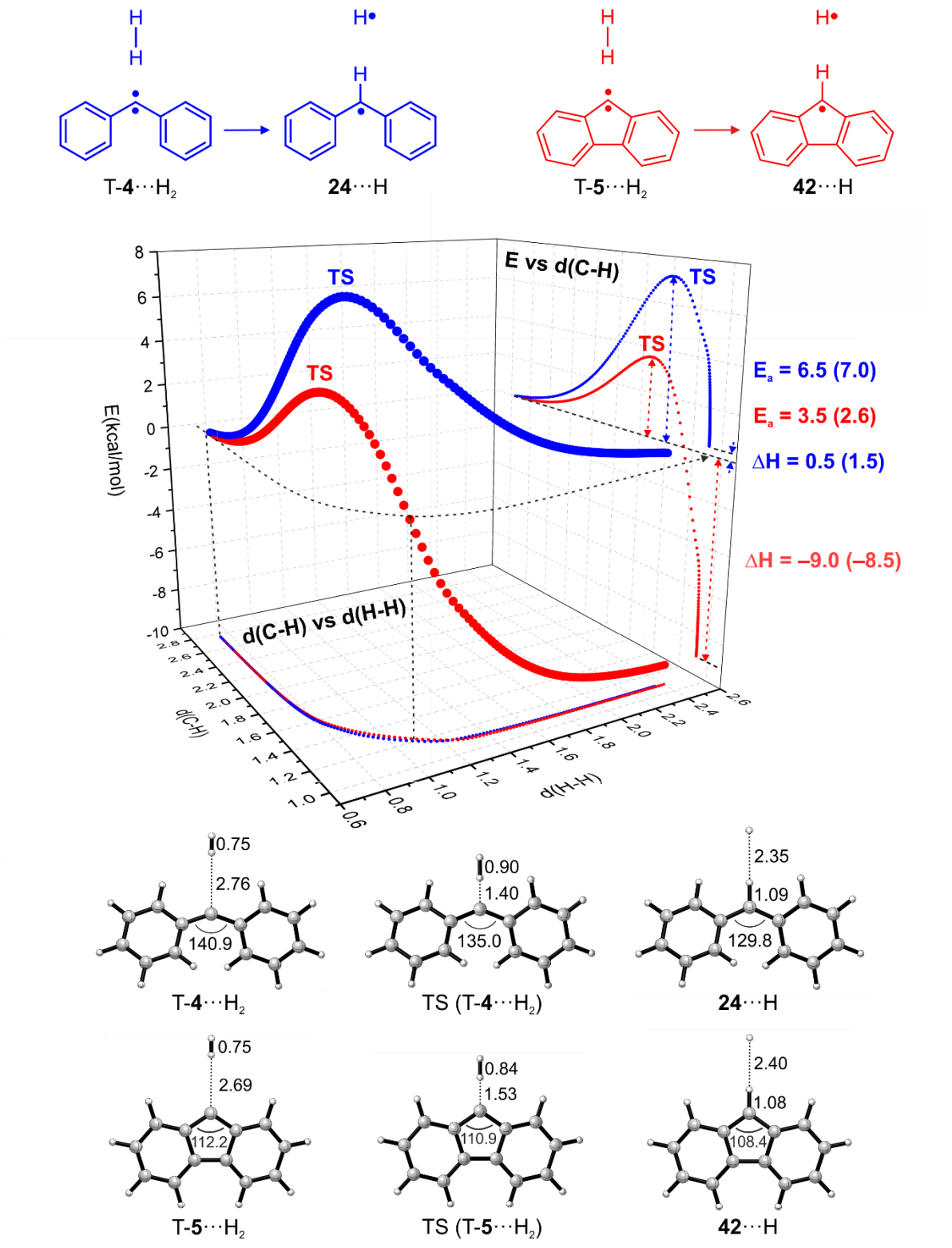

Figure 25. Hydrogen-abstraction by diphenylcarbene T-**4** (blue) and fluorenylidene T-**5** (red) on the triplet PES calculated at the B3LYP-D3/def2-TZVP level of theory. The reaction profiles show the change in energy as a function of the intermolecular C–H and intramolecular H–H distances, along the intrinsic reaction path. Energies are given in kcal/mol and values in parentheses include ZPE correction. Selected bond lengths and angles are given in Å and °, respectively.

This simplified reaction model shows that tunneling through the barrier at the reactant-energy level (projection of the curves on the xy plane) follows a very similar pathway for carbenes **4** and **5**. The high reactivity of **5** toward H_2 and D_2 at low temperatures can be explained by a relatively short tunneling path through the barrier, even at the lowest energy vibrational level. An estimation of 1.6–1.7 Å for the barrier width is obtained for **5** by calculating the arc length of the tunneling path at the reactant-energy level. This value is expected to be considerably lower if taking into account the ZPE and due to the flatness of the surface at longer C–H distances. Moreover, calculations also suggest the formation of an early TS for the exothermic H-abstraction by **5**, in agreement with Hammond`s postulate.[154] Indeed, TS (T-**5**···H) is formed at a larger intermolecular C–H distance (1.53 Å) and a shorter H–H distance (0.84 Å) compared to the values found for TS (T-**4**···H), which are 1.40 and 0.90 Å, respectively. Overall, DFT calculations predict a considerable smaller and narrower barrier for carbene **4** compared to carbene **5**, in agreement with the reactivity trends observed in H_2 matrices.

The vibrationally-assisted tunneling of **4** can be understood since the reaction cannot proceed through a very large tunneling path at 3 K that can become shorter upon increasing the potential energy. The computed enthalpy is slightly endothermic according to DFT calculations (0.5–1.5 kcal/mol) but becomes isothermic at the CCSD(T) level of theory. Hence, small changes in the thermal energy might have dramatic effects in reaction rates considering the flatness of the PES at both sides of the TS. Even though, the thermal energy at 30 K is not sufficient to significantly excite C–H or H–H vibrational levels, it can excite the solid noble gas host material, whose Debye frequencies are in the range of 40–70 cm^{-1}.[155] As the matrix softens at higher temperatures, it can better accommodate the structural changes required for the tunneling of **4**. Besides thermal considerations, the unreactivity of carbene **4** in solid H_2 might be explained by a stabilization of the reactants (matrix solvation), which would make the reaction slightly endothermic, and thus less probable to proceed through deep tunneling at 3–5 K. For example, rotamerization tunneling rates are found to be strongly dependent on the environment (matrix host, temperature, and interaction with other molecules).[69,81,156]

Finally, the marked differences in the enthalpy of the H-abstraction process for carbenes **4** and **5** can be rationalized based on the relative stability of both reactants and products. Fluorenyl radical **42** and diphenylmethyl radical **24** are found to have a similar stability, since the experimental C–H BDE of the corresponding hydrocarbons **41** and **47** are 82.0 and 84.5 kcal/mol, respectively.[60] Hence, the imbalance on the calculated H-abstraction enthalpies

should come from the relative stability of carbenes **4** and **5**. However, assessing stability for carbenes can be challenging, in part because they can have different reaction patterns, but also because of the lack of physical measurements. In this work, carbene stability is assessed by using the concept of carbene stabilization energy (CSE), as described by O´Ferral et al.[104,157] In this theoretical model, the CSE is defined as the enthalpy of the homodesmotic reaction involving the conversion of the carbene center to a tetravalent carbon, with methylene as the standard reference. The CSE can be calculated with the carbene in either the singlet or triplet state (although the product is considered in its singlet ground state). By this definition, a positive CSE value indicates that the substituent provides greater stabilization to the carbene than the H atoms in CH_2 (Scheme 13).

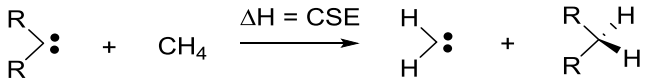

Scheme 13. Carbene stabilization energy (CSE) as measure of the hydrogenation enthalpy of carbenes.

Likewise, either using enthalpies or electronic energies, the singlet–triplet gap of a designated carbene (R_2C:) should be directly correlated to the difference on the CSE of the carbene in both electronic states as shown in Eq. (9).

$$\Delta E_{ST}(R_2C:) = \Delta E_{ST}(H_2C:) - (CSE(\,^1R_2C:) - CSE(\,^3R_2C:)) \qquad (9)$$

Following the methodology used by O`Ferral et al.,[157] CCSD(T) energy calculations of CH_2, **4**, and **5**, as well as their corresponding hydrogenated species, were performed by using geometries optimized at the B3LYP-D3/def2-TZVP level of theory. These values were used to estimate the CSE of carbenes **4** and **5** relative to triplet and singlet CH_2 as shown in Table 5. Carbene **4** has higher CSE in both the singlet and triplet states (31.6 and 22.6 kcal/mol) than **5** (25.5 and 16.5 kcal/mol) at the CCSD(T)/cc-PVTZ level of theory. The relative lower stability of S-**5** in comparison to S-**4**, gives insights into the impact of antiaromaticity in S-**5**. As for the triplet states, T-**5** is expected to be less stable than T-**4**, by having a smaller C–C–C angle (almost 30^o closer than T-**4**). Larger C–C–C angles will favor triplet states by reducing the hybridization difference, and therefore the energy separation between the nonbonding orbitals. An extreme and rare case is triplet cyclopropylidene with a negative CSE, indicating that it is less stable than CH_2 with respect to the corresponding reference species.[104] Moreover, lowering the central bond angle as in T-**5** increases the amount of s character in the singly occupied orbitals of the carbene, hence making it more reactive.

Table 5. Calculated CSE values and singlet-triplet energy gap (kcal/mol) of several carbenes.

Carbene	Method	CSE (Singlet)	CSE (Triplet)	ΔE_{ST}
Methylene	CCSD(T)/cc-PVDZ	0	0	12.6
	CCSD(T)/cc-PVTZ	0	0	11.0
Diphenylcarbene **4**	CCSD(T)/cc-PVDZ	30.3	21.0	3.3
	CCSD(T)/cc-PVTZ	31.6	22.6	1.9
Fluorenylidene **5**	CCSD(T)/cc-PVDZ	24.6	15.4	3.4
	CCSD(T)/cc-PVTZ	25.5	16.5	2.0

Overall, the relative destabilization of triplet fluorenylidene **5** compared to triplet diphenylcarbene **4** seems to explain the experimental differences in the reactivity toward H_2 under cryogenic conditions. Carbenes **4** and **5** are similar looking triplet ground state intermediates that show a distinct reactivity pattern on the reaction with H_2, in contrast to the reactions with other small molecules at low temperatures. Under these conditions, both carbenes quickly react with O_2,[131,145] and switch the spin state from triplet to singlet, upon interaction with H_2O,[17,158] ICF_3,[19,159] and BF_3.[20,159] On the other hand, at temperatures higher than 77 K, carbene **5** is more reactive than carbene **4** toward C–H bonds, with shorter lifetimes, and showing smaller KIE in cyclohexane glasses/solutions.[84,87,89] Such reactivity differences toward C–H bonds were explained by a smaller S–T gap in **5** (although, not reflected by CCSD(T) calculations), allowing singlet reactions to contribute, and only to a lesser extent to a variation in triplet reactivity.[15] However, experiments in H_2 matrices at low temperatures, show that the H-abstraction by carbenes **4** and **5** is controlled by triplet reactivity. Carbene geometrical structure (and relative energetic stabilization) rather than philicity[103] or the S–T gap,[159] seems to be the key factor in the hydrogenation of these triplet arylcarbenes.

Arylnitrenes

Nitrenes, the subvalent nitrogen analogues of carbenes, are reactive intermediates which might activate H_2, based on their electron deficiency and the strength of the resulting N–H bonds. However, as explained previously, the large amount of 2s character in the lone pair orbital on nitrogen makes triplet nitrenes more thermodynamically stable (and less reactive) than triplet carbenes.[55] For example, triplet carbenes react with O_2 at low temperatures with rates that approach diffusion control to form carbonyl *O*-oxides,[139] whereas triplet nitrenes react much slower. For instance, phenylnitrene **6** can be isolated in pure solid O_2, and its thermal reaction

to form nitroso *O*-oxide is only observed by annealing an O_2-doped Xe matrix at temperatures higher than 40 K.[160] Such results are rationalized by the formation of weak N–O bonds and strong C–O bonds in the oxygenation of nitrenes and carbenes, respectively. Regarding the H-abstraction by triplet nitrenes, a comprehensive theoretical study pointed to NH and nitrenes substituted with electronic-withdrawing groups, as the potential nitrenes to abstract H atoms (because of having the less positive enthalpies).[161] A novel borylnitrene is so far the only "nitrene" reported to insert into H_2 under cryogenic conditions.[162] This highly reactive BN vinylidene analogue also reacts with N_2, O_2, and CO upon visible light irradiation.[163] In order to shed light into the scarcely studied activation of H_2 by nitrenes, two common arylnitrenes (2,6-dimethylphenylnitrene **7** and 2,6-difluorophenylnitrene **8**) were tested experimentally.

Hydrogen Matrices

The spectrum of 2,6-dimethylphenylazide **54** in solid H_2 at 3 K is shown in Figure 26. Irradiation of **54** with UV light (λ = 254 nm) at 3 K results in a decrease of the IR signals assigned to **54** (1475, 1422, 1307, 1290, and 769 cm^{-1}), accompanied by the formation of new signals at 1568, 1455, 1435, 1205, and 758 cm^{-1}.

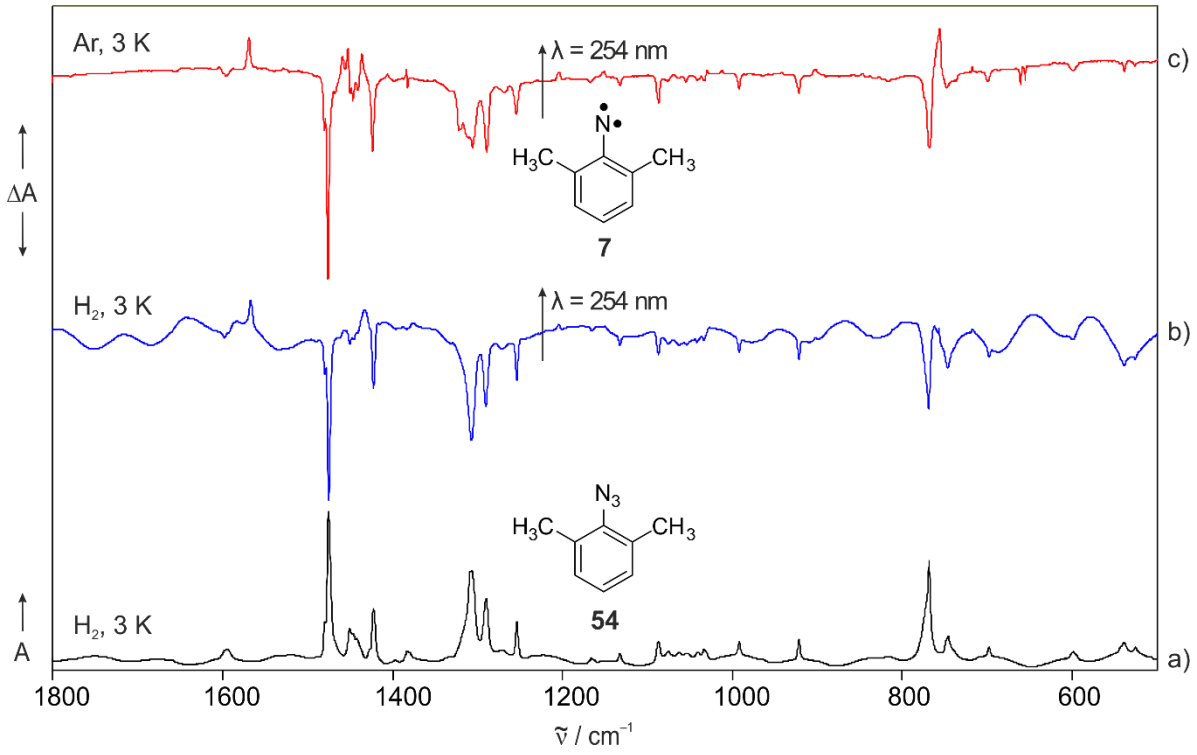

Figure 26. IR spectra showing the formation of 2,6-dimethylphenylnitrene **7** in H_2 and Ar matrices. a) IR spectrum of 2,6-dimethylphenylazide **54** in H_2 at 3 K. b) Difference IR spectrum obtained after irradiating **54** with λ = 254 nm in H_2 at 3 K. c) Difference IR spectrum obtained after irradiating **54** with λ = 254 nm in Ar at 3 K.

The spectroscopic features observed after the photolysis are assigned to matrix-isolated 2,6-dimethylphenylnitrene **7** and are in excellent agreement with values from literature.[164] Under the same experimental conditions, photolysis of **54** in either H_2 or Ar matrices at 3 K, produces similar spectra, but no even traces of the expected H_2-insertion product, 2,6-dimethylaniline **55**. Likewise, annealing of a H_2-doped Ar matrix containing nitrene **7** at 30 K does not produce new spectral features. This shows that neither thermal nor photochemical reaction between nitrene **7** and H_2 occurs under such cryogenic conditions. Moreover, there is no indication of formation of benzazirine ($\tilde{\nu}$(C=N) ~ 1730 cm^{-1}), ketenimine ($\tilde{\nu}$(C=N=N) ~ 1890 cm^{-1}), or the product of nitrene insertion into one of the methyl groups ($\tilde{\nu}$(N–H) ~ 3400 cm^{-1}).

2,6-Difluorophenylnitrene **8** is another triplet ortho-disubstituted phenylnitrene that can be efficiently generated in the matrix, by photolysis of the precursor 2,6-difluorophenylazide **56** (Figure 27). Similarly as for nitrene **7**, ring expansion processes are suppressed due to electronic and steric effects of the ortho substituents.[165]

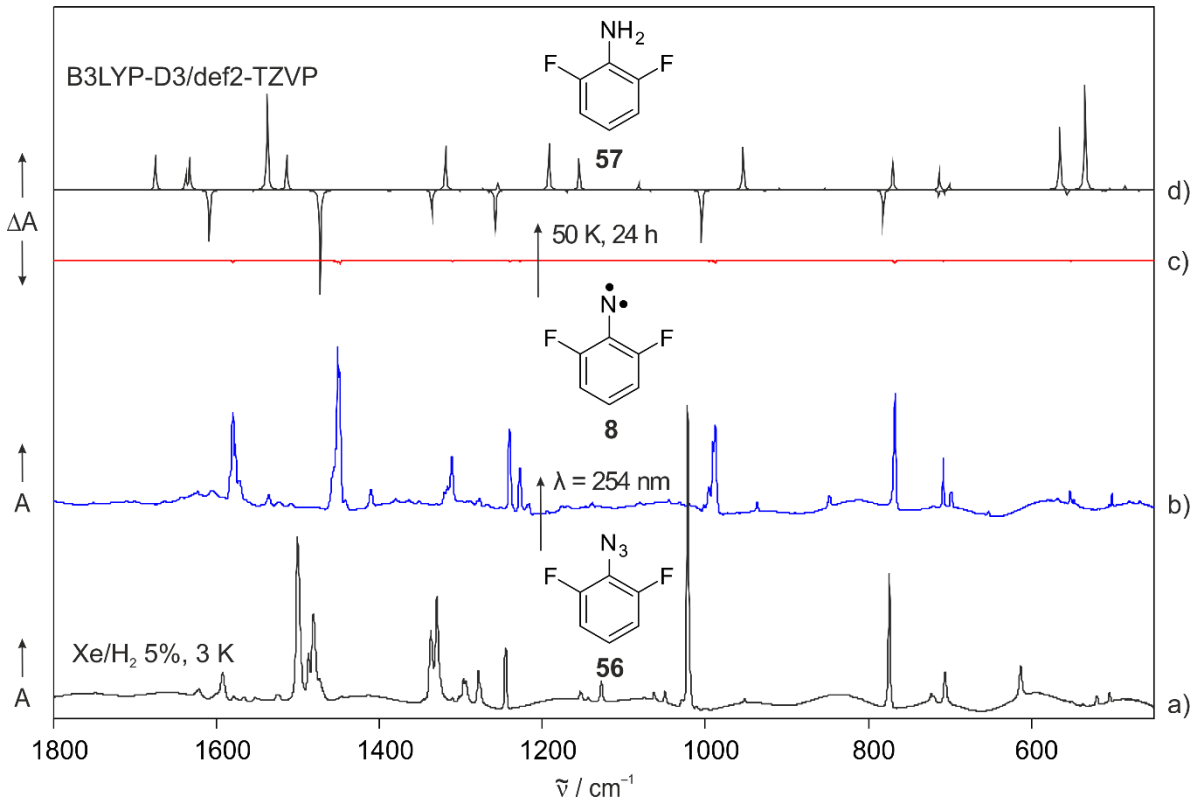

Figure 27. IR spectra showing the formation of 2,6-difluorophenylnitrene **8** in H_2-doped Xe matrices. a) IR spectrum of 2,6-difluorophenylazide **56** in 5% H_2-doped Xe at 3 K. b) IR spectrum obtained after irradiating **56** with λ = 254 nm in 5% H_2-doped Xe at 3 K. c) Difference IR spectrum obtained after annealing the matrix at 50 K for 24 h. d) Difference IR spectrum for the conversion **8**→**57** calculated at the B3LYP-D3//def2-TZVP level of theory.

Irradiation of precursor **56** with UV light (λ = 254 nm) in 5% H_2-doped Xe at 3 K results in complete depletion of the IR signals assigned to **56** (1502, 1331, 1022, 775, and 613 cm^{-1}) and formation of a new set of signals. New absorptions at 1579, 1452, 1241, 988, and 768 cm^{-1} are in agreement with the IR spectrum of matrix-isolated **8** reported in N_2 at 10 K.[45] Even after annealing of the Xe matrix at 50 K for 24 h, nitrene **8** is stable and the hydrogenation reaction does not occur. The experiment was also performed in 5% H_2-doped Ar matrices (annealing at 30 K) and a similar result is obtained, H_2-insertion product 2,6-difluoroaniline **57** is again not detected (Scheme 14).

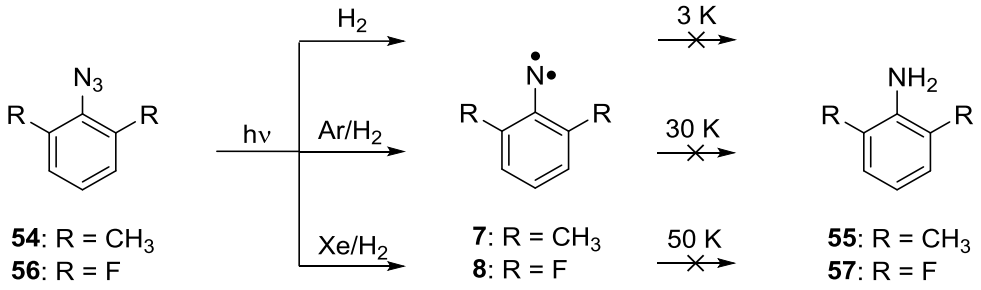

Scheme 14. Reactivity of 2,6-dimethylphenylnitrene **7** and 2,6-difluorophenylnitrene **8** with hydrogen in solid H_2 and in doped inert gas matrices.

Calculations

The stability of triplet arylnitrenes **7** and **8** toward H_2 at low temperatures can be explained by the high barrier and endothermicity of the H-abstraction step. Activation energies calculated at the B3LYP-D3/def2-TZVP level of theory are 19.5 and 16.0 kcal/mol for nitrenes **7** and **8**, respectively. Likewise, endothermic enthalpies (18.2 and 14.5 kcal/mol) are obtained, showing that aminyl radicals are not expected to be formed. Even with a better H-donor like methanol, phenylnitrene **6** faces a quite endothermic H-abstraction (6.5 kcal/mol), according to CBS-QB3 calculations.[161] Hence, experimental observations are consistent with the above calculations, which are not supportive of H-abstraction by phenylnitrene derivatives.

Overall, it is well established that triplet carbenes and nitrenes react with H-donors through H-abstraction followed by recombination of the resulting radical pair to give the insertion product. Experimental observations supported by calculations, show that both the shape of the barrier (height and width) and the enthalpy associated to the H-abstraction step, are crucial variables regarding low-temperature reactivity of triplet intermediates. A compilation of the calculated activation energies and enthalpies for H-abstraction reactions involving triplet carbenes and nitrenes is shown in Figure 28.

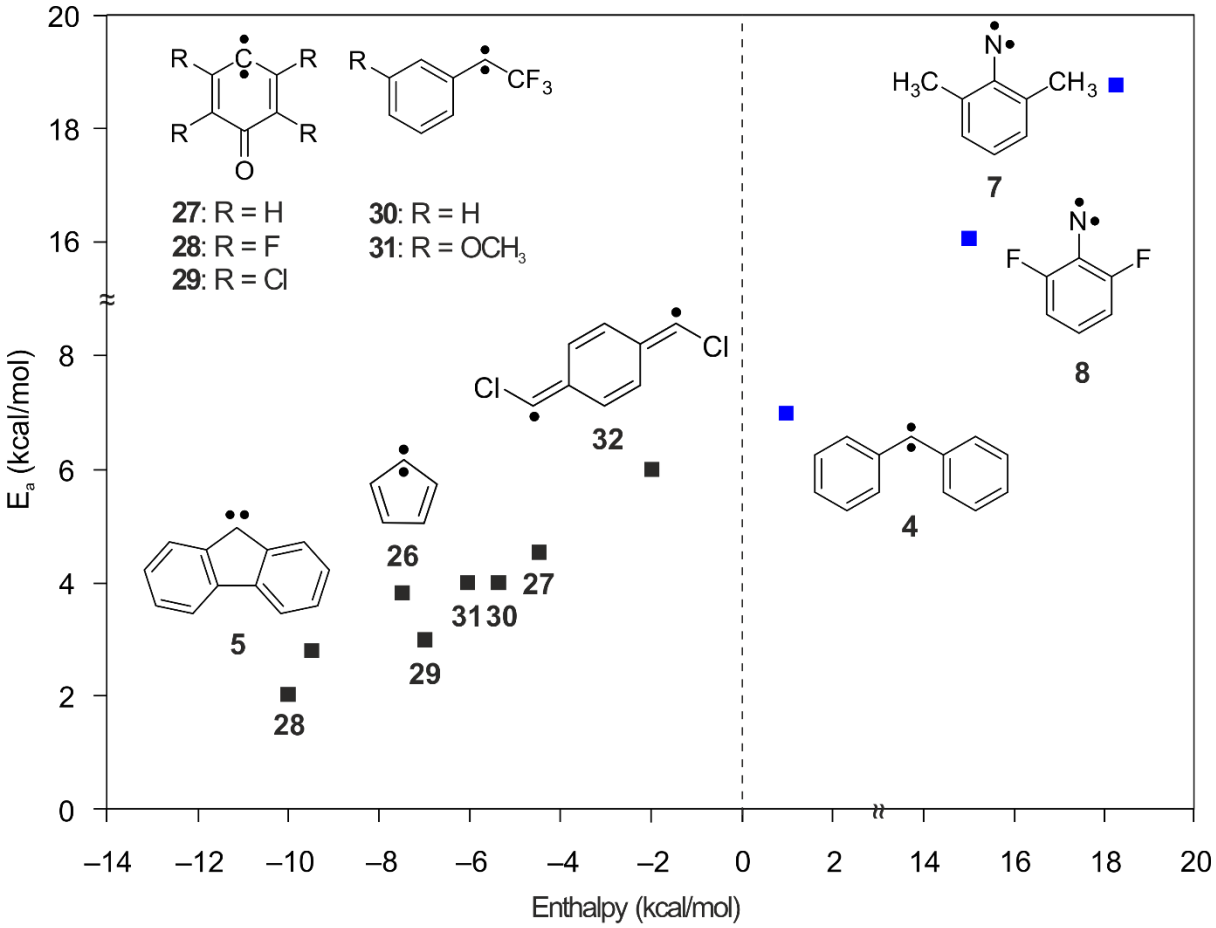

Figure 28. Triplet carbenes and nitrenes for which the reaction with H_2 has been investigated at low temperatures (including this work). Activation energies and enthalpies for the H-abstraction step are calculated at the B3LYP-D3/def2-TZVP level of theory. Triplet carbenes **5, 26**–**31** and open-shell singlet diradical **32** react with H_2, but triplet nitrenes **7**–**8** (in blue) do not react. Triplet carbene **4** (in blue) displays a temperature-dependent reactivity toward H_2. Energies are given in kcal/mol and include ZPE correction (see appendix, Table A1)

All triplet carbenes and nitrenes for which the reaction with H_2 has been investigated at low temperatures, in addition to the species investigated in this work, are summarized above. Experiments show that, in general, most of the triplet carbenes investigated (such as triplet **5**, **26**–**31** and open-shell singlet diradical **32**) readily react with H_2 in either solid H_2 at 3 K or in H_2-doped Ar matrices at 25–30 K.[98,102] Indeed, such triplet species find a tunneling pathway which is predicted to be exothermic (in between –4 and –10 kcal/mol) and with not so high barriers (1–6 kcal/mol). Interesting cases are the highly electrophilic triplet carbenes **28** and **29**, which have strongly depopulated π orbitals and might insert directly into H_2 showing a singlet-like chemistry.[97] Indeed, for carbenes **28** and **29**, no H/D isotope effects are observed, and DFT calculations predict no barrier for the concerted reaction (although E_a = 2–3 kcal/mol for H-abstraction). On the other hand, carbene **4** shows an unusual temperature-dependent reactivity at such low temperatures, which is interpreted as tunneling through a slightly

endothermic H-abstraction that can become exothermic upon vibrational excitation of the reactants. Following the trend, nitrenes **7** and **8** are found to be unreactive toward H_2, which can be explained by the high barriers and more positive enthalpies compared to those of triplet carbenes.

Overall, the examples shown in Figure 28 are triplet intermediates for which low-temperature reactivity toward H_2 has been studied. So far, variables like chemical identity of the triplet intermediate (carbene or nitrene), barrier shape, enthalpy, and philicity have been taken into account. However, reactivity of carbenes is also governed by the spin state involved in the reactions, this additional variable will be covered in the next chapter.

Spin-Selective Hydrogenation of Carbenes

Introduction

The chemistry of carbenes is controlled by their spin states, which can be either singlet or triplet, resulting in spin-dependent reactions.[2,12] For example, reactions of carbenes with alcohols have been widely investigated to understand the spin-selective chemistry of carbenes.[14,84,87] Singlet carbenes are assumed to insert into O–H bonds, whereas triplet carbenes add to C–H bonds. The reaction pattern of carbenes in solution mainly depends on the population of the equilibrated spin states. However, at cryogenic temperatures, excited spin states cannot be populated, and carbenes are usually formed in their ground spin states.

Trapping experiments with H_2 and O_2 are frequently used in matrix to provide chemical evidence for the formation of triplet carbenes, whereas CO and HCl are probes for singlet reactivity.[143] For example, the ground state multiplicity of the isomeric aryl(trifluoromethyl)carbenes **31** and **39** was established from their thermal reactions with H_2, O_2, and HCl in N_2 matrices.[102] Triplet *m*-methoxyphenyl(trifluoromethyl) carbene **31** thermally reacts with H_2 and O_2 to form adducts **58** and **59**, respectively. On the other hand, the singlet *para* isomer **39** selectively adds to HCl to form a stable chloride **60** (Scheme 15).

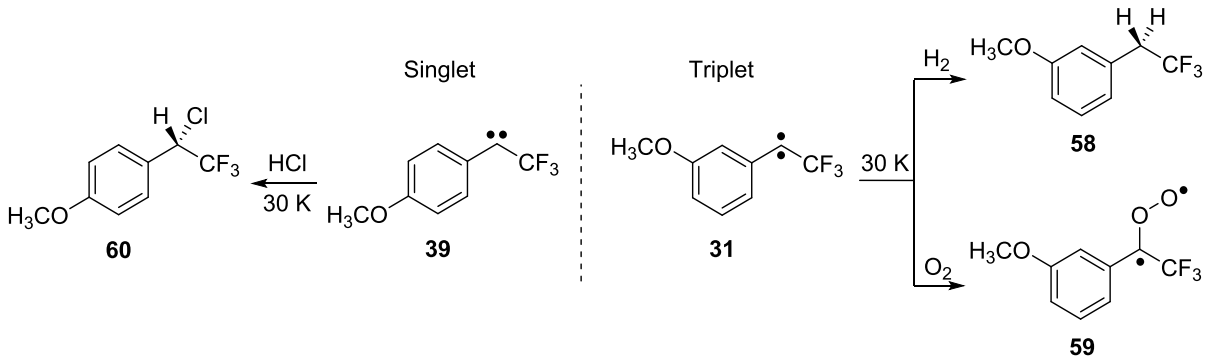

Scheme 15. Spin-selective reaction of isomeric aryl(trifluoromethyl)carbenes **31** and **39** with H_2, O_2, and HCl in low temperature matrices.

Matrix isolation experiments also indicate that H_2 additions might serve as probe not only for triplet carbenes, but also for diradicaloid biscarbenes.[98] Open-shell singlet ($\sigma^2\pi^2$) *p*-bis(chloromethylene)phenylene **32** reacts with H_2 to form singlet chlorophenylcarbene **37**, upon warming of a 2% H_2-doped Ar matrix to 30 K. In contrast, singlet **37**, whether generated from **32** or from the diazirine precursor, does not insert into H_2 under analogue experimental

conditions. Interestingly, close-shell singlet ($\sigma^2\sigma^2$) *p*-bis(fluoromethylene)phenylene **38** is reported to be unreactive toward H_2, in clear contrast to its analogue diradical **32**. This shows that radical-like stepwise hydrogenation of arylcarbenes at low temperatures is more favored than a concerted mechanism.

In general, comparisons of the reactivity of singlet and triplet carbenes toward a chosen substrate are based on kinetic and spectroscopic data, obtained from separated experiments (e.g. isomeric aryl(trifluoromethyl)carbenes **31** and **39**). However, uncertain reproducibility of conditions involving different reactants might spoil the veracity of the results. In this context, bis(*p*-methoxyphenyl)carbene **61** is an interesting case, because its lowest singlet S-**61** and triplet states T-**61** can be simultaneously isolated under matrix isolation conditions.[128] The spin states can be switched via photolysis; 365 nm light irradiation shifts the photostationary equilibrium toward T-**61**, whereas photolysis with $\lambda = 450$ nm photochemically populates S-**61**. Upon annealing at higher temperatures (> 10 K), T-**61** is converted into S-**61**, however, cooling back to 3 K does not restore T-**61**. Hence, depending on temperature and irradiation conditions, matrices containing mainly triplet or singlet carbene can be generated (Scheme 16).

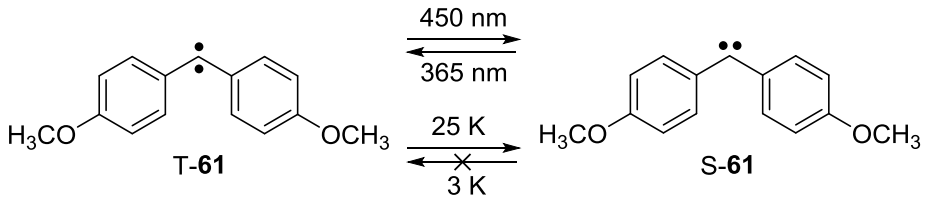

Scheme 16. Singlet-triplet interconversion of bis(*p*-methoxyphenyl)carbene **61** in low-temperature matrices.

Another magnetically bistable carbene, 3-methoxy-9-fluorenylidene **62**, was recently isolated in low-temperatures matrices and fully characterized with IR, UV–vis, and EPR spectroscopy by I. Trosien and T. Thomanek at the Department of Organic Chemistry II of the Ruhr-Universität Bochum. Its spin-specific intermolecular reactivity is currently under investigation.

Other carbenes that show magnetic bistability at low temperatures are 2-naphthyl-(carbomethoxy)carbene[166] and *p*-tolyl(trifluoromethyl)carbene.[167] Rather than being a feature of particular carbenes, magnetic bistability seems to be a general phenomenon that solely depends on the singlet−triplet gap of the carbene, and a similar behavior has recently been discovered for furoylnitrenes.[168] Controlling the spin state of carbenes by thermo- and photochemistry allows to probe the spin-specific reactions of carbenes in a single experiment. In this work, the spin-selective hydrogenation of carbenes **61** and **62** is studied at cryogenic

temperatures. This topic might be useful for applications such as information storage, radical-initiated polymerization processes, as well as in H_2 activation or storage.

Bis(*p*-methoxyphenyl)carbene

Hydrogen matrices

Irradiation of bis(*p*-methoxyphenyl)diazomethane **63** in H_2 matrices at 3 K upon visible light (λ = 560 nm) results in the disappearance of the signals assigned to **63** (1515, 1251, 1048, and 830 cm^{-1}), and a complex spectrum is obtained, which differs noticeably from the one reported in Ar matrices (Figure 29).[128] Photolysis of an Ar matrix containing **63** with λ = 520–560 nm produces S-**61** and T-**61** in a ratio of approximately 50:50, which is determined by analysis of the signals located at 831 cm^{-1} (S-**61**) and 816 cm^{-1} (T-**61**).

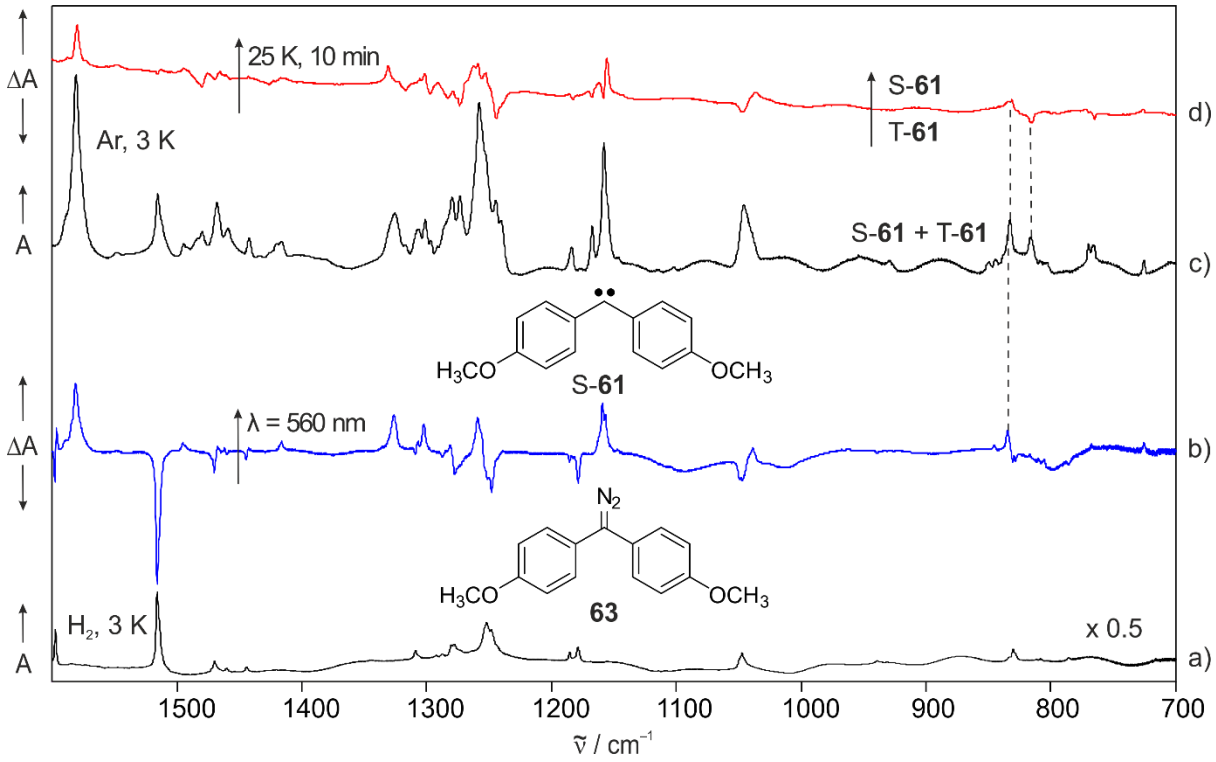

Figure 29. IR spectra showing the photochemistry of bis(*p*-methoxyphenyl)diazomethane **63** in H_2 matrices. a) IR spectrum of **63** in H_2 at 3 K. b) Difference IR spectrum obtained after irradiating **63** with λ = 560 nm in H_2 at 3 K. c) IR spectrum of bis(*p*-methoxyphenyl)carbene **61** in Ar at 3 K, obtained after irradiating **63** with λ = 560 nm. The ratio S-**61**/T-**61** is approximately 50:50. d) Difference IR spectrum showing the interconversion of T-**61** into S-**61**, after annealing an Ar matrix containing both T-**61** and S-**61** at 25 K for 10 min. The dashed lines indicate the signal positions of S-**61** and T-**61**; only S-**61** is observed in (b).

Analysis of the spectra obtained after photolysis in H_2 shows a selective formation of S-**61** with characteristic IR signals at 1582, 1326, 1259, and 834 cm^{-1}. In contrast to the experiments in Ar, triplet T-**61** is generated only in traces with a 98:2 ratio of S-**61** to T-**61**. In H_2, the characteristic signals of S-**61** and T-**61** are slightly blue-shifted and appear at 834 and 817 cm^{-1}, respectively. The signals corresponding to S-**61** diminish as the matrix is irradiated with λ = 365 nm for several hours. Simultaneously, a set of new signals appear at 1515, 1251, and 1048 cm^{-1} and are assigned to the H_2-insertion product, bis(*p*-methoxyphenyl)methane **64**. The spectrum obtained after complete photochemistry is in good agreement with a spectrum of matrix-isolated **64**, as independently recorded in Ar at 3 K (Figure 30).

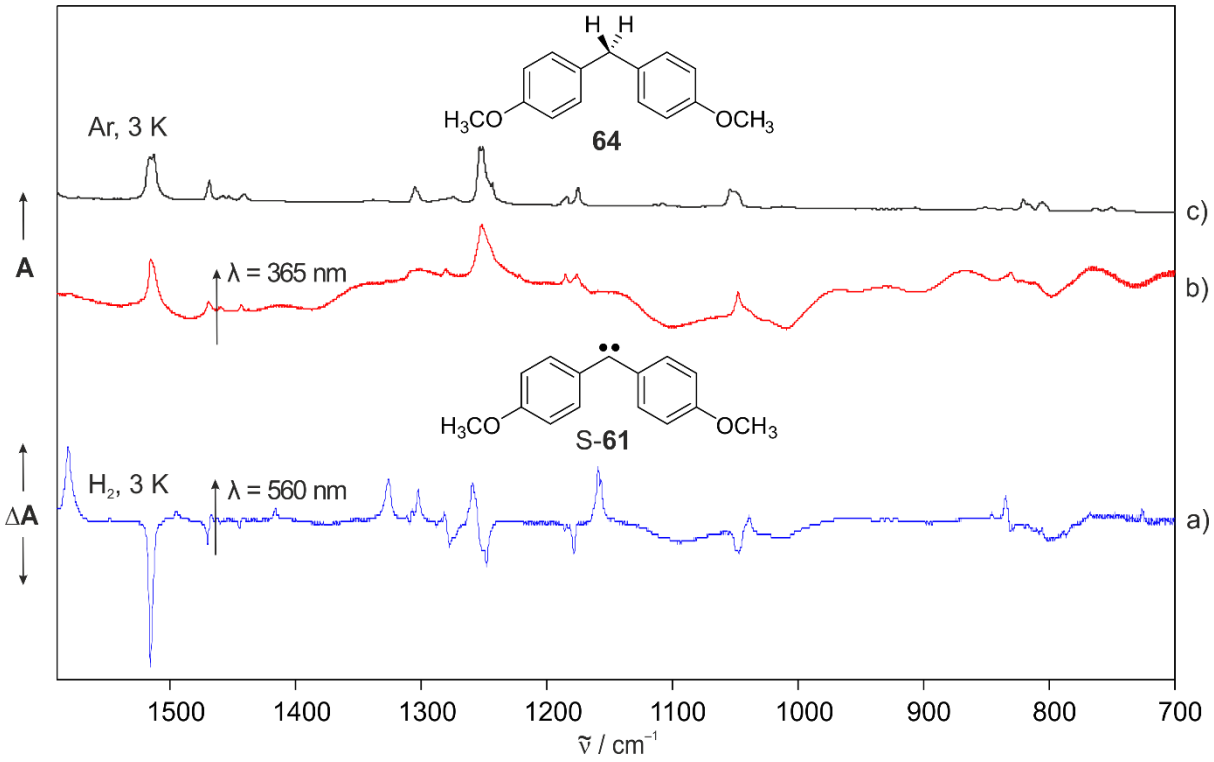

Figure 30. IR spectra showing the photochemistry of bis(*p*-methoxyphenyl)carbene **61** in H_2 matrices. a) Difference IR spectrum obtained after irradiating bis(*p*-methoxyphenyl)diazomethane **63** with λ = 560 nm in H_2 at 3 K. b) IR spectrum obtained after irradiating S-**61** with λ = 365 nm in H_2 at 3 K. c) IR spectrum of bis(*p*-methoxyphenyl)methane **64** in Ar at 3 K.

It should be noticed that some of the spectral features of **64** (e.g. 1309 and 1170 cm^{-1}) do not appear in H_2 as intense as in Ar. This discrepancy could be a result of comparing spectra measured in different matrices and/or related to the rich conformational landscape of **64**. In principle, deposition of **64** from room temperature onto the cold window should result in a mixture of the nearly-degenerate conformers (arising from the orientation of the methoxy groups) to be trapped in the matrix. For carbene T-**61**, three nearly-degenerate conformers were

detected by electron-nuclear double resonance (ENDOR) spectroscopic measurements in MTHF glasses at 10 K.[128] However, a photochemical generation of **64** at 3 K without thermal equilibration, could be more conformational-specific, resulting in a slightly different spectrum. From these experiments, it is possible to conclude that the hydrogenation reaction of carbene **61** occurs selectively from the triplet state T-**61**. Signals corresponding to T-**61** are extremely weak and might correspond to carbene molecules trapped in non-reactive matrix sites. In contrast, S-**61** is indefinitely stable in H_2 matrices at 3 K and does not react upon annealing the matrix at 4–5 K. Rather, S-**61** reacts with H_2 upon irradiation with $\lambda = 365$ nm, which is known to initiate the conversion of S-**61** into T-**61**. The higher reactivity of triplet carbenes compared to singlets toward H_2 was already suggested by Sheridan et al., by studying the thermal reactions in H_2-doped Ar matrices.[98,102] However, if T-**61** readily reacted with H_2 upon generation from precursor **63**, then product **64** should be detectable in the matrix. This encounter the problem that the remaining **63** has a very similar spectrum than the produced **64**, making it difficult to detect the latter compound with certainty. Another open question is whether the photochemical conversion of S-**61** into **64** occurs via T-**61** or not. Both questions will be adressed in the next sections.

Deuterium matrices

Similar experiments were carried out in D_2 matrices. Since D_2 matrices are less volatile than H_2 matrices, a wider range of photolytic and annealing conditions can be explored with less risk of boiling off the matrix. Moreover, isotope effects are important to assess the role of QMT in these reactions. Irradiation of matrix-isolated precursor **63** at 3 K with $\lambda = 560$ nm gives a spectrum that resembles previous results; singlet carbene S-**61** is predominantly formed (96%), whereas only traces of triplet carbene T-**61** (4%) are detected (Figure 31).

In general, most of the signals assigned to **61** in H_2, D_2 and Ar matrices are quite broad due to the presence of a mixture of conformers. Nevertheless, a careful examination of the spectrum obtained in D_2 reveals additional signals that are not present in the experiments in Ar. These signals at 1252, 1082, and 1047 cm^{-1} match with the spectrum of the matrix-isolated D_2-insertion product, 1,1-dideuterobis(*p*-methoxyphenyl)methane d_2-**64**. Moreover, the signal at 1515 cm^{-1} (C=C str. ring) that is assigned to both **63** and d_2-**64**, is much more intense than the expected contribution from unconverted precursor **63** in the matrix after long time photolysis (by correlating intensities of the signals of **63** with its unperturbed C=N=N

stretching vibration at 2044 cm^{-1}). This shows that the absence of T-**61** is a consequence of the reaction with D_2 and not a result of a selective formation of S-**61** in D_2 matrices, which would have been an extreme case of host effect (since both S-**61** and T-**61** are equally produced in Ne, Ar, or Xe matrices). Moreover, the spin-selective formation of S-**61** is independent of both the irradiation time (from a few minutes to several hours) and the extent of the conversion from **63** into **61** (either small fraction or complete). This could mean that the reaction of T-**61** with H_2/D_2 is faster than its generation. However, it is not clear if the photolysis of **63** forms S-**61** and T-**61** directly in one step, or the photoequilibration of the spin states occurs before reaction. In any case, the time resolution of the spectrometer (minute scale) does not allow to withdraw any conclusion in this regard.

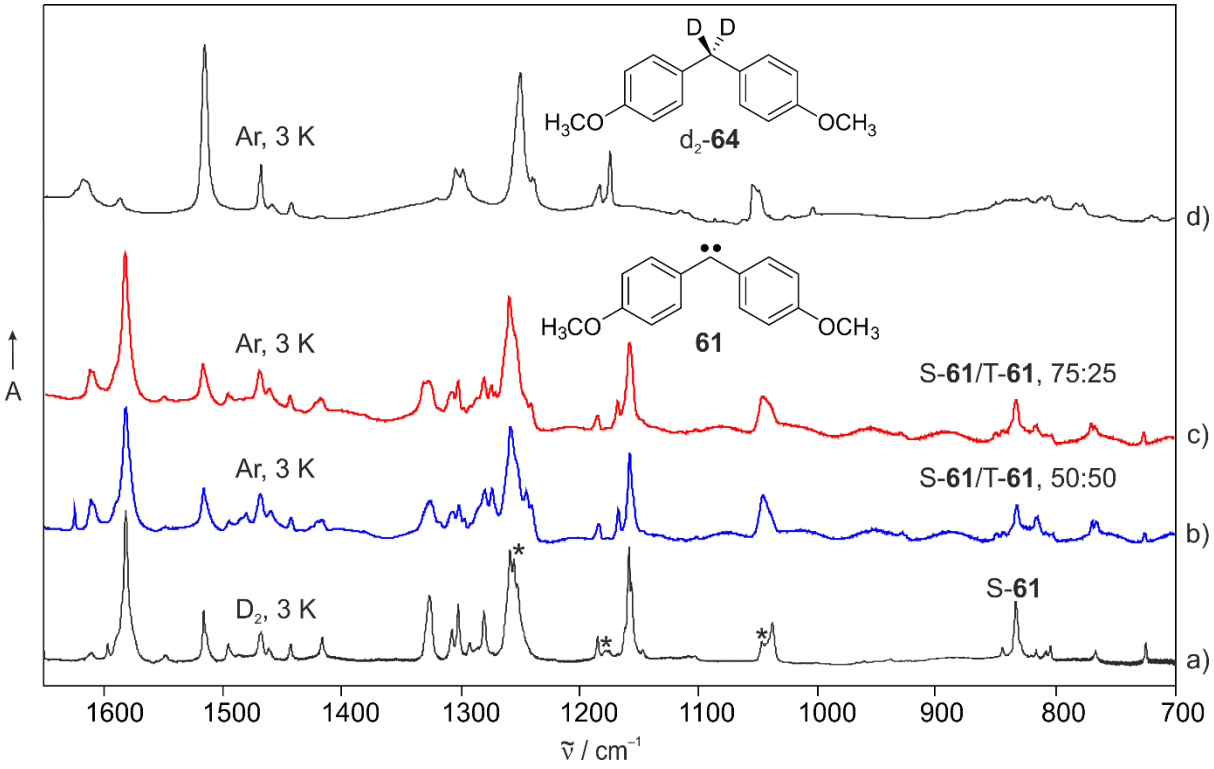

Figure 31. IR spectra showing the photochemistry of bis(*p*-methoxyphenyl)diazomethane **63** in D_2 matrices. a) IR spectrum of bis(*p*-methoxyphenyl)carbene **61** in D_2 at 3 K, obtained after irradiating **63** with λ = 560 nm. b) IR spectrum of bis(*p*-methoxyphenyl)carbene **61** in Ar at 3 K, obtained after irradiating **63** with λ = 560 nm. The ratio S-**61**/T-**61** is approximately 50:50. c) IR spectrum of bis(*p*-methoxyphenyl)carbene **61** in Ar at 3 K, obtained after annealing an Ar matrix containing both T-**61** and S-**61** at 25 K for 10 min. The ratio S-**61**/T-**61** is approximately 75:25. d) IR spectrum of 1,1-dideuterobis(*p*-methoxyphenyl)methane d_2-**64** in Ar at 3 K. IR signals marked as (*) in spectrum (a) are assigned to d_2-**64**.

Similar to the behavior observed in H_2 matrices, S-**61** remains stable in D_2 matrices upon annealing the matrix at 6 K for 24 h. The reaction of S-**61** with D_2 is only activated upon photolysis with λ < 500 nm. Irradiation with λ = 450 or 365 nm produces a decrease of the

signals corresponding to S-**61**, accompanied by an increase of the features assigned to d_2-**64**. Irradiation with λ = 365 nm is more efficient, and a complete conversion of S-**61** into d_2-**64** is achieved after several hours of photolysis (Figure 32).

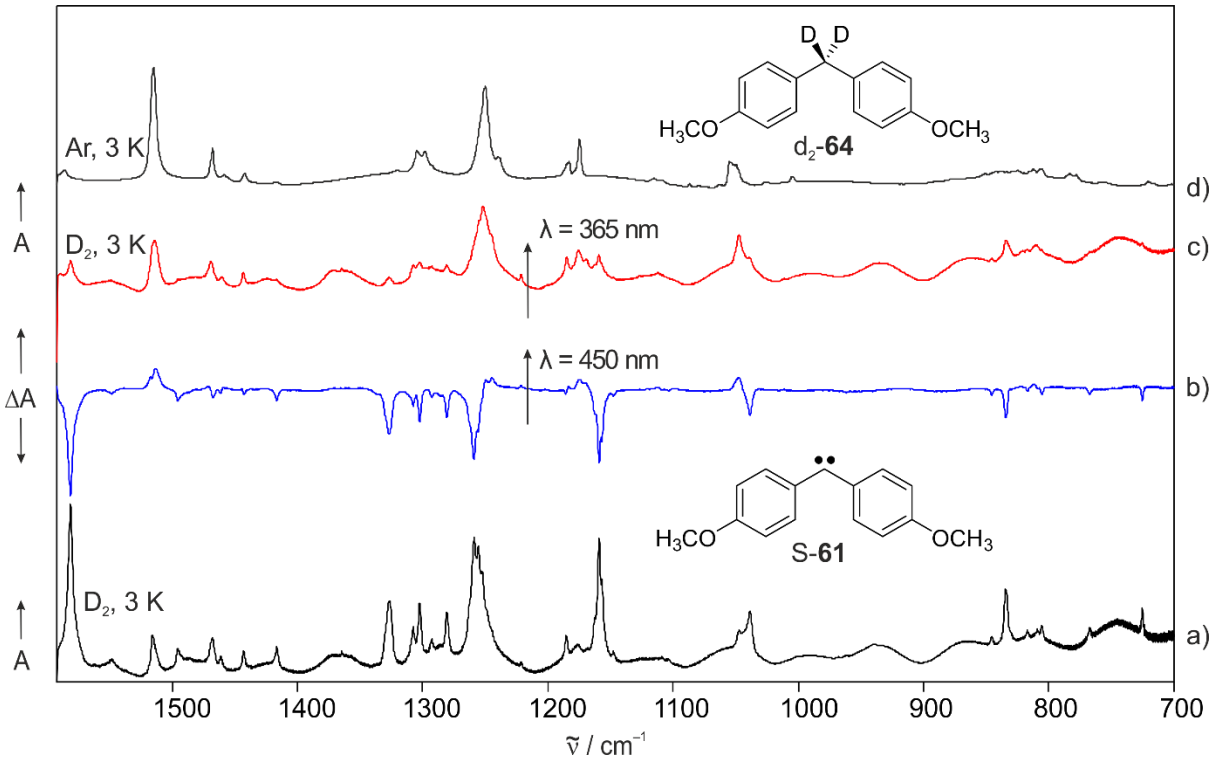

Figure 32. IR spectra showing the photochemistry of bis(*p*-methoxyphenyl)carbene **61** in D_2 matrices. a) IR spectrum of **61** in D_2 at 3 K, obtained after irradiating bis(*p*-methoxyphenyl)diazomethane **63** with λ = 560 nm. b) Difference IR spectrum obtained after irradiating **61** with λ = 450 nm in D_2 at 3 K. c) IR spectrum obtained after irradiating **61** with λ = 365 nm in D_2 at 3 K. d) IR spectrum of 1,1-dideuterobis(*p*-methoxyphenyl) methane d_2-**64** in Ar at 3 K.

In Ar matrices, the interconversion between S-**61** and T-**61** can be induced photochemically. The initial S-**61**/T-**61** ratio of 50:50 (once the photostationary equilibrium is formed) changes to 75:25 (maximum ratio) upon visible-light irradiation (450 nm) for 10 min. In contrast, 365 nm irradiation for several hours leads to S-**61**/T-**61** ratios greater than 20:80.[128] From the experimental observations it can be concluded that if T-**61** is not present, the amount of S-**61** in an Ar matrix is invariable upon 450 nm photolysis. However, 450 nm photolysis in D_2 matrices converts S-**61** into d_2-**64**. The mechanism might involve the formation of an excited singlet state S*-**61** since the formation of the reactive T-**61** is excluded by using visible light. In case of the efficient 365 nm photolysis, the most probable pathway from S-**61** to d_2-**64** might proceed via T-**61**, although a photoactivated singlet reaction cannot be ruled out. Therefore, upon 365 nm light, one cannot clearly state whether S-**61** is decreasing because is reacting via

S*-**61** or is converting into the T-**61**. It is also possible that both pathways (S-**61**→S*-**61**→**64**) and **(**S-**61**→T-**61**→**64**) are competing processes.

Additionally, UV–vis experiments were carried out to further investigate on the spin-selectivity found in the hydrogenation of carbene **61**. Precursor **63** was deposited along with an excess of D_2 at 3 K. Its UV–vis spectrum features two strong bands at 280 and 230 nm, and a very weak and broad band centered at 535 nm (assigned to the n→π* transition). These bands decrease in intensity as the matrix is irradiated with λ = 560 nm, and a strong band at 380 nm is formed concomitantly (Figure 33).

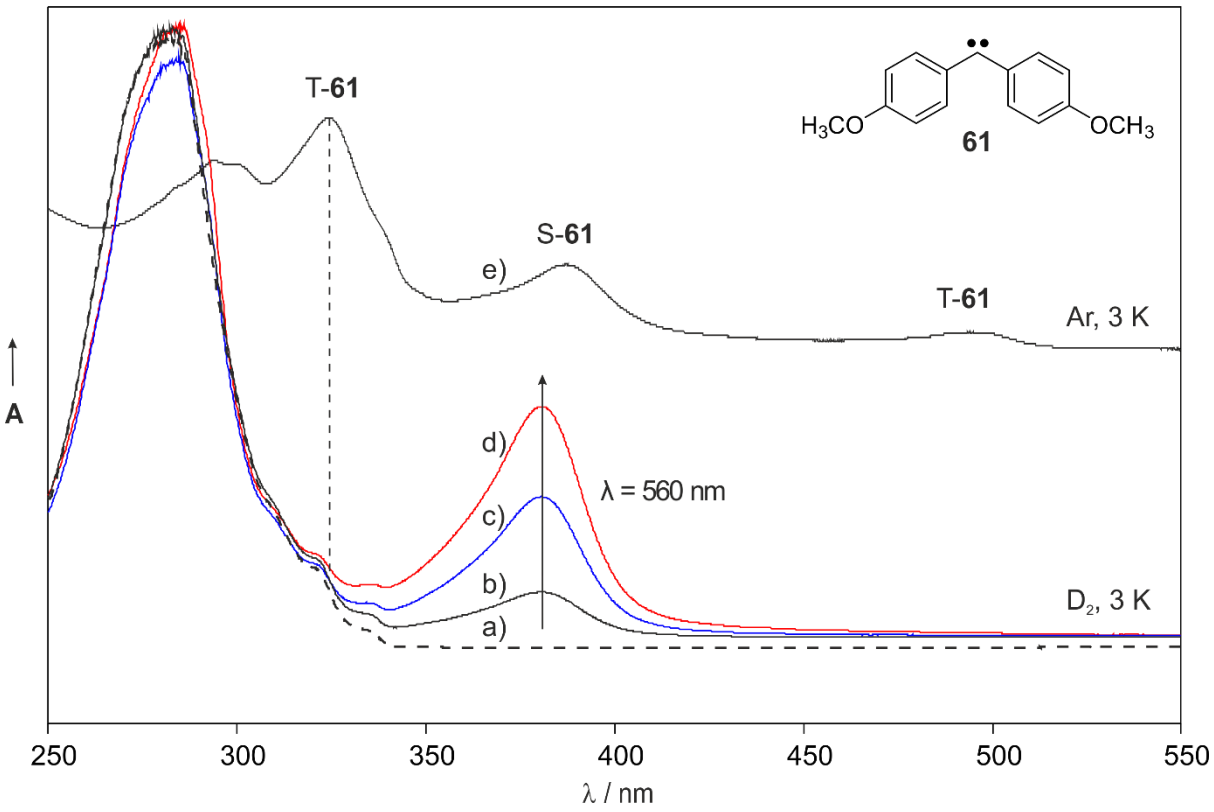

Figure 33. UV–vis spectra showing the photochemistry of bis(*p*-methoxyphenyl)diazomethane **63** in D_2 matrices. a) UV–vis spectrum of **63** in D_2 at 3 K b-d) UV–vis spectra obtained after irradiating **63** with λ = 560 nm for 30 min, 1 h, and 4 h, respectively. e) UV–vis spectrum of bis(*p*-methoxyphenyl)carbene **61** in Ar at 3 K, obtained after irradiating **63** with λ = 560 nm for 12 h. The dashed line indicates the strongest band position of T-**61**; no corresponding band was observed in (b-d).

This band is assigned to the singlet state of carbene **61** by comparison to the UV–vis spectrum of **61**, which is obtained by photolysis of precursor **63** in Ar matrices.[128] The triplet state of **61** is characterized by two absorption bands located at 483 nm (weak) and 316 nm (strong), which are not present in the D_2 matrix. This finding agrees with the results obtained from the IR measurements, only the singlet state of **61** is observed in D_2 matrices at 3 K. Although traces

of T-**61** are identified in the IR experiments, the characteristic band of T-**61** at 384 nm is not observed in the UV–vis spectra recorded in D_2 matrices. This is surprising considering the higher sensitivity of UV–vis spectroscopy compared to IR spectroscopy. A possible reason might be that the very weak absorption bands of T-**61** (being present as traces) are overlapped by the strong bands of the precursor **63** and the singlet S-**61**. The D_2-insertion product d_2-**64** cannot be identified in these spectra, since all bands are located at wavelengths lower than 300 nm and overlap with those of precursor **63**.

Although it was possible to detect small amounts of T-**61** in all IR experiments, such species could not be identified by the more sensitive UV–vis spectroscopy in D_2 matrices. To shed light into the formation of T-**61**, matrix X-band (9.5 GHz) EPR experiments were carried out. As a highly sensitive technique for paramagnetic species, even traces of T-**61** are easily detected, and with the advantage of having no interference of the other EPR-silent species like S-**61** and **64**. Photolysis of **63** in solid Ar or D_2 at 5 K results in the formation of T-**61**, albeit its characteristic signals are much more intense in Ar than in D_2 matrices (Figure 34).

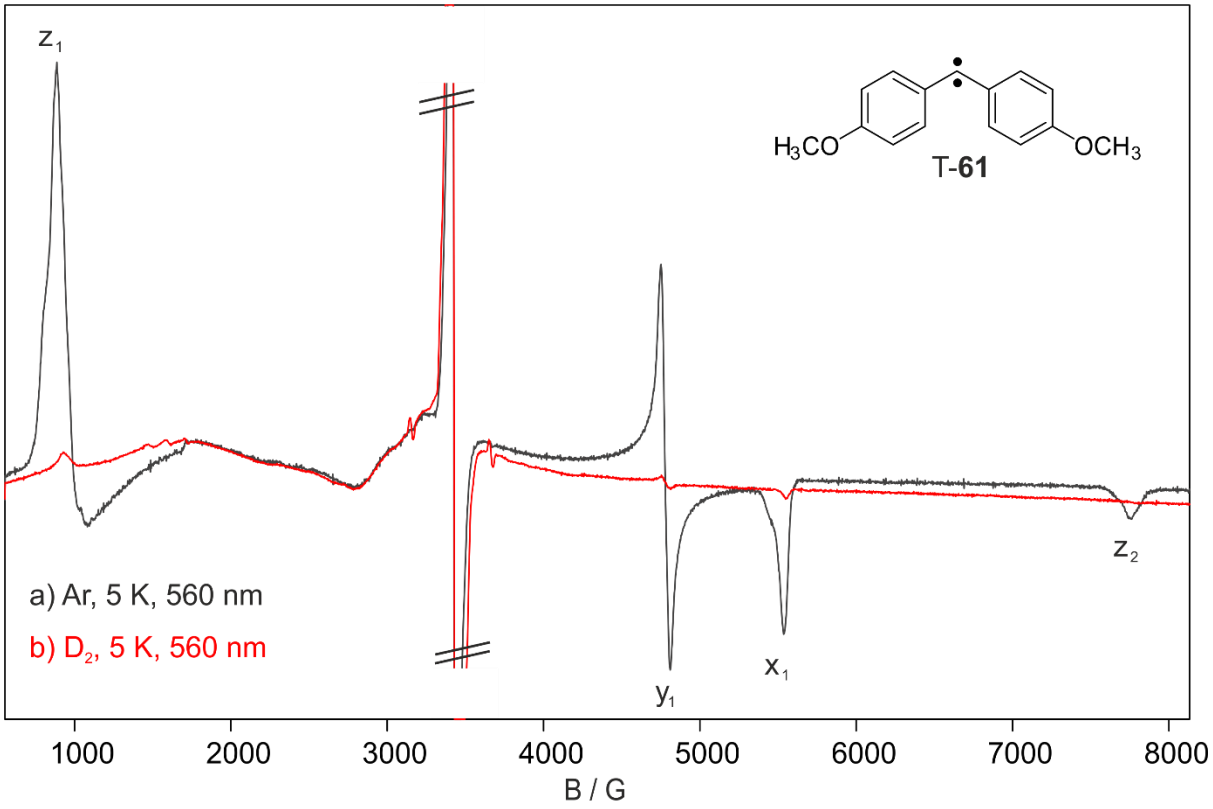

Figure 34. EPR spectra showing the formation of triplet bis(*p*-methoxyphenyl)carbene T-**61** in Ar and D_2 matrices. a) EPR spectrum obtained after irradiating bis(*p*-methoxyphenyl)diazomethane **63** with λ = 560 nm in D_2 at 5 K. b) EPR spectrum obtained after irradiating **63** with λ = 560 nm in D_2 at 5 K. Both experiments were performed under experimental conditions as similar as possible.

The EPR spectrum of T-**61** obtained in Ar matrices agrees with the one reported in literature.[128] Carbene T-**61** shows a characteristic spectrum, which is dominated by a large zero-field splitting (zfs) due to the anisotropic dipolar interaction of the two electron magnetic moments. Spin-Hamiltonian-based simulations yield zfs parameters of $|D/hc| = 0.4096\ cm^{-1}$ and $|D/hc| = 0.0190\ cm^{-1}$; those are close to the values reported for the parent diphenylcarbene **4** ($|D/hc| = 0.417\ cm^{-1}$ and $|E/hc| = 0.019\ cm^{-1}$).[18] The experiment was repeated in D_2 matrices using the same experimental procedure for deposition of sample, photolysis, and recording spectra. However, irradiation with $\lambda = 560$ nm in D_2 matrices produces very weak signals, which are only formed after several hours of irradiation. The integrated intensity of the z_1 canonical transition in D_2 is 1/50 of the value obtained in the Ar matrix. These values cannot be directly compared since the amount of the EPR-silent precursor **63** present in the matrix is unknown. Nevertheless, the results are qualitatively consistent with the observations from the IR and UV–vis experiments. The carbene signals are formed together with an intense, unresolved signal centered at 3430 G, which is attributed to an unknown radical species. In addition, small signals corresponding to D atoms (3340, 3418, 3496 G; hyperfine coupling 78 G) are observed and could be products of the reaction of T-**61** with D_2, but could also be originated from the photochemical cleavage of D_2 itself. Further irradiation with $\lambda = 365$ nm results in a small increase of the triplet signals, whereas upon 450 nm irradiation the triplet signals are bleached. These observations are not conclusive since the amount of unreacted precursor (if some) is again unknown. The experiments described above (IR, UV–vis and EPR spectroscopy) show that both H_2 or D_2 selectively react with the triplet state of carbene **61** upon photochemical generation in matrices at 3 K. Moreover, no appreciable isotope effects are found, suggesting that the reaction is activated by photochemistry (Scheme 17).

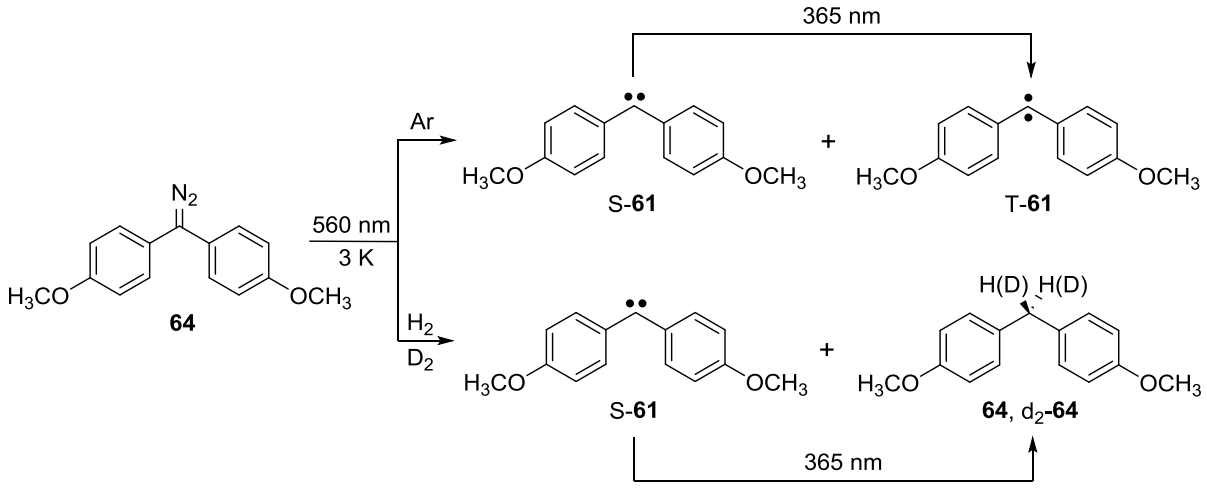

Scheme 17. Spin-selective reactivity of bis(*p*-methoxyphenyl)carbene **61** in H_2 and D_2 matrices.

Hydrogen-doped Inert Gas Matrices

Experiments in H_2-doped inert gas matrices allow to produce and trap carbenes in high yields, before permitting H_2 molecules to diffuse and potentially react. This methodology allows studying the thermal reaction (most probably assisted by tunneling) of carbene **61** and H_2 at different temperatures with no influence of light. Precursor **63** was deposited along with an excess of 5% H_2-doped Ar at 3 K and irradiated with λ = 560 nm to generate carbene **61**. The resulting spectrum shows, as expected, the formation of both S-**61** and T-**61** in a 50:50 ratio, approximately (Figure 35).

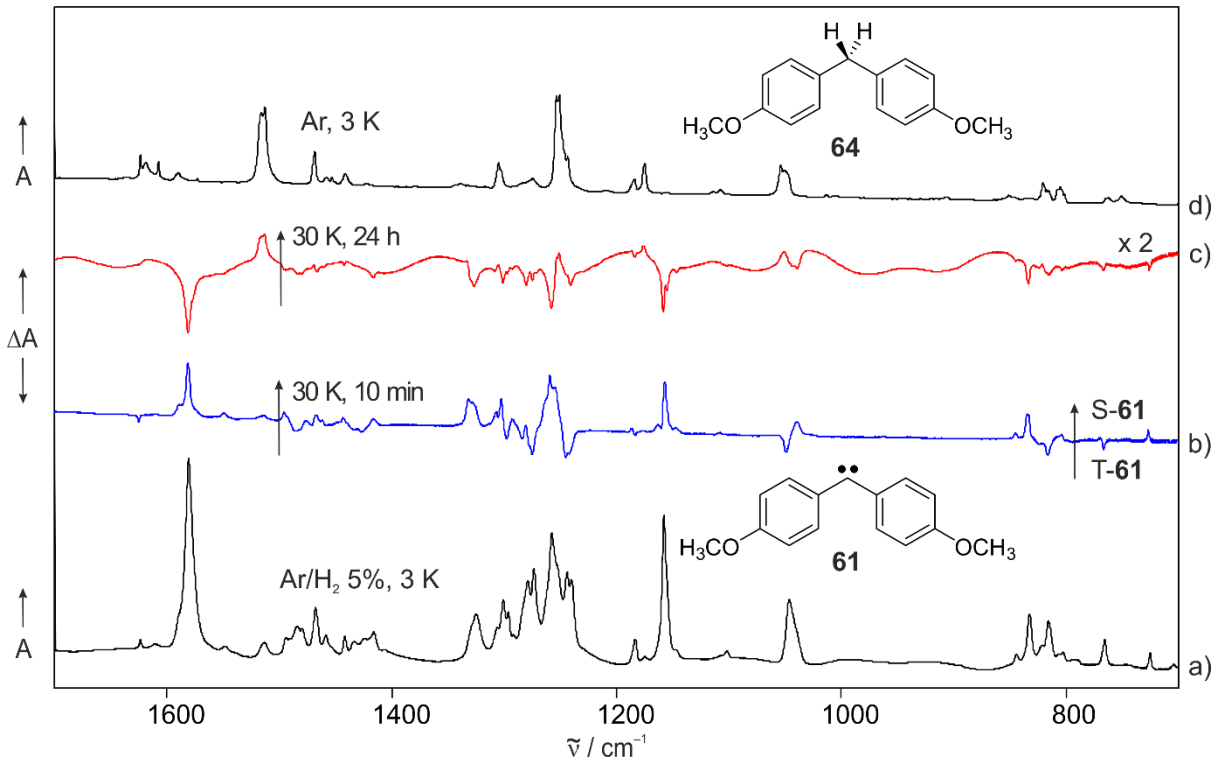

Figure 35. IR spectra showing the reaction of bis(*p*-methoxyphenyl)carbene **61** with H_2 in Ar matrices. a) IR spectrum of **61** in Ar at 3 K, obtained after irradiating bis(*p*-methoxyphenyl)diazomethane **63** with λ = 560 nm. The ratio S-**61**/T-**61** is approximately 50:50. b) Difference IR spectrum showing the interconversion of T-**61** into S-**61** after annealing an Ar matrix containing both T-**61** and S-**61** at 30 K for 10 min. c) Difference IR spectrum obtained after annealing **61** in 5% H_2-doped Ar at 30 K for 24 h. d) IR spectrum of bis(*p*-methoxyphenyl) methane **64** in Ar at 3 K.

In Ar matrices, the S-**61**/T-**61** ratio increases upon annealing due to the irreversible conversion of T-**61** into S-**61**. Upon annealing, the Ar matrix become softer, which enables the conformational relaxation of carbene **61**, and hence the interconversion of states seems to occur (by crossing over a small barrier). In this experiment, the relative population of S-**61** increases upon annealing to 10 K (55:45), and even more when reaching 20 K (73:27). At 25–30 K, the equilibration of states fully takes place by reaching the maximum ratio observed in Ar matrices

(76:24).[128] Overall, annealing the matrix from 3 to 30 K (over 10 min) is dominated by the ISC process, and there is initially no formation of the H_2-insertion product **64**. However, keeping the matrix at 30 K for 24 h results in a decrease of all bands assigned to both S-**61** and T-**61**, accomplished by an increase of the spectral features assigned to the H_2-insertion product **64**.

The kinetics of the reaction of carbene **61** in 5% H_2-doped Ar matrices was followed by observing the temporal change of the intensities corresponding to the characteristic IR signals at 1515 cm^{-1} (**64**), 831 cm^{-1} (S-**61**), and 816 cm^{-1} (T-**61**). Likewise, the evolution of the S-**61**/T-**61** ratio was monitored during 15 h and compared to the values obtained during warming up (3→30 K). Since this is a complex reaction, the values of the integrated signals corresponding to the three species (S-**61**, T-**61**, and **64**) were separately fitted to a pseudo-first order kinetics,[133] as shown in Figure 36.

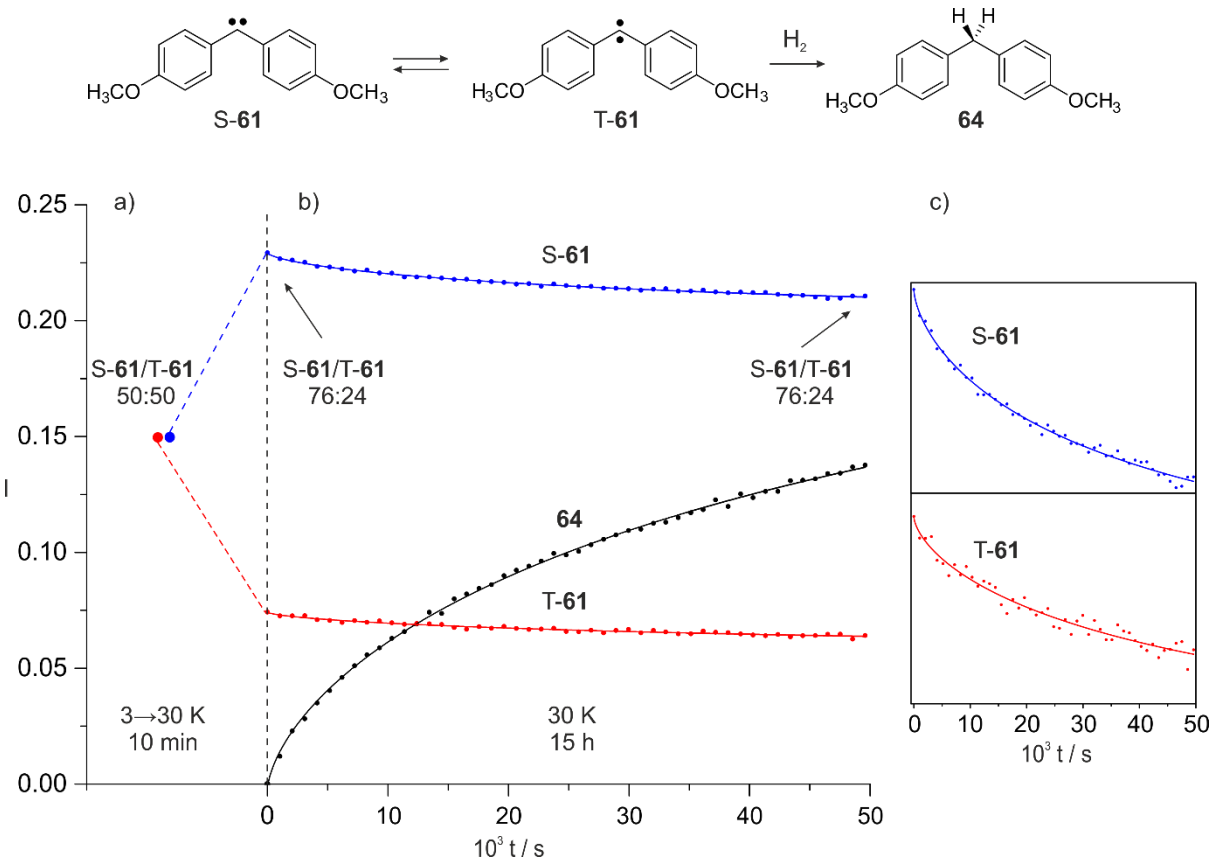

Figure 36. Dynamics of the reaction of bis(*p*-methoxyphenyl)carbene **61** with H_2 in Ar matrices. a) Diagram showing the interconversion of T-**61** into S-**61** after annealing an Ar matrix containing both S-**61** and T-**61** at 30 K for 10 min. The S-**61**/T-**61** ratio increases from (50:50) to (76:24). b) Plot of the increasing intensity of the IR signal at 1515 cm^{-1} (**64**), and the decreasing intensity of the IR signals at 831 cm^{-1} (S-**61**) and 816 cm^{-1} (T-**61**) to Eq. (8), as recorded in 5% H_2-doped Ar matrices at 3 K. c) Zoom-in of the plots corresponding to the decay of T-**61** and S-**61** at 30 K. Integrated intensities of the signal at 831 cm^{-1} (S-**61**) were divided by a factor of 2.15, which is the ratio between the molar absorptivities of the signals at 831 cm^{-1} and 816 cm^{-1}.

Kinetics measurements show that after the fast equilibration of S-**61** and T-**61** takes place at 30 K, both S-**61** and T-**61** decay about a 10 % within 15 h. The relative population of T-**61** with respect to the total amount of carbene **61** remains constant (in between 23.6 and 24.4%) throughout the duration of the annealing at 30 K. Moreover, the pseudo-first order rate constants reflecting the decay of S-**61** and T-**61**, and the formation of product **64** are comparable and in the order of 1.7–2.1 × 10^{-5} s^{-1} as shown in Table 6.

Table 6. Rate constants (as fitted to Eq. (8) with β = 0.65) for the reaction of bis(*p*-methoxyphenyl) carbene **61** with H_2 and D_2 under different experimental conditions.

Exp.	Host	Temp	Species	k (s^{-1})	S-**61**/T-**61** ratio
1	Ar/H_2	30 K	S-**61**	2.1 ± 0.5 × 10^{-5}	76:24
			T-**61**	1.6 ± 0.9 × 10^{-5}	
			64	1.7 ± 0.1 × 10^{-5}	
2	Ar/D_2	30 K	S-**61**	7 ± 3 × 10^{-6}	76:24
			d_2-**64**	5.1 ± 0.8 × 10^{-6}	
3	Ne/H_2	8 K	**64**	6 ± 1 × 10^{-6}	82:18

The integrated signals corresponding to the three species (S-**61**, T-**61**, and **64**) were independently fitted to pseudo-first order kinetics. In the Ar/D_2 and Ne/H_2, the change in the intensities of the signals of S-**61** and T-**61** is too small to allow for a proper kinetic analysis.

The rate constants should be interpreted with caution, because they represent an average of a distribution of reaction rates associated with multiple matrix sites. In these experiments, dispersive plots are found with dispersion coefficients of β = 0.65, which are far from the ideal value of one, and the corresponding rate constants strongly depend on the choice of β. Another complication is that the IR signals of S-**61** and T-**61** used for the analysis are very weak (the others overlap between them), generating intrinsic errors during integration. However, both the rate constants and the relative population of S-**61** and T-**61** allow to shed light into the complex mechanism of hydrogenation of carbene **61**.

Several ideas regarding the reaction mechanism might be considered: i) S-**61** reacts with H_2 to form **64** at the same rate as T-**61** does; ii) S-**61** converts into T-**61** and the latter subsequently produces **64** as a consecutive reaction; iii) S-**61** and T-**61** are in equilibrium and react with H_2 from one state, perhaps via a more feasible triplet PES. It is unlikely that S-**61** and T-**61** parallelly react at the same rate (i), based on the contrasting reactivity displayed in H_2 and D_2 matrices at 3 K. Moreover, numerous examples in literature show that triplet carbenes are generally more reactive than singlets toward H_2 in low-temperature matrices.[65,85,98,102] In hypothesis (ii), the S-**61**/T-**61** ratio should not remain constant during the reaction. A faster

rate constant for the reaction with H_2 of either S-**61** or T-**61** would change the relative population of the states. It is therefore suggested that the reaction proceeds through T-**61** and S-**61** rearranges to T-**61** in order to recover the decreasing amount of T-**61**, maintaining the equilibrium between both spin states (iii). This implies that the ISC between states is faster than the hydrogenation reaction. For example, the thermal rearrangement of triplet *p*-tolyl(trifluoromethyl)carbene to its singlet state takes place at rates of $1–2 \times 10^{-4}$ s^{-1} in Ar (25–30 K) and Xe (40–50 K), showing that the ISC process does not depend on temperature, but it is activated once the matrix host is soft enough.[167] Moreover, the interconversion between states is about one order of magnitude faster than the rates observed ($\sim 10^{-5}$ s^{-1}) for the reactions of carbenes **4** and **61** with H_2 or H_2O.[17,128]

Singlet-to-triplet interconversion in bimagnetically stable carbenes is reported to reach high yields (S/T ratio <20%) after prolonged 365 nm irradiation.[128,167] In H_2-doped Ar matrices, photolysis of the matrix (while at 30 K) with 365 nm light for 12 h completely transforms carbene **61** into product **64**. This process is very efficient (in contrast to separated photolysis or annealing) because it facilitates the constant generation of T-**61** while H_2 is freely diffusing. These observations suggest than the thermal reaction of **61** with H_2 at 30 K proceeds via the more reactive triplet state.

Further investigations on this reaction were performed by repeating the experiment in 5% D_2-doped Ar matrices. Carbene **61** was generated at 3 K, and upon annealing the matrix at 30 K, signals assigned to S-**61** and T-**61** decrease and the concomitant formation of product d_2-**64** is observed. The rate constant for the formation of d_2-**64** is determined to be $5.1 \pm 0.8 \times 10^{-6}$ s^{-1}, which is about three times smaller than that of **64** obtained in Ar/H_2 ($1.7 \pm 0.1 \times 10^{-5}$ s^{-1}). Such a small isotopic ratio agrees with the results from the experiments in solid H_2 and D_2, where no KIE was observed. On the other hand, the S-**61**/T-**61** ratio remains constant (76:24) during annealing at 30 K, in agreement with the "equilibration" hypothesis.

In Ne/H_2 matrices, irradiation of **63** with $\lambda = 560$ nm (OPO laser at low power) at 3 K produces S-**61** in higher quantities, as indicated by a S-**61**/T-**61** ratio of 55:45. This ratio differs from the one obtained in pure Ne matrices (47:53), and is a consequence of the photoannealing that permits H_2 molecules to diffuse and readily react with T-**61**. If the photolysis is conducted with an intense 530 nm LED placed close to the cold window, the relative population of T-**61** decreases even more (62:38). These results show that T-61, photoproduced at 3 K, readily reacts with accessible H_2 molecules. The yield of the reaction depends on the softness of the

host and the concentration of H_2 in the matrix (S-**61**/T-**61** ratio of 98:2 (H_2), 96:4 (D_2), 55:45 (Ne/H_2), and 50:50 (Ar/H_2)). The rate constant for the formation of **64** in H_2-doped Ne matrices at 8 K is determined to be $6 \pm 0.8 \times 10^{-6}$ s^{-1}, showing a temperature dependence, like in case of diphenylcarbene **4**. At this temperature, the S-**61**/T-**61** ratio is found to be (82:18), which is intermediate compared to the values obtained in H_2 and Ar matrices.

Overall, monitoring the relative population of the spin states of **61** throughout the hydrogenation reaction was shown to shed light into the reaction mechanism and spin-dependent processes. However, comparing those ratios in different matrices might be misleading since the hosts interact differently with the trapped carbenes, and the more polar singlet states could be more stabilized than the triplet states. Moreover, the dispersive matrix environment is likely to produce a distribution of S/T ratios and S–T energy splittings.

Calculations

In order to understand the remarkable spin-selectivity observed for the hydrogenation of carbene **61**, the reactions of both S-**61** and T-**61** with H_2 have been studied computationally. The S–T splitting of **61** is calculated to be 2.2 kcal/mol at the B3LYP-D3/def2-TZVP level of theory, and –0.3 kcal/mol (with S-**61** as ground state) when the energy is refined at the CCSD(T)/cc-pVDZ level of theory. Likewise, the latter method predicts S-**61** to be 0.2–0.4 kcal/mol more stable than T-**61**, when considering all combinations of conformers. This agrees with the experimental observations, which indicate a slightly more stable singlet state (irreversible thermal T→S interconversion), but at the same time, expecting a ground state triplet or nearly degenerate singlet and triplet states (linear Curie-Weiss plot).[128]

Reaction profiles for bis(*p*-methoxyphenyl)carbene **61** in the singlet (blue) and triplet (red) spin states are reported in Figure 37. Energy calculations along the intrinsic reaction path were carried out at the B3LYP-D3/def2-TZVP level of theory and all relevant stationary points recomputed at the CCSD(T)/cc-pVDZ level of theory. Because of the contrasting reaction mechanisms of singlet and triplet carbenes, a reaction coordinate (e.g. d(C–H) or d(H–H) as in Figure 25) which is physically meaningful for both states cannot be chosen. Instead, standard IRCs are used for a qualitative comparison on the singlet and triplet energy curves. By definition, IRC in mass-weighted coordinates (in units of amu $^{1/2}$bohr) encompasses the reduced masses and the traveled arc lengths of all atoms in the molecule, thus representing the reaction path in a single dimension. The use of these coordinates is controversial for predicting

tunneling pathways and barrier widths, however, they have extensively been used for comparing carbene reactions.[69-71]

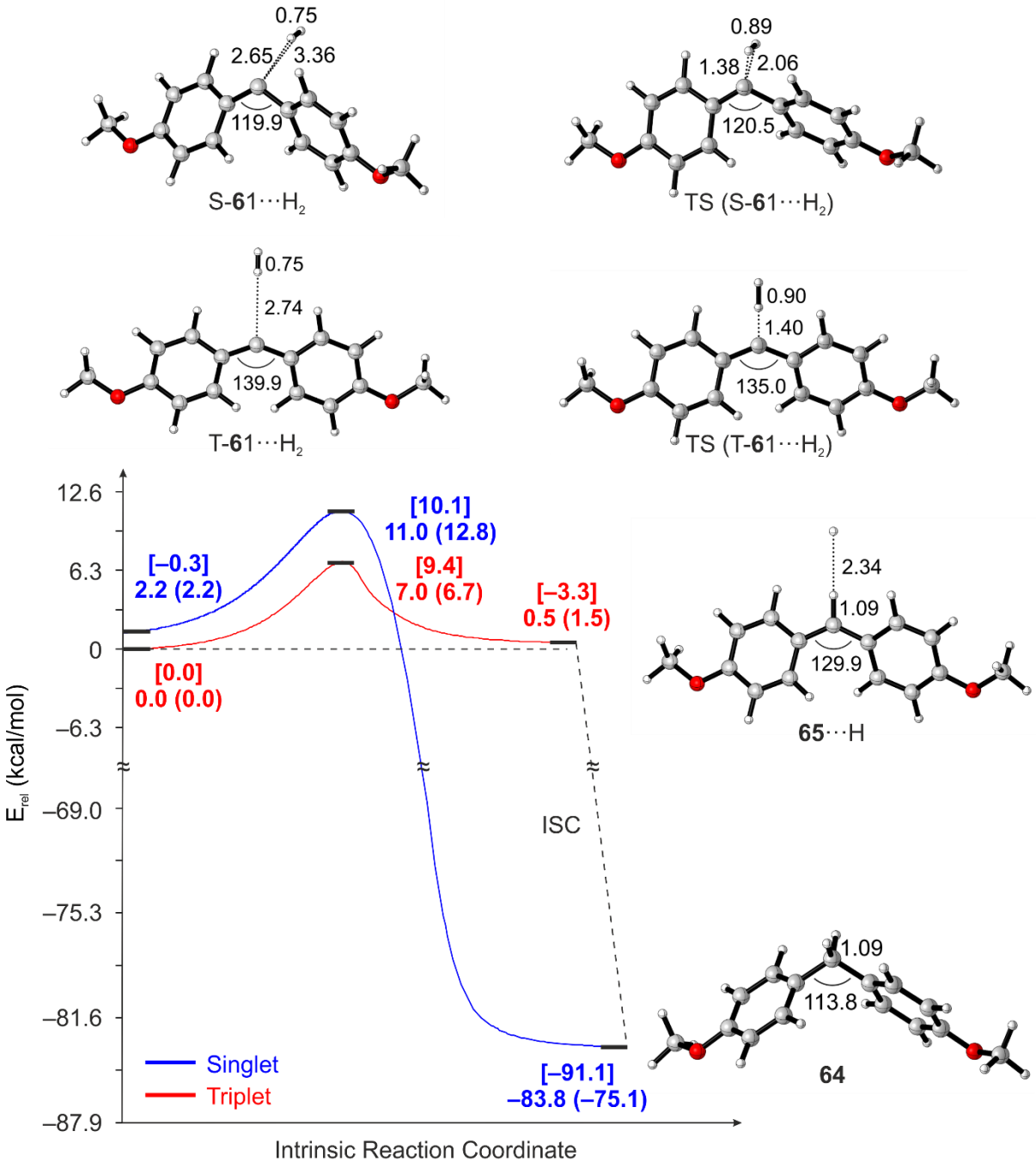

Figure 37. Hydrogenation of bis(*p*-methoxyphenyl)carbene **61** on the singlet (blue) and triplet (red) PES along the intrinsic reaction path. Energy profiles were calculated at the B3LYP-D3/def2-TZVP level of theory. Values in parentheses include ZPE correction. Values in brackets correspond to CCSD(T)/cc-PVDZ// B3LYP-D3/def2-TZVP energies. Energies are given in kcal/mol and selected bond lengths and angles are given in Å and °, respectively.

The H-abstraction by carbene T-**61** is calculated to be 6.7 kcal/mol at the DFT level, although CCSD(T) calculations predict a higher value of 9.5 kcal/mol. Calculations also estimate that

the activation barrier is not significantly affected by the ZPE of deuterium (6.8 kcal/mol). Regardless of the method, the activation barriers are much higher than the thermal energy available at 30 K, suggesting that H- and D-abstractions occur by tunneling. However, only a small isotope effect (~3) is measured for the reaction in Ar matrices doped with H_2/D_2 at 30 K, and no differences in reactivity are found in solid H_2 and D_2 at 3 K. The formation of radical **65** is predicted to be slightly endothermic (1.5 kcal/mol) by the B3LYP-D3/def2-TZVP approach, but with CCSD(T), the reaction becomes exothermic with an energy of –3.3 kcal/mol. While these enthalpy values are contrasting, they are decisive for a proper interpretation of the implication of tunneling phenomena, and therefore a thermochemistry analysis was also performed by using the isolated species T-**61**, H_2, **65**, and H radical (instead of complexes T-**61**$\cdots H_2$ and **65**$\cdots$H), and an enthalpy of –4.0 kcal/mol is obtained. An exothermic H-abstraction by T-**61** is in line with its reactivity observed in solid H_2, and correlates well with the general depiction of low-temperature triplet reactivity previously shown in Figure 28.

Carbene T-**61** is found to be more reactive than the parent diphenylcarbene **4** in solid H_2. Both carbenes have similar geometries with C–C–C angles of about 140° but have different electronic structures. The methoxy substitution in the para position of carbene **4** preferentially stabilizes the electrophilic singlet state because of electron-donating resonance interactions between the empty π orbital on the carbenic carbon and the substituent,[102] hence rendering a bimagnetically stable carbene as **61**. Calculations show that triplet states are generally not stabilized by electron donors, since the unpaired electron is less delocalized into the π system.[57] The effect of this electron donation on the singly occupied σ-orbital of the triplet state is not well understood, although atomic charges on the carbene center are reported to slightly increase upon the para substitution. Transition state geometries of T-**61**$\cdots H_2$ and T-**4**$\cdots H_2$ suggest that H_2 linearly approach the carbene center, allowing the interaction of the singly occupied σ orbital of the triplet carbene with the empty σ* orbital of H_2.[90] Strong π-donor groups might increase the electron density at the carbene center, resulting in a more favored radical attack to H_2. The *p*-methoxybenzyl radical is classified as a moderate nucleophile, and has a larger nucleophilicity index than the parent benzyl radical.[169] This could explain why the H-abstraction by T-**61** (–3.3 kcal/mol) is more favorable than that of T-**4** (isothermic), in agreement with the reactivity trends detected in solid H_2.

In line with the spin-selectivity observed in solid H_2 or D_2, calculations predict higher barriers for S-**61** than for T-**61**. However, the magnitude of such difference is quite contrasting for DFT

and CCSD(T) methods. At the B3LYP-D3/def2-TZVP level of theory, the activation barrier of T-**61** amounts to 6.7 kcal/mol, and for S-**61** a much higher value of 12.8 kcal/mol is obtained. This trend was also predicted for carbenes **4** and **5** with singlet barriers about twice as high as that of triplet states. At this level of theory, high barriers are also predicted for the unreactive singlet carbenes **35–38** (9–13 kcal/mol), again much higher than the values estimated for the reactive triplet carbenes **26**–**31** (2–5 kcal/mol), previously shown in Figure 28. In contrast, CCSD(T) calculations predict quite similar barriers on the singlet and triplet state surfaces (E_a (S-**61**$\cdots H_2$) = 9.4 kcal/mol and E_a (T-**61**$\cdots H_2$) = 10.4 kcal/mol). Likewise, isomeric aryl(trifluoromethyl)carbenes (triplet **31**) and (singlet **39**) are predicted to have relatively similar barriers (4.0 and 5.7 kcal/mol, respectively), even though they show a contrasting reactivity in H_2-doped Ar matrices.[102] This brings into doubt the argument that single carbenes are in general less reactive than triplets because of higher barriers in the former case.[15,65,85,98] Nevertheless, the role of tunneling in the H_2 addition to carbenes is well established, which strongly depends on the geometrical change from reactants to products.[99,100] Contrary to the transition state of T-**61** (C_2 symmetry), H_2 approaches the carbene center of S-**61** from one side (C_s symmetry), to achieve maximal orbital overlapping of both σ→π (electrophilic phase) and σ→σ* (nucleophilic phase).[101] The orientation of H_2 to S-**61** in the calculated TS is not completely perpendicular to the molecular plane because of steric hindrance, instead it points towards both the π and σ orbitals of the carbene. Hence, it appears a four-electron repulsion of the occupied σ orbitals of S-**61** and H_2, which is believed to be the origin of the barrier height.[129] This repulsion is not expected to be present in singlet $CH_2\cdots H_2$, which explains the direct overlapping of σ→π in the prereactive complex and the lack of activation barrier. Finally, the interpretation of Sheridan et al. that the unreactivity of singlet carbenes is attributed to the lower probability of QMT involving two hydrogens simultaneously, also seems to explain the spin-selectivity observed, although is not exempted from controversy.[98]

3-Methoxy-9-fluorenylidene

As described before, the ground-state multiplicity of arylcarbenes like **4** or **30** may selectively be tuned by introducing methoxy groups, which strongly stabilize the singlet state via resonance.[102,128] Fluorenylidene **5** has a small S–T gap, which suggests that the ordering of states might also be reversed by electron-donating substituents. In analogy to the design of carbene **61**, 3,6-dimethoxy-9-fluorenylidene **67** is reported to have a singlet ground state in frozen media.[170] It inserts directly into the C–H bonds of cyclohexane, and it adds to olefins

with total retention of stereochemistry. The singlet chemistry displayed by carbene **67** diverges from the radical-like reactivity of the parent triplet carbene **5**. The sequence of carbenes (**5**→**67**) is completed by considering the monosubstituted derivative 3-methoxy-9-fluorenylidene **62**, which is predicted to have a S–T gap of 0.5 kcal/mol. Noteworthy, the stabilizing effect of the singlet state upon introducing one methoxy group is more pronounced for carbene **5** than for carbene **4**. This can be related to the planarity of **5** that favors the interaction of the empty orbital with the occupied orbitals of the fluorenyl residue (Figure 38).

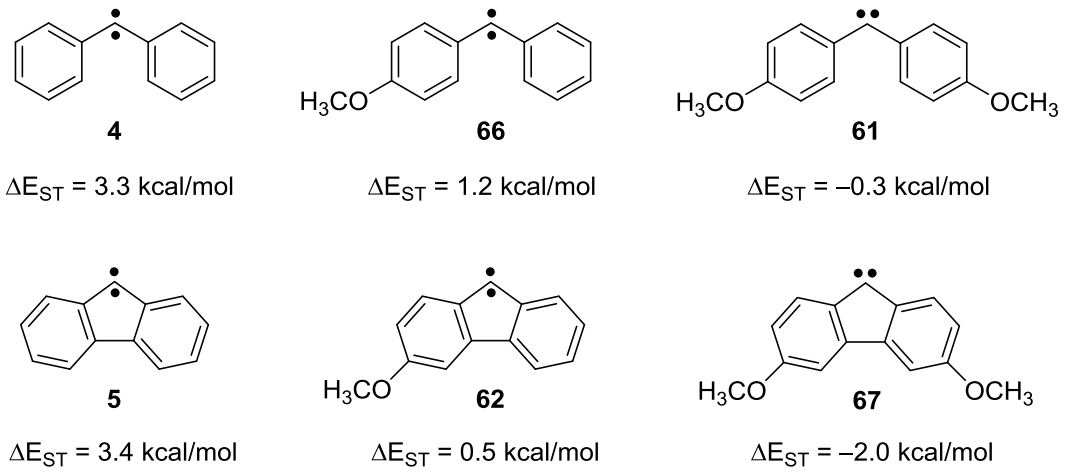

Figure 38. Singlet-triplet splittings of diphenylcarbene **4**, fluorenylidene **5**, and their corresponding methoxy-substituted derivatives (**66**→**61** and **62**→**67**), calculated at the CCSD(T)/cc-PVDZ//B3LYP-D3/def2-TZVP level of theory.

Bistable carbene **62** can be isolated in both its lowest energy singlet S-**62** and triplet T-**62** states. In Ar matrices at 3 K, both states coexist indefinitely under these conditions. It is found that visible and UV light irradiation (with λ = 530 or 405 nm) results predominantly in the formation of T-**62**, whereas 650 or 455 nm light shifts the photostationary equilibrium toward S-**62**. Contrary to carbene **61**, a thermal interconversion between the singlet and triplet states is not observed (Scheme 18).

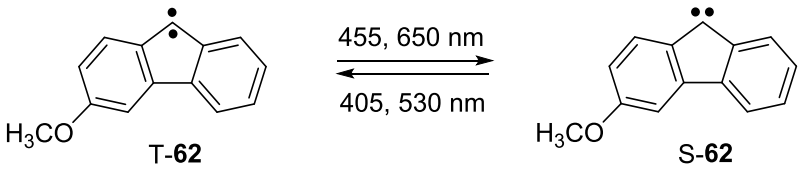

Scheme 18. Singlet-triplet interconversion of 3-methoxy-9-fluorenylidene **62** in low-temperature matrices.

Hydrogen Matrices

The spectrum of 3-methoxy-9-diazofluorene **68** in solid H_2 at 3 K is shown in Figure 39. Irradiation of **68** with UV light (λ = 365 nm) at 3 K results in a complete depletion of the IR signals assigned to **68** and formation of a new set of signals (1498, 1288, 1219, 1177, and 1047 cm^{-1}). The spectrum obtained after complete photolysis matches with the IR spectrum of the H_2-insertion product, 3-methoxyfluorene **69**, calculated at the B3LYP-D3/def2-TZVP level of theory.

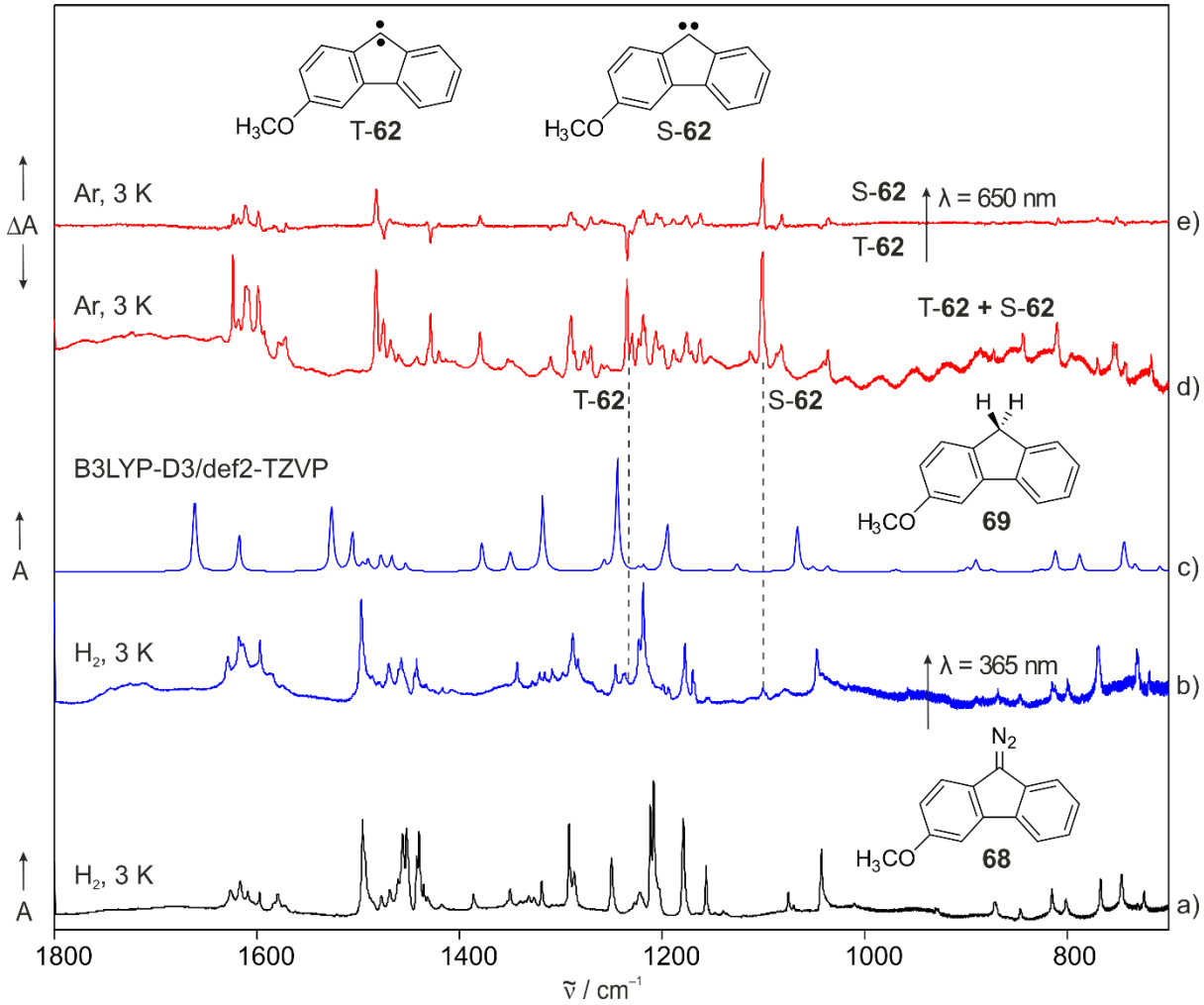

Figure 39. IR spectra showing the photochemistry of 3-methoxy-9-diazofluorene **68** in H_2 matrices. a) IR spectrum of **68** in H_2 at 3 K. b) IR spectrum obtained after irradiating **68** with λ = 365 nm in H_2 at 3 K. c) IR spectrum of 3-methoxyfluorene **69** calculated at the B3LYP-D3/def2-TZVP level of theory. d) IR spectrum of 3-methoxy-9-fluorenylidene **62** in Ar at 3 K, obtained after irradiating **68** with λ = 365 nm. The ratio S-**62**/T-**62** is approximately 45:55. e) Difference IR spectrum showing the interconversion of T-**62** into S-**62** after irradiating an Ar matrix containing both T-**62** and S-**62** with λ = 650 nm for 30 min. The dashed lines indicate the signal positions of S-**62** and T-**62**; none of them are observed in (b).

In Ar matrices, irradiation of **68** with λ = 365 nm produces S-**62** and T-**62** in a ratio of approximately 45:55. The most intense signals of carbene **62** are located at 1101 cm^{-1} (S-**62**) and 1235 cm^{-1} (T-**62**), and are not present in the spectra recorded in H_2 matrices. Carbene **62**, in either its singlet or triplet state, is not detected throughout the photolysis, indicating that its reaction with H_2 is very fast even at temperatures as low as 3 K. Hydrogenation product **69** is generated even after irradiating for a few minutes and continues to increase until precursor **68** is completely photobleached (2 h of photolysis). Such direct insertion into H_2 was also observed for the parent carbene **5** in H_2 matrices.

Deuterium Matrices

Following the procedure executed in H_2 matrices, precursor **68** was deposited in a D_2 matrix at 3 K and irradiated with λ = 365 nm for 2 h (Figure 40). The characteristic diazo signal is completely photobleached, resulting in a spectrum which looks not as simple as the one obtained in H_2 matrices. Signals appearing at 1497, 1442, 1317, 1284, 1220, 1177, and 1051 cm^{-1} are assigned to the D_2-insertion product, 9,9-dideutero-3-methoxyfluorene d_2-**69**, based on the comparison with the spectrum predicted by the B3LYP-D3/def2-TZVP method. In addition, spectral features located at 1612, 1598, 1483, 1381, 1220, and 1102 cm^{-1} correspond to singlet carbene S-**62**. These features match with the signals that increase after irradiating an Ar matrix containing both T-**62** and S-**62** with λ = 650 nm for 30 min. Interestingly, the characteristic signals of T-**62** at 1475, 1429, and 1235 cm^{-1} are not detected in D_2. The finding tells about the high reactivity of T-**62** toward H_2, since no KIE in D_2 matrices is observed. In contrast, the parent carbene **5** was shown to abstract D atoms with tunneling rates in the order of 10^{-5} s^{-1}.

Similar to S-**61**, carbene S-**62** remains stable in D_2 matrices upon keeping the matrix in the dark at 3 K for 24 h. The reaction of S-**62** with D_2 is only activated upon photolysis with the wavelengths, at which the photostationary equilibrium is shifted toward T-**62** (λ = 530 or 405 nm). Irradiation with λ = 405 nm produces a decrease of the signals corresponding to S-**62**, accompanied by a concomitant grow of the features assigned to d_2-**69**. This photochemistry is efficient and no byproducts are observed, resulting in a clean and complete conversion of S-**62** into d_2-**69** after several hours of irradiation.

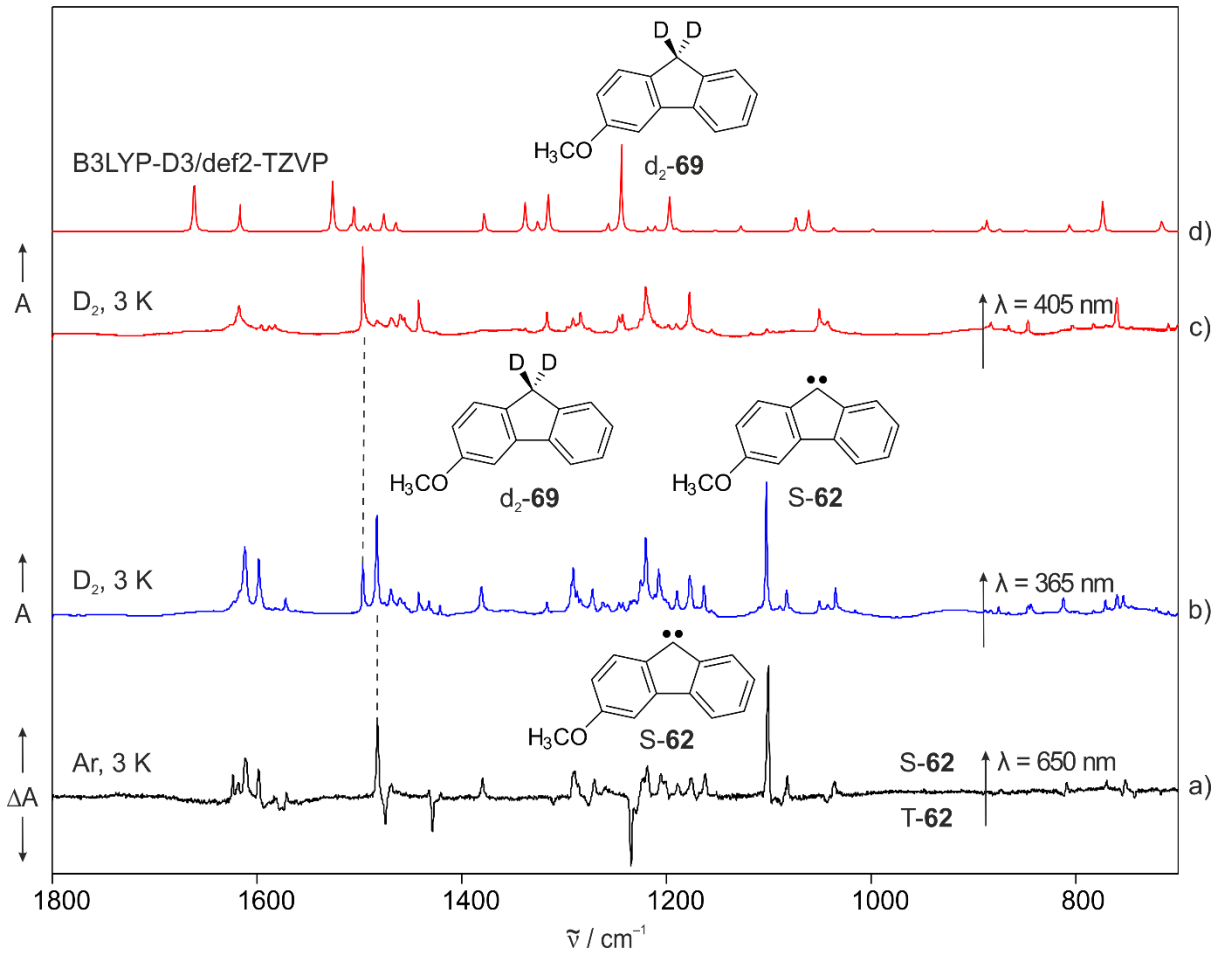

Figure 40. IR spectra showing the photochemistry of 3-methoxy-9-diazofluorene **68** in D_2 matrices. a) Difference IR spectrum showing the interconversion of T-**62** into S-**62**, after irradiating an Ar matrix containing both T-**62** and S-**62** with λ = 650 nm for 30 min. b) IR spectrum obtained after irradiating **68** with λ = 365 nm in D_2 at 3 K. c) IR spectrum obtained after subsequent irradiation of matrix (b) with λ = 405 nm in D_2 at 3 K. d) IR spectrum of 9,9-dideutero-3-methoxyfluorene d_2-**69** calculated at the B3LYP-D3/def2-TZVP level of theory. The dashed lines indicate the signal positions of S-**62** and d_2-**69**; both are observed in (b).

The UV–vis spectrum of carbene S-**62** in Ar matrices shows a band at about 410 nm. This electronic transition is activated with λ = 405 ± 20 nm light, and a shift of the photostationary equilibrium toward T-**62** is induced. Under the same photolytic conditions, a photochemical reaction of S-**62** to form d_2-**69** is observed in D_2 matrices. This reaction might proceed via the reactive triplet state T-**62** based on the high reactivity found for T-**62** in both H_2 and D_2 matrices, and the inertness of S-**62** upon photolysis with other wavelengths (e.g. 365, 450, and 650 nm). However, as discussed for carbene **61**, a photoactivated singlet reaction cannot be ruled out **(**S-**62**→S*-**62**→d_2-**69**).

Contrary to the spectral features of **61**, the IR signals of matrix-isolated **62** in its singlet and triplet states do not overlap with those assigned to d_2-**69**. This is probably related to the planarity of the structure and, for the same reason, the signals of carbenes **5** and **62** tend to be

sharper than those belonging to **4** and **61**. A careful examination of the spectra obtained in Ar and D_2 allows to analyze the relative population of S-**62** and T-**62** in these matrices. Integration of the characteristic signals of carbene **62** located at 1483 cm^{-1} (S-**62**), 1429 cm^{-1} (T-**62**), and 1498 cm^{-1} (d_2-**69**) results in a S-**62**/T-**62**/d_2-**69** ratio of approximately 44:2:54, after 365 nm photolysis of precursor **68** in D_2 matrices. When compared to the S-**62**/T-**62** ratio obtained in Ar matrices (45:55), it can be concluded that product d_2-**69** is exclusively formed from T-**62**. Moreover, upon subsequent irradiation with λ = 405 nm, the spectrum mostly contains d_2-**69** and only traces (2%) of unreacted S-**62**. The formation of S-**62** and d_2-**69** is independent of both the irradiation time with λ = 365 nm (a few minutes to several hours) and the extent of the conversion from **68** into d_2-**69** (either small fraction or complete reaction). In Ar matrices, both S-**62** and T-**62** are found to be stable under prolonged irradiation with λ = 365 nm (Figure 41).

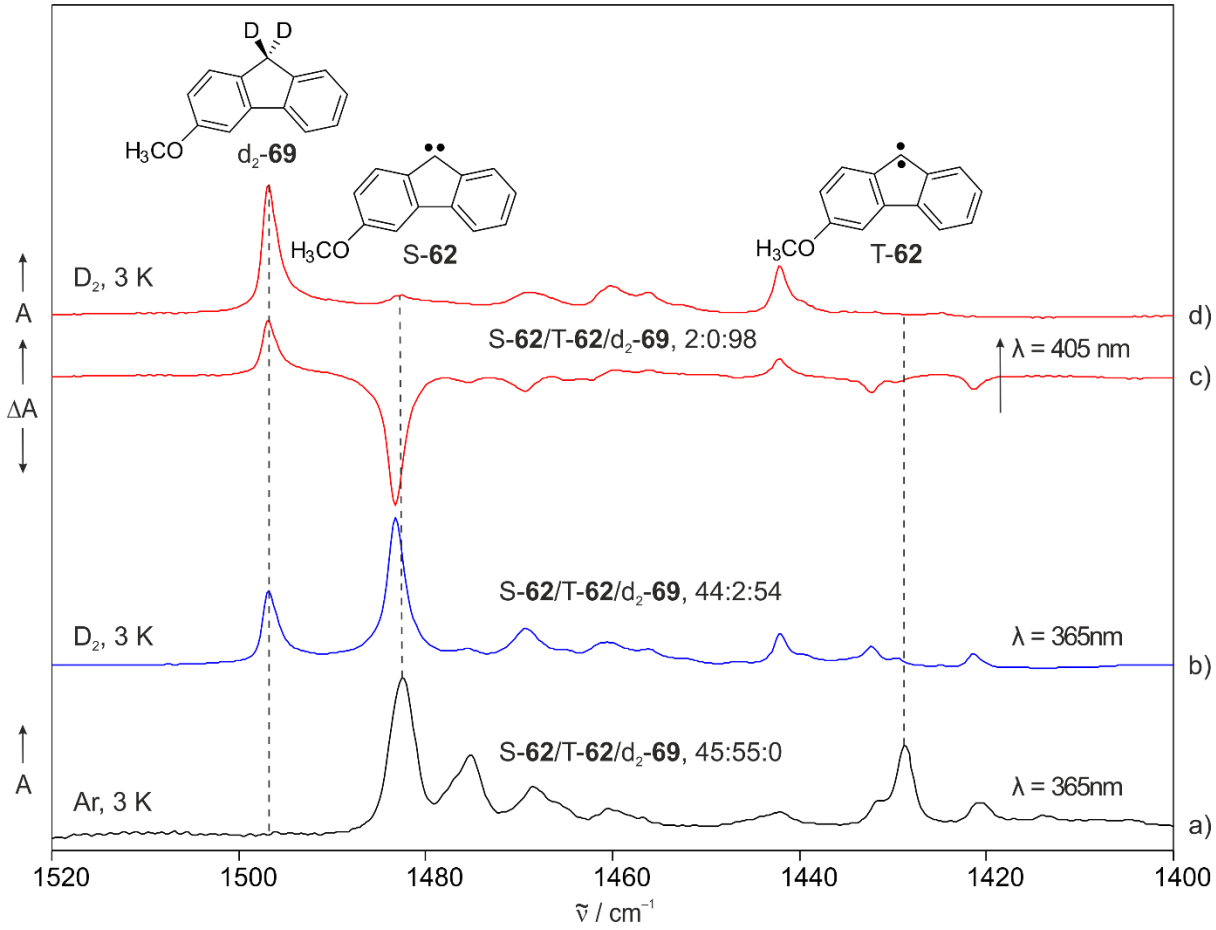

Figure 41. IR spectra showing the spin-selective reaction of triplet 3-methoxy-9-fluorenylidene T-**62** with D_2. a) IR spectrum of **62** in Ar at 3 K, obtained after irradiating **68** with λ = 365 nm. The ratio S-**62**/T-**62**/d_2-**69** is approximately 45:55:0. b) IR spectrum obtained after irradiating **68** with λ = 365 nm in D_2 at 3 K. The ratio S-**62**/T-**62**/d_2-**69** is approximately 44:2:54. c-d) Difference and final IR spectrum obtained after subsequent irradiation of matrix (b) with λ = 405 nm in D_2 at 3 K. The ratio S-**62**/T-**62**/d_2-**69** is approximately 2:0:98.

Overall, the experiments described above show that D_2 selectively reacts with the triplet state of carbene **62** upon photochemical generation in matrices at 3 K. In contrast, S-**62** is thermally stable but can be photochemically induced to react with D_2 upon 405 nm photolysis, probably via T-**62**. In H_2 matrices, S-**62** and T-**62** react completely, showing a remarkable isotope effect and indicating that these reactions might be assisted by tunneling (Scheme 19).

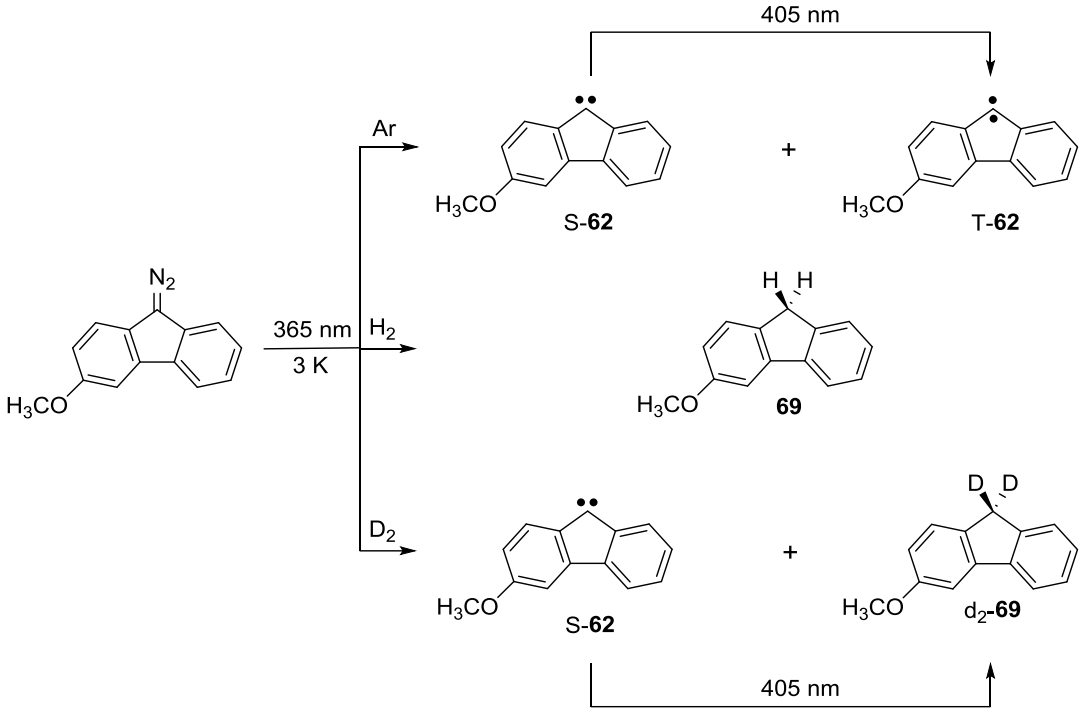

Scheme 19. Spin-selective reactivity of 3-methoxy-9-fluorenylidene **62** in H_2 and D_2 matrices.

Calculations

Similar to the carbenes discussed in the previous chapters, the reactions of both S-**62** and T-**62** with H_2 have been studied by means of theoretical methods. The S–T splitting of **62** is calculated to be 1.8 kcal/mol at the B3LYP-D3/def2-TZVP level of theory and 0.5 kcal/mol at the CCSD(T)/cc-pVDZ level of theory. The higher correlated CCSD(T) approach gives a better simulation of the properties of carbene **62** as it predicts its magnetically bistability. Energy curves for the addition of H_2 to 3-methoxy-9-fluorenylidene **62**, in the singlet (blue) and triplet (red) spin states, are reported in Figure 42. Energy calculations along the intrinsic reaction path are carried out at the B3LYP-D3/def2-TZVP level of theory, and all relevant stationary points were consequently recalculated at the CCSD(T)/cc-pVDZ level of theory.

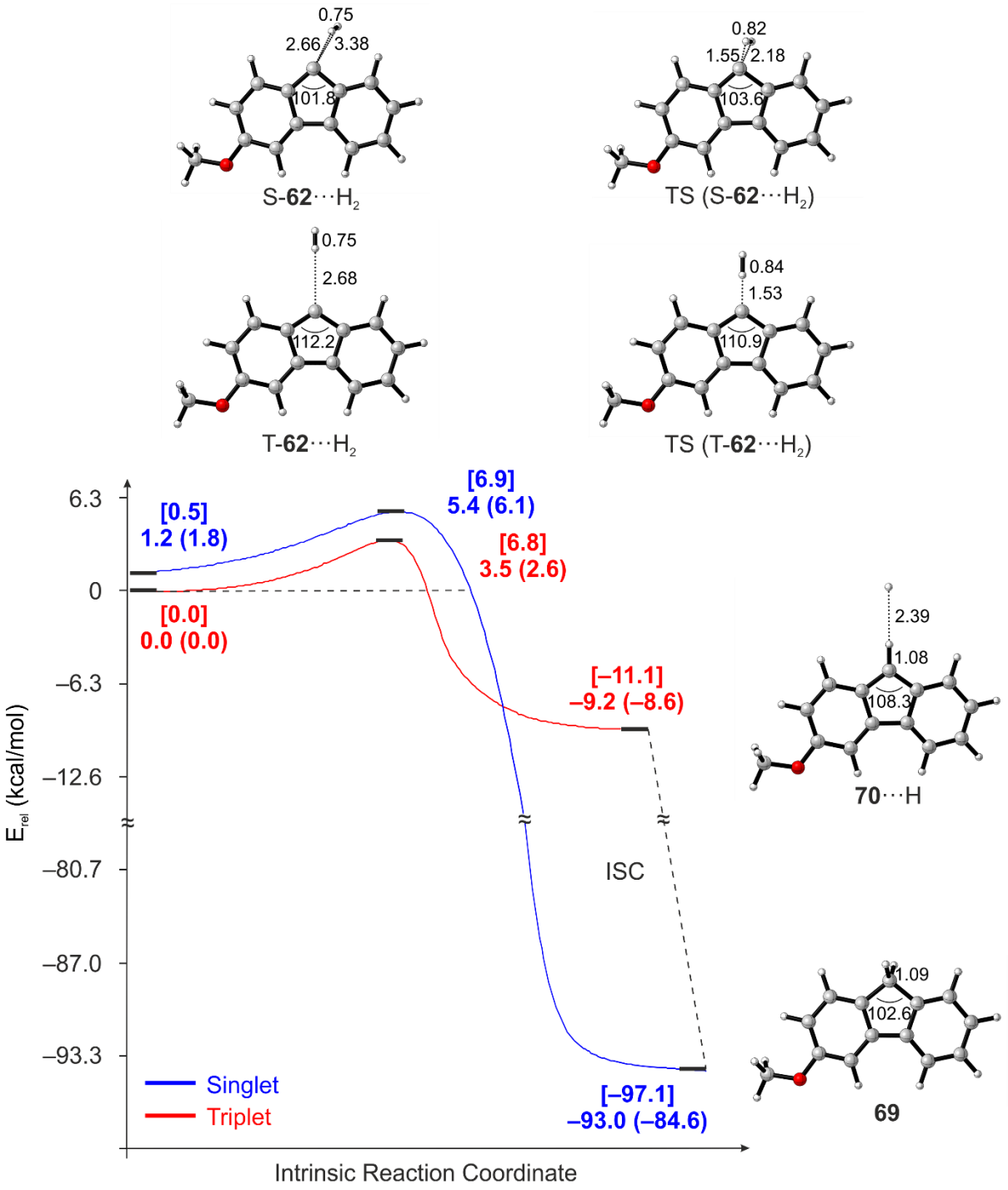

Figure 42. Hydrogenation of 3-methoxy-9-fluorenylidene **62** on the singlet (blue) and triplet (red) PES along the intrinsic reaction path. Energy profiles were calculated at the B3LYP-D3/def2-TZVP level of theory. Values in parentheses include ZPE correction. Values in brackets correspond to CCSD(T)/cc-PVDZ//B3LYP-D3/def2-TZVP energies. Energies are given in kcal/mol and selected bond lengths and angles are given in Å and °, respectively.

The geometries of the hydrogen complex T-**62**···H_2 and the corresponding transition state TS (T-**62**···H_2) are predicted to be very similar to the related structures calculated for the parent carbene **5**. Such geometrical similarity is reflected in having almost identical H-abstraction

activation barriers and enthalpies, according to both DFT and CCSD(T) methods. These predictions agree with the experimental observations that both triplet carbenes **5** and T-**62** readily insert into H_2 at temperatures as low as 3 K. Nevertheless, calculations fail to explain why T-**62** reacts much faster (not detected at all) than carbene **5** ($\tau_{1/2}$ = 5–6 h) in solid D_2 at 3 K. Given the experimental evidences that strongly suggest a tunneling mechanism, such contrasting kinetic rates are probably a consequence of small differences in the shape of the barrier that are not properly simulated by the calculations. For example, equation (10) can be used to estimate the tunneling rate of a D atom penetrating a parabolic barrier with a calculated width of 1.6 Å, height of 7 kcal/mol, and considering the D atom vibrating at a typical D–D stretching frequency of approximately 3000 cm^{-1}.

$$k = \tilde{\nu}(D-D) \times c \times e^{-\pi^2 w\sqrt{2m(V-E)}/\hbar} \quad (10)$$

The rate of tunneling is estimated to be 2×10^{-5} s^{-1}, which matches the experimental value determined for carbene **5** ($2–5 \times 10^{-5}$ s^{-1} at 3–6 K). However, if the width is increased to 1.7 Å or the barrier lowered to 6 kcal/mol (both differences beyond the accuracy of the calculations), this rate changes to 1×10^{-6} s^{-1} and 4×10^{-4} s^{-1}, respectively. Such simple model calculations illustrate that small changes in barrier shapes can have profound impact in the predicted tunneling rates of carbenes **5** and T-**62**. Furthermore, bimagnetically stable carbenes have only been observed in matrices recently,[128,166,167] resulting in scarce experimental data and limited understanding of the formation and dynamics of such bistable species.[171,172]

Concerning the spin-selectivity observed for **62** in solid D_2, DFT calculations predict a higher and broader barrier for S-**62** compared to T-**62**. However, this could be an artefact of the intrinsic reaction coordinates by taking into account the displacement of two H/D atoms. On the other hand, CCSD(T) calculations predict similar barriers on the singlet and triplet energy curves (E_a (S-**62**$\cdots H_2$) = 6.4 kcal/mol and E_a (T-**62**$\cdots H_2$) = 6.8 kcal/mol). The reason why triplets can find a tunneling pathway, whereas singlet carbenes cannot, is not really understood. There are now multiples examples showing a higher reactivity of triplet carbenes toward H_2 at low temperatures. These observations are in line with the assumption of Sheridan et al. on the lower probability of QMT involving two hydrogens simultaneously.[98] However, multidimensional SCT computations[151] are perhaps necessary for an accurate prediction of tunneling paths and reaction rates.

A compendium of the results on the low-temperature hydrogenation of the arylcarbenes investigated in this work is shown in Table 7. The results provide additional insights into the chemical differences between diphenylcarbene **4** and fluorenylidene **5**. The higher reactivity of carbene **5** upon H-abstraction might be explained by the demanded contraction of the C–C–C angle to 112º, which is much smaller than the typical angles of triplet carbenes 135–145º.[15] The enthalpy of the H-abstraction step is a key factor in the reaction of triplet carbenes with H_2 via H-atom tunneling at low temperatures. Likewise, the spin-selective hydrogenation of bistable species bis(*p*-methoxyphenyl)carbene **61** and 3-methoxy-9-fluorenylidene **62** show that triplet arylcarbenes are generally more reactive than the corresponding singlets, even though the reason for this behavior is not yet completely understood. These results do not contradict the observations that highly electrophilic carbenes insert directly into H_2, irrespective of its spin state.[97,103]

Table 7. Summary of the reactivity of the arylcarbenes investigated in this work in H_2 and D_2 matrices.

Carbene	Ar	H_2	D_2
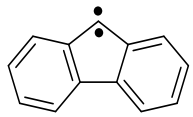 **5**	T-**5**	**41**	T-**5**→d_2-**41**
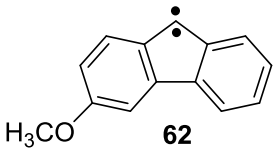 **62**	S-**62** + T-**62**	**69**	**S-62** + d_2-**69**
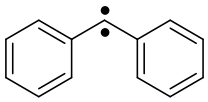 **4**	T-**4**	T-**4**	T-**4**
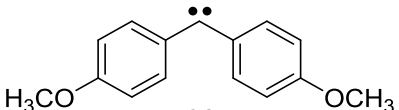 **61**	S-**61** + T-**61**	S-**61** + **64**	S-**61** + d_2-**64**

Tentative ground state multiplicities are singlet for carbene **61** and triplet for carbene **62**, based on experimental observations in matrices and calculated S–T splittings. However, a distribution of S–T splittings values rather than a well-defined value is envisaged in disordered media.

On the other hand, arylnitrenes are found to be unreactive toward H_2 in low-temperature matrices. Although not interesting from a mechanistic point of view, this relative stability is an advantage in applications where H-abstraction processes can spoil potential use. Further investigation on stable arylnitrenes is discussed on the next section.

Trinitrenes

Introduction

The quest for developing organic magnets comes up because of being potentially both more cost effective and lighter than the more traditional metal magnets.[173] The properties of organic magnets are quite different from conventional metallic magnets: lightweight, transparent, flexible, or even liquid magnets could be designed. One approach toward the synthesis of organic magnets is to use molecular high-spin systems with many spin centers as building blocks. The building blocks for constructing high-spin molecules are based on non-Kekulé molecules such as trimethylenemethane **71**, *m*-xylylene **72** or 1,3,5-trimethylenebenzene **73**. These planar π-conjugated polyradicals are characterized by strong ferromagnetic couplings between the spin centers leading to high-spin ground states ($S \geq 1$). A number of very high-spin polyradicals (e.g. $S = 5000$) have been published by Rajca et al.[174,175] In addition, triplet diarylcarbenes have also been used as units to construct "superparamagnetic" polycarbenes.[176,177] While this approach was successfully used to synthesize very high-spin organic polymers with magnetic ordering, the drawback of these systems is the high chemical reactivity.

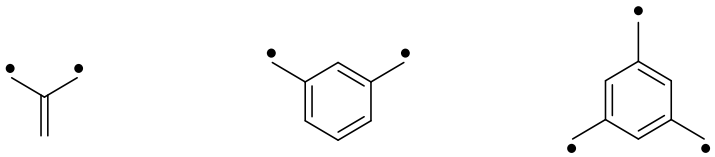

71 **72** **73**

Arylnitrenes with robust triplet ground states and large S–T splittings, have been much less considered as basic units for the construction of high-spin molecules than carbenes. The advantage of arylnitrenes is that there are convenient precursors available for their synthesis, and that the magnetic interaction between the unpaired electrons is very large. The magnetic parameter D of arylnitrenes is in the order of 1 cm^{-1}, which is about three times larger than that of arylcarbenes (typically 0.2–0.4 cm^{-1}).[173] High-spin arylnitrenes are obtained by arranging two or three nitrene centers in meta position of an aromatic core, which results in ferromagnetic-coupled dinitrenes with quintet ground states or trinitrenes with septet ground states.[178] A number of trinitrenes (e.g. **74**–**78**) have been studied by the very sensitive EPR spectroscopy in solid media [179-183] Only a few of these high-spin nitrenes could be synthesized

in high enough yields to be characterized by IR[179,184,185] or UV–vis spectroscopy[186] in inert gas matrices.

74 **75** **76** **77** **78**

In most cases the yield of trinitrenes is low due to incomplete photolysis of the precursor leading to mono- or dinitrenes, or because of secondary photoreactions that produce rearranged products such as azirines, ketenimines, or nitriles.[185,187,188] Experimental and theoretical studies suggest that by blocking the positions adjacent to the nitrene units in arylnitrenes with halogen atoms, the rearrangements of di- and trinitrenes are effectively suppressed.[45,165] Therefore, photolysis of 1,3,5-triazido-2,4,6-trichlorobenzene **79** and its bromo-analogue **83** should give high yields of septet trinitrenes **82** and **86**, respectively (Scheme 20). This hypothesis is supported by the EPR (X-band 9 GHz) studies by Misochko et al., which reported that septet trinitrene **82** is the major paramagnetic product of the photolysis of precursor **79** in Ar matrices at 15 K.[189] Similarly, trinitrene **86** was also produced in low-temperature matrices, albeit in this case, the more sensitive W-band 94 GHz EPR allowed to characterize all paramagnetic species (**84**–**86**) formed at different stages of the photolysis.[190]

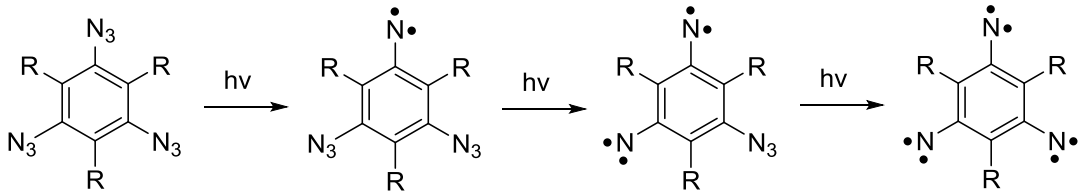

79: R = Cl
83: R = Br

80: R = Cl
84: R = Br

81: R = Cl
85: R = Br

82: R = Cl
86: R = Br

Scheme 20. Photochemical synthesis of 1,3,5-trichloro-2,4,6-trinitrenobenzene **82** and 1,3,5-bromo-2,4,6-trinitrenobenzene **86**.

Herein, the isolation and complete spectroscopic characterization (IR and UV–vis) of septet trinitrenes **82** and **86** in both inert (Ne, Ar, and Xe) and reactive (H_2, O_2, and H_2O) low-temperature matrices is reported.

1,3,5-Trichloro-2,4,6-trinitrenobenzene

IR Spectroscopy

The spectrum of matrix-isolated 1,3,5-triazido-2,4,6-trichlorobenzene **79** in Ar at 3 K is shown in Figure 43. Triazide **79** shows strong IR signals at 2129 and 1408 cm^{-1} and less intense spectral features at 1543, 1277, 791, and 524 cm^{-1}. The band centered at 2129 cm^{-1} is divided into several components (similar to Fermi resonance phenomenon on aldehydes) and assigned to the N=N=N stretching vibrations of the three azido groups. The IR spectrum is reasonably reproduced by calculations at the B3LYP/aug-cc-PVTZ level of theory, however, some deviations in both the position and intensity of the signals located on the finger-print region are observed. Moreover, most of the spectral features appear as broad bands with bandwidths of up to 20 cm^{-1}. Such broadening is explained by the existence of at least six conformers within 0.5 kcal/mol of energy separation between them. The rich conformational landscape of **79** is probably a consequence of having a flexible structure with dihedral angles of about 40º between the azide groups and the aromatic plane, according to DFT calculations.

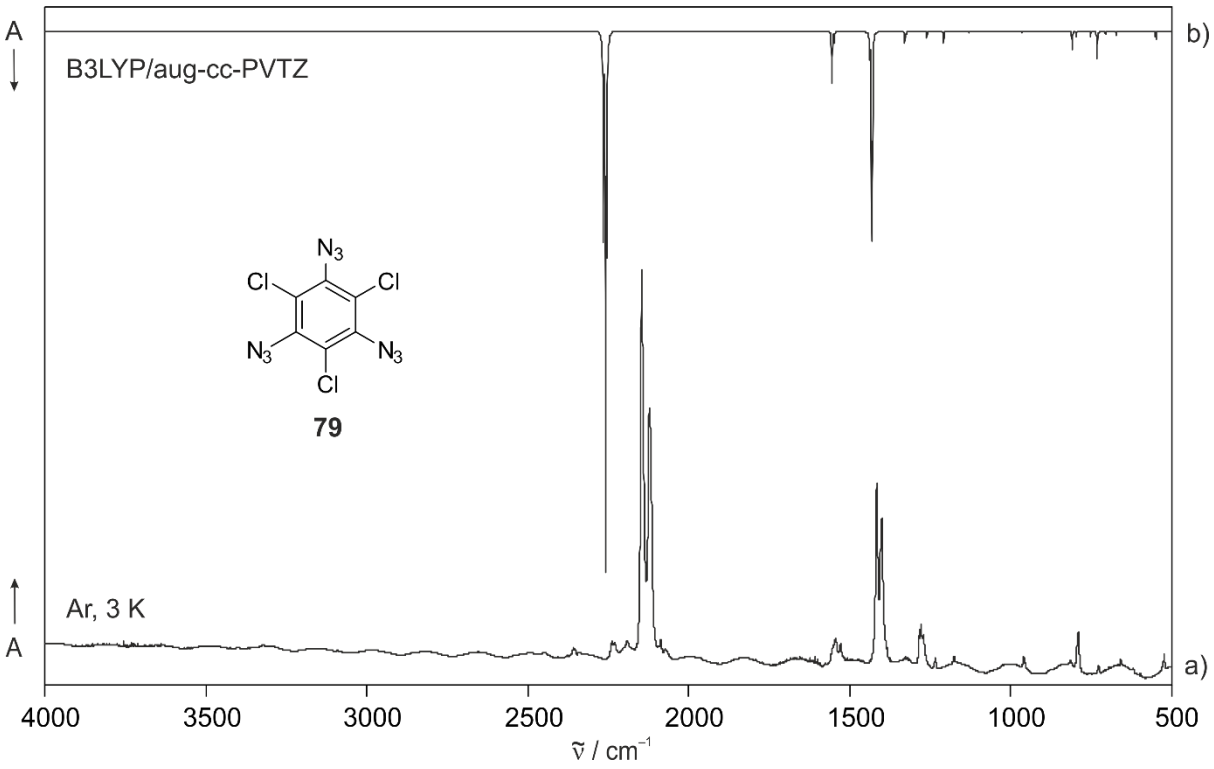

Figure 43. a) IR spectrum of 1,3,5-triazido-2,4,6-trichlorobenzene **79** in Ar matrices at 3 K. b) IR spectrum of **79** calculated at the B3LYP/aug-cc-PVTZ level of theory. Only the lowest-energy conformer is shown.

Triazide **79** was irradiated with λ = 365 nm light for 4 h and neither precursor **79**, triplet **80**, nor quintet **81** is found at the end of the irradiation. Moreover, typical photoproducts of nitrenes, such as azirines and cyclic ketenimines are not observed in this case.[45] A clean spectrum with few but unambiguous signals is obtained, suggesting the presence of a unique and highly symmetric photoproduct (Figure 44).

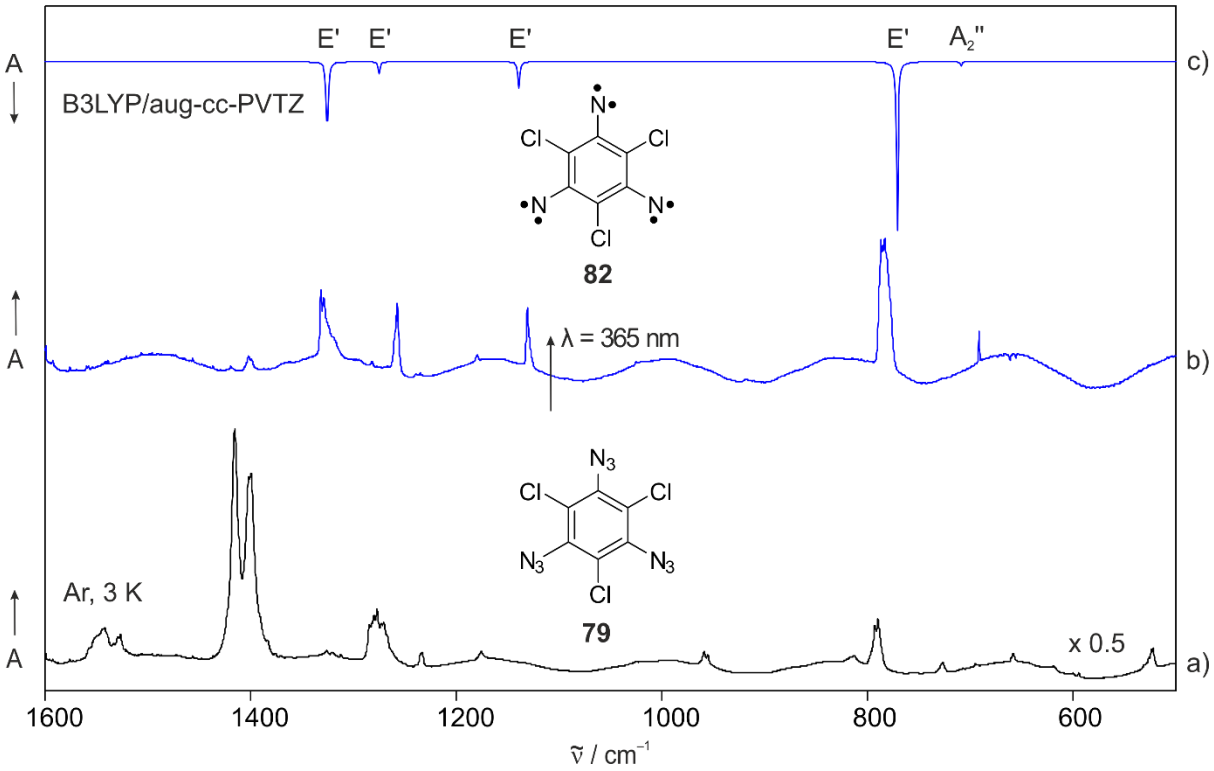

Figure 44. IR spectra showing the photochemistry of 1,3,5-triazido-2,4,6-trichlorobenzene **79** in Ar matrices. a) IR spectrum of **79** in Ar at 3 K. b) IR spectrum obtained after irradiating **79** with λ = 365 nm for 4 h. c) IR spectrum of septet 1,3,5-trichloro-2,4,6-trinitrenobenzene **82** calculated at the B3LYP/aug-cc-PVTZ level of theory.

Observed new signals at 1329, 1257, 1131, 783, and 691 cm^{-1} are therefore assigned to septet trinitrene 1,3,5-trichloro-2,4,6-trinitrenobenzene **82**. By comparing the matrix IR spectrum with the one calculated at the B3LYP/aug-cc-PVTZ level of theory, a good agreement concerning both signals position and intensity pattern is found. Such good matching is not a surprise since the electronic structure of trinitrene **82**, with a robust septet ground state, is expected to be properly described by single determinant calculations. Indeed, geometry optimization of trinitrene **82** with CASSCF/cc-PVTZ and B3LYP/cc-PVTZ methods gives very similar structures, where the characteristic bond distances differ in max. 0.01 Å.

Trinitrene **82** is predicted to have 30 vibrational degrees of freedom (3N–6), however, its D_{3h} symmetry forces some of the modes to be IR-inactive, making them observable by Raman

spectroscopy. Indeed, 17 vibrational modes are IR-active but only nine of them are located in the range 4000–400 cm^{-1}, making them detectable by the MCT detector of the spectrometer. Furthermore, four of these potentially observable signals of **82** are doubly degenerate vibrational modes (E'), hence simplifying the spectrum to only five signals. The most intense signal at 783 cm^{-1} correspond to the antisymmetric C–Cl stretching (Table 8).

Table 8. Vibrational frequencies of 1,3,5-trichloro-2,4,6-trinitrenobenzene **82** measured in Ar at 3 K and calculated at the B3LYP/aug-cc-PVTZ level of theory.

Mode	Symmetry	$\tilde{\nu}_{exp.}$ /cm^{-1}	$I_{rel., exp.}$	$\tilde{\nu}_{calc.}$/cm^{-1}	$I_{rel., calc}$	Assignment
19	A_2''	691	0.02	715	0.23	ring def. (oop)
20, 21	E'	783	1.00	772	1.00	C–Cl str.
23, 24	E'	1131	0.19	1140	0.33	ring def. (ip)
25, 26	E'	1257	0.22	1276	0.38	C–N str.
28, 29	E'	1329	0.47	1326	0.54	C–C str.

Relative intensities based on the strongest absorption. Modes (E') are doubly degenerate.

Although several trinitrenes have been already detected by the sensitive EPR,[178] IR spectroscopy has the advantage of detecting diamagnetic species that are produced during the photolysis of aromatic polyazides, hence allowing to estimate the yield of formation of high-spin nitrenes. Septet **82** is the first trinitrene that is obtained in high yields and free of unwanted side products. Triazide **79** can be completely photolyzed within a few hours of UV irradiation and neither triplet mononitrene **80** nor quintet dinitrene **81** species is observed at the end of the photolysis. In contrast, trinitrenes as **76** were generated in very low yields, and only a few of its IR bands could be assigned.[179] Likewise, trinitrene **78** is found to be very unstable and readily decomposes to triplet cyanonitrene, NCN, even after short photolysis times.[184]

In a complementary EPR study, Misochko et al. reported that UV irradiation of triazide **79** with λ = 297 nm in Ar matrices at 15 K produces EPR lines that are assigned to quintet dinitrene **81**, which decay after longer irradiation.[189] Likewise, septet **82** was found to be the main paramagnetic product, and triplet **80** was not detected at all throughout the photolysis. For completing the IR characterization of all potential photoproducts of triazide **79**, matrix experiments were repeated by using a more compact host as Ne in order to facilitate the identification of these additional elusive intermediates (Figure 45).

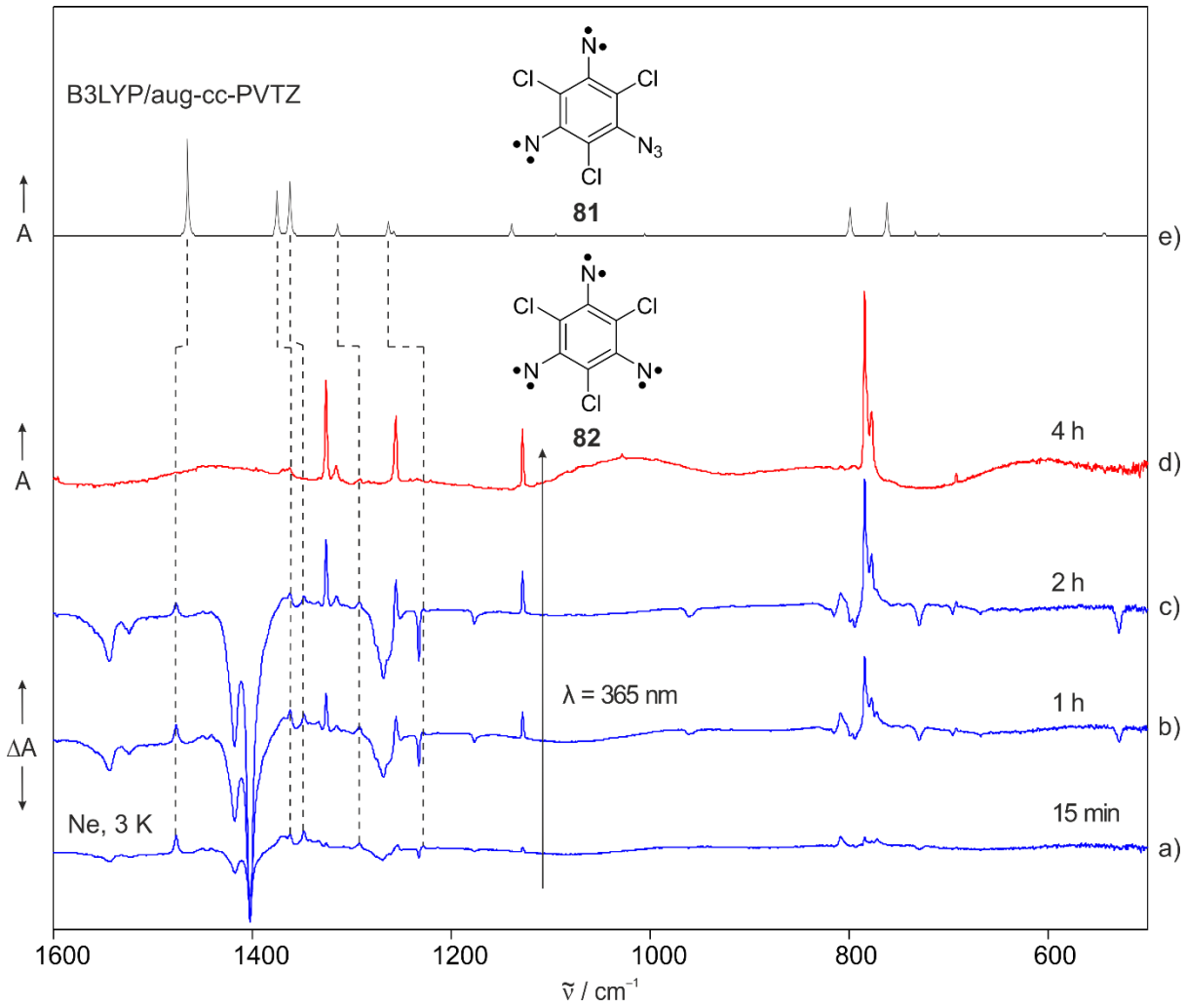

Figure 45. IR spectra showing the photochemistry of 1,3,5-triazido-2,4,6-trichlorobenzene **79** in Ne matrices. a-c) IR difference spectra obtained after irradiating **79** with λ = 365 nm in Ne at 3 K for 15 min, 1 h, and 2 h, respectively. d) IR spectrum obtained after irradiating **79** with λ = 365 nm for 4 h. e) IR spectrum of quintet dinitrene **81** calculated at the B3LYP/aug-cc-PVTZ level of theory. The dashed lines indicate the signal positions assigned to **81**; they appear as weak signals in (a-c) but are not present in (d).

Irradiation of precursor **79** in Ne matrices with λ = 365 nm for 15 min does not result in the formation of appreciable amounts of trinitrene **82**. Instead, weak peaks at 1478, 1363, 1348, 1292, and 1229 cm^{-1} appear in the spectrum, and match with the calculated frequencies of quintet dinitrene **81**, albeit some of the predicted spectral features are missing. The signals assigned to **81** reached the maximum intensity after 1 h of irradiation and gradually decayed upon further irradiation. Since all the signals follow a similar evolution during the course of the photolysis, they can be assigned to the same photoproduct, that is **81**. A different scenario was observed during the photogeneration of 3,5-dichloropyridyl-2,4,6-trinitrene **76** in Ar matrices at 7 K; the IR signals of the corresponding quintet dinitrene persist after 36 h of photolysis with λ = 334 nm.[179]

On the other hand, if triplet mononitrene **80** would be present as well, an additional signal at 1450–1500 cm^{-1} (C=C str.) would appear in the spectra. Calculations predict such vibration to appear at 1465 cm^{-1} for dinitrene **81** and 1491 cm^{-1} for mononitrene **80**. Moreover, it is unlikely that triplet **80** would be detected by IR but not by the more sensitive EPR spectroscopy in matrices. Hence, experiments in Ne matrices show that the main photoproduct is trinitrene **82**, and quintet **81** is presumably formed in low concentrations at early stages of the photolysis.

UV–vis Spectroscopy

Matrix UV–vis experiments were also carried out in Ar matrices at 8 K as shown in Figure 46. Matrix-isolated triazide **79** shows a broad and strong absorption centered at 246 nm, as typically observed for aromatic compounds. Irradiation of the matrix with $\lambda = 365$ nm results in a decreasing of the band assigned to **79** and the appearance of new spectral features that increase proportionally, which indicate that only one species is forming. These new bands are located at 310–345, 221, 204 nm as well as some very weak features at 289, 283, and 237 nm. To analyze the UV–vis data, time-dependent (TD)DFT calculations were performed using a variety of functionals and basis sets. Calculations at the M06-2X/aug-cc-PVTZ level of theory predict the electronic transitions of trinitrene **82** at 338, 292, 268, 252, 214 (very intense), 209, and 208 nm, in reasonable agreement with the most intense observed bands. The five bands very closed to each other between 310 and 345 nm seem to be part of a vibrational progression, which results from the coupling of vibrational and electronic levels. As expected, calculations predict a single purely electronic transition above 300 nm.

The signals assigned to **82** persist upon prolonged irradiation with $\lambda = 365$ nm, in agreement with the IR observations. However, dinitrene **81** is not detected at any time. This intermediate is expected to have a noticeable band around 450–500 nm because of its similarity to dinitrene 2,4,6-trichloro-3,5-dinitreno-(allyloxy)-benzene; the latter reported to have bands at 483 and 450 nm in Ar matrices.[191] Interestingly, strong UV irradiation at 254 nm produces a decrease in all bands because of the photobleaching of trinitrene **82**. This is confirmed by scanning the photostability of triazide **79** and trinitrene **82** at the UV–vis wavelength range (200–800 nm). Irradiation was performed with broadband UV–vis light coming from a high-pressure mercury lamp, and by using cut-off filters to select the different wavelengths to scan. Triazide **79** and trinitrene **82** are photostable upon irradiation above 385 nm and 335 nm, respectively. The photoreactivity of trinitrene **82** at $\lambda < 335$ nm confirms its spectral assignment.

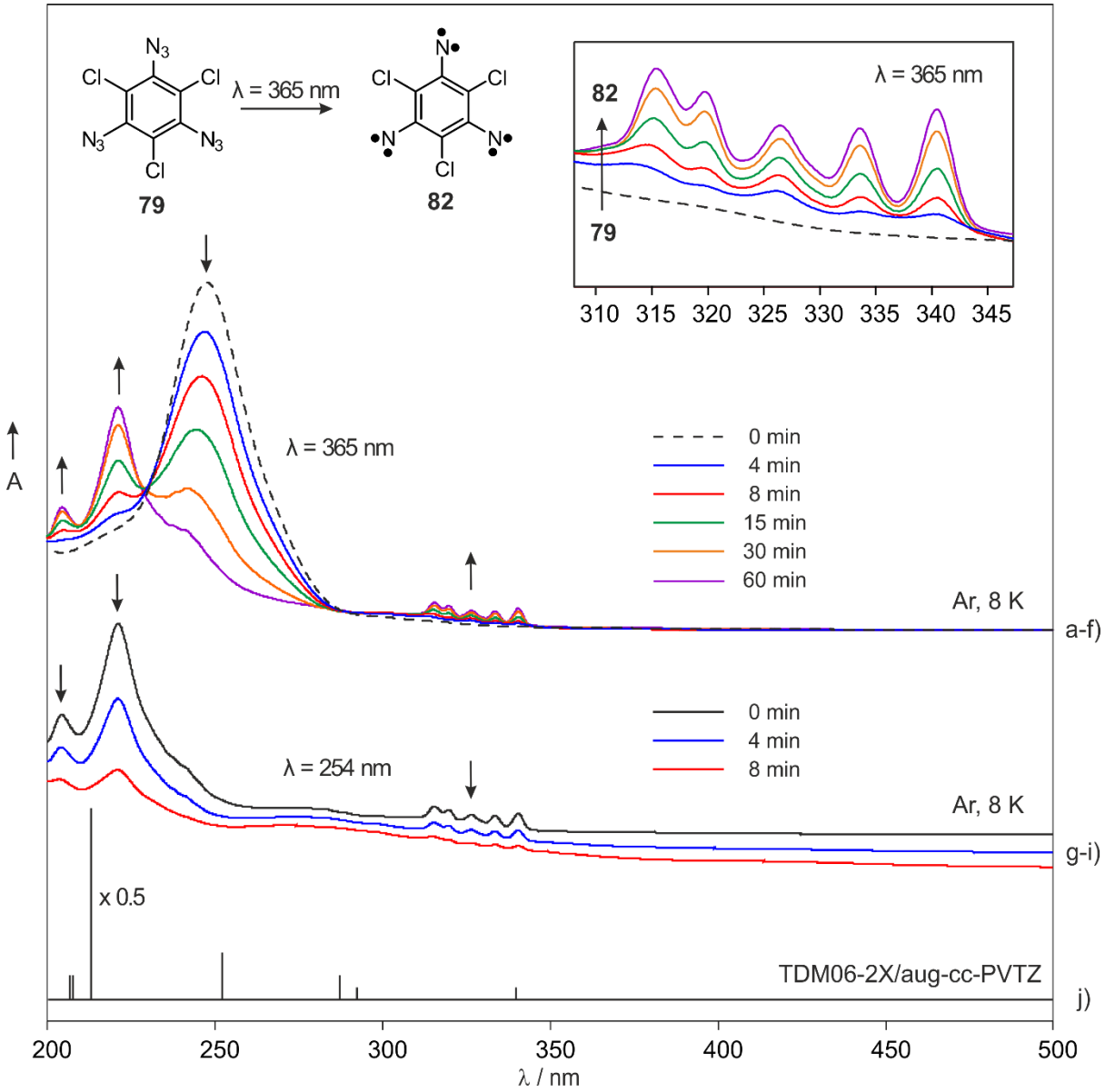

Figure 46. UV–vis spectra showing the photochemistry of 1,3,5-triazido-2,4,6-trichlorobenzene **79** in Ar matrices. a) UV–vis spectrum of **79** in Ar at 8 K. b-f) UV–vis spectra obtained after irradiating **79** with λ = 365 nm for 4, 8, 15, 30, and 60 min, respectively. g) UV–vis spectra of 1,3,5-trichloro-2,4,6-trinitrenobenzene **82**, obtained after irradiating **79** with λ = 365 nm for 4 h. h-i) UV–vis spectra after irradiating **82** with λ = 254 nm during 4 and 8 min, respectively. j) Electronic transitions of septet trinitrene **82** calculated at the (TD)M06-2X/aug-cc-PVTZ level of theory. Inset shows the increase of the signals at 310–345 nm upon irradiation with λ = 365 nm.

This is the first electronic absorption spectrum free from lower-spin intermediates recorded for an organic molecule with a septet ground state. Previous attempts on septet trinitrene **76** were unsuccessful because of a substantial contamination with the quintet dinitrene, and because longer photolysis (>5 min) gradually destroyed both species.[186] Likewise, a careful analysis of the UV–vis spectra indicates the possible presence of two isosbestic points at 288 and 229 nm. At these wavelengths, the total absorbance should not change during the chemical reaction, hence suggesting a direct conversion from triazide **79** into trinitrene **82**. Such direct

photoconversion would probably occur via a multiphoton process. However, this hypothesis is unlikely since quintet dinitrene **82** was detected by IR and EPR spectroscopy. Hence, there is probably a photostationary equilibrium, in which the lower-spin species **80** and **81** are always present in low concentrations. This could be the reason behind the slightly out-of-focus isosbestic points, although those small shifts could be related to changes of transparency of the matrix while irradiating (see appendix, Figure A2).

In some cases, experimental evidence obtained by UV–vis spectroscopy cannot directly be compared to information gained from IR measurements because of the different sensitivity of these spectroscopic techniques. Herein, both IR and UV–vis spectra are parallelly recorded over the same matrix, instead of doing two separated experiments. However, UV–vis spectra below 260 nm cannot be recorded because the cold CsI window and the external CsBr windows strongly absorb the incident light (Figure 47).

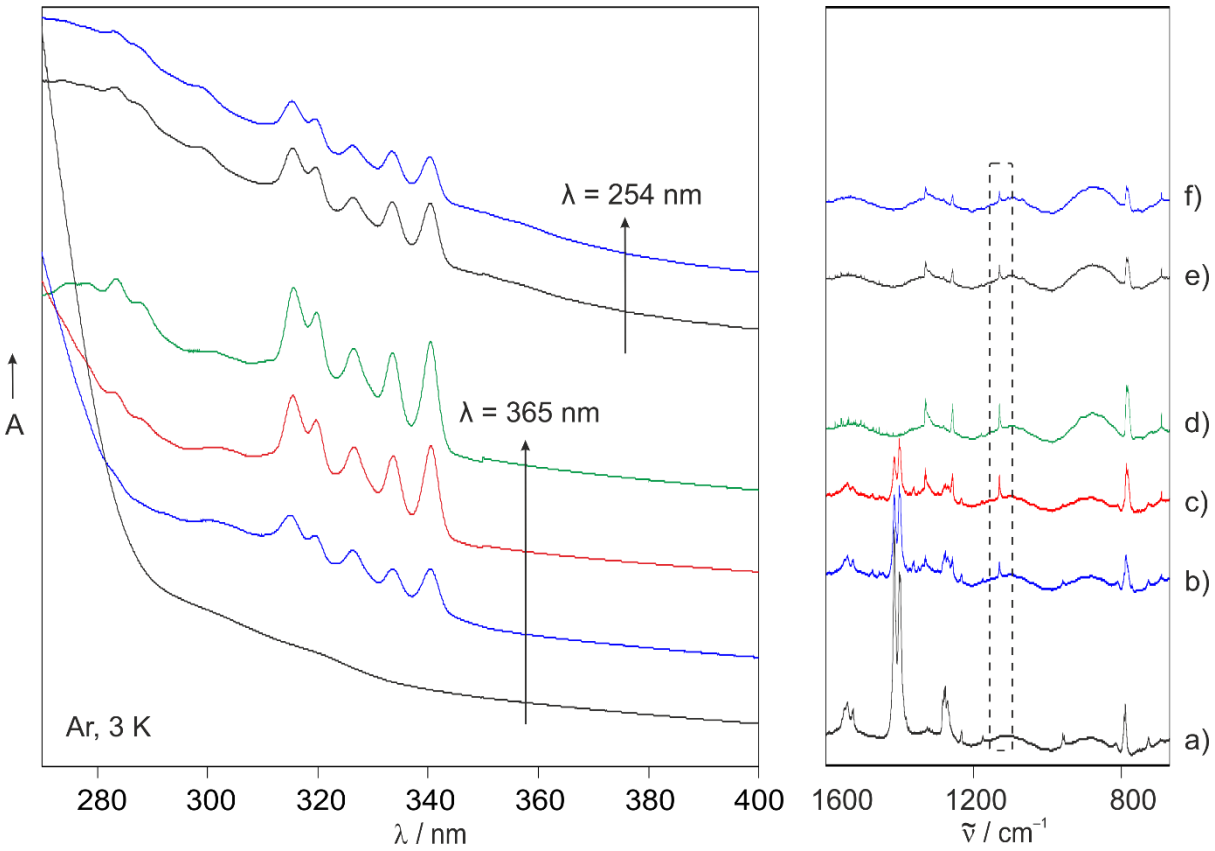

Figure 47. UV–vis and IR spectra showing the formation of 1,3,5-trichloro-2,4,6-trinitrenobenzene **82** and its photoreaction in Ar matrices. a) UV–vis and IR spectra of 1,3,5-triazido-2,4,6-trichlorobenzene **79** in Ar at 3 K. b-d) UV–vis and IR spectra obtained after irradiating **79** with λ = 365 nm during 15, 30, and 4 h respectively. e-f) UV–vis and IR spectra obtained after subsequent irradiation with λ = 254 nm during 15 and 30 min, respectively. UV–vis and IR spectra are recorded over the same Ar matrix.

By monitoring one of the characteristic IR signals at 1131 cm^{-1} and the vibrational progression at 310–345 nm, the generation (with $\lambda = 365$ nm) and photoreaction (with $\lambda = 254$ nm) of trinitrene **82** can simultaneously be followed by using both UV–vis and IR spectroscopy. Hence, the assignment of the UV–vis bands is confirmed by the correlation with the IR features that were unequivocally assigned to trinitrene **82**.

Irradiation of **82** with UV light ($\lambda = 254$ nm) in Ar at 3 K results in a decrease of all IR signals assigned to **82** accompanied by the formation of very weak signals, although a well-defined peak at 2302 cm^{-1}. However, this signal is blue-shifted in almost 100 cm^{-1} compared to the typical –C≡N vibrations. For example, photolysis of 1,3-diazidobenzene is reported to produce the corresponding nitrene, which subsequently inserts into the 1,6-aromatic bond inducing ring-opening and resulting in the formation of aminoacetylenes. IR signals at 2220 and 2110 cm^{-1} were detected and assigned to –C≡N and –C≡C–H fragments, respectively.[187] An identification of the photoproducts obtained from trinitrene **82** is not possible because of the low intensity of most of the formed peaks, however, the signal at 2302 cm^{-1} indicates that Cl atoms should be bonded in closer positions to the –C≡N group. Indeed, IR signals at 2297 and 2290 cm^{-1} are reported for chlorocyanoacetylene in the gas and solid phase, respectively.[192]

Reactive Matrices

Since trinitrene **82** can be generated in good yields in inert gas matrices, it would be interesting to explore its potential reactions with small molecules like O_2. There is no reference on literature about O_2 trapping of high-spin polynitrenes yet. The parent phenylnitrene **6** can be isolated in solid Ar, Xe, mixtures of these inert gases with O_2, and even in pure solid O_2.[44] Annealing of a 4% O_2-doped Xe matrix containing nitrene **6** at temperatures above 40 K, results in the formation of phenylnitroso *O*-oxide **87**. Upon visible light irradiation (450 nm), intermediate **87** rapidly rearranges to the more stable nitrobenzene **88** (Scheme 21).

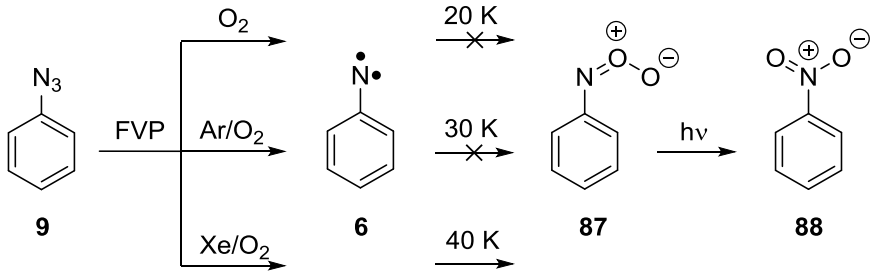

Scheme 21. Reaction of phenylnitrene **6** with O_2 in low-temperature matrices.

To investigate the reaction of trinitrene **82** with O_2, Ar and Xe matrices were doped with 5% of O_2. This content of O_2 in the matrix is high enough since the ratio of O_2/**82** would be in the order of 50:1. Carbenes are completely oxidized when photoproduced in Ar/O_2 matrices with a content of O_2 higher than 4%.[139] Doped matrices containing precursor **79** are deposited at the lowest temperature and irradiated with λ = 365 nm for 4 h in order to completely convert **79** into trinitrene **82**. The matrices are warmed up to 32 K (Ar) or 50 K (Xe) for 12 h and the reaction is monitored by recording spectra every 15 min. At these relatively high temperatures, O_2 molecules will diffuse and potentially interact with the guest molecules. Indeed, the more volatile H_2 has been detected in Xe matrices even after 60 h of uninterrupted annealing at 50 K.[100] However, trinitrene **82** does not react at all with O_2 in doped Ar or Xe matrices. Likewise, trinitrene **82** is also trapped in solid O_2 and no reaction was observed at temperatures up to 20 K, when the O_2 matrix starts subliming (Figure 48).

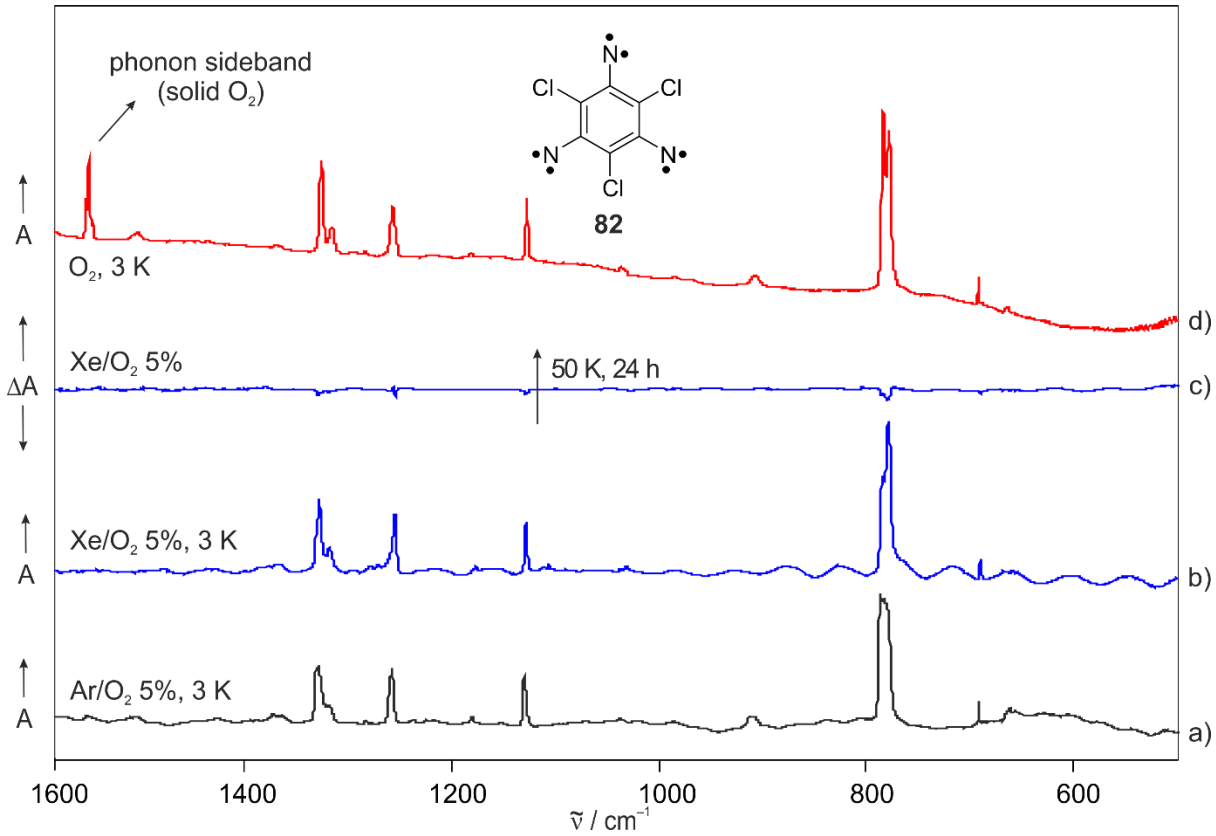

Figure 48. IR spectra showing the formation of 1,3,5-trichloro-2,4,6-trinitrenobenzene **82** in O_2 matrices. a) IR spectrum of **82** in 5% O_2-doped Ar at 3 K, obtained after irradiating 1,3,5-triazido-2,4,6-trichlorobenzene **79** with λ = 365 nm for 4 h. b) IR spectrum of **82** in 5% O_2-doped Xe at 3 K, obtained after irradiating **79** with λ = 365 nm for 4 h. c) Difference IR spectrum obtained after annealing the matrix (b) at 50 K for 24 h. d) IR spectrum of **82** in solid O_2 at 3 K, obtained after irradiating **79** with λ = 365 nm for 4 h. The marked signal is an IR-active phonon sideband of O_2.[193]

The finding shows that trinitrene **82** is less reactive than phenylnitrene **6** toward O_2 despite having six unpaired electrons. For the spin-allowed reaction of triplet **6** and triplet O_2, an activation barrier was determined to be 4.3 ± 0.5 kcal/mol by flash photolysis experiments.[194] In case of the oxygenation of septet **82**, the barrier would probably be higher due to electronic and steric effects originated by the Cl substituents, albeit spin restrictions cannot be rule out. Trinitrenes in general have robust septet ground states with large energy gaps between the ground state and the lower-spin excited states (quintet, triplet, and open-shell singlet).[178]

Low-density amorphous water–ice (LDA ice) has a peculiar structure characterized by the absence of long-range periodic structures. At cryogenic temperatures, it is a polar matrix that has proven to be a suitable medium to synthesize and stabilize organic cations by protonation of the corresponding carbenes.[17,158] Although arylnitrenes are in general less reactive toward H-abstraction or protonation,[161] trinitrene **82**, with three subvalent nitrogen atoms, is not expected to remain inert in such an acidic host like LDA ice. Hence, triazide **79** was deposited together with an excess of water onto a cold window at 50 K. The temperature was lowered to 8 K and the matrix was irradiated with λ = 365 nm light for 4 h until complete depletion of all bands assigned to **79** (Figure 49).

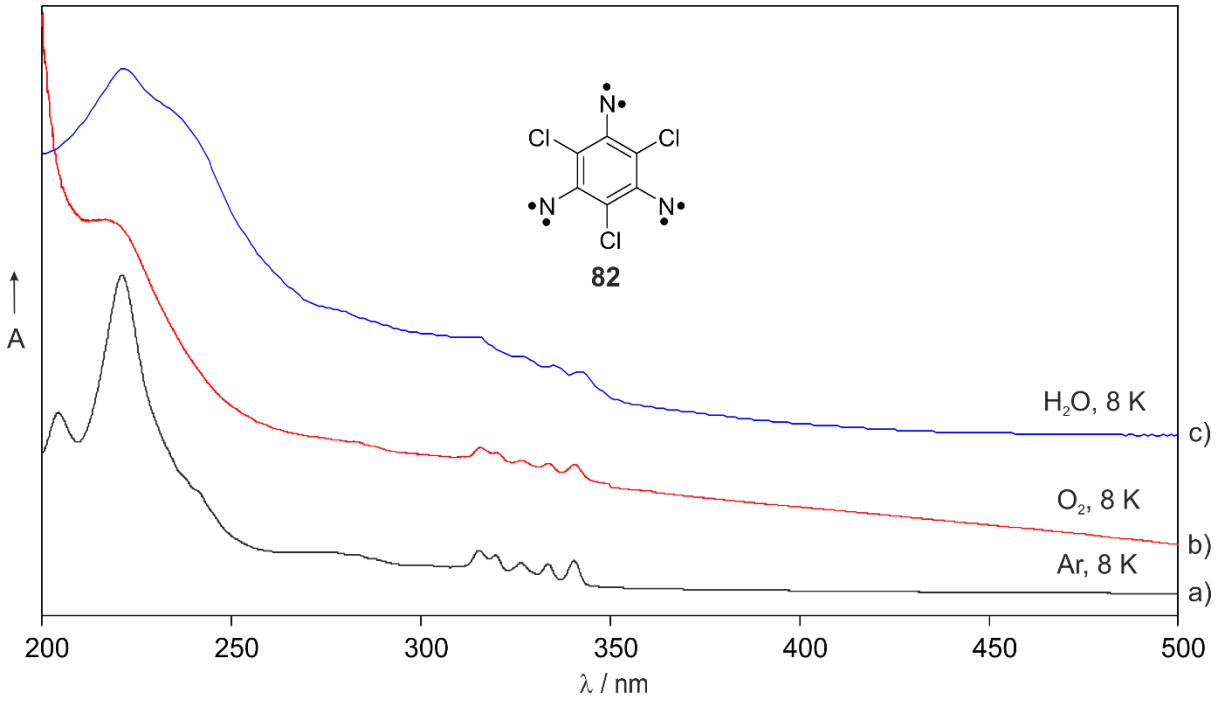

Figure 49. UV–vis spectra showing the formation of 1,3,5-trichloro-2,4,6-trinitrenobenzene **82** in reactive matrices. a-c) UV-vis spectra obtained after irradiating 1,3,5-triazido-2,4,6-trichlorobenzene **79** with λ = 365 nm in Ar, O_2, and H_2O at 8 K. Trinitrene **82** is stable in the H_2O matrix up to 160 K, at this point H_2O starts subliming.

The spectrum obtained after complete photolysis of **79** in LDA ices matches with the one recorded in Ar and pure O_2 matrices, albeit some the spectral features are not as resolved as in Ar matrices. Such broadening of the bands in LDA ice is explained by the multiple orientations of the water molecules, resulting in a highly heterogeneous matrix.[17] Annealing of the LDA ice containing trinitrene **82** was carefully performed from 8 to 120 K (transition temperature to crystalline ice) and further on to 170 K, where ice starts subliming.[195] Surprisingly, trinitrene **82** was stable up to 160 K, just before the degradation point of the matrix. Trinitrene **82** is therefore trapped in LDA ices in high yields, in clear contrast to triplet diphenylcarbene **4** or singlet phenylchlorocarbene **36**, which quantitatively form benzhydryl cation and singlet complex **36**$\cdots H_2O$, respectively. Hydrogen abstraction by nitrenes is generally associated with endothermic processes involving high activations barriers (as previously shown in Figure 28), which are less probable to be overcome or penetrated even at temperatures as high as 160 K. Solvation of nitrenes is predicted to reduce the enthalpy of the H-abstraction by triplet nitrenes, resulting in exothermic processes as for acyl- and alkoxycarbonylnitrenes.[161] As for phenylnitrene **6**, the enthalpy decreases from 5.7 kcal/mol in the gas phase to 4.5 kcal/mol in benzene, and further down to 2.4 kcal/mol in methanol.

On the other hand, there is not much experimental data about isolating nitrenium ions at cryogenic conditions since most of studies have been done in solution by using ultrafast spectroscopy.[22] Several ways of generating nitrenium ions in matrix have so far been described in literature such as: upon X-irradiation of nitrenes,[196] laser irradiation of amines[197] and production of nitrenes in HCl-doped inert gas matrices.[198] Herein, the latter procedure is used by depositing triazide **79** in HCl-doped Ar matrices, followed by 365 nm irradiation and successive warming of the matrix up to 30 K. Trinitrene **82** is formed in 1% HCl-doped Ar matrices and is invariant upon annealing or photolysis with 365 and 405 nm light. In addition, the experiment was repeated by using a higher content of HCl in the matrix (5%), resulting in very small amount of trinitrene **82** formed. Only weak and broad IR signals are detected suggesting that triazide **79** reacts photochemically with the neighboring HCl molecules to form multiple products in low concentration.

As a further step in studying the stability of trinitrene **82** in reactive matrices, X-band EPR experiments were carried out. Triazide **79** was sublimed and deposited with an excess of H_2 on the tip of a cooper rod at 5 K. In contrast to D_2, the more volatile H_2 is not expected to be held as a solid matrix at 5 K for a prolonged time. Hence, precursor **79** was probably deposited onto

the rod as a neat matrix. After photolysis of the neat matrix with 365 nm light for 30 min, all the observed EPR signals match to the ones reported in Ar matrices at 15 K, and previously assigned to the symmetric septet trinitrene **82** (Figure 50).[189]

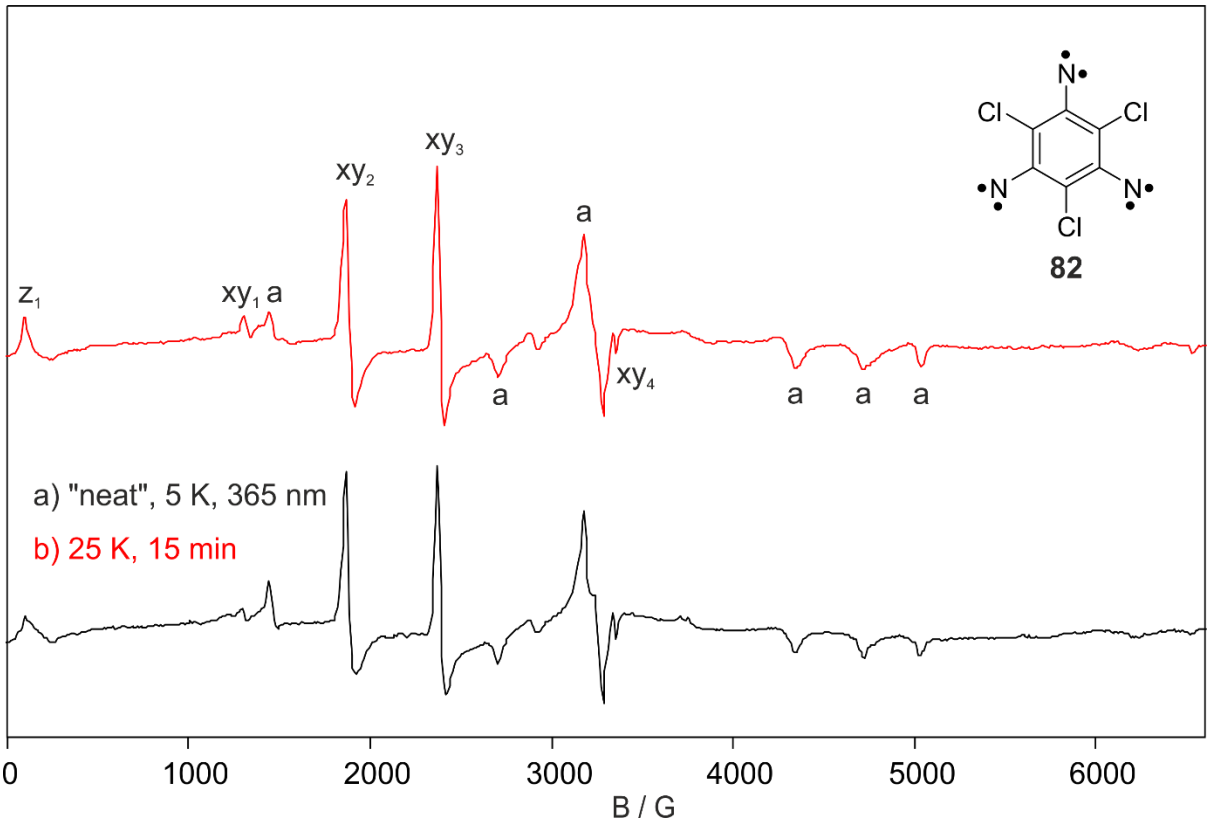

Figure 50. EPR spectra showing the formation of 1,3,5-trichloro-2,4,6-trinitrenobenzene **82** in "neat" matrices. a) EPR spectrum obtained after irradiating 1,3,5-triazido-2,4,6-trichlorobenzene **79** with λ = 365 nm for 30 min at 5 K. b) EPR spectrum obtained after annealing the matrix for 15 min at 25 K and subsequent cool down to 5 K. EPR signals are labeled as Z-transitions, XY-transitions, and off-principal-axis transitions (a).

Although the signals in the EPR spectrum are much broader than those reported in Ar, septet trinitrene **82** (S = 3, g = 2.0023, |D/hc| = 0.0957 cm^{-1}, and |E/hc| = 0 cm^{-1}) is basically the only paramagnetic product produced.[189] The EPR signals are assigned to one Z-transition at 180 mT (z_1), four XY-transitions at 1530 (xy_1), 1950 (xy_2), 2380 (xy_3), and 3400 (xy_4) mT, and additional six off-principal-axis transitions (denoted as a). Upon annealing to 25 K for 15 min and cooling back to 5 K, no change in the intensity of all signals is observed, showing that trinitrene **82** was initially produced in a matrix of neat triazide **79**. If H_2 were initially deposited, layers of matrix would immediately boil off at 25 K, producing a decrease in the concentration of the septet species. The trapping of the septet trinitrene **82** in reactive hosts like precursor **79** tells about the unreactivity of nitrenes toward organic compounds at low temperatures. This agree to the observations that the main deactivation path of triplet

phenylnitrene **6**, when warming organic glasses gradually up to room temperature, is the dimerization to form azobenzene **13**.

1,3,5-Tribromo-2,4,6-trinitrenobenzene

Among all organic polyradicals, high-spin nitrenes have the highest D values and exhibit the strongest magnetic properties. The dominant contribution to the parameter D usually arises from the dipolar spin-spin interaction (D_{SS}), which is proportional to the spin density at the nitrene center.[199] However, the introduction of heavy bromine atoms in polynitrenes leads to unprecedently large values of D because of a dominant spin-orbit coupling contribution (D_{SO}).[200] In this regard, septet 2,4,6-tribromo-1,3,5-trinitrenobenzene **86** was generated in methylcyclohexane glasses at 5 K and characterized by W-band EPR spectroscopy.[190] A large |D/hc| value of 0.203 cm^{-1} was determined, which is twice the value reported for the chloro-based trinitrene **82** (|D/hc| = 0.0957 cm^{-1}). Albeit trinitrenes **82** and **86** are predicted to have a similar spin density at the nitrene center (~1.54), a strong spin-orbit coupling increases the magnetic anisotropy of trinitrene **86**, resulting in stronger magnetic properties (Figure 51). Hence, it would be important to explore the chemical reactivity of trinitrene **86**, as a potential candidate for designing molecular magnets

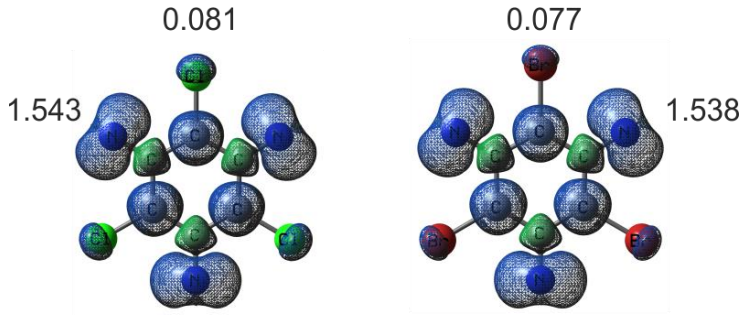

Figure 51. Spin density distribution of D_{3h} symmetric septet 1,3,5-trichloro-2,4,6-trinitrenobenzene **82** and 1,3,5-tribromo-2,4,6-trinitrenobenzene **86**, calculated at the B3LYP/aug-cc-PVTZ level of theory. Blue color indicates an excess of α-spin density at the atom (positive spin density), and green color shows an excess of β-spin density at the atom (negative spin density). Only values of the spin density at nitrogen and halogen atoms are indicated.

IR and UV–vis Spectroscopy

Matrix isolated 1,3,5-triazido-2,4,6-tribromobenzene **83** was irradiated with λ = 405 nm light for 15 h in Ar matrices. After the prolonged photolysis, all IR signals assigned to triazide **83** (2140, 1531, 1384, 1267, 638, and 522 cm^{-1}) are depleted and a clean spectrum containing several spectral features is recorded (Figure 52).

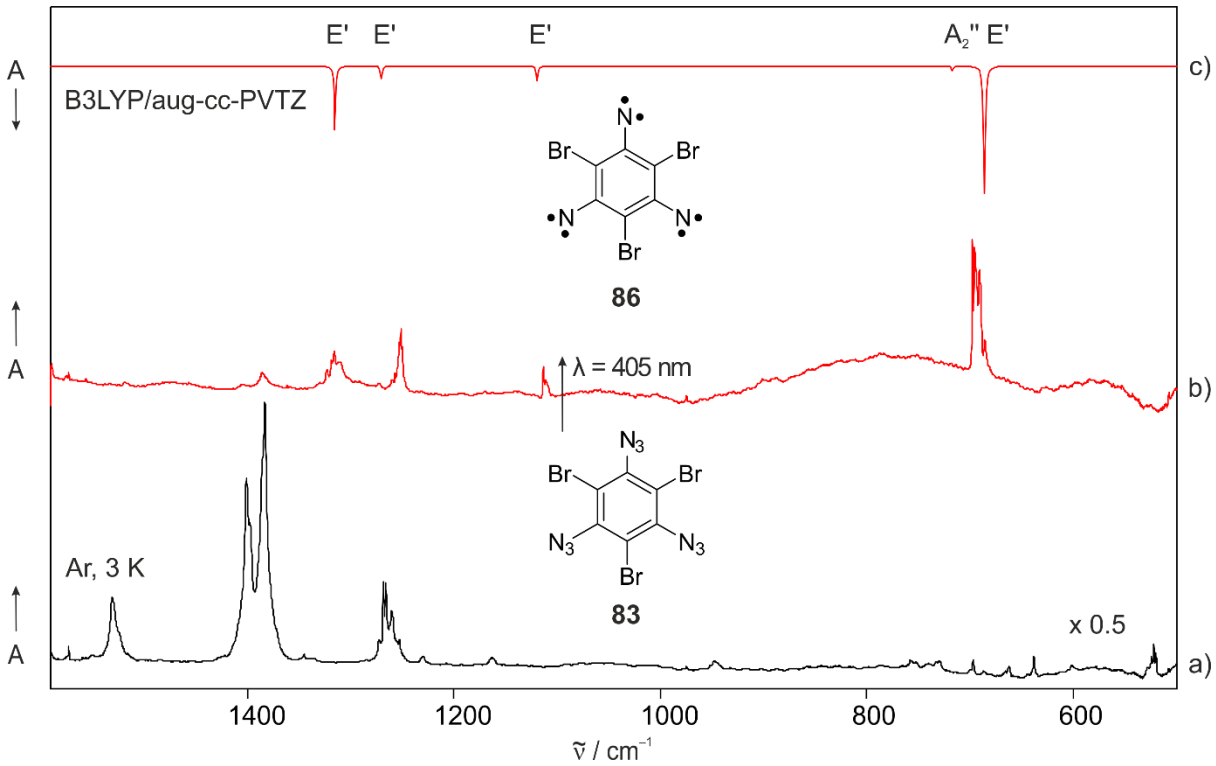

Figure 52. IR spectra showing the photochemistry of 1,3,5-triazido-2,4,6-tribromobenzene **83** in Ar matrices. a) IR spectrum of **83** in Ar at 3 K. b) IR spectrum obtained after irradiating **83** with λ = 405 nm for 15 h. c) IR spectrum of septet 1,3,5-tribromo-2,4,6-trinitrenobenzene **86** calculated at the B3LYP/aug-cc-PVTZ level of theory.

The new signals are assigned to septet trinitrene 1,3,5-tribromo-2,4,6-trinitrenobenzene **86**. By comparing the obtained IR spectrum with the one calculated at the B3LYP/aug-cc-PVTZ level of theory, a good matching concerning the position and intensity of the doubly degenerate modes (E') is found. On the other hand, there is no precursor remaining and neither triplet **84** nor quintet **85** species is detected at the end of the irradiation. Once again, typical photoproducts of nitrenes, such as azirines and cyclic ketenimines are not observed for this molecule either, and a clean spectrum is obtained (Table 9).

Table 9. Vibrational frequencies of 1,3,5-tribromo-2,4,6-trinitrenobenzene **86** measured in Ar at 3 K and calculated at the B3LYP/aug-cc-PVTZ level of theory.

Mode	Symmetry	$\tilde{\nu}_{exp.}$ /cm^{-1}	$I_{rel., exp.}$	$\tilde{\nu}_{calc.}$/cm^{-1}	$I_{rel., calc}$	Assignment
21	A_2"	686	0.05	718	0.08	ring def. (oop)
19, 20	E'	690–697	1.00	686	1.00	C–Br str.
23, 24	E'	1108–1113	0.12	1119	0.13	ring def. (ip)
25, 26	E'	1249–1256	0.14	1270	0.13	C–N str.
28, 29	E'	1310–1322	0.68	1315	0.50	C–C str.

Relative intensities based on the strongest absorption. Modes (E') are doubly degenerate.

The IR signals assigned to trinitrene **86** are in general red-shifted only a few wavenumbers (5–20 cm^{-1}) with respect to trinitrene **82** because of the structural similarity between them. However, the most intense signals for both nitrenes are separated by about 90 cm^{-1} and are assigned to the C–X stretching vibration. Such large frequency shift is explained since the C–Cl bonds are more polar and stronger than the C–Br, being also reflected in the calculated bond distances as shown in Figure 53.

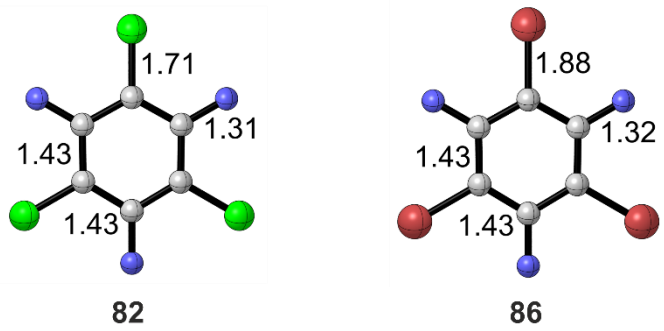

Figure 53. Selected bond distances (Å) of septet 1,3,5-trichloro-2,4,6-trinitrenobenzene **82** and septet 1,3,5-tribromo-2,4,6-trinitrenobenzene **86**, calculated at the B3LYP/aug-cc-PVTZ level of theory.

Moreover, it can be noticed a remarkable broadening on the signals of trinitrene **86** and their splitting into several components. A careful analysis on the shape of the vibration centered at 693 cm^{-1} reveal the existence of four intense peaks at 690–697 cm^{-1} and a weaker one at 686 cm^{-1}. Such weak signal can be assigned to the ring deformation (oop) mode of trinitrene **86**, since it appears at a similar frequency that the equivalent mode in trinitrene **82** (691 cm^{-1}), and such mode should not be sensitive to the exchange of Br by Cl atoms. It seems that the large red-shift in the C–X stretching (Cl→Br) causes an overlapping of the E' and A_2" modes in trinitrene **86**. On the other hand, the four peaks observed at 690–697 cm^{-1} could perhaps arise from the isotopic distribution in trinitrene **86**. However, calculations predict a frequency difference of 0.6 cm^{-1} between the lighter ($^{79}Br^{79}Br^{79}Br$) and heavier ($^{81}Br^{81}Br^{81}Br$) isotope distributions, and that is much smaller than the observed broadening.

Matrix UV–vis experiments were also carried out in Ar matrices at 8 K. Matrix-isolated triazide **83** shows a broad and strong absorption centered at 244 nm. Irradiation of the matrix with λ = 365 nm results in a decrease of the band assigned to **83** and new spectral features (315–350, 233, and 219 nm) arise. The spectrum in general resemblances the one obtained for trinitrene **82**, albeit the bands are more intense and resolved for the chloro-based trinitrene. Hence, based on the similarity of both spectra, the characteristic vibrational progression

observed, and the formation of trinitrene **86** in high yields in the IR experiments, it is reasonable that all bands observed in the UV–vis experiment also belong to trinitrene **86** (Figure 54).

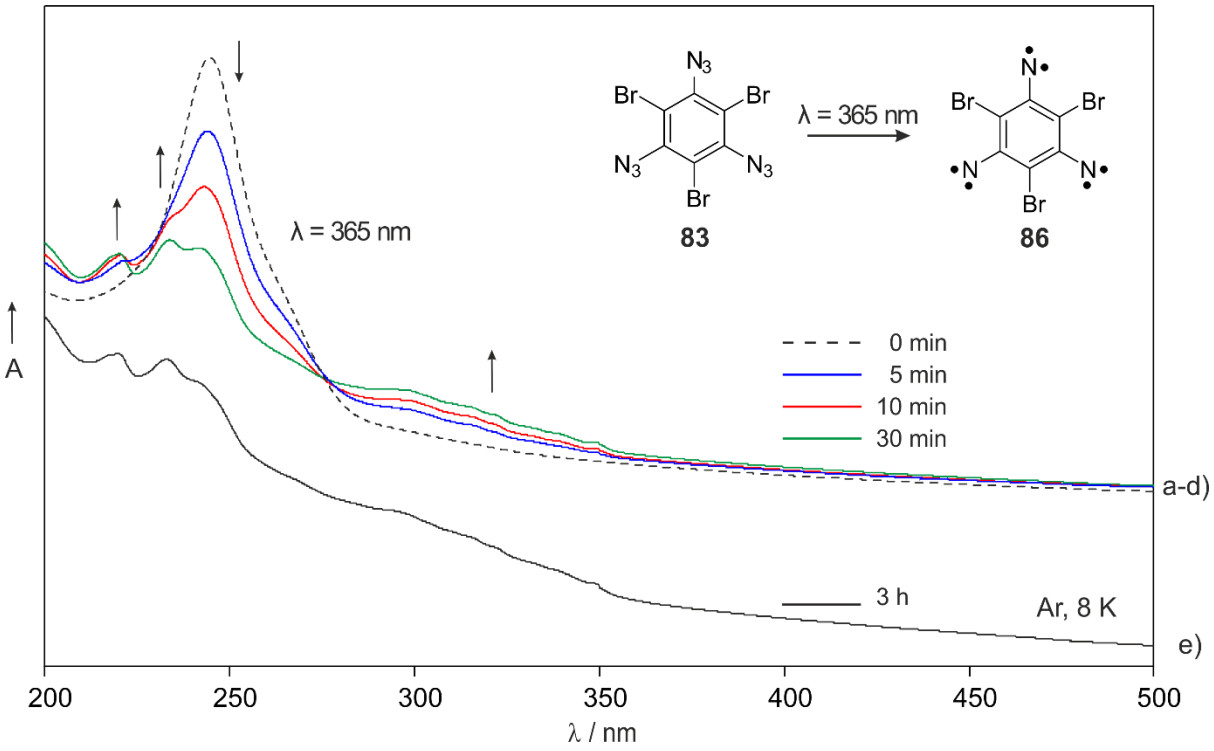

Figure 54. UV–vis spectra showing the photochemistry of 1,3,5-triazido-2,4,6-tribromobenzene **83** in Ar matrices. a) UV–vis spectrum of **83** in Ar at 8 K. b-d) UV–vis spectra obtained after irradiating **83** with λ = 365 nm for 5, 10, and 30 min, respectively. e) UV–vis spectra of 1,3,5-tribromo-2,4,6-trinitrenobenzene **86**, obtained after irradiating **83** with λ = 365 nm for 3 h.

Finally, triazide **83** was deposited along with an excess of *p*-H_2 matrix onto a cold window at 3 K. Irradiation of the matrix with λ = 405 nm for 15 h, results in the formation of the signals previously assigned to trinitrene **86**. Under the same experimental conditions, photolysis of **83** in either *p*-H_2 or Ar matrices at 3 K, produces similar spectra and no even traces of any other product are observed. Moreover, it is interesting that the broad band of trinitrene **86** at 686–697 cm^{-1} containing five peaks, appears in *p*-H_2 as a sharp signal at 691.5 cm^{-1} with a bandwidth of only 1 cm^{-1}. Hence, the splitting of the signals observed in Ar could probably be related to matrix effects that are inexistent in a "soft" solid as *p*-H_2 (Figure 55).

The H-abstraction by trinitrene **86** to form a sextet dinitrenoaminyl radical is an endothermic process (14.4 kcal/mol) with a high barrier of 19.1 kcal/mol, according calculations at the B3LYP-D3/def2-TZVP level of theory. In case of trinitrene **82**, very similar enthalpies (14.0 kcal/mol) and activation barriers (18.3 kcal/mol) are predicted. These unfavorable energy

values are also similar to the ones predicted for arylnitrenes **7** and **8**, as previously shown in Figure 28.

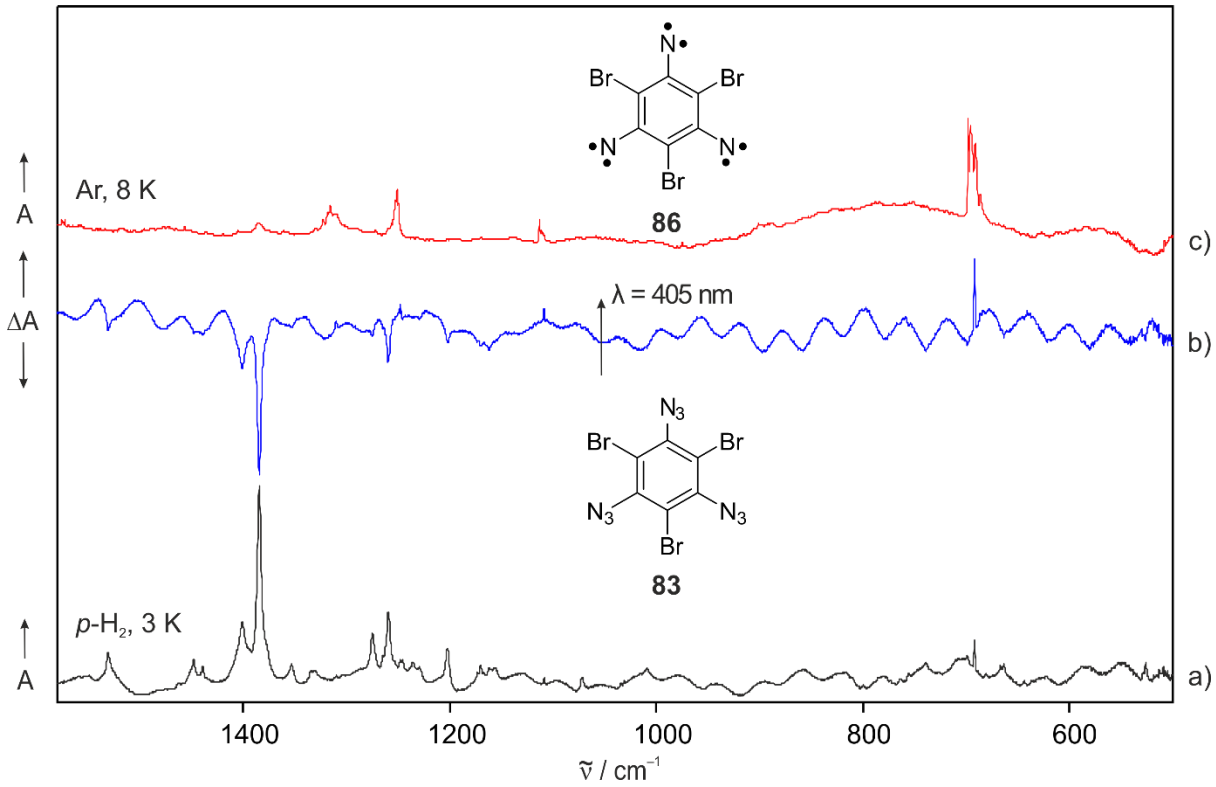

Figure 55. IR spectra showing the photochemistry of 1,3,5-triazido-2,4,6-tribromobenzene **83** in *p*-H_2 matrices. a) IR spectrum of **83** in *p*-H_2 at 3 K. b) IR spectrum obtained after irradiating **83** with λ = 405 nm for 15 h in *p*-H_2 at 3 K. c) IR spectrum of septet 1,3,5-tribromo-2,4,6-trinitrenobenzene **86**, obtained after irradiating **83** with λ = 405 nm for 15 h in Ar at 3 K.

Overall, highly symmetric trinitrenes **82** and **86** shows an unprecedent stability in both inert gas and reactive matrices, as compared to other high-spin polynitrenes and arylnitrenes in general. In water matrices, trinitrene **82** is surprisingly stable up to 160 K, which tells that this high-spin nitrene might have the potential to be generated and characterized not only under cryogenic conditions, but also under conventional organic chemistry conditions. The stability toward reactive molecules, the robust ground states, and the strong magnetic properties suggest that these septet species could be used as building blocks for the synthesis of organic magnetic materials. Moreover, water matrices are stable up to 170 K, temperature where ice starts subliming, hence water can be used as a novel matrix host for studying elusive species at unusual higher temperatures.

Experimental Section

Methods

Matrix Isolation: Experiments were performed by using standard techniques as described in literature.[201,202] To reach cryogenic temperatures, Sumitomo Heavy Industries two-staged closed-cycle helium refrigerator systems (3 K) or Air Products Diplex close-cycle helium refrigerator systems (8 K) are used. High vacuum (10^{-5}–10^{-7} mbar) is reached by using an oil diffusion pump for IR and UV–vis experiments, while a turbo pump is used for X-band EPR experiments. Matrices were generated by co-deposition of the substance of interest along with an excess of gas onto a cesium iodide window (IR), a sapphire window (UV–vis), or an oxygen-free high-conductivity copper rod (EPR). The windows are connected to the copper framework of the cryostat, and the thermal contact is made using an indium wire. The temperature of the window is measured by using a silicon diode at the copper holder and an Oxford ITC4 temperature controller. Inert gases used for matrix isolation were Ar (Air Liquide, 99.999%), Ne (Air Liquide, 99.999%) or Xe (Messer, 99.99%). As reactive hosts, O_2 (Air Liquide, 99.9995%), H_2 (Air Liquide, 99.999%) or D_2 (Merck Schuchardt, 99.5%) were used. Deposition times varied between 30 min and 4 h and a flow rate of about 1 mbar/min was typically used for the host gas. The gas flow was controlled by a MKS mass flow controller. The experiments in low-density amorphous ice were performed in a similar manner by using H_2O vapor as host.[195] Ultra-pure water was degassed in several freeze–thaw cycles and deposited onto the cold window held at 50 K, by controlling the deposition rate with a fine metering valve.

Low-Temperature Spectroscopy: Matrix isolation IR spectra were recorded with a Bruker IFS66, a Bruker IFS66s or a Bruker Vertex V70 FTIR spectrometer with a resolution of 0.5 cm^{-1}. To block light of wavenumbers greater than 4000 cm^{-1}, the IR beam of the spectrometer was passed through a IR long pass interference filter (Edmund, LP2400 nm) to avoid the formation of vibrationally excited H_2 upon absorption of the unfiltered IR light.[148] The spectrometer and outer windows were purged with dry air in order to get rid of both CO_2 and water from the atmosphere. Matrix-isolation UV–vis spectra were recorded with a Varian Cary 5000 spectrometer with a resolution of 0.2 nm. Matrix-isolation EPR spectra were recorded on a Bruker Elexsys 500 X-band spectrometer.

Standard Spectroscopy: IR spectra were recoded with an Equinox 55 FTIR spectrometer. NMR spectra were recorded with a Bruker DPX 200 (200 MHz ^{1}H-NMR, 50.3 MHz ^{13}C-NMR) spectrometer. NMR shifts are reported in parts per million (ppm) downfield from tetramethylsilane and referenced with respect to the solvent signal. Signal multiplicities are reported according to standard assignments. Mass spectrometric analyses were carried out by the SC department of the Ruhr-Universität Bochum using a VG Autospec mass spectrometer for standard mass spectra (MS), and a Joel AccuTOF GCv JMS-T100GCV spectrometer for high resolution mass spectra (HRMS). Ionization methods were electron ionization (EI) or fast atom bombardment (FAB).

Light Sources: Broadband photolysis of the matrices was performed using a high-pressure mercury lamp (Ushio 500 W) equipped with dichroic mirrors (Oriel) and long pass cut-off filters (Schott, 50% transmission), and custom-made LEDs with λ = 650, 530, 505, 450, 405 or 365 nm (max. 5 W). A low-pressure mercury arc lamp with λ = 254 nm (Gräntzel) was used for narrowband irradiation. Monochromatic irradiation was conducted with a 308 nm XeCl-excimer laser. For visible (λ = 560 nm) and IR irradiation (>4000 cm^{-1}), a lamp-pumped OPO laser (InnoLas Laser model SpitLight 600 midband) was used.

***p*-Hydrogen:** This description corresponds to the experiments conducted in Taiwan. As the experimental procedure for converting *o*-H_2 into *p*-H_2 is well established, only a brief information is herein given.[203,204] Normal H_2 (99.9999%, Scott Specialty Gases) is allowed to flow through a cold trap at 77 K before entering the *p*-H_2 converter. The converter contains a copper coil filled with hydrated iron (III) oxide catalyst (30−50 mesh, Sigma-Aldrich) that is cooled with a closed-cycle refrigerator (Advanced Research Systems, DE204AF). The efficiency of conversion is controlled by the temperature of the catalyst, e.g. at 13 K the concentration of *o*-H_2 is less than 100 ppm, according to Boltzmann distribution. Precursors are premixed with the freshly prepared *p*-H_2 and deposited onto a gold-plated copper block, cooled to 3.2 K with a closed-cycle cryostat (Sumitomo Heavy Industries, RDK-415). The cold plate serves as both a matrix sample substrate and a mirror to reflect the incident IR beam to the detector. IR absorption spectra at resolution 0.25 cm^{-1} were recorded with a FTIR spectrometer (Bruker Vertex V80v), equipped with a KBr beam splitter and a HgCdTe detector cooled to 77 K.

Calculations: Geometry optimizations, vibrational frequencies, and IRC profiles were calculated using the B3LYP[205,206] hybrid functional with D3 empirical dispersion correction.[207] Excited state calculations (TDDFT) were perfomed using the M06-2X[208] functional. Several basis sets such as def2-TZVP,[209] cc-pV(D/T)Z,[210] and aug-cc-pV(T/Q)Z[211] were employed. Tight convergence criteria for gradients and a full (99 590) integration grid, having 99 radial shells per atom and 590 angular points per shell, were used throughout. CCSD(T) single point calculations on top of DFT geometries were performed to recalculate S–T energy gaps, enthalpies, and activation barriers of arylcarbenes. In case of CH_2, more accurate methods such as CCSD(T), QCISD(T), MRCI, and CBS-APNO[212] were employed. DFT and CBS calculations were done with the Gaussian 09[213] suite of programs, whereas CCSD(T), QCISD(T), and MRCI calculations were performed using the Molpro 2012 program[214]. Experimental EPR spectra were analyzed using the Easyspin program package.[215]

Synthesis

All starting materials and reagents were purchased from commercial suppliers and used without further purification. Solvents were purified by standard procedures. TLC analysis was carried out using Polygram G/UV_{254} silica gel pre-coated plates. Spots were analyzed using a CAMAG UV lamp. ICN silica 32–63 (60 Å) or aluminum oxide (stage 1) were used as stationary phase for column chromatography. Aluminum oxide was deactivated (stage 4) before use by mixing it with water in a ratio of 100 g/8ml.

9-Diazofluorene 40: The sample was synthesized from 9-fluorenone, according to literature.[216] ^{1}H-NMR (200 MHz, DMSO-d_6): δ = 8.08 (d, 2 H, ArH), 7.71 (d, 2 H, ArH), 7.45–7.29 (m, 4 H, ArH) ppm. IR (Ar, 3 K): $\tilde{\nu}$ = 3071, 2088, 2061, 1608, 1448, 1443, 1378, 1331, 1310, 1225, 1220, 1155, 752, 725, 653, 618, and 561 cm^{-1}.

Diphenyldiazomethane 45: The sample was synthesized from benzophenone hydrazone, according to literature.[217] Before use, precursor **45** was purified by flash column chromatography (alumina, pentane). ^{1}H-NMR (200 MHz, DMSO-d_6): δ = 7.42 (t, 4 H, ArH), 7.27–7.17 (m, 6 H, ArH) ppm. IR (Ar, 3 K): $\tilde{\nu}$ = 3070, 2047, 1600, 1582, 1503, 1497, 1457, 1447, 1320, 1305, 1270, 1263, 1035, 937, 756, 750, 697, 692, and 651 cm^{-1}.

Bis(*p*-methoxyphenyl)diazomethane 63: The sample was synthesized according to literature[218] by two reaction steps: synthesis of the corresponding hydrazone,

bis(*p*-methoxyphenyl)methylenehydrazone, followed by oxidation with HgO to form **63** as a purple solid. ^{1}H-NMR (200 MHz, DMSO): δ = 3.77 (s, 6 H, OCH_3), 7.00–7.05 (d, 4 H, ArH), 7.15–7.19 (d, 4 H, ArH) ppm. IR (Ar, 3 K): 3020–2843 (broad), 2040, 1515, 1469, 1443, 1309, 1279, 1252, 1184, 1177, 1048, 827, and 606 cm^{-1}.

3-Methoxy-9-diazofluorene 68: The sample was synthesized by I. Trosien (Ruhr-Universität Bochum). It was deposited in matrix as received. IR (Ar, 3 K): $\tilde{\nu}$ = 2075, 2058, 1495, 1469, 1452, 1439, 1291, 1249, 1207, 1178, 1156, 1043, 811, 765, 744, and 650 cm^{-1}.

Tetraphenylethylene 46: The sample was deposited in matrix as received. IR (Ar, 3 K): $\tilde{\nu}$ = 3120–3020 (broad), 1605, 1495, 1446, 1077, 1032, 781, 761, 747, 701, 626, 616, and 570 cm^{-1}.

Fluorene 41: Deposited in matrix as received. IR (Ar, 3 K): $\tilde{\nu}$ = 3110–3000 (broad), 2920, 1483, 1456, 1451, 1408, 1313, 1299, 1190, 1106, 955, 740, 695, and 622 cm^{-1}.

9,9-Dideuterofluorene d_2**-41:** The sample was synthesized by I. Trosien (Ruhr-Universität Bochum). It was deposited in matrix as received. IR (Ar, 3 K): $\tilde{\nu}$ = 3110–3000 (broad), 2920, 1481, 1453, 1449, 1307, 1284, 1231, 1193, 1101, 1041, 1037, 1002, 941, 829, 739, 669, and 622 cm^{-1}.

Diphenylmethane 47: The sample was deposited in matrix as received. IR (Ar, 3 K): $\tilde{\nu}$ = 3120–3010 (broad), 2930, 2850, 1604, 1498, 1459, 1455, 1080, 1032, 737, 725, 700, 695, 609, and 554 cm^{-1}.

1,1-Dideuterodiphenylmethane d_2**-47:** Deuterated compounds were synthesized according to literature.[219] ^{1}H-NMR (200 MHz $CDCl_3$): δ = 7.23–7.42 ppm (m, 10 H, ArH). ^{13}C NMR (50 MHz, $CDCl_3$): δ = 126.13, 128.51, 128.97, 141.11 ppm. MS (EI): *m/z* (%) 170.1 (100) [M^+], 169.1 (90), [M^+-H]. IR (Ar, 3 K): $\tilde{\nu}$ = 3120–3000 (broad), 2211, 2139, 2108, 1604, 1497, 1452, 1079, 1038, 1014, 733, 726, 700, 698, 693, 603, and 554 cm^{-1}.

Bis(*p*-methoxyphenyl)methane 64: The sample was synthesized from bis(4-methoxyphenyl) methanone, according to literature.[220] ^{1}H-NMR (200 MHz, $CDCl_3$): δ = 3.79 (s, 6 H, OCH_3), 3.87 (s, 2 H, CH), 6.83 (d, 4 H, ArH), 7.10 (d, 4 H, ArH) ppm. ^{13}C NMR (50 MHz, DMSO-d_6): δ = 40.26, 55.39, 113.99, 129.86, 133.86, 158.05 ppm. IR (Ar, 3 K): $\tilde{\nu}$ = 3015, 2980–2900

(broad), 2856, 2841, 1619, 1607, 1590, 1515, 1469, 1443, 1305, 1274, 1254, 1184, 1175, 1054, 820, 805, and 577 cm^{-1}.

1,1-Dideuterobis(*p*-methoxyphenyl)methane d_2**-64:** The sample was synthesized from **64**, according to literature.[219] ^{1}H-NMR (200 MHz, $CDCl_3$): δ = 3.78 (s, 6 H, OCH_3), 6.82 (d, 4 H, ArH), 7.09 (d, 4 H, ArH) ppm. ^{13}C NMR (50 MHz, $CDCl_3$): δ = 55.40, 113.99, 129.84, 133.79, 158.04 ppm. MS (EI): *m/z* (%) 230.1 (100) [M^+], 229.1 (22) [M^+ -H]. HRMS *m/z* calcd. for $C_{15}H_{14}D_2O_2$: 230.12758, found: 230.09413. IR (Ar, 3 K): $\tilde{\nu}$ = 3014, 2980–2900 (broad), 2841, 1617, 1586, 1515, 1468, 1442, 1305, 1298, 1274, 1250, 1183, 1175, 1055, 805, 756, 720, and 574 cm^{-1}.

2,6-Dimethylphenylazide 54: The sample was synthesized from 2,6-dimethylaniline, according to literature.[221] ^{1}H-NMR (200 MHz, $CDCl_3$): δ = 7.06 (s, 3 H), 2.42 (s, 6 H) ppm. IR (Ar, 3 K): $\tilde{\nu}$ = 3079, 2990–2900 (broad), 2879, 2859, 2134, 2105, 1599, 1476, 1450, 1424, 1383, 1306, 1289, 1254, 1087, 1055, 1032, 992, 922, 768, 748, 699, 599, and 539 cm^{-1}.

2,6-Difluorophenylazide 56: The sample was synthesized from 2,6-difluoroaniline, according to literature.[221] ^{1}H-NMR (200 MHz, $CDCl_3$): δ = 6.88−6.95 (m, 2 H), 7.00−7.08 (m, 1 H) ppm. IR (Ar, 3 K): $\tilde{\nu}$ = 2058, 2144, 2122, 1593, 1501, 1487, 1481, 1337, 1330, 1297, 1278, 1245, 1154, 1128, 1063, 1050, 1022, 774, 723, 706, 613, 519, and 504 cm^{-1}.

1,3,5-Triazido-2,4,6-trichlorobenzene 79: The sample was synthesized by S. V. Chapyshev (Institute of Problems of Chemical Physics, Russian Academy of Sciences).[222] It was deposited in matrix as received. IR (Ar, 3 K): $\tilde{\nu}$ = 2192, 2146, 2123, 1542, 1527, 1416, 1400, 1277, 1233, 1176, 959, 793, 727, 658, and 522 cm^{-1}.

1,3,5-Triazido-2,4,6-tribromobenzene 83: The sample was synthesized by S. V. Chapyshev (Institute of Problems of Chemical Physics, Russian Academy of Sciences).[222] It was deposited in matrix as received. IR (Ar, 3 K): $\tilde{\nu}$ = 2215, 2137, 2102, 1531, 1401, 1383, 1268, 1260, 1163, 948, 758, 730, 697, 662 and 638 cm^{-1}.

Literature

(1) Eisenthal, K. B.; Moss, R. A.; Turro, N. J. *Science* **1984**, *225*, 1439.

(2) Kirmse, W. *Carbene Chemistry*; Academic Press: New York, London, 1971.

(3) Gleiter, R.; Hoffmann, R. *J. Am. Chem. Soc.* **1968**, *90*, 5457.

(4) Mulliken, R. S. *Phys. Rev.* **1932**, *41*, 751.

(5) Herzberg, G. *Proc. Roy. Soc. (London) A262* **1961**, *262*, 291.

(6) Wasserman, E.; Yager, W. A.; Kuck, V. J. *Chem. Phys. Lett.* **1970**, *7*, 409.

(7) Bernheim, R. A.; Bernard, H. W.; Wang, P. S.; Wood, L. S.; Skell, P. S. *J. Chem. Phys.* **1971**, *54*, 3223.

(8) Wasserman, E.; Kuck, V. J.; Hutton, R. S.; Anderson, E. D.; Yager, W. A. *J. Chem. Phys.* **1971**, *54*, 4120.

(9) McKellar, A. R. W.; Bunker, P. R.; Sears, T. J.; Evenson, K. M.; Saykally, R. J.; Langhoff, S. R. *J. Chem. Phys.* **1983**, *79*, 5251.

(10) Sulzbach, H. M.; Bolton, E.; Lenoir, D.; Schleyer, P. v. R.; Schaefer, H. F. *J. Am. Chem. Soc.* **1996**, *118*, 9908.

(11) Nemirowski, A.; Schreiner, P. R. *J. Org. Chem.* **2007**, *72*, 9533.

(12) Moss, R. A. *Acc. Chem. Res.* **1989**, *22*, 15.

(13) Jones, M.; Ando, W.; Hendrick, M. E.; Kulczycki, A.; Howley, P. M.; Hummel, K. F.; Malament, D. S. *J. Am. Chem. Soc.* **1972**, *94*, 7469.

(14) Eisenthal, K. B.; Turro, N. J.; Aikawa, M.; Butcher, J. A.; DuPuy, C.; Hefferon, G.; Hetherington, W.; Korenowski, G. M.; McAuliffe, M. J. *J. Am. Chem. Soc.* **1980**, *102*, 6563.

(15) Hirai, K.; Itoh, T.; Tomioka, H. *Chem. Rev.* **2009**, *109*, 3275.

(16) Liu, M. T. H.; Bonneau, R.; Jefford, C. W. *J. Chem. Soc., Chem. Commun.* **1990**, 1482.

(17) Costa, P.; Fernandez-Oliva, M.; Sanchez-Garcia, E.; Sander, W. *J. Am. Chem. Soc.* **2014**, *136*, 15625.

(18) Costa, P.; Sander, W. *Angew. Chem. Int. Ed.* **2014**, *53*, 5122.

(19) Henkel, S.; Costa, P.; Klute, L.; Sokkar, P.; Fernandez-Oliva, M.; Thiel, W.; Sanchez-Garcia, E.; Sander, W. *J. Am. Chem. Soc.* **2016**, *138*, 1689.

(20) Costa, P.; Mieres-Perez, J.; Özkan, N.; Sander, W. *Angew. Chem. Int. Ed.* **2017**, *56*, 1760.

(21) Lwowski, W. *Nitrenes*; John Wiley & Sons, Inc.: New York, 1920.

(22) *Nitrenes and Nitrenium Ions*; Falvey, D. E.; Gudmundsdottir, A. D., Eds.; John Wiley & Sons, Inc.: Hoboken, NJ, 2013; Vol. 6.

(23) Han, C. C.; Corelli, J. C. *J. Vac. Sci. Technol. B* **1988**, *6*, 219.

(24) Wang, J. F.; Downs, W. D.; Cech, T. R. *Science* **1993**, *260*, 504.

(25) Platz, M. S. In *Reactive Intermediate Chemistry*; Moss, R. A., Platz, M. S., Jones, M. S., Eds.; John Wiley & Sons, Inc.: Hoboken, NJ, 2004, p 501.

(26) Fairchild, P. W.; Smith, G. P.; Crosley, D. R.; Jeffries, J. B. *Chem. Phys. Lett.* **1984**, *107*, 181.

(27) Engelking, P. C.; Lineberger, W. C. *J. Chem. Phys.* **1976**, *65*, 4223.

(28) McCarty, M.; Robinson, G. W. *J. Am. Chem. Soc.* **1959**, *81*, 4472.

(29) Esser, H.; Langen, J.; Schurath, U. *Ber. Bunsenges. Phys. Chem.* **1983**, *87*, 636.

(30) Fischer, P. H. H.; Charles, S. W.; McDowell, C. A. *J. Chem. Phys.* **1967**, *46*, 2162.

(31) Davis, J. H.; Goddard, W. A. *J. Am. Chem. Soc.* **1977**, *99*, 7111.

(32) Gritsan, N.; Platz, M. In *Organic Azides Syntheses and Applications*; Bräse, S., Banert, K., Eds.; John Wiley & Sons, Ltd: Chichester, U.K., 2010, p 311.

(33) Bucher, G. In *CRC Handbook of Organic Photochemistry and Photobiology, Second Edition*; Press: Boca Raton, FL, 2004.

(34) Albini, A.; Bettinetti, G.; Minoli, G. *J. Am. Chem. Soc.* **1997**, *119*, 7308.

(35) Gritsan, N. P.; Platz, M. S. *Chem. Rev.* **2006**, *106*, 3844.

(36) Schrock, A. K.; Schuster, G. B. *J. Am. Chem. Soc.* **1984**, *106*, 5228.

(37) Huisgen, R. *Angew. Chem.* **1955**, *67*, 756.

(38) Gritsan, N. P.; Platz, M. S. *Adv. Phys. Org. Chem.* **2001**, *36*, 255.

(39) Wentrup, C. *Chem. Rev.* **2017**, *117*, 4562.

(40) Kvaskoff, D.; Luerssen, H.; Bednarek, P.; Wentrup, C. *J. Am. Chem. Soc.* **2014**, *136*, 15203.

(41) Schuster, G. B.; Platz, M. S. *Adv. Photochem.* **1992**, *17*, 69.

(42) Shields, C. J.; Chrisope, D. R.; Schuster, G. B.; Dixon, A. J.; Poliakoff, M.; Turner, J. J. *J. Am. Chem. Soc.* **1987**, *109*, 4723.

(43) Tsao, M.-L.; Platz, M. S. *J. Am. Chem. Soc.* **2003**, *125*, 12014.

(44) Mieres-Perez, J.; Mendez-Vega, E.; Velappan, K.; Sander, W. *J. Org. Chem.* **2015**, *80*, 11926.

(45) Morawietz, J.; Sander, W. *J. Org. Chem.* **1996**, *61*, 4351.

(46) Wijeratne, N. R.; Fonte, M. D.; Ronemus, A.; Wyss, P. J.; Tahmassebi, D.; Wenthold, P. G. *J. Phys. Chem. A* **2009**, *113*, 9467.

(47) Winkler, M. *J. Phys. Chem. A* **2008**, *112*, 8649.

(48) Hrovat, D. A.; Waali, E. E.; Borden, W. T. *J. Am. Chem. Soc.* **1992**, *114*, 8698.

(49) Moss, R. A.; Dolling, U. H. *J. Am. Chem. Soc.* **1971**, *93*, 954.

(50) Admasu, A.; Gudmundsdottir, A. D.; Platz, M. S. *J. Phys. Chem. A* **1997**, *101*, 3832.

(51) Warmuth, R.; Marvel, M. A. *Angew. Chem. Int. Ed.* **2000**, *39*, 1117.

(52) Gritsan, N. P.; Zhu, Z. D.; Hadad, C. M.; Platz, M. S. *J. Am. Chem. Soc.* **1999**, *121*, 1202.

(53) Platz, M. S. *Acc. Chem. Res.* **1995**, *28*, 487.

(54) Karney, W. L.; Borden, W. T. *J. Am. Chem. Soc.* **1997**, *119*, 1378.

(55) Kemnitz, C. R.; Karney, W. L.; Borden, W. T. *J. Am. Chem. Soc.* **1998**, *120*, 3499.

(56) Borden, W. T.; Gritsan, N. P.; Hadad, C. M.; Karney, W. L.; Kemnitz, C. R.; Platz, M. S. *Acc. Chem. Res.* **2000**, *33*, 765.

(57) Geise, C. M.; Hadad, C. M. *J. Org. Chem.* **2000**, *65*, 8348.

(58) Knorr, J.; Sokkar, P.; Schott, S.; Costa, P.; Thiel, W.; Sander, W.; Sanchez-Garcia, E.; Nuernberger, P. *Nat. Commun.* **2016**, *7*, 12968.

(59) Gritsan, N. P.; Yuzawa, T.; Platz, M. S. *J. Am. Chem. Soc.* **1997**, *119*, 5059.

(60) Luo, Y.-R. *Comprehensive Handbook of Chemical Bond Energies*; CRC Press: Boca Raton, FL, 2007.

(61) Bell, R. P. *The Tunnel Effect in Chemistry*; Chapman and Hall: New York, 1980.

(62) Dewar, M. J. S.; Merz, K. M.; Stewart, J. J. P. *J. Chem. Soc., Chem. Commun.* **1985**, 166.

(63) Borden, W. T. *WIREs Comput. Mol. Sci.* **2016**, *6*, 20.

(64) Caldin, E. F. *Chem. Rev.* **1969**, *69*, 135.

(65) Sheridan, R. S. In *Reviews of Reactive Intermediate Chemistry*; Moss, R. A., Platz, M. S., Jones, M. S., Eds.; John Wiley & Sons, Inc.: Hoboken, NJ, 2006, p 415.

(66) Meisner, J.; Kastner, J. *Angew. Chem. Int. Ed.* **2016**, *55*, 5400.

(67) Ertelt, M.; Hrovat, D. A.; Borden, W. T.; Sander, W. *Chem. Eur. J.* **2014**, *20*, 4713.

(68) Eyring, H. *J. Chem. Phys.* **1935**, *3*, 107.

(69) Amiri, S.; Reisenauer, H. P.; Schreiner, P. R. *J. Am. Chem. Soc.* **2010**, *132*, 15902.

(70) Schreiner, P. R.; Reisenauer, H. P.; Pickard, F. C.; Simmonett, A. C.; Allen, W. D.; Matyus, E.; Csaszar, A. G. *Nature* **2008**, *453*, 906.

(71) Gerbig, D.; Schreiner, P. R. In *Contemporary Carbene Chemistry*; Moss, R. A., Doyle, M. P., Eds.; John Wiley & Sons, Inc: Hoboken, NJ, 2013; Vol. 7, p 193.

(72) Kim, Y. H.; Kreevoy, M. M. *J. Am. Chem. Soc.* **1992**, *114*, 7116.

(73) Greer, E. M.; Kwon, K.; Greer, A.; Doubleday, C. *Tetrahedron* **2016**, *72*, 7357.

(74) Brunton, G.; Gray, J. A.; Griller, D.; Barclay, L. R. C.; Ingold, K. U. *J. Am. Chem. Soc.* **1978**, *100*, 4197.

(75) Hammes-Schiffer, S. *Acc. Chem. Res.* **2006**, *39*, 93.

(76) Hiraoka, K.; Sato, T.; Takayama, T. *Science* **2001**, *292*, 869.

(77) Wonchoba, S. E.; Hu, W. P.; Truhlar, D. G. *Phys. Rev. B* **1995**, *51*, 9985.

(78) McMahon, R. J. *Science* **2003**, *299*, 833.

(79) Carpenter, B. K. *J. Am. Chem. Soc.* **1983**, *105*, 1700.

(80) Pettersson, M.; Lundell, J.; Khriachtchev, L.; Rasanen, M. *J. Am. Chem. Soc.* **1997**, *119*, 11715.

(81) Pettersson, M.; Macoas, E. M. S.; Khriachtchev, L.; Lundell, J.; Fausto, R.; Rasanen, M. *J. Chem. Phys.* **2002**, *117*, 9095.

(82) Mcmahon, R. J.; Chapman, O. L. *J. Am. Chem. Soc.* **1987**, *109*, 683.

(83) Nunes, C. M.; Knezz, S. N.; Reva, I.; Fausto, R.; McMahon, R. J. *J. Am. Chem. Soc.* **2016**, *138*, 15287.

(84) Platz, M. S.; Senthilnathan, V. P.; Wright, B. B.; Mccurdy, C. W. *J. Am. Chem. Soc.* **1982**, *104*, 6494.

(85) Tomioka, H. In *Atom Tunneling Phenomena in Physics, Chemistry and Biology*; Miyazaki, T., Ed.; Springer Berlin Heidelberg: Berlin, Heidelberg, 2004, p 147.

(86) Morawietz, J.; Sander, W.; Traubel, M. *J. Org. Chem.* **1995**, *60*, 6368.

(87) Senthilnathan, V. P.; Platz, M. S. *J. Am. Chem. Soc.* **1980**, *102*, 7637.

(88) Lin, C.-T.; Gaspar, P. P. *Tetrahedron Lett.* **1980**, *21*, 3553.

(89) Platz, M. S. *Acc. Chem. Res.* **1988**, *21*, 236.

(90) Bauschlicher, C. W.; Bender, C. F.; Schaefer, H. F. *J. Am. Chem. Soc.* **1976**, *98*, 3072.

(91) McGrady, G. S.; Guilera, G. *Chem. Soc. Rev.* **2003**, *32*, 383.

(92) Stephan, D. W. *Chem. Commun.* **2010**, *46*, 8526.

(93) Frey, G. D.; Lavallo, V.; Donnadieu, B.; Schoeller, W. W.; Bertrand, G. *Science* **2007**, *316*, 439.

(94) Welch, G. C.; San Juan, R. R.; Masuda, J. D.; Stephan, D. W. *Science* **2006**, *314*, 1124.

(95) Peng, Y.; Guo, J.-D.; Ellis, B. D.; Zhu, Z.; Fettinger, J. C.; Nagase, S.; Power, P. P. *J. Am. Chem. Soc.* **2009**, *131*, 16272.

(96) Kötting, C.; Sander, W. *J. Am. Chem. Soc.* **1999**, *121*, 8891.

(97) Sander, W.; Hubert, R.; Kraka, E.; Grafenstein, J.; Cremer, D. *Chem. Eur. J.* **2000**, *6*, 4567.

(98) Zuev, P. S.; Sheridan, R. S. *J. Am. Chem. Soc.* **2001**, *123*, 12434.

(99) Henkel, S.; Ertelt, M.; Sander, W. *Chem. Eur. J.* **2014**, *20*, 7585.

(100) Henkel, S.; Sander, W. *Angew. Chem. Int. Ed.* **2015**, *54*, 4603.

(101) Kollmar, H. *J. Am. Chem. Soc.* **1978**, *100*, 2660.

(102) Song, M.-G.; Sheridan, R. S. *J. Am. Chem. Soc.* **2011**, *133*, 19688.

(103) Sander, W.; Kotting, C.; Hubert, R. *J. Phys. Org. Chem.* **2000**, *13*, 561.

(104) Gronert, S.; Keeffe, J. R.; O'Ferrall, R. A. M. *J. Am. Chem. Soc.* **2011**, *133*, 3381.

(105) W. Braun, A. M. B., M. Pilling *J. Chem. Phys.* **1970**, *52*, 5131.

(106) Tsang, W.; Hampson, R. *J. Phys. Chem. Ref. Data* **1986**, *15*, 1087.

(107) Pickard, J. M.; Rodgers, A. S. *Int. J. Chem. Kinet.* **1983**, *15*, 569.

(108) Lu, K.-W.; Matsui, H.; Huang, C.-L.; Raghunath, P.; Wang, N.-S.; Lin, M. C. *J. Phys. Chem. A* **2010**, *114*, 5493.

(109) Lee, P.-F.; Matsui, H.; Wang, N.-S. *J. Phys. Chem. A* **2012**, *116*.

(110) Gannon, K. L.; Blitz, M. A.; Pilling, M. J.; Seakins, P. W.; Klippenstein, S. J.; Harding, L. B. *J. Phys. Chem. A* **2008**, *112*, 9575.

(111) Bahou, M.; Das, P.; Lee, Y. F.; Wu, Y. J.; Lee, Y. P. *Phys. Chem. Chem. Phys.* **2014**, *16*, 2200.

(112) Fushitani, M.; Sogoshi, N.; Wakabayashi, T.; Momose, T.; Shida, T. *J. Chem. Phys.* **1998**, *109*, 6346.

(113) Lee, Y.-F.; Lee, Y.-P. *Mol. Phys.* **2015**, *113*, 2148.

(114) Sehested, J.; Ellermann, T.; Nielsen, O. J. *Int. J. Chem. Kinet.* **1994**, *26*, 259.

(115) Hoshina, H.; Fushitani, M.; Momose, T.; Shida, T. *J. Chem. Phys.* **2004**, *120*, 3706.

(116) Moore, C. B.; Pimentel, G. C. *J. Chem. Phys.* **1964**, *41*, 3504.

(117) Maier, G.; Reisenauer, H. P. *Angew. Chem. Int. Ed.* **1986**, *98*, 829.

(118) Milligan, D. E.; Pimentel, G. C. *J. Chem. Phys.* **1958**, *29*, 1405.

(119) Lee, Y. P.; Pimentel, G. C. *J. Chem. Phys.* **1981**, *75*, 4241.

(120) Jacox, M. E. *J. Phys. Chem. Ref. Data* **2003**, *32*.

(121) Baskin, C. P.; Bender, C. F.; W., B. C.; Schaefer, H. F. *J. Am. Chem. Soc.* **1974**, *96*, 2709.

(122) Bauschlicher, C. W.; Schaefer, H. F.; Bender, C. F. *J. Am. Chem. Soc.* **1976**, *98*, 1653.

(123) Bauschlicher, C. W.; Haber, K.; Schaefer, H. F.; Bender, C. F. *J. Am. Chem. Soc.* **1977**, *99*, 3610.

(124) Woodward, R. B.; Hoffmann, R. *Angew. Chem. Int. Ed.* **1969**, *8*, 781.

(125) Ignatyev, I. S.; Schaefer, H. F. *J. Am. Chem. Soc.* **1997**, *119*, 12306.

(126) Carr, R. W. *J. Phys. Chem.* **1972**, *76*, 1581.

(127) Woodcock, H. L.; Moran, D.; Brooks, B. R.; Schleyer, P. V.; Schaefer, H. F. *J. Am. Chem. Soc.* **2007**, *129*, 3763.

(128) Costa, P.; Lohmiller, T.; Trosien, I.; Savitsky, A.; Lubitz, W.; Fernandez-Oliva, M.; Sanchez-Garcia, E.; Sander, W. *J. Am. Chem. Soc.* **2016**, *138*, 1622.

(129) Sosa, C.; Schlegel, H. B. *J. Am. Chem. Soc.* **1984**, *106*, 5847.

(130) Kastner, J. *Chem. Eur. J.* **2013**, *19*, 8207.

(131) Bell, G. A.; Dunkin, I. R. *J. Chem. Soc., Faraday Trans. 2* **1985**, *81*, 725.

(132) Davydov, E. Y.; Vorotnikov, A. P.; Pustoshnyi, V. P. *J. Phys. Chem.* **1996**, *100*, 12403.

(133) Siebrand, W.; Wildman, T. A. *Acc. Chem. Res.* **1986**, *19*, 238.

(134) Hutchison, C. A.; Pearson, G. A. *J. Chem. Phys.* **1965**, *43*, 2545.

(135) Jr., C. A. H.; Pearson, G. A. *J. Chem. Phys.* **1967**, *47*, 520.

(136) Anderson, L. W.; Pipkin, F. M.; Baird, J. C. *Phys. Rev. Lett.* **1960**, *4*, 69.

(137) Grasse, P. B.; Brauer, B. E.; Zupancic, J. J.; Kaufmann, K. J.; Schuster, G. B. *J. Am. Chem. Soc.* **1983**, *105*, 6833.

(138) Wang, J.; Kubicki, J.; Hilinski, E. F.; Mecklenburg, S. L.; Gustafson, T. L.; Platz, M. S. *J. Am. Chem. Soc.* **2007**, *129*, 13683.

(139) Sander, W. W. *J. Org. Chem.* **1989**, *54*, 333.

(140) Costa, P.; Sander, W. *J. Phys. Org. Chem.* **2015**, *28*, 71.

(141) Baird, M. S.; Dunkin, I. R.; Poliakoff, M. *J. Chem. Soc., Chem. Commun.* **1974**, 904b.

(142) Dunkin, I. R.; Mccluskey, A. *Spectrochim. Acta, Part A* **1993**, *49*, 1179.

(143) Sander, W.; Bucher, G.; Wierlacher, S. *Chem. Rev.* **1993**, *93*, 1583.

(144) Sander, W. W.; Patyk, A.; Bucher, G. *J. Mol. Struct.* **1990**, *222*, 21.

(145) Sander, W. *Angew. Chem. Int. Ed.* **1986**, *25*, 255.

(146) Dunkin, I. R.; Shields, C. J. *J. Chem. Soc., Chem. Commun.* **1986**, 154.

(147) Gush, H. P.; Allin, E. J.; Welsh, H. L.; Hare, W. F. J. *Can. J. Phys.* **1960**, *38*, 176.

(148) Raston, P. L.; Anderson, D. T. *Phys. Chem. Chem. Phys.* **2006**, *8*, 3124.

(149) Korolyuk, O. A.; Krivchikov, A. I.; Gorodilov, B. Y. *J. Low Temp. Phys.* **2001**, *122*, 203.

(150) Truhlar, D. G.; Garrett, B. C. *Annu. Rev. Phys. Chem.* **1984**, *35*, 159.

(151) Fernandez-Ramos, A.; Ellingson, B. A.; Garrett, B. C.; Truhlar, D. G. In *Rev. Comput. Chem.*; Lipkowitz, K. B., Cundari, T. R., Eds.; John Wiley & Sons, Inc.: Hoboken, NJ, 2007; Vol. 23, p 125.

(152) Langer, J. S. *Ann. Phys.* **1967**, *41*, 108.

(153) Razavy, M. *Quantum Theory of Tunneling*; World Scientific: Singapore, 2003.

(154) Hammond, G. S. *J. Am. Chem. Soc.* **1955**, *77*, 334.

(155) Wagner, J. P.; Reisenauer, H. P.; Hirvonen, V.; Wu, C.-H.; Tyberg, J. L.; Allen, W. D.; Schreiner, P. R. *Chem. Commun.* **2016**, *52*.

(156) Tsuge, M.; Khriachtchev, L. *J. Phys. Chem. A* **2015**, *119*, 2628.

(157) Gronert, S.; Keeffe, J. R.; O'Ferrall, R. A. M. In *Contemporary Carbene Chemistry*; Moss, R. A., Doyle, M. P., Eds.; John Wiley & Sons, Inc: Hoboken, NJ, 2013; Vol. 7, p 3.

(158) Costa, P.; Trosien, I.; Fernandez-Oliva, M.; Sanchez-Garcia, E.; Sander, W. *Angew. Chem. Int. Ed.* **2015**, *54*, 2656.

(159) Raut, A. H.; Costa, P.; Sander, W. unpublished results.

(160) Mieres-Perez, J.; Mendez-Vega, E.; Velappan, K.; Sander, W. *J. Org. Chem.* **2015**, *80*, 11926.

(161) Sankaranarayanan, J.; Rajam, S.; Hadad, C. M.; Gudmundsdottir, A. D. *J. Phys. Org. Chem.* **2010**, *23*, 370.

(162) Bettinger, H. F.; Filthaus, M.; Neuhaus, P. *Chem. Commun.* **2009**, 2186.

(163) Bettinger, H. F.; Bornemann, H. *J. Am. Chem. Soc.* **2006**, *128*, 11128.

(164) Dunkin, I. R.; Donnelly, T.; Lockhart, T. S. *Tetrahedron Lett.* **1985**, *26*, 359.

(165) Karney, W. L.; Borden, W. T. *J. Am. Chem. Soc.* **1997**, *119*, 3347.

(166) Zhu, Z. D.; Bally, T.; Stracener, L. L.; McMahon, R. J. *J. Am. Chem. Soc.* **1999**, *121*, 2863.

(167) Tsegaw, Y. A.; Kadam, P. E.; Totsch, N.; Sanchez-Garcia, E.; Sander, W. *J. Am. Chem. Soc.* **2017**, *139*, 12310.

(168) Feng, R. J.; Lu, Y.; Deng, G. H.; Xu, J.; Wu, Z.; Li, H. M.; Liu, Q.; Kadowki, N.; Abe, M.; Zeng, X. Q. *J. Am. Chem. Soc.* **2018**, *140*, 10.

(169) De Vleeschouwer, F.; Van Speybroeck, V.; Waroquier, M.; Geerlings, P.; De Proft, F. *Org. Lett.* **2007**, *9*, 2721.

(170) Chuang, C.; Lapin, S. C.; Schrock, A. K.; Schuster, G. B. *J. Am. Chem. Soc.* **1985**, *107*, 4238.

(171) Wang, Y. H.; Yuzawa, T.; Hamaguchi, H. O.; Toscano, J. P. *J. Am. Chem. Soc.* **1999**, *121*, 2875.

(172) Zhang, Y. L.; Kubicki, J.; Wang, J.; Platz, M. S. *J. Phys. Chem. A* **2008**, *112*, 11093.

(173) *Magnetic Properties of Organic Materials*; Lahti, P. M., Ed.; Marcel Dekker: New York 1999.

(174) Rajca, A. *Chem. Eur. J.* **2002**, *8*, 4834.

(175) Gallagher, N. M.; Olankitwanit, A.; Rajca, A. *J. Org. Chem.* **2015**, *80*, 1291.

(176) Teki, Y.; Takui, T.; Itoh, K.; Iwamura, H.; Kobayashi, K. *J. Am. Chem. Soc.* **1986**, *108*, 2147.

(177) Iwamura, H.; Nakamura, N.; Koga, N.; Sasaki, S. *Mol. Cryst. Liq. Cryst.* **1992**, *216-18*, 207.

(178) Chapyshev, S. V. *Russ. Chem. Bull.* **2011**, *60*, 1274.

(179) Chapyshev, S. V.; Kuhn, A.; Wong, M. H.; Wentrup, C. *J. Am. Chem. Soc.* **2000**, *122*, 1572.

(180) Chapyshev, S. V.; Grote, D.; Finke, C.; Sander, W. *J. Org. Chem.* **2008**, *73*, 7045.

(181) Chapyshev, S. V.; Misochko, E. Y.; Akimov, A. V.; Dorokhov, V. G.; Neuhaus, P.; Grote, D.; Sander, W. *J. Org. Chem.* **2009**, *74*, 7238.

(182) Chapyshev, S. V.; Neuhaus, P.; Grote, D.; Sander, W. *J. Phys. Org. Chem.* **2010**, *23*, 340.

(183) Chapyshev, S. V.; Korchagin, D. V.; Budyka, M. F.; Gavrishova, T. N.; Neuhaus, P.; Sander, W. *ChemPhysChem* **2012**, *13*, 2721.

(184) Sato, T.; Narazaki, A.; Kawaguchi, Y.; Niino, H.; Bucher, G.; Grote, D.; Wolff, J. J.; Wenk, H. H.; Sandert, W. *J. Am. Chem. Soc.* **2004**, *126*, 7846.

(185) Finke, C.; Grote, D.; Seidel, R. W.; Chapyshev, S. V.; Sander, W. *J. Phys. Org. Chem.* **2012**, *25*, 486.

(186) Chapyshev, S. V. *Mendeleev Commun.* **2002**, 168.

(187) Chapyshev, S. V.; Tomioka, H. *Bull. Chem. Soc. Jpn.* **2003**, *76*, 2075.

(188) Gritsan, N. P.; Platz, M. S. *Adv. Phys. Org. Chem.* **2001**, *36*, 255.

(189) Misochko, E. Y.; Akimov, A. V.; Masitov, A. A.; Korchagin, D. V.; Aldoshin, S. M.; Chapyshev, S. V. *J. Chem. Phys.* **2013**, *138*.

(190) Akimov, A.; Masitov, A.; Korchagin, D.; Chapyshev, S.; Misochko, E.; Savitsky, A. *J. Chem. Phys.* **2015**, *143*.

(191) Mieres-Perez, J.; Henkel, S.; Mendez-Vega, E.; Schleif, T.; Lohmiller, T.; Savitsky, A.; Sander, W. *J. Phys. Org. Chem.* **2017**, *30*.

(192) Shimanouchi, T. *J. Phys. Chem. Ref. Data* **1977**, *6*, 993.

(193) Jones, L. H.; Agnew, S. F.; Swanson, B. I.; Ekberg, S. A. *J. Chem. Phys.* **1986**, *85*, 428.

(194) Safiullin, R. L.; Khursan, S. L.; Chainikova, E. M.; Danilov, V. T. *Kinet. Catal.* **2004**, *45*, 640.

(195) Gudipati, M. S. *J. Phys. Chem. A* **2004**, *108*, 4412.

(196) Carra, C.; Nussbaum, R.; Bally, T. *ChemPhysChem* **2006**, *7*, 1268.

(197) Gee, C.; Douin, S.; Crepin, C.; Brechignac, P. *Chem. Phys. Lett.* **2001**, *338*, 130.

(198) Wang, J.; Burdzinski, G.; Zhu, Z.; Platz, M. S.; Carra, C.; Bally, T. *J. Am. Chem. Soc.* **2007**, *129*, 8380.

(199) Misochko, E. Y.; Korchagin, D. V.; Bozhenko, K. V.; Chapyshev, S. V.; Aldoshin, S. M. *J. Chem. Phys.* **2010**, *133*, 064101.

(200) Misochko, E. Y.; Akimov, A. V.; Masitov, A. A.; Korchagin, D. V.; Yakushchenko, I. K.; Chapyshev, S. V. *J. Chem. Phys.* **2012**, *137*.

(201) Dunkin, I. R. *Matrix-Isolation Techniques: A Practical Approach.*; Oxford University Press: New York, 1998.

(202) Bally, T. In *Reactive Intermediate Chemistry*; Moss, R. A., Platz, M. S., Jones, M. S., Eds.; John Wiley & Sons, Inc.: Hoboken, NJ, 2004, p 797.

(203) Tam, S.; Fajardo, M. E. *Rev. Sci. Instrum.* **1999**, *70*, 1926.

(204) Tom, B. A.; Bhasker, S.; Miyamoto, Y.; Momose, T.; McCall, B. J. *Rev. Sci. Instrum.* **2009**, *80*, 016108.

(205) Lee, C. T.; Yang, W. T.; Parr, R. G. *Phys. Rev. B* **1988**, *37*, 785.

(206) Raghavachari, K. *Theor. Chem. Acc.* **2000**, *103*, 361.

(207) Grimme, S.; Antony, J.; Ehrlich, S.; Krieg, H. *J. Chem. Phys.* **2010**, *132*.

(208) Zhao, Y.; Schultz, N. E.; Truhlar, D. G. *J. Chem. Theory Comput.* **2006**, *2*, 364.

(209) Weigend, F.; Ahlrichs, R. *Phys. Chem. Chem. Phys.* **2005**, *7*, 3297.

(210) Dunning, T. H. *J. Chem. Phys.* **1989**, *90*, 1007.

(211) Kendall, R. A.; Jr., T. H. D.; Harrison, R. J. *J. Chem. Phys.* **1992**, *96*, 6796.

(212) Ochterski, J. W.; Petersson, G. A.; Jr., J. A. M. *J. Chem. Phys.* **1996**, *104*, 2598.

(213) Frisch, M. J. T., G. W.; Schlegel, H. B.; Scuseria, G. E.; Robb, M. A.; Cheeseman, J. R.; Scalmani, G.; Barone, V.; Mennucci, B.; Petersson, G. A.; Nakatsuji, H.; Caricato, M.; Li, X.; Hratchian, H. P.; Izmaylov, A. F.; Bloino, J.; Zheng, G.; Sonnenberg, J. L.; Hada, M.; Ehara, M.; Toyota, K.; Fukuda, R.; Hasegawa, J.; Ishida, M.; Nakajima, T.; Honda, Y.; Kitao, O.; Nakai, H.; Vreven, T.; Montgomery, Jr., J. A.; Peralta, J. E.; Ogliaro, F.; Bearpark, M.; Heyd, J. J.; Brothers, E.; Kudin, K. N.; Staroverov, V. N.; Kobayashi, R.; Normand, J.; Raghavachari, K.; Rendell, A.; Burant, J. C.; Iyengar, S. S.; Tomasi, J.; Cossi, M.; Rega, N.; Millam, N. J.; Klene, M.; Knox, J. E.; Cross, J. B.; Bakken, V.; Adamo, C.; Jaramillo, J.; Gomperts, R.; Stratmann, R. E.; Yazyev, O.; Austin, A. J.; Cammi, R.; Pomelli, C.; Ochterski, J. W.; Martin, R. L.; Morokuma, K.; Zakrzewski, V. G.; Voth, G. A.; Salvador, P.; Dannenberg, J. J.; Dapprich, S.; Daniels, A. D.; Farkas, Ö.; Foresman, J. B.; Ortiz, J. V.; Cioslowski, J.; Fox, D. J. ; Revision D.1 ed.; Gaussian, Inc.: Wallingford CT, 2009.

(214) Werner, H. J.; Knowles, P. J.; Knizia, G.; Manby, F. R.; Schutz, M. *WIREs Comput. Mol. Sci.* **2012**, *2*, 242.

(215) Stoll, S.; Schweiger, A. *J. Magn. Reson.* **2006**, *178*, 42.

(216) Zeng, W.; Ballard, T. E.; Tkachenko, A. G.; Burns, V. A.; Feldheim, D. L.; Melander, C. *Bioorg. Med. Chem. Lett.* **2006**, *16*, 5148.

(217) Miller, J. *J. Org. Chem.* **1959**, *24*, 560.

(218) Davis, P. J.; Harris, L.; Karim, A.; Thompson, A. L.; Gilpin, M.; Moloney, M. G.; Pound, M. J.; Thompson, C. *Tetrahedron Lett.* **2011**, *52*, 1553.

(219) Hu, Y.; Liang, L.; Wei, W.-T.; Sun, X.; Zhang, X.-J.; Yan, M. *Tetrahedron* **2015**, *71*, 1425.

(220) Li, Z.; Deng, G.; Li, Y.-C. *Synlett* **2008**, *2008*, 3053.

(221) Hu, M. Y.; Li, J. Q.; Yao, S. Q. *Org. Lett.* **2008**, *10*, 5529.

(222) Chapyshev, S. V.; Chernyak, A. V. *J. Fluorine Chem.* **2013**, *156*, 303.

Acknowledgments

First, I would like to express my sincere gratitude to Prof. Wolfram Sander for giving me the opportunity to carry out this work, constant scientific support and encouragement, and for showing the way on how scientific research should be conducted. Moreover, many thanks to Prof. Elsa Sánchez-García for her feedbacks concerning calculations, publishing papers, and for all the help on non-chemical problems.

I am also very thankful to Prof. Yuan-Pern Lee for accepting me in his group at NCTU, Taiwan, providing me with all support during the three-month internship, and helping me out in Bochum with the *p*-H_2 converter, spectroscopic analysis, and proofreading.

I am grateful for all the help I have received from the technical and administrative staff over the years. In this regard, I thank Dirk, Heidi, Torsten, Klaus, Catharina, Robin, Sabine, Jacinta, Hannah, and Pamela. Particularly, I thank Heidi for showing me the secrets of matrix isolation; Catharina for always being willing to dive into any new equipment; and Torsten for his help and the nice meetings about IT stuffs. Many thanks are also extended to Dirk Grote and Christian Merten for answering my constant spectroscopic questions. However, chemistry is not everything, so I am thankful to Jacinta for preparing letters in no time, and Gundula Talbot for taking care of the Cuban guys and finding solutions for any kind of problems.

Of course, many thanks to the current and former group colleagues: Y am, Saonli, Andre, Fee, Sandra, Melanie, Andreas, Nadja, Geneviève, Stefan, Paolo, Arun, Pritam, Soumya, Bishnu, Akshay, Yetsedaw, Tim, Corina, Iris, Linda, Mika, Adam, Nesli, Mohamed, Tobi, Liang, Melania, Adrián, Julian, Nora, Tino, Tobias, Karoline, as well as the guests, Katelyn, Ana, Teddy, and Das (with his students), for all the help and for keeping a nice atmosphere in the lab. Likewise, I thank the group members in Taiwan, particularly Masa and Karolina.

I would also like to thank Stefan, Mika, Iris, Akshay, and Paolo for proofreading some of the sections of this manuscript, and for all the help concerning synthesis, measurements, and data analysis. Many thanks to Iris, Mika, Corina, Tim, and Klaus for teaching me German and for being there, whenever I needed help or just to say silly things. Also to Stefan, Paolo, the Indians, and Yetsedaw for all the fun inside Lab and for the outdoor activities.

Por último y no menos importante, mi agradecimiento va dirigido al piquete cubano-alemán (y los amigos que andan regados por otros países también), mis primos y tíos en España, Miami y Cuba … y en especial a mis padres, hacia ellos va dedicada esta tesis.

Appendix

Figures

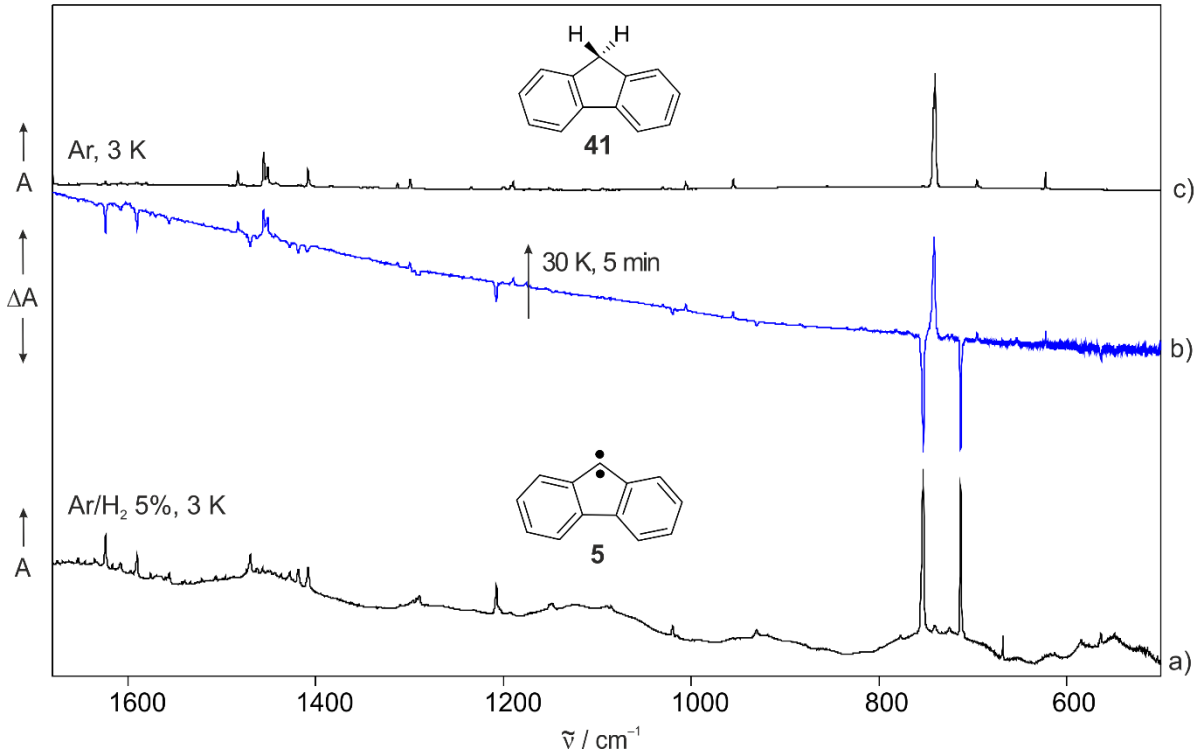

Figure A1. IR spectra showing the reaction of fluorenylidene **5** with H_2 in Ar matrices. a) IR spectrum obtained after irradiating 9-diazofluorene **40** with $\lambda = 365$ nm for 2 h in 5% H_2-doped Ar at 3 K. b) Difference IR spectrum obtained after annealing the matrix at 30 K for 5 min. c) IR spectrum of fluorene **41** in Ar at 3 K.

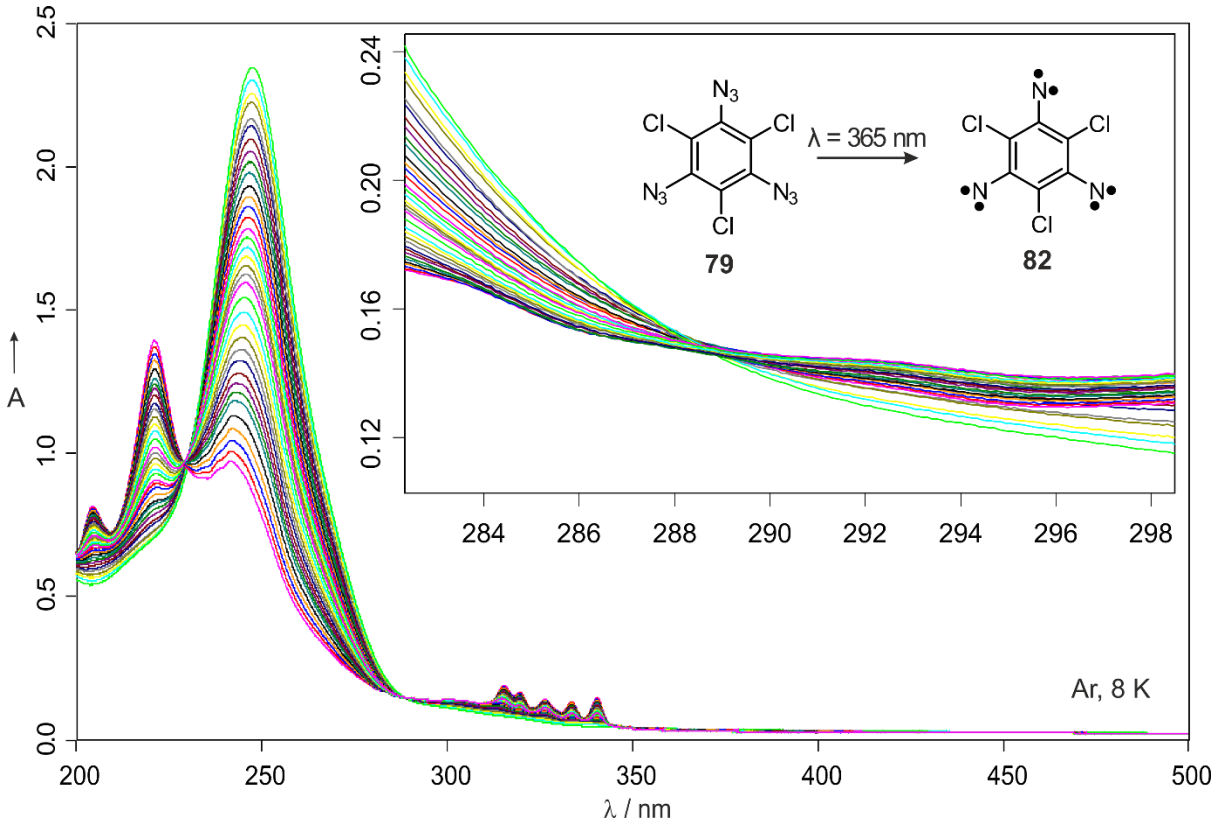

Figure A2. UV–vis spectra showing the photochemistry of 1,3,5-triazido-2,4,6-trichlorobenzene **79** in Ar matrices at 8 K. UV–vis spectra are recorded by starting from precursor **79** and upon subsequent irradiation with λ = 365 nm during steps of 30 s (from the beginning to 10 min), 1 min (from 10 to 20 min), and every 2 min (from 20 to 30 min).

Tables

Table A1. Energetics of the reactions of carbenes and nitrenes with H_2, calculated at the B3LYP-D3 /def2-TZVP level of theory.

Spin State	Intermediate	Transition State	Triplet Radical Pair RH + H	Singlet Product RH_2
Triplet Carbenes	**4**	7.0	1.5	–76.1
	5	2.6	–8.5	–85.7
	26	3.6	–7.4	–85.5
	27	4.5	–4.5	–69.9
	28 (concerted)	0	–	–78.1
	28 (H-abstraction)	1.9	–10.1	–78.1
	29 (concerted)	0	–	–74.6
	29 (H-abstraction)	3.1	–6.8	–74.6
	30	4.1	–5.2	–91.7
	31	4.0	–5.4	–91.3
	32	6.0	–2.1	–70.8
Triplet Nitrenes	**7**	19.5	18.2	–75.5
	8	16.0	14.5	–75.4
Singlet Carbenes	**33**	0	–	–113.2
	34	5.4	–	–83.3
	35	13.1	–	–74.3
	36	12.0	–	–78.7
	37	11.7	–	–78.9
	38	9.3	–	–78.7
	39	5.7	–	–90.2

ZPE-corrected energies are given in kcal/mol. Activation energies are relative to carbene + H_2. Transition states are calculated assuming concerted addition for singlet carbenes and H-abstraction mechanism for triplet carbenes (unless otherwise noted).

Optimized Geometries

Triplet Fluorenylidene T-**5**
Method: B3LYP-D3/def2-TZVP
Multiplicity: 3
E = –500.2879651 a.u.
E + ZPE = –500.125329 a.u.
$E_{CCSD(T)/cc\text{-}PVDZ}$ = –498.67812438 a.u.
$E_{CCSD(T)/cc\text{-}PVTZ}$ = –499.14154672 a.u.

Atomic Symbol	X	Y	Z
C	1.65954900	0.00000000	-1.44102295
C	0.73259400	0.00000000	-0.41618795
C	1.17548400	0.00000000	0.94891205
C	2.53882600	0.00000000	1.24851405
C	3.45318400	0.00000000	0.20139705
C	3.02180600	0.00000000	-1.12696995
H	1.33909400	0.00000000	-2.47598295
H	2.87394500	0.00000000	2.27756905
H	4.51390500	0.00000000	0.41712305
H	3.75297400	0.00000000	-1.92518895
C	-1.65954900	0.00000000	-1.44102295
C	-3.02180600	0.00000000	-1.12696995
C	-3.45318400	0.00000000	0.20139705
C	-2.53882600	0.00000000	1.24851405
C	-1.17548400	0.00000000	0.94891205
C	-0.73259400	0.00000000	-0.41618795
H	-1.33909400	0.00000000	-2.47598295
H	-3.75297400	0.00000000	-1.92518895
H	-4.51390500	0.00000000	0.41712305
H	-2.87394500	0.00000000	2.27756905
C	0.00000000	0.00000000	1.73954205

Singlet Fluorenylidene S-**5**
Method: B3LYP-D3/def2-TZVP
Multiplicity: 1
E = –500.2801553 a.u.
E + ZPE = –500.117596 a.u.
$E_{CCSD(T)/cc\text{-}PVDZ}$ = –498.67272901 a.u.
$E_{CCSD(T)/cc\text{-}PVTZ}$ = –499.13840211 a.u.

Atomic Symbol	X	Y	Z
C	1.66839000	0.00000000	1.46126412
C	0.73940400	0.00000000	0.44896312
C	1.13719800	0.00000000	-0.91533088
C	2.48513200	0.00000000	-1.24339888
C	3.43817800	0.00000000	-0.21651888
C	3.03223000	0.00000000	1.10998012
H	1.37638300	0.00000000	2.50456212
H	2.78057400	0.00000000	-2.28507788
H	4.49392000	0.00000000	-0.45460588
H	3.77886900	0.00000000	1.89476212
C	-1.66839000	0.00000000	1.46126412
C	-3.03223000	0.00000000	1.10998012
C	-3.43817800	0.00000000	-0.21651888
C	-2.48513200	0.00000000	-1.24339888
C	-1.13719800	0.00000000	-0.91533088
C	-0.73940400	0.00000000	0.44896312
H	-1.37638300	0.00000000	2.50456212
H	-3.77886900	0.00000000	1.89476212
H	-4.49392000	0.00000000	-0.45460588
H	-2.78057400	0.00000000	-2.28507788
C	0.00000000	0.00000000	-1.84313088

Triplet Complex T-**5**···H_2
Method: B3LYP-D3/def2-TZVP
Multiplicity: 3
E = –501.4685996 a.u.
E + ZPE = –501.294638 a.u.
$E_{CCSD(T)/cc\text{-}PVDZ}$ = –499.84197613 a.u.

Atomic Symbol	X	Y	Z
C	0.00000000	1.66053400	-1.55025416
C	0.00000000	0.73276100	-0.52619416
C	0.00000000	1.17562200	0.83899084
C	0.00000000	2.53852900	1.14002084
C	0.00000000	3.45346400	0.09346884
C	0.00000000	3.02264600	-1.23508216
H	0.00000000	1.34101700	-2.58549916
H	0.00000000	2.87241800	2.16944384
H	0.00000000	4.51406600	0.30969884
H	0.00000000	3.75425800	-2.03288816
C	0.00000000	-1.66053400	-1.55025416
C	0.00000000	-3.02264600	-1.23508216
C	0.00000000	-3.45346400	0.09346884
C	0.00000000	-2.53852900	1.14002084
C	0.00000000	-1.17562200	0.83899084
C	0.00000000	-0.73276100	-0.52619416
H	0.00000000	-1.34101700	-2.58549916
H	0.00000000	-3.75425800	-2.03288816
H	0.00000000	-4.51406600	0.30969884
H	0.00000000	-2.87241800	2.16944384
C	0.00000000	0.00000000	1.62843984
H	0.00000000	0.00000000	4.31532584
H	0.00000000	0.00000000	5.06112384

Singlet Complex S-**5**···H_2
Method: B3LYP-D3/def2-TZVP
Multiplicity: 1
E = –501.4616731 a.u.
E + ZPE = –501.286987 a.u.
$E_{CCSD(T)/cc\text{-}PVDZ}$ = –499.83816794 a.u.

Atomic Symbol	X	Y	Z
C	1.54018802	0.12286372	1.66879700
C	0.53720301	-0.01080417	0.73946800
C	-0.81745501	-0.17286102	1.13739100
C	-1.14704201	-0.18817899	2.48488900
C	-0.13066699	-0.04248110	3.43784200
C	1.18755802	0.10687876	3.03227700
H	2.57664704	0.24324161	1.37738900
H	-2.18176702	-0.30869788	2.78004000
H	-0.37011699	-0.04792207	4.49322900
C	1.54018802	0.12286372	-1.66879700
C	1.18755802	0.10687876	-3.03227700
C	-0.13066699	-0.04248110	-3.43784200
C	-1.14704201	-0.18817899	-2.48488900
C	-0.81745501	-0.17286102	-1.13739100
C	0.53720301	-0.01080417	-0.73946800
H	2.57664704	0.24324161	-1.37738900
H	1.96469003	0.21520967	-3.77903500
H	-0.37011699	-0.04792207	-4.49322900
H	-2.18176702	-0.30869788	-2.78004000
C	-1.73357202	-0.30474493	0.00000000
H	-3.64734682	1.58170628	0.00000000
H	-3.96754774	2.25809432	0.00000000
H	1.96469003	0.21520967	3.77903500

Triplet Transition State TS (T-**5**···H_2)
Method: B3LYP-D3/def2-TZVP
Multiplicity: 3
E = –501.4628936 a.u.
E + ZPE = –501.290431 a.u.
$E_{CCSD(T)/cc\text{-}PVDZ}$ = –499.83098004 a.u.

Atomic Symbol	X	Y	Z
C	0.00000000	-1.66069187	-1.52732420
C	0.00000000	-0.73242397	-0.50375211
C	0.00000000	-1.17003911	0.86052385
C	0.00000000	-2.53257914	1.16397571
C	0.00000000	-3.45062303	0.11968762
C	0.00000000	-3.02249090	-1.20957434
H	0.00000000	-1.34327876	-2.56318917
H	0.00000000	-2.86534624	2.19406168
H	0.00000000	-4.51079506	0.33815351
H	0.00000000	-3.75577282	-2.00591141
C	0.00000000	1.66069187	-1.52732420
C	0.00000000	3.02249090	-1.20957434
C	0.00000000	3.45062303	0.11968762
C	0.00000000	2.53257914	1.16397571
C	0.00000000	1.17003911	0.86052385
C	0.00000000	0.73242397	-0.50375211
H	0.00000000	1.34327876	-2.56318917
H	0.00000000	3.75577282	-2.00591141
H	0.00000000	4.51079506	0.33815351
H	0.00000000	2.86534624	2.19406168
C	0.00000000	0.00000000	1.66625997
H	0.00000000	0.00000000	3.19535297
H	0.00000000	0.00000000	4.03841497

Singlet Transition State TS (S-**5**···H_2)
Method: B3LYP-D3/def2-TZVP
Multiplicity: 1
E = –501.4573198 a.u.
E + ZPE = –501.282082 a.u.
$E_{CCSD(T)/cc\text{-}PVDZ}$ = –499.82947746 a.u.

Atomic Symbol	X	Y	Z
C	-0.02107197	-1.52161095	-1.66221300
C	0.00840501	-0.49805497	-0.73622099
C	0.07355990	0.85696305	-1.15172097
C	0.06002081	1.17214807	-2.50502396
C	-0.02570717	0.14042208	-3.43967997
C	-0.05278707	-1.18793093	-3.02184799
H	-0.02475089	-2.56029496	-1.35480702
H	0.11197773	2.20647007	-2.82136295
H	-0.05229825	0.36936909	-4.49718597
C	-0.02107197	-1.52161095	1.66221300
C	-0.05278707	-1.18793093	3.02184799
C	-0.02570717	0.14042208	3.43967997
C	0.06002081	1.17214807	2.50502396
C	0.07355990	0.85696305	1.15172097
C	0.00840501	-0.49805497	0.73622099
H	-0.02475089	-2.56029496	1.35480702
H	-0.09223664	-1.97765804	3.76185300
H	-0.05229825	0.36936909	4.49718597
H	0.11197773	2.20647007	2.82136295
C	0.31323991	1.72893104	0.00000000
H	-0.73982017	2.98989497	0.00000000
H	-1.53404617	3.01751292	0.00000000
H	-0.09223664	-1.97765804	-3.76185300

Triplet Radical Pair **42**···H
Method: B3LYP-D3/def2-TZVP
Multiplicity: 3
E = –501.4830737 a.u.
E + ZPE = –501.308127 a.u.
$E_{CCSD(T)/cc\text{-}PVDZ}$ = –499.85932240 a.u.

Atomic Symbol	X	Y	Z
C	0.00000000	1.66183300	-1.53917911
C	0.00000000	0.73151300	-0.51798811
C	0.00000000	1.15694300	0.84578589
C	0.00000000	2.52006100	1.15414689
C	0.00000000	3.44494100	0.11568289
C	0.00000000	3.02311100	-1.21567211
H	0.00000000	1.34943600	-2.57646011
H	0.00000000	2.85051200	2.18574089
H	0.00000000	4.50415300	0.33933189
H	0.00000000	3.76014300	-2.00867611
C	0.00000000	-1.66183300	-1.53917911
C	0.00000000	-3.02311100	-1.21567211
C	0.00000000	-3.44494100	0.11568289
C	0.00000000	-2.52006100	1.15414689
C	0.00000000	-1.15694300	0.84578589
C	0.00000000	-0.73151300	-0.51798811
H	0.00000000	-1.34943600	-2.57646011
H	0.00000000	-3.76014300	-2.00867611
H	0.00000000	-4.50415300	0.33933189
H	0.00000000	-2.85051200	2.18574089
C	0.00000000	0.00000000	1.68051989
H	0.00000000	0.00000000	2.76136689
H	0.00000000	0.00000000	5.16232489

Fluorene **41**
Method: B3LYP-D3/def2-TZVP
Multiplicity: 1
E = –501.6184352 a.u.
E + ZPE = –501.431094 a.u.
$E_{CCSD(T)/cc-PVDZ}$ = –499.99759052 a.u.
$E_{CCSD(T)/cc-PVTZ}$ = –500.47308154 a.u.

Atomic Symbol	X	Y	Z
C	1.64381600	0.00000000	1.49898690
C	0.73204100	0.00000000	0.44819690
C	1.18008300	0.00000000	-0.88338310
C	2.53496400	0.00000000	-1.16844810
C	3.44769900	0.00000000	-0.11434010
C	3.00398500	0.00000000	1.20760490
H	1.30342200	0.00000000	2.52717790
H	2.88536700	0.00000000	-2.19394410
H	4.51008800	0.00000000	-0.32313610
H	3.72634600	0.00000000	2.01425390
C	-1.64381600	0.00000000	1.49898690
C	-3.00398500	0.00000000	1.20760490
C	-3.44769900	0.00000000	-0.11434010
C	-2.53496400	0.00000000	-1.16844810
C	-1.18008300	0.00000000	-0.88338310
C	-0.73204100	0.00000000	0.44819690
H	-1.30342200	0.00000000	2.52717790
H	-3.72634600	0.00000000	2.01425390
H	-4.51008800	0.00000000	-0.32313610
H	-2.88536700	0.00000000	-2.19394410
C	0.00000000	0.00000000	-1.82570410
H	0.00000000	-0.87815363	-2.47891905
H	0.00000000	0.87815363	-2.47891905

Triplet Diphenylcarbene T-**4**
Method: B3LYP-D3/def2-TZVP
Multiplicity: 3
E = –501.5015229 a.u.
E + ZPE = –501.318119 a.u.
$E_{CCSD(T)/cc\text{-}PVDZ}$ = –499.86975724 a.u.
$E_{CCSD(T)/cc\text{-}PVTZ}$ = –500.34214055 a.u.

Atomic Symbol	X	Y	Z
C	0.00000000	0.00000000	-0.87393705
C	0.01553500	1.31831702	-0.41491213
C	-0.48247992	2.38058396	-1.21301426
C	0.56221987	1.64846010	0.85660390
C	-0.44858896	3.68481299	-0.75799034
H	-0.89441482	2.14999790	-2.18687528
C	0.58355183	2.95788513	1.29744481
H	0.96912681	0.85755714	1.47280999
C	0.07974791	3.98521108	0.49842269
H	-0.83789890	4.47910195	-1.38277444
H	1.00163473	3.18671420	2.27015984
H	0.10286988	5.00877310	0.84915362
C	-0.01553500	-1.31831702	-0.41491213
C	0.48247992	-2.38058396	-1.21301426
C	-0.56221987	-1.64846010	0.85660390
C	0.44858896	-3.68481299	-0.75799034
H	0.89441482	-2.14999790	-2.18687528
C	-0.58355183	-2.95788513	1.29744481
H	-0.96912681	-0.85755714	1.47280999
C	-0.07974791	-3.98521108	0.49842269
H	0.83789890	-4.47910195	-1.38277444
H	-1.00163473	-3.18671420	2.27015984
H	-0.10286988	-5.00877310	0.84915362

Singlet Diphenylcarbene S-**4**
Method: B3LYP-D3/def2-TZVP
Multiplicity: 1
E = –501.4934233 a.u.
E + ZPE = –501.309054 a.u.
$E_{CCSD(T)/cc\text{-}PVDZ}$ = –499.86447933 a.u.
$E_{CCSD(T)/cc\text{-}PVTZ}$ = –500.33906552 a.u.

Atomic Symbol	X	Y	Z
C	0.00000000	0.00000000	-1.29656995
C	-0.04308291	1.23024801	-0.57675799
C	0.58213123	2.36769099	-1.14105688
C	-0.74146017	1.39929604	0.64555885
C	0.57425110	3.58388801	-0.48369190
H	1.08004444	2.25184197	-2.09488376
C	-0.81363329	2.64015906	1.25623981
H	-1.25289228	0.55006106	1.07903576
C	-0.13853316	3.72842704	0.70765094
H	1.08813820	4.43528199	-0.91197281
H	-1.37945649	2.76125908	2.17178569
H	-0.18056025	4.69299905	1.19810691
C	0.04308291	-1.23024801	-0.57675799
C	0.74146017	-1.39929604	0.64555885
C	-0.58213123	-2.36769099	-1.14105688
C	0.81363329	-2.64015906	1.25623981
H	1.25289228	-0.55006106	1.07903576
C	-0.57425110	-3.58388801	-0.48369190
H	-1.08004444	-2.25184197	-2.09488376
C	0.13853316	-3.72842704	0.70765094
H	1.37945649	-2.76125908	2.17178569
H	-1.08813820	-4.43528199	-0.91197281
H	0.18056025	-4.69299905	1.19810691

Triplet Complex T-4···H_2
Method: B3LYP-D3/def2-TZVP
Multiplicity: 3
E = –502.6825581 a.u.
E + ZPE = –502.487455 a.u.
$E_{CCSD(T)/cc\text{-}PVDZ}$ = –501.03399700 a.u.

Atomic Symbol	X	Y	Z
C	0.00000000	0.00000000	0.81024289
C	-0.02146341	1.31589997	0.34213889
C	0.45437508	2.38991909	1.13724189
C	-0.54672183	1.62791621	-0.94286511
C	0.42611568	3.68785884	0.66366389
H	0.84633654	2.17455281	2.12257589
C	-0.56037308	2.93056482	-1.40293411
H	-0.94233880	0.82879195	-1.55545811
C	-0.07398974	3.96954426	-0.60844211
H	0.79897003	4.49180251	1.28610089
H	-0.95941413	3.14480549	-2.38689211
H	-0.09026392	4.98796129	-0.97420011
C	0.02146341	-1.31589997	0.34213889
C	-0.45437508	-2.38991909	1.13724189
C	0.54672183	-1.62791621	-0.94286511
C	-0.42611568	-3.68785884	0.66366389
H	-0.84633654	-2.17455281	2.12257589
C	0.56037308	-2.93056482	-1.40293411
H	0.94233880	-0.82879195	-1.55545811
C	0.07398974	-3.96954426	-0.60844211
H	-0.79897003	-4.49180251	1.28610089
H	0.95941413	-3.14480549	-2.38689211
H	0.09026392	-4.98796129	-0.97420011
H	0.00000000	0.00000000	3.57140289
H	0.00000000	0.00000000	4.31724689

Singlet Complex S-4···H_2
Method: B3LYP-D3/def2-TZVP
Multiplicity: 1
E = –502.6745564 a.u.
E + ZPE = –502.478228 a.u.
$E_{CCSD(T)/cc\text{-}PVDZ}$ = –501.02921822 a.u.

Atomic Symbol	X	Y	Z
C	2.60614700	-1.53113909	-0.45078877
C	1.36791501	-0.91107807	-0.47156687
C	1.23815704	0.46596898	-0.15969110
C	2.41126606	1.17422002	0.19625677
C	3.63194505	0.53278001	0.28407386
C	3.73574802	-0.81704205	-0.05850291
H	2.69549498	-2.57422114	-0.72808860
H	0.48909300	-1.46520211	-0.77304577
H	2.32111208	2.23262406	0.40251059
H	4.51548506	1.08369804	0.58082476
C	0.01444505	1.18505298	-0.30064821
C	-1.22654596	0.51232704	-0.10862909
C	-2.30739996	0.83815591	-0.96159013
C	-1.46010997	-0.42712378	0.92608307
C	-3.52502897	0.19401296	-0.84244301
H	-2.14613995	1.58832578	-1.72470026
C	-2.71169698	-0.99593173	1.09640418
H	-0.65454196	-0.66765768	1.60756211
C	-3.73817198	-0.71060486	0.19856814
H	-4.32778897	0.42259986	-1.53226004
H	-2.88586098	-1.68386058	1.91463830
H	-0.11177389	3.10850531	1.59289046
H	-0.10903088	3.38245542	2.28829541
H	4.70137001	-1.30682406	-0.03271183
H	-4.70743499	-1.17803282	0.31892923

Triplet Transition State TS (T-4···H_2)
Method: B3LYP-D3/def2-TZVP
Multiplicity: 3
E = –502.6710948 a.u.
E + ZPE = –502.476331 a.u.
$E_{CCSD(T)/cc\text{-}PVDZ}$ = –501.01883345 a.u.

Atomic Symbol	X	Y	Z
C	0.00000000	0.00000000	0.94517207
C	0.02047317	-1.30584992	0.40401001
C	-0.41548883	-2.41045496	1.17563895
C	0.51147419	-1.57162385	-0.90026200
C	-0.39177080	-3.69331194	0.66145589
H	-0.77789184	-2.23619801	2.18030895
C	0.53041022	-2.86024783	-1.40200506
H	0.89633419	-0.75548782	-1.49603396
C	0.07510522	-3.92942187	-0.63143511
H	-0.73814080	-4.51960597	1.26972085
H	0.91236223	-3.03798978	-2.39985306
H	0.09341724	-4.93553985	-1.02980816
C	-0.02047317	1.30584992	0.40401001
C	0.41548883	2.41045496	1.17563895
C	-0.51147419	1.57162385	-0.90026200
C	0.39177080	3.69331194	0.66145589
H	0.77789184	2.23619801	2.18030895
C	-0.53041022	2.86024783	-1.40200506
H	-0.89633419	0.75548782	-1.49603396
C	-0.07510522	3.92942187	-0.63143511
H	0.73814080	4.51960597	1.26972085
H	-0.91236223	3.03798978	-2.39985306
H	-0.09341724	4.93553985	-1.02980816
H	0.00000000	0.00000000	2.34539407
H	0.00000000	0.00000000	3.24590307

Singlet Transition State TS (S-4···H_2)
Method: B3LYP-D3/def2-TZVP
Multiplicity: 1
E = –502.6619538 a.u.
E + ZPE = –502.464854 a.u.
$E_{CCSD(T)/cc\text{-}PVDZ}$ = –501.01516249 a.u.

Atomic Symbol	X	Y	Z
C	2.56719884	-1.45037208	-0.62968637
C	1.34136888	-0.80704304	-0.49957324
C	1.25982296	0.51032489	0.00083897
C	2.46723200	1.13045276	0.39777605
C	3.67275496	0.46801470	0.31290592
C	3.73416688	-0.82718621	-0.21333329
H	2.60344578	-2.45046502	-1.04382354
H	0.44055685	-1.30543493	-0.82966631
H	2.42942307	2.13639469	0.79616721
H	4.57986900	0.95889360	0.64309898
C	0.02515400	1.25151997	-0.08317089
C	-1.25110904	0.54971102	0.01059402
C	-2.28695303	0.95466222	-0.84589889
C	-1.50764808	-0.48824711	0.92386386
C	-3.51821906	0.31545128	-0.82520197
H	-2.09820800	1.77167732	-1.53042276
C	-2.75385411	-1.09351805	0.97912978
H	-0.71972308	-0.79773227	1.59871879
C	-3.75630810	-0.70189985	0.09473487
H	-4.30038206	0.62389644	-1.50725991
H	-2.94626414	-1.87435916	1.70433466
H	0.03862908	2.33616381	0.87354329
H	0.05121009	2.24964067	1.72145828
H	4.68571885	-1.33689125	-0.29420539
H	-4.72591813	-1.18300681	0.13018380

Triplet Radical Pair **24**···H
Method: B3LYP-D3/def2-TZVP
Multiplicity: 3
E = –502.6819489 a.u.
E + ZPE = –502.485200 a.u.
$E_{CCSD(T)/cc\text{-}PVDZ}$ = –501.03401038 a.u.

Atomic Symbol	X	Y	Z
C	0.00000000	0.00000000	1.00825800
C	-0.01962266	1.29454029	0.40159400
C	0.34749170	2.41756137	1.18165600
C	-0.44104633	1.54349767	-0.92583900
C	0.33702250	3.69650360	0.65727400
H	0.65692031	2.26026208	2.20826800
C	-0.46093470	2.82844983	-1.44007000
H	-0.79977195	0.72531575	-1.53341400
C	-0.06259446	3.91324979	-0.66113600
H	0.63661283	4.53299435	1.27646600
H	-0.80194434	2.99032799	-2.45528800
H	-0.07705508	4.91501068	-1.07064400
C	0.01962266	-1.29454029	0.40159400
C	-0.34749170	-2.41756137	1.18165600
C	0.44104633	-1.54349767	-0.92583900
C	-0.33702250	-3.69650360	0.65727400
H	-0.65692031	-2.26026208	2.20826800
C	0.46093470	-2.82844983	-1.44007000
H	0.79977195	-0.72531575	-1.53341400
C	0.06259446	-3.91324979	-0.66113600
H	-0.63661283	-4.53299435	1.27646600
H	0.80194434	-2.99032799	-2.45528800
H	0.07705508	-4.91501068	-1.07064400
H	0.00000000	0.00000000	2.09432100
H	0.00000000	0.00000000	4.44360700

Diphenylmethane **47**
Method: B3LYP-D3/def2-TZVP
Multiplicity: 1
E = –502.8179984 a.u.
E + ZPE = –502.608840 a.u.
$E_{CCSD(T)/cc\text{-}PVDZ}$ = –501.18023934 a.u.
$E_{CCSD(T)/cc\text{-}PVTZ}$ = –501.66397306 a.u.

Atomic Symbol	X	Y	Z
C	0.00000000	0.00000000	1.47868203
H	-0.04357027	-0.87392347	2.13422447
H	0.04357027	0.87392347	2.13422447
C	-1.26604115	0.05878253	0.64954999
C	-1.46915106	1.10531212	-0.25282135
C	-2.24910919	-0.92184251	0.76140330
C	-2.62579501	1.17167965	-1.01699137
H	-0.70582302	1.86684016	-0.36205281
C	-3.41017114	-0.86116397	-0.00463973
H	-2.10655426	-1.74250796	1.45515078
C	-3.60243505	0.18647761	-0.89572607
H	-2.76635093	1.99136310	-1.71075686
H	-4.16209918	-1.63408101	0.09600373
H	-4.50394401	0.23632102	-1.49321009
C	1.26604115	-0.05878253	0.64954999
C	2.24910919	0.92184251	0.76140330
C	1.46915106	-1.10531212	-0.25282135
C	3.41017114	0.86116397	-0.00463973
H	2.10655426	1.74250796	1.45515078
C	2.62579501	-1.17167965	-1.01699137
H	0.70582302	-1.86684016	-0.36205281
C	3.60243505	-0.18647761	-0.89572607
H	4.16209918	1.63408101	0.09600373
H	2.76635093	-1.99136310	-1.71075686
H	4.50394401	-0.23632102	-1.49321009

Triplet Bis(*p*-methoxyphenyl)carbene T-**61**
Method: B3LYP-D3/def2-TZVP
Multiplicity: 3
E = –730.65125320 a.u.
E + ZPE = –730.40285700 a.u.
$E_{CCSD(T)/cc\text{-}PVDZ}$ = –728.34008914 a.u.

Atomic Symbol	X	Y	Z
C	-0.03655804	1.31378694	0.58873002
C	-0.60606708	1.63741393	-0.67820096
C	0.45485299	2.39379994	1.36083199
C	-0.65337710	2.93461493	-1.13045797
H	-1.01151911	0.84060093	-1.28785794
C	0.39882998	3.70077894	0.90763498
H	0.88649803	2.18433595	2.33097498
C	-0.15219606	3.98339993	-0.34580300
H	-1.08339213	3.17437992	-2.09449196
H	0.78874101	4.49070594	1.53296496
C	0.03655804	-1.31378694	0.58873002
C	0.60606708	-1.63741393	-0.67820096
C	-0.45485299	-2.39379994	1.36083199
C	0.65337710	-2.93461493	-1.13045797
H	1.01151911	-0.84060093	-1.28785794
C	-0.39882998	-3.70077894	0.90763498
H	-0.88649803	-2.18433595	2.33097498
C	0.15219606	-3.98339993	-0.34580300
H	1.08339213	-3.17437992	-2.09449196
H	-0.78874101	-4.49070594	1.53296496
C	0.00000000	0.00000000	1.05627103
O	0.25170988	-5.22718708	-0.88742193
C	-0.23100710	-6.33484507	-0.14412290
H	-0.05011613	-7.21186307	-0.76147190
H	0.30357193	-6.44421106	0.80474408
H	-1.30392609	-6.24743206	0.05403914
O	-0.25170988	5.22718708	-0.88742193
C	0.23100710	6.33484507	-0.14412290
H	0.05011613	7.21186307	-0.76147190
H	-0.30357193	6.44421106	0.80474408
H	1.30392609	6.24743206	0.05403914

Singlet Bis(*p*-methoxyphenyl)carbene S-**61**
Method: B3LYP-D3/def2-TZVP
Multiplicity: 1
E = –730.64906530 a.u.
E + ZPE = –730.39934900 a.u.
$E_{CCSD(T)/cc\text{-}PVDZ}$ = –728.34053001 a.u.

Atomic Symbol	X	Y	Z
C	0.06972700	-1.22877500	0.85306093
C	0.70234297	-1.39870498	-0.40938309
C	-0.46063195	-2.39112801	1.45627295
C	0.78723399	-2.63255998	-1.01312609
H	1.16494994	-0.54324697	-0.88355010
C	-0.45047194	-3.62067501	0.82373095
H	-0.90381593	-2.28864602	2.43837896
C	0.18987203	-3.75097700	-0.41517507
H	1.29998997	-2.76785997	-1.95675510
H	-0.90200590	-4.47408202	1.30789696
C	-0.06972700	1.22877500	0.85306093
C	-0.70234297	1.39870498	-0.40938309
C	0.46063195	2.39112801	1.45627295
C	-0.78723399	2.63255998	-1.01312609
H	-1.16494994	0.54324697	-0.88355010
C	0.45047194	3.62067501	0.82373095
H	0.90381593	2.28864602	2.43837896
C	-0.18987203	3.75097700	-0.41517507
H	-1.29998997	2.76785997	-1.95675510
H	0.90200590	4.47408202	1.30789696
C	0.00000000	0.00000000	1.57262793
O	-0.30363520	4.91306799	-1.09979206
C	0.26227878	6.09648601	-0.55196207
H	0.05499574	6.88543800	-1.27092207
H	-0.19703120	6.35003100	0.40772294
H	1.34399879	5.99795403	-0.42283010
O	0.30363520	-4.91306799	-1.09979206
C	-0.26227878	-6.09648601	-0.55196207
H	-0.05499574	-6.88543800	-1.27092207
H	0.19703120	-6.35003100	0.40772294
H	-1.34399879	-5.99795403	-0.42283010

Triplet Complex T-**61**···H_2
Method: B3LYP-D3/def2-TZVP
Multiplicity: 3
E = –731.83236670 a.u.
E + ZPE = –731.57219300 a.u.
$E_{CCSD(T)/cc\text{-}PVDZ}$ = –729.50446129 a.u.

Atomic Symbol	X	Y	Z
C	2.89608095	0.62620170	-1.20365048
C	1.60859330	0.58857237	-0.72479852
C	1.31035601	0.04765682	0.56070852
C	2.40669019	-0.41147300	1.32877407
C	3.70504317	-0.36183103	0.84974511
C	3.96095655	0.14850885	-0.42648777
H	3.11570710	1.03031326	-2.18353917
H	0.80011063	0.97758170	-1.32935074
H	2.21829439	-0.81530440	2.31492278
H	4.50875607	-0.72760312	1.47210581
C	0.00000000	0.00000000	1.03984802
C	-1.31035601	-0.04765682	0.56070852
C	-2.40669019	0.41147300	1.32877407
C	-1.60859330	-0.58857237	-0.72479852
C	-3.70504317	0.36183103	0.84974511
H	-2.21829439	0.81530440	2.31492278
C	-2.89608095	-0.62620170	-1.20365048
H	-0.80011063	-0.97758170	-1.32935074
C	-3.96095655	-0.14850885	-0.42648777
H	-4.50875607	0.72760312	1.47210581
H	-3.11570710	-1.03031326	-2.18353917
O	-5.19188131	-0.22946033	-0.99903674
O	5.19188131	0.22946033	-0.99903674
C	-6.31692415	0.22637178	-0.26503324
H	-6.23497505	1.29146933	-0.02657003
H	-7.17913241	0.06773249	-0.90878290
H	-6.44778392	-0.34195010	0.66122100
C	6.31692415	-0.22637178	-0.26503324
H	6.23497505	-1.29146933	-0.02657003
H	7.17913241	-0.06773249	-0.90878290
H	6.44778392	0.34195010	0.66122100
H	-0.00000000	0.00000000	3.78413050
H	-0.00000000	0.00000000	4.53039767

Singlet Complex S-**61**···H_2
Method: B3LYP-D3/def2-TZVP
Multiplicity: 1
E = –731.83041938 a.u.
E + ZPE = –731.56859100 a.u.
$E_{CCSD(T)/cc\text{-}PVDZ}$ = –729.50557692 a.u.

Atomic Symbol	X	Y	Z
C	-1.24829032	0.45842366	-2.60525052
C	-0.63582071	0.43527603	-1.37337485
C	0.74632387	0.12998896	-1.23258181
C	1.45086355	-0.17299453	-2.42047709
C	0.83213199	-0.22003149	-3.65489940
C	-0.52336485	0.12316693	-3.75712423
H	-2.28838309	0.73649644	-2.71684649
H	-1.20388169	0.71061261	-0.49488981
H	2.51035085	-0.37723862	-2.33675024
H	1.40700680	-0.47772813	-4.53224635
C	1.47468149	0.23222052	-0.01181609
C	0.80316435	0.05107945	1.23199824
C	1.24150502	0.80182558	2.34507926
C	-0.24494500	-0.88048653	1.46337247
C	0.62268322	0.71796231	3.57933947
H	2.07259604	1.47970418	2.19958440
C	-0.80724579	-1.03593292	2.71055218
H	-0.57647074	-1.50959392	0.64759526
C	-0.40159172	-0.21675914	3.77318016
H	0.96266914	1.34555468	4.38999552
H	-1.57947319	-1.77153828	2.89540682
O	-1.04405530	-0.41741862	4.94873641
O	-1.21127666	0.18551785	-4.91930467
C	-0.53802180	-0.08946449	-6.14152780
H	-0.15642444	-1.11415518	-6.16442230
H	-1.28185176	0.03613157	-6.92452936
H	0.28601220	0.61019383	-6.30685836
C	-0.68712269	0.37379018	6.07411202
H	-0.85287926	1.43789564	5.88180883
H	-1.33530426	0.04826674	6.88424380
H	0.35693432	0.21428333	6.35861765
H	3.43124441	-1.55006243	0.05299807
H	3.78080678	-2.21200344	0.04734646

Triplet Transition State TS (T-**61**···H_2)
Method: B3LYP-D3/def2-TZVP
Multiplicity: 3
E = –731.82120762 a.u.
E + ZPE = –731.56146400 a.u.
$E_{CCSD(T)/cc\text{-}PVDZ}$ = –729.48955648 a.u.

Atomic Symbol	X	Y	Z
C	-2.84903300	-1.19509500	0.57151100
C	-1.56978000	-0.69033300	0.53146800
C	-1.30348100	0.61695900	0.03924900
C	-2.41993000	1.37828400	-0.37288600
C	-3.70873300	0.87366000	-0.33081200
C	-3.93483600	-0.42419800	0.13557800
H	-3.04391500	-2.19010500	0.95037400
H	-0.75113400	-1.29167500	0.90229700
H	-2.26026000	2.38500000	-0.73647400
H	-4.52755200	1.49524700	-0.66266800
C	0.00000100	1.15779100	0.00001200
C	1.30348100	0.61695700	-0.03923300
C	2.41993400	1.37828600	0.37288500
C	1.56977500	-0.69033800	-0.53144600
C	3.70873600	0.87366200	0.33080300
H	2.26026700	2.38500400	0.73646900
C	2.84902800	-1.19510000	-0.57149800
H	0.75112600	-1.29168300	-0.90226200
C	3.93483600	-0.42419900	-0.13558000
H	4.52755800	1.49525000	0.66264700
H	3.04390600	-2.19011200	-0.95035600
O	5.15476700	-1.01931000	-0.21486800
O	-5.15476800	-1.01930800	0.21485700
C	6.29777800	-0.28895300	0.20149300
H	6.23415200	-0.01432300	1.25906500
H	7.14728700	-0.95163100	0.05281000
H	6.43550100	0.61572200	-0.39896300
C	-6.29777500	-0.28895400	-0.20151900
H	-6.23414000	-0.01433100	-1.25909300
H	-7.14728600	-0.95163000	-0.05283900
H	-6.43550400	0.61572600	0.39893000
H	0.00000100	2.56036400	0.00000500
H	0.00000100	3.46154200	0.00000200

Singlet Transition State TS (S-**61**···H_2)
Method: B3LYP-D3/def2-TZVP
Multiplicity: 1
E = –731.81477662 a.u.
E + ZPE = –731.55176900 a.u.
$E_{CCSD(T)/cc\text{-}PVDZ}$ = –729.48839782 a.u.

Atomic Symbol	X	Y	Z
C	2.59740300	-1.17116300	-0.53745500
C	1.36937500	-0.54574800	-0.42314400
C	1.25569900	0.79726500	0.00533100
C	2.45881300	1.45282500	0.34065300
C	3.68459700	0.82219600	0.27890300
C	3.76570500	-0.50287300	-0.17437500
H	2.67394200	-2.18820800	-0.89934500
H	0.48105300	-1.08348800	-0.72379600
H	2.41197400	2.47718600	0.68807200
H	4.57227100	1.36290600	0.57324500
C	0.01142100	1.52032900	-0.08411300
C	-1.25908200	0.82195400	0.04060700
C	-2.34713700	1.29319000	-0.70629500
C	-1.48880900	-0.27832900	0.89350700
C	-3.59143100	0.68205700	-0.66073700
H	-2.19339500	2.15417200	-1.34453000
C	-2.72746600	-0.87544000	0.98060400
H	-0.67642600	-0.64214700	1.50933100
C	-3.78751300	-0.40786600	0.19213400
H	-4.39661800	1.06501800	-1.26997300
H	-2.91159100	-1.70463700	1.65114900
O	-4.96096600	-1.06783200	0.33608100
O	4.92155900	-1.20684400	-0.29103400
C	6.14778000	-0.57128300	0.03662400
H	6.17293000	-0.26635100	1.08737900
H	6.92458400	-1.31154300	-0.14076200
H	6.32835400	0.30175900	-0.59789800
C	-6.08788900	-0.64364600	-0.41926100
H	-5.90072100	-0.72508200	-1.49394200
H	-6.89984000	-1.31195600	-0.14287200
H	-6.36613100	0.38571800	-0.17548200
H	0.03102400	2.64072300	0.72590100
H	0.05505500	2.68253200	1.61524400

Triplet Radical Pair **65**···H
Method: B3LYP-D3/def2-TZVP
Multiplicity: 3
E = –731.83156428 a.u.
E + ZPE = –731.56987900 a.u.
$E_{CCSD(T)/cc\text{-}PVDZ}$ = –729.50971921 a.u.

Atomic Symbol	X	Y	Z
C	2.82504264	0.48596578	-1.22752158
C	1.54733793	0.44516877	-0.71470427
C	1.29331378	0.03453910	0.61864843
C	2.42517313	-0.30027937	1.39404199
C	3.71206549	-0.27279706	0.88314531
C	3.92338312	0.11690756	-0.44189595
H	3.00721887	0.81804331	-2.24144667
H	0.72911267	0.78291999	-1.33406418
H	2.27941088	-0.60263449	2.42449241
H	4.53880874	-0.55073672	1.52057299
C	0.00000000	0.00000000	1.22339219
C	-1.29331378	-0.03453910	0.61864843
C	-2.42517313	0.30027937	1.39404199
C	-1.54733793	-0.44516877	-0.71470427
C	-3.71206549	0.27279706	0.88314531
H	-2.27941088	0.60263449	2.42449241
C	-2.82504264	-0.48596578	-1.22752158
H	-0.72911267	-0.78291999	-1.33406418
C	-3.92338312	-0.11690756	-0.44189595
H	-4.53880874	0.55073672	1.52057299
H	-3.00721887	-0.81804331	-2.24144667
O	-5.13998879	-0.18596610	-1.04763783
O	5.13998879	0.18596610	-1.04763783
C	-6.29126832	0.17873454	-0.30402489
H	-6.24129689	1.22127276	0.02597405
H	-7.13569769	0.05551097	-0.97846588
H	-6.42799992	-0.46915902	0.56766786
C	6.29126832	-0.17873454	-0.30402489
H	6.24129689	-1.22127276	0.02597405
H	7.13569769	-0.05551097	-0.97846588
H	6.42799992	0.46915902	0.56766786
H	0.00000000	0.00000000	2.30957454
H	0.00000000	0.00000000	4.65054837

Bis(*p*-methoxyphenyl)methane **64**
Method: B3LYP-D3/def2-TZVP
Multiplicity: 1
E = –731.96593950 a.u.
E + ZPE = –731.69188000 a.u.
$E_{CCSD(T)/cc\text{-}PVDZ}$ = –729.64969778 a.u.

Atomic Symbol	X	Y	Z
C	1.25207133	-2.58237902	-0.59512464
C	1.14227506	-1.43377703	0.16446634
C	0.10039778	-1.26447009	1.08380204
C	-0.82810921	-2.28944513	1.20267776
C	-0.73767193	-3.45691012	0.44311377
C	0.30939734	-3.60682406	-0.46128192
H	2.05866355	-2.71207897	-1.30485540
H	1.87181406	-0.64239200	0.03825757
H	-1.64886942	-2.18669018	1.90350152
H	-1.48402793	-4.22771216	0.56767654
C	0.00000000	0.00000000	1.91022802
C	-0.10039778	1.26447009	1.08380204
C	0.82810921	2.28944513	1.20267776
C	-1.14227506	1.43377703	0.16446634
C	0.73767193	3.45691012	0.44311377
H	1.64886942	2.18669018	1.90350152
C	-1.25207133	2.58237902	-0.59512464
H	-1.87181406	0.64239200	0.03825757
C	-0.30939734	3.60682406	-0.46128192
H	1.48402793	4.22771216	0.56767654
H	-2.05866355	2.71207897	-1.30485540
O	-0.50164681	4.69840091	-1.25539607
O	0.50164681	-4.69840091	-1.25539607
C	-0.42252835	-5.76906609	-1.16777016
H	-1.43413029	-5.45013713	-1.43952446
H	-0.08102811	-6.52021506	-1.87671007
H	-0.44066663	-6.20335710	-0.16278217
C	0.42252835	5.76906609	-1.16777016
H	1.43413029	5.45013713	-1.43952446
H	0.08102811	6.52021506	-1.87671007
H	0.44066663	6.20335710	-0.16278217
H	0.87089428	0.07604093	2.56766828
H	-0.87089428	-0.07604093	2.56766828

Triplet 3-Methoxy-9-fluorenylidene T-**62**
Method: B3LYP-D3/def2-TZVP
Multiplicity: 3
E = –614.86323540 a.u.
E + ZPE = –614.66811900 a.u.
$E_{CCSD(T)/cc\text{-}PVDZ}$ = –612.91339336 a.u.

Atomic Symbol	X	Y	Z
C	-1.11757502	-0.89830007	0.00000000
C	-0.00969700	-0.08360809	0.00000000
C	-0.15945398	1.34821791	0.00000000
C	-1.43692097	1.90666094	0.00000000
C	-2.55178398	1.07638095	0.00000000
C	-2.39662601	-0.31715205	0.00000000
H	-1.03898203	-1.97801807	0.00000000
H	-1.56453295	2.98140194	0.00000000
H	-3.53669297	1.51829697	0.00000000
C	2.11775197	-1.58048512	0.00000000
C	3.51425097	-1.55556415	0.00000000
C	4.20935899	-0.34331016	0.00000000
C	3.53179601	0.87016585	0.00000000
C	2.13584901	0.86044588	0.00000000
C	1.42268999	-0.38515011	0.00000000
H	1.58886496	-2.52618211	0.00000000
H	4.06540396	-2.48718016	0.00000000
H	5.29192499	-0.35079918	0.00000000
H	4.07338703	1.80719884	0.00000000
C	1.14832203	1.87806389	0.00000000
O	-3.42956702	-1.20005303	0.00000000
C	-4.75988901	-0.70493501	0.00000000
H	-5.40415803	-1.58108800	0.00000000
H	-4.96355900	-0.10589498	0.89276706
H	-4.96355900	-0.10589498	-0.89276706

Singlet 3-Methoxy-9-fluorenylidene S-**62**
Method: B3LYP-D3/def2-TZVP
Multiplicity: 1
E = –614.86038380 a.u.
E + ZPE = –614.66510700 a.u.
$E_{CCSD(T)/cc\text{-}PVDZ}$ = –612.91254296 a.u.

Atomic Symbol	X	Y	Z
C	-1.12156999	-0.92929804	0.00000000
C	-0.01933001	-0.12418002	0.00000000
C	-0.12973803	1.30025598	0.00000000
C	-1.39314204	1.87790396	0.00000000
C	-2.53558503	1.07602793	0.00000000
C	-2.40003600	-0.31431806	0.00000000
H	-1.07048297	-2.01074704	0.00000000
H	-1.48120606	2.95729495	0.00000000
H	-3.51282304	1.53417192	0.00000000
C	2.13152302	-1.60369398	0.00000000
C	3.53719602	-1.53745396	0.00000000
C	4.19943000	-0.31856894	0.00000000
C	3.47408297	0.88097204	0.00000000
C	2.08907498	0.83377302	0.00000000
C	1.42776400	-0.42284499	0.00000000
H	1.63195904	-2.56524099	0.00000000
H	4.11056503	-2.45635595	0.00000000
H	5.28173300	-0.29723792	0.00000000
H	3.97605696	1.84036305	0.00000000
C	1.15250295	1.97502700	0.00000000
O	-3.43427399	-1.17779508	0.00000000
C	-4.76648000	-0.67397711	0.00000000
H	-5.41275398	-1.54793512	0.00000000
H	-4.96151702	-0.07485706	0.89324995
H	-4.96151702	-0.07485706	-0.89324995

Triplet Complex T-**62**···H_2
Method: B3LYP-D3/def2-TZVP
Multiplicity: 3
E = –616.04390835 a.u.
E + ZPE = –615.83747200 a.u.
$E_{CCSD(T)/cc\text{-}PVDZ}$ = –614.07726173 a.u.

Atomic Symbol	X	Y	Z
C	1.17899296	-0.96132094	0.00000000
C	0.04868798	-0.17796291	0.00000000
C	0.15978501	1.25751108	0.00000000
C	1.42083203	1.85177505	0.00000000
C	2.55812401	1.05284802	0.00000000
C	2.44149297	-0.34446498	0.00000000
H	1.13082393	-2.04282394	0.00000000
H	1.51783706	2.92967305	0.00000000
H	3.53039402	1.52184899	0.00000000
C	-2.03989407	-1.73052786	0.00000000
C	-3.43671407	-1.74143882	0.00000000
C	-4.16327603	-0.54777480	0.00000000
C	-3.51737300	0.68275618	0.00000000
C	-2.12178700	0.70842314	0.00000000
C	-1.37561203	-0.51780488	0.00000000
H	-1.48708609	-2.66243887	0.00000000
H	-3.96348909	-2.68704781	0.00000000
H	-5.24526203	-0.58345277	0.00000000
H	-4.08238798	1.60581519	0.00000000
C	-1.16143297	1.75084412	0.00000000
H	-1.77481790	4.35555313	0.00000000
H	-1.94175788	5.08238614	0.00000000
O	3.49881895	-1.19776701	0.00000000
C	4.81470696	-0.66511204	0.00000000
H	5.48346594	-1.52269706	0.00000000
H	5.00126698	-0.06058828	-0.89278453
H	5.00126698	-0.06058828	0.89278453

Singlet Complex S-**62**···H_2
Method: B3LYP-D3/def2-TZVP
Multiplicity: 1
E = –616.04201400 a.u.
E + ZPE = –615.83461000 a.u.
$E_{CCSD(T)/cc\text{-}PVDZ}$ = –614.07813383 a.u.

Atomic Symbol	X	Y	Z
C	-1.17224794	-0.97866894	0.04463597
C	-0.05500589	-0.20015801	-0.04660298
C	-0.13882980	1.21978900	-0.18185197
C	-1.39045676	1.82235808	-0.20624701
C	-2.54735181	1.04868315	-0.10445105
C	-2.43843890	-0.33917286	0.01377094
H	-1.14219500	-2.05650094	0.14188296
H	-1.45785769	2.89885908	-0.30304100
H	-3.51531978	1.52573820	-0.12167008
C	2.06811202	-1.71248114	0.09874207
C	3.47477802	-1.67097722	0.10630411
C	4.15950810	-0.47048326	-0.01302185
C	3.45667517	0.73457478	-0.14932387
C	2.07111117	0.71147487	-0.15680291
C	1.38623909	-0.52570909	-0.02774294
H	1.55101196	-2.65969611	0.19595304
H	4.03105296	-2.59463226	0.20879212
H	5.24192410	-0.46795633	-0.00137082
H	3.97639123	1.67964075	-0.24444584
C	1.15517525	1.86167592	-0.27632293
H	1.63870729	3.64455088	1.63817310
H	1.73771529	3.94300586	2.31756111
O	-3.48849695	-1.17750580	0.10695090
C	-4.81106492	-0.64908772	0.08013786
H	-5.47344797	-1.50710568	0.16062683
H	-4.98300590	0.02607128	0.92241886
H	-5.00621786	-0.12283370	-0.85782814

Triplet Transition State TS (T-**62**···H_2)
Method: B3LYP-D3/def2-TZVP
Multiplicity: 3
E = –616.03831078 a.u.
E + ZPE = –615.83337200 a.u.
$E_{CCSD(T)/cc\text{-}PVDZ}$ = –614.06643320 a.u.

Atomic Symbol	X	Y	Z
C	-1.16589103	-0.95332605	0.00000000
C	-0.04261305	-0.16023403	0.00000000
C	-0.16185107	1.27223297	0.00000000
C	-1.42764708	1.85717395	0.00000000
C	-2.55997306	1.05069193	0.00000000
C	-2.43311904	-0.34573707	0.00000000
H	-1.10987902	-2.03441705	0.00000000
H	-1.53332609	2.93452095	0.00000000
H	-3.53564807	1.51264492	0.00000000
C	2.05872598	-1.69425700	0.00000000
C	3.45573898	-1.69089598	0.00000000
C	4.16961696	-0.48980297	0.00000000
C	3.50989294	0.73384602	0.00000000
C	2.11405794	0.74531300	0.00000000
C	1.38378296	-0.48742201	0.00000000
H	1.51551199	-2.63176201	0.00000000
H	3.99246099	-2.63094697	0.00000000
H	5.25194896	-0.51402595	0.00000000
H	4.06623093	1.66248003	0.00000000
C	1.15297292	1.79370799	0.00000000
H	1.49599390	3.28807999	0.00000000
H	1.68269489	4.10904100	0.00000000
O	-3.48365103	-1.20722208	0.00000000
C	-4.80381404	-0.68539910	0.00000000
H	-5.46555702	-1.54841811	0.00000000
H	-4.99525708	-0.08238104	0.89276267
H	-4.99525708	-0.08238104	-0.89276267

Singlet Transition State TS (S-**62**···H_2)
Method: B3LYP-D3/def2-TZVP
Multiplicity: 1
E = –616.03525311 a.u.
E + ZPE = –615.82769100 a.u.
$E_{CCSD(T)/cc\text{-}PVDZ}$ = –614.06706778 a.u.

Atomic Symbol	X	Y	Z
C	-1.15882099	-0.95788501	-0.00818708
C	-0.04431801	-0.15668498	-0.01214701
C	-0.15184804	1.26203702	-0.06734689
C	-1.41195606	1.84686299	-0.07515184
C	-2.55251504	1.05061596	-0.01388691
C	-2.42700700	-0.34410404	0.00791998
H	-1.10582996	-2.03892001	-0.01653017
H	-1.50678708	2.92477599	-0.12080275
H	-3.52662805	1.51540593	-0.00295087
C	2.06875803	-1.68218793	0.01470886
C	3.46738303	-1.65683190	0.04536086
C	4.16399900	-0.45080388	0.02655495
C	3.47867997	0.76238411	-0.04563994
C	2.09039797	0.75251008	-0.06294294
C	1.39111900	-0.47857394	-0.01050204
H	1.53858106	-2.62690994	0.01512678
H	4.01677006	-2.58945189	0.07842478
H	5.24620100	-0.45842785	0.05211195
H	4.01590095	1.70176313	-0.08626287
C	1.15237694	1.86915407	-0.26997885
H	1.44658892	3.01847500	0.72342525
H	1.48699392	3.03571493	1.54007025
O	-3.47395998	-1.19984007	0.03479291
C	-4.79762499	-0.68012211	0.04012095
H	-5.45575097	-1.54527112	0.06141988
H	-4.97882601	-0.06357518	0.92504300
H	-4.99727701	-0.09308104	-0.86071100

Triplet Radical Pair **70**···H
Method: B3LYP-D3/def2-TZVP
Multiplicity: 3
E = –616.05858193 a.u.
E + ZPE = –615.85118000 a.u.
$E_{CCSD(T)/cc\text{-}PVDZ}$ = –614.09489362 a.u.

Atomic Symbol	X	Y	Z
C	1.17161195	-0.96118607	0.00000000
C	0.04434697	-0.17433203	0.00000000
C	0.14762403	1.25544397	0.00000000
C	1.41148105	1.84925892	0.00000000
C	2.55139602	1.05356388	0.00000000
C	2.43483197	-0.34398512	0.00000000
H	1.12416991	-2.04257607	0.00000000
H	1.51122909	2.92787392	0.00000000
H	3.52360604	1.52296684	0.00000000
C	-2.05257908	-1.71297595	0.00000000
C	-3.45016508	-1.70838490	0.00000000
C	-4.16196504	-0.50595088	0.00000000
C	-3.49806999	0.71569510	0.00000000
C	-2.10081799	0.72680305	0.00000000
C	-1.37898604	-0.50560098	0.00000000
H	-1.51081312	-2.65120897	0.00000000
H	-3.98841412	-2.64767688	0.00000000
H	-5.24447504	-0.52820884	0.00000000
H	-4.05548496	1.64455812	0.00000000
C	-1.16200895	1.80428301	0.00000000
H	-1.40841991	2.85654302	0.00000000
H	-1.94282283	5.18942504	0.00000000
O	3.49211094	-1.19784016	0.00000000
C	4.80797596	-0.66624120	0.00000000
H	5.47646992	-1.52412023	0.00000000
H	4.99500801	-0.06159693	-0.89267158
H	4.99500801	-0.06159693	0.89267158

Triplet 3-Methoxy-9-fluorene **69**
Method: B3LYP-D3/def2-TZVP
Multiplicity: 1
E = –616.19206280 a.u.
E + ZPE = –615.97230500 a.u.
$E_{CCSD(T)/cc\text{-}PVDZ}$ = –614.23203193 a.u.

Atomic Symbol	X	Y	Z
C	-1.14746197	-0.92576300	0.00000000
C	-0.03576101	-0.10001394	0.00000000
C	-0.17205609	1.30039605	0.00000000
C	-1.43174012	1.86437498	0.00000000
C	-2.56262408	1.04382392	0.00000000
C	-2.41891400	-0.34685307	0.00000000
H	-1.06406991	-2.00468900	0.00000000
H	-1.55806318	2.94073997	0.00000000
H	-3.54249010	1.49729286	0.00000000
C	2.04377007	-1.65589683	0.00000000
C	3.43451207	-1.67737176	0.00000000
C	4.16318401	-0.48836072	0.00000000
C	3.51024694	0.74361725	0.00000000
C	2.12576994	0.77042117	0.00000000
C	1.39135200	-0.42721387	0.00000000
H	1.48042212	-2.58091986	0.00000000
H	3.95759012	-2.62546773	0.00000000
H	5.24539001	-0.52310166	0.00000000
H	4.08188689	1.66432128	0.00000000
C	1.18873687	1.95539812	0.00000000
O	-3.46271595	-1.22512713	0.00000000
C	-4.78442698	-0.71397520	0.00000000
H	-5.44131993	-1.58113624	0.00000000
H	-4.98308804	-0.11155023	0.89239582
H	-4.98308804	-0.11155023	-0.89239582
H	1.34052181	2.59077711	0.87830607
H	1.34052181	2.59077711	-0.87830607

Septet 1,3,5-Trichloro-2,4,6-trinitrenobenzene **82**
Method: B3LYP/aug-cc-PVTZ
Multiplicity: 7
E = –1773.435803 a.u.
E + ZPE = –1773.391336 a.u.

Atomic Symbol	X	Y	Z
C	0.00000000	1.44656382	0.00000000
C	-1.22884756	0.70947547	0.00000000
C	-1.25276102	-0.72328191	0.00000000
C	1.25276102	-0.72328191	0.00000000
C	1.22884756	0.70947547	0.00000000
N	-2.39095207	-1.38041682	0.00000000
N	2.39095207	-1.38041682	0.00000000
N	0.00000000	2.76083364	0.00000000
C	0.00000000	-1.41895094	0.00000000
Cl	0.00000000	-3.13330192	0.00000000
Cl	-2.71351906	1.56665096	0.00000000
Cl	2.71351906	1.56665096	0.00000000

Septet 1,3,5-Tribromo-2,4,6-trinitrenobenzene **86**
Method: B3LYP/aug-cc-PVTZ
Multiplicity: 7
E = –8115.4183554 a.u.
E + ZPE = –8115.375831 a.u.

Atomic Symbol	X	Y	Z
C	0.00000000	1.44510196	0.00000000
C	-1.22839554	0.70921450	0.00000000
C	-1.25149501	-0.72255098	0.00000000
C	1.25149501	-0.72255098	0.00000000
C	1.22839554	0.70921450	0.00000000
N	-2.39069719	-1.38026967	0.00000000
N	2.39069719	-1.38026967	0.00000000
N	0.00000000	2.76053933	0.00000000
C	0.00000000	-1.41842899	0.00000000
Br	-2.85354850	1.64749700	0.00000000
Br	0.00000000	-3.29499399	0.00000000
Br	2.85354850	1.64749700	0.00000000